Fatigue Behavior and Modeling of Polyether Ether Ketone under Variable Amplitude and Multiaxial Loading

by

Rakish Shrestha

A dissertation submitted to the Graduate Faculty of
Auburn University
in partial fulfillment of the
requirements for the Degree of
Doctor of Philosophy

Auburn, Alabama
August 8, 2020

Thermoplastic, Fatigue, Cyclic behavior, Frequency effect, Energy approach, Multiaxial fatigue

Approved by

Nima Shamsaei, Chair, Philpott-WestPoint Stevens Distinguished Associate Professor, Department of Mechanical Engineering
Jeffrey Suhling, Quina Professor, Department of Mechanical Engineering
Hareesh Tippur, McWane Chair Professor, Department of Mechanical Engineering
Asha-Dee Celestine, Assistant Professor, Department of Aerospace Engineering

Table of Contents

ABSTRACT

Experimental and analytical roadmap to thoroughly understand and establish benchmark material properties for unfilled polyether ether ketone (PEEK) under monotonic tension and compression, as well as uniaxial and multiaxial fatigue loading conditions along with the obtained results are documented in the present dissertation. A systematic experimental program was designed to study the effects of various loading characteristics, including strain amplitude, test frequency (i.e. cyclic strain rate), control modes (i.e. strain-controlled versus force-controlled), self-heating, mean stress/strains, pre-loadings, and several multiaxial load paths. Knowledge gained from investigating the cyclic deformation behavior was then used to determine a suitable fatigue life model capable of correlating fatigue life of the PEEK polymer under various types of loading conditions.

Monotonic tension and compression tests revealed that the quasi-static tensile and compressive properties of PEEK polymers were significantly affected by the applied strain rate. Similarly, under fatigue loading, the applied test frequency not only affected the rise in temperature on the gage section of the specimen, but it also had an impact on the resulting fatigue life. Cyclic deformation behavior represented by the stress responses under strain-controlled loading revealed significant cyclic softening under fully-reversed loadings, while stress relaxation was evident under tensile mean strain loadings. Variations in loading condition were also seen to affect the resulting deformation response, which was represented by the hysteresis loops. Under variable amplitude block loading tests, the beneficial effect of load history was observed to be significant and irrespective to the loading sequence. Characterizing PEEK polymer under more realistic multiaxial loading

revealed that the fatigue lives were dependent on the applied loading path, among which the non-proportional loading was observed to be the most detrimental compared to proportional and uniaxial loading. It was also realized that due to the complex failure mechanisms in polymeric materials, which were significantly different to those in the metallic materials, traditional fatigue life models were not able to accurately correlate the fatigue data of PEEK thermoplastic. Furthermore, reasonably well correlations of fatigue data under different types of uniaxial and multiaxial loading conditions were obtained using an energy based model that was capable of capturing the effect of cyclic deformation on the fatigue behavior.

Keywords: Thermoplastic, Fatigue, Cyclic behavior, Frequency effect, Energy approach, Multiaxial fatigue

Acknowledgments

I would like to dedicate this dissertation first to my family and especially to my parents who supported, believed, and advised me in all of the decision that I took.

I would like to thank my advisor Dr. Nima Shamsaei, first of all for giving me an opportunity to join his prestigious research team. His advice, guidance, patience, and most importantly his knowledge and expertise was pivotal to the successful completion of this dissertation.

I would like thank my committee members, Dr. Jeffrey Suhling, Dr. Hareesh Tippur, and Dr. Asha-Dee Celestine, for their valuable feedback and suggestion, which helped to improve the quality of this dissertation.

I would also like to thank Dr. Jutima Simsiriwong for being my mentor and for teaching and guiding me through every step of my graduate school.

I am very thankful to all of the funding committees, for funding all of the research works that were included in this dissertation.

I would like to thank all of my lab mates who made my journey through the graduate school memorable, enjoyable as well as easier.

List of Tables

List of Figures

Nomenclature

A	Alternating stress ratio/Cross-section area
a	Exponent related to the DCD method
a_f	Final crack length
a_o	Initial crack length
B	Material constant in the temperature rise equation
b	Fatigue strength exponent
C	Material constant in the temperature rise equation
c	Fatigue ductility exponent
D	Cumulative damage
D_i	Damage induced by a specific stress/strain level of i
E	Modulus of elasticity
E'	Cyclic modulus of elasticity
f	Test frequency
i	Block of loading under specific stress/strain level
K'	Cyclic strength coefficient
k	Material constant in Fatemi-Socie damage parameter
N	Number of cycles
N_a	Number of cycles required to reach a crack length of a
N_f	Cycles to failure
$N_{f,experimental}$	Experimentally obtained fatigue life
N_{f_i}	Cycles to failure for a specific stress/strain level of i
$N_{f,predicted}$	Predicted fatigue life
N_i	Number of cycles for a specific stress/strain level of i
N_t	Transition fatigue life
$2N_f$	Reversals to failure
n'	Cyclic strain hardening exponent
R, R_ε	Ratio of minimum to maximum strain
r_{mid}	Mid-section radius at the gage

r_{surf}	Surface radius at the gage
S	Stress
T_g	Glass transition temperature
ΔT	Temperature rise on the surface of specimen
W^E	Elastic strain energy density
ΔW^{E+}	Tensile elastic strain energy density
$W^P, \Delta W^P$	Plastic strain energy density
$W^T, \Delta W^T$	Total strain energy density
W_0	Total strain energy at the fatigue limit endurance level
ΔW_{HL}^E	Elastic strain energy density at half-life cycle
W_{avg}^E	Average elastic strain energy density
$W_{HL}^P, \Delta W_{HL}^P$	Plastic strain energy density at the half-life cycle
W_{avg}^P	Average plastic strain energy density
$W_{HL}^T, \Delta W_{HL}^T$	Total strain energy densities at half-life cycle
α	Material constant in the damage curve approach
γ	Material constant in the total strain energy density equation
ε_0	Strain amplitude at the fatigue limit
ε_f'	Fatigue ductility coefficient
ε_m	Mean strain
$\frac{\Delta\varepsilon}{2}$, ε_a	Total/axial strain amplitude
$\bar{\varepsilon}_a$	Equivalent strain amplitude
$\bar{\varepsilon}_{a\_mid}$	Equivalent strain amplitude at mid-section
$\frac{\Delta\varepsilon_e}{2}$	Axial elastic strain amplitude
$\frac{\Delta\bar{\varepsilon}_e}{2}$	Equivalent elastic strain amplitude
$\frac{\Delta\varepsilon_p}{2}$	Axial plastic strain amplitude
$\frac{\Delta\bar{\varepsilon}_p}{2}$	Equivalent plastic strain amplitude

ε_{a_tr}	Transverse strain amplitude
γ_a	Shear strain amplitude
γ_{a_mid}	Shear strain amplitude at mid-section
γ_{a_surf}	Shear strain amplitude at the surface
λ	Ratio of axial to shear strain
κ	Material constant in the total strain energy density equation
σ_0	Stress amplitude at the fatigue limit
$\frac{\Delta\sigma}{2}, \sigma_a$	Stress amplitude
$\bar{\sigma}_a$	Equivalent stress amplitude
$\bar{\sigma}_{a\_mid}$	Equivalent stress amplitude at mid-section
σ'_f	Fatigue strength coefficient
σ_y	Yield strength
σ'_y	Cyclic yield strength
σ_m	Mean stress
$\bar{\nu}$	Equivalent Poisson's ratio
ν_e	Elastic Poisson's ratio
τ_a	Shear stress amplitude
τ_{a_mid}	Shear stress amplitude at mid-section
τ_{a_surf}	Shear stress amplitude at surface
ψ_0	Fatigue limit
ΣW^{E+}	Cumulative tensile elastic strain energy density
$\sum W^{E+}_{axial}$	Cumulative axial elastic strain energy density
$\sum W^{E+}_{shear}$	Cumulative shear elastic strain energy density
ΣW^{P}	Cumulative plastic strain energy density
$\sum W^{P}_{axial}$	Cumulative axial plastic strain energy density
$\sum W^{P}_{shear}$	Cumulative shear plastic strain energy density

ΣW^T	Cumulative total strain energy density
$\sum W_{axial}^T$	Cumulative total axial strain energy density
ΣW_i^T	Cumulative total strain energy density at particular strain or stress level applied in the loading block i
$\sum W_{MA}^T$	Cumulative total strain energy density for multiaxial loading
$\sum W_{shear}^T$	Cumulative total shear strain energy density

CHAPTER 1 INTRODUCTION

With the advances in the field of polymer science and technology, high strength polymers with improved load-bearing capabilities are gaining special interest from engineering communities. Following the increase in demand for better fuel efficiency in an attempt to reduce carbon footprint, while still maintaining a high level of performance, these engineering thermoplastics have gained attention from aerospace and automotive industries as a lightweight alternative to metallic materials for manufacturing structural components [1]. Due to good chemical and corrosion resistance, lubricity, ease of processing, and cost-effectiveness, polymers are also being used in various applications in oil and gas and biomedical industries [2, 3]. Particularly, the resistance of some of the polymeric materials, such as polyether ether ketone (PEEK), to in-vivo degradation and radiation sterilization, biocompatibility, and low elastic modulus make them an ideal candidate for fabricating orthopedic implants in biomedical applications [2, 4-7].

PEEK polymers are also extensively used as a matrix material of composite structures in aerospace and automotive applications. In such applications, most of the PEEK composite structures, systems, and components are typically subjected to different cyclic loading conditions including uniaxial fully-reversed constant amplitude, mean strain/stress and/or variable amplitude and multiaxial. Experimental studies have also shown that the cyclic damage process in polymer matrix composites is primarily initiated from the cracks in the matrix [8]. Hence, a complete understanding of the fatigue behavior of PEEK under different forms of

loading conditions is of practical importance and should be an inevitable part of the engineering design.

Unlike metals, the fatigue behavior of polymeric materials has not been studied extensively. Thus, the fundamental knowledge on the fatigue behavior of polymeric materials is not fully understood and is absent from the current literature. Further, the complexities of polymeric microstructures, sensitivity to loading conditions, frequency (i.e. strain rate), temperature, etc. result in the presence of completely different failure mechanisms in polymer systems compared to metals. It is also noteworthy to mention that the majority of the fatigue life models, employed to correlate fatigue data in polymers, were first developed based on the failure mechanisms observed in metals. Hence, establishing new fatigue models or adjusting the existing models based on the failure mechanisms inherent to polymeric materials is essential to accurately predict their fatigue lives.

The main goal of this study is to test the hypothesis that an energy based model, capable of incorporating cyclic deformation behavior unique to different types of fatigue loadings, would be able to correlate the fatigue data of PEEK polymer. The cyclic deformation behavior of PEEK would be significantly affected by the different types of fatigue loadings, which can be constant or variable amplitude, fully-reversed, with tensile mean strain/stress, block loading, and multiaxial in nature. Even under identical loading conditions, the cyclic deformation behavior of PEEK will be significantly affected by the cyclic strain rate as it can be directly associated with the rise in temperature of the specimen.

Under block loading test, the order of loading sequence would result in variation in the stress response, and consequently, on the fatigue resistance of the part.

Similarly, in the case of multiaxial loading, different loading paths will have different effects on the cyclic deformation behavior. Therefore, the damage induced by different types of fatigue loadings can significantly vary based on the applied loading conditions. The cumulative total strain energy density, which is measured as the sum of plastic (i.e. area of the hysteresis loop) and tensile elastic strain energy density (i.e. under the hysteresis loop) and calculated from each cycle could incorporate the damages induced by different loading types and test variables. As a result an energy based model with cumulative total strain energy density as a damage parameter could correlate the fatigue life of PEEK polymer under various types of fatigue loading conditions.

Therefore, the specific objectives of the proposed study for attending the desired final aim are:

1. To understand the cyclic deformation behavior, which would be represented by the stress responses, rise in temperature, and stress-strain hysteresis loops and will govern the fatigue life of PEEK polymer under various types of fatigue loading and test conditions.

2. To establish a fatigue life prediction model that is capable of correlating the fatigue data for PEEK (and potential other polymers) obtained from different types of fatigue loadings.

At the conclusion of the study, an energy based fatigue model with an ability to incorporate the damage induced throughout the cyclic loading process and

capable of providing a good correlation of fatigue data under different types of uniaxial as well as multiaxial fatigue loading conditions will be proposed.

An investigation into the mechanical properties of PEEK at ambient temperature under uniaxial monotonic (tension and compression) at different strain rates and uniaxial fully-reversed strain-controlled cyclic tests at strain amplitudes ranging from 0.02 mm/mm to 0.04 mm/mm at various frequencies are presented in Chapter 2. Additionally, force-controlled cyclic tests that utilized applied loads corresponding to stress responses obtained from the strain-controlled fatigue tests are also performed. Three types of fatigue models including a strain based (Coffin-Manson) model, a strain-stress based (Smith-Watson-Topper) model, and an energy based model are employed to investigate their ability to correlate the data obtained from different loading conditions.

In Chapter 3, the fatigue behavior of PEEK polymer investigated under uniaxial strain-controlled cyclic loading conditions with various mean strains (R_ε = 0, 0.20, and 0.25) are presented. Results obtained from the fractography analyses utilizing a scanning electron microscope performed on the fracture surface of PEEK specimens under tensile mean strain loading are also included in this chapter. Information such as different stages of crack growth and types of defects observed on the fracture surfaces and their effect on the fatigue resistance of PEEK are reported.

An investigation into the effect of load history and sequence on the cyclic deformation and fatigue behavior of PEEK is presented in Chapter 4. Various uniaxial strain-controlled multi-block fatigue tests are conducted to investigate the

effect of pre-loading and/or mean stress/strain on cyclic deformation and fatigue behavior of PEEK. Fatigue tests to be included are (1) fully-reversed (R_ε = -1) two-, three-, and four-block loadings with adjusted frequencies to maintain a nominal temperature rise on the specimen gage surface, (2) fully-reversed two-block loading to study the frequency effect, and (3) pulsating tension (R_ε = 0) two-block loading.

Chapter 5 includes a detailed study on the applicability of several damage models to correlate the fatigue life of PEEK under mean strain/stress and variable amplitude multi-block loadings. The employed models are assessed against experimental data for PEEK under various cyclic loading conditions, including (1) constant amplitude loading with non-zero mean strains, (2) two-block loading with zero and non-zero mean strains, and (3) three- and four-block loading with a zero mean strain. Several fatigue models, including strain based, strain-stress based, and energy based approaches are employed to correct for the effect of mean strain and stress. For the specimens subjected to block loading, different damage accumulation models are employed, including both linear and non-linear damage rules. Additionally, a Direct Cumulative Damage (DCD) approach using an energy based parameter is used to account for the load history and sequence effects on the fatigue resistance of PEEK polymer.

The fatigue behavior of PEEK is also investigated under fully-reversed strain-controlled torsion and axial-torsion multiaxial loading in Chapter 6. Combined axial-torsion multiaxial tests are conducted under proportional in-phase (IP) and non-proportional 90° out of phase (OP) loading. The stress responses under torsion, IP, and OP loadings are investigated to understand the cyclic deformation

behavior and its effect on fatigue lives of PEEK. Fatigue models based on the von-Mises equivalent strain amplitude and cumulative total strain energy density are employed to correlate the fatigue data of PEEK under torsion and multiaxial loading. Finally, major conclusions obtained from each of the chapters and future studies are summarized in Chapter 7.

CHAPTER 2 DEFORMATION AND FATIGUE BEHAVIOR OF POLYETHER ETHER KETONE (PEEK) UNDER UNIAXIAL CYCLIC LOADING

(International Journal of Fatigue, 2016, 82, 411-427)

2.1 Abstract

In this study, the fatigue behavior of a semi-crystalline thermoplastic polyether ether ketone (PEEK) is investigated. A series of tests at ambient temperature, including uniaxial monotonic (tension and compression) at different strain rates and uniaxial fully-reversed strain-controlled cyclic tests at strain amplitudes ranging from 0.02 mm/mm to 0.04 mm/mm at various frequencies, were conducted. The frequency influence on the strain-controlled fatigue lives of unfilled PEEK specimens was found to be highly dependent on the strain level. A minimal frequency effect was observed at a lower strain amplitude of 0.02 mm/mm, whereas increasing the test frequency at higher strain amplitudes resulted in longer fatigue lives. Additionally, load-controlled cyclic tests that utilized applied loads corresponding to stress responses obtained from the strain-controlled fatigue tests were performed. The cyclic behavior under the two control modes were compared and discussed. Three types of fatigue models including a strain based (Coffin-Manson) model, a strain-stress based (Smith-Watson-Topper) model, and an energy based model were employed to correlate the data in this study. Among the three fatigue models, the energy approach was found to better correlate the PEEK experimental data at various frequencies.

2.2 Introduction

Durable lightweight materials have gained increased interest over the past decades in different applications such as automotive and aerospace industries. This tendency has pushed the engineering community to further investigate the use of polymers as lightweight materials in different structural applications to enhance fuel efficiency while maintaining a high level of performance reliability. Other important advantages of polymers are low cost and their capability to be processed into a wide range of fabricated forms such as films, fibers, membranes, filters, moldings, and extrudates [9].

The material of interest in this study is a thermoplastic polyether ether ketone (PEEK). PEEK polymer exhibits excellent mechanical and electrical properties at elevated temperature as well as high toughness, low tendency to creep, and good dimensional stability over a wide range of temperatures. Due to these reasons, PEEK is an ideal candidate as a matrix in composite materials, which are widely used in various applications such as aerospace, automotive, oil and gas, and medical industries. Examples include brackets, clamps, thermal acoustic insulation and fasteners in aerospace applications, gears, bearings, brushings, shift fork wear pads in automotive applications, and as biomaterials to replace metal implant components in orthopedics and trauma [2, 3]. Experimental studies have indicated that the cyclic damage process of polymer matrix composites is initiated from the cracks in polymer matrix [8]. Since most PEEK composite structures, systems, and components in these applications are typically subjected to cyclic loadings,

understanding the fatigue behavior of PEEK is of practical importance and is an inevitable part of the engineering design.

While there has been a large amount of research performed over the past decades to gain an understanding of fatigue failure in metals, considerably less work has been focused on polymers. Unlike metals, the fatigue behavior of polymeric materials is significantly affected by their inherent viscoelastic (time- and frequency-dependent) properties [10]. At high frequencies, the softening and melting of polymers can also occur in which the fatigue failure can be accelerated through thermal softening [11].

Nonetheless, various well-established fatigue prediction models for metals have been explored to obtain their applicability to polymeric materials. The fatigue model, which was originally proposed for metallic materials (steels, aluminum, and copper) by Kujawski and Ellyin [12, 13], has been employed for the life prediction of an epoxy (thermoset polymer) under uniaxial strain-controlled tests [13] and a polyacetal (thermoplastic polymer) under uniaxial load controlled tests [14]. In [13, 14], the relationship between the fatigue life and the damage parameter ψ, which can be based on either stress, strain, or strain energy density, was expressed as:

$$\psi = \kappa\left(N_f\right)^{\gamma} + \psi_0 \tag{2.1}$$

where, ψ is the equivalent damage parameter, κ and γ are the material constants, and N_f represents the total fatigue life. The nomenclature ψ_0 in Eq. (2.1) represents the stress, strain, or strain energy density associated with the material endurance limit, based on the approach chosen. For a uniaxial fully reversed cyclic loading,

the stress, strain, and strain energy approaches can be expressed as Eqs. (2.2)-(2.4), respectively [13, 14].

$$\sigma_a = \kappa\left(N_f\right)^{\gamma} + \sigma_0 \tag{2.2}$$

$$\varepsilon_a = \kappa\left(N_f\right)^{\gamma} + \varepsilon_0 \tag{2.3}$$

$$W^T = W^P_{avg} + W^E_{avg} = \kappa\left(N_f\right)^{\gamma} + W_0 \tag{2.4}$$

where σ_a is the stress amplitude, ε_a is the strain amplitude, and W^T is the total strain energy density. In Eq. (2.4), W^P_{avg} is the average value of dissipated strain energy density and W^E_{avg} is the average value of elastic strain energy density, which are obtained for all cycles [13]. While each of the three approaches provided a good correlation between the predictions and the experimental data in [13], using the strain energy density as the damage parameter was found to be more successful in predicting fatigue life of an epoxy polymer that was subjected to the strain-controlled cyclic loading. For a polycetel polymer under load-controlled tests, however, both stress and energy approaches provided a better correlation than the strain based approach [14].

Mellott and Fatemi [15] conducted a number of cyclic tests to evaluate fatigue behavior of two thermoplastics; a polypropylene copolymer (PP) and a compounded polymer referred to as PO. Uniaxial load controlled tests were performed under various test conditions to evaluate the effects of mold flow direction, specimen thickness, mean stress, test temperature, and test frequency on fatigue life. In their study [15], the Modified Goodman, Goodman-Boller, and

Walker models that are commonly used for metallic materials were employed to correlate the experimental data of the PP and PO polymers. They reported that the Walker model with a correction factor predicted fatigue life of both thermoplastics under cyclic test with and without (ratio of minimum to maximum stress, R_ε = -1) mean stresses fairly well, while the Modified Goodman and Goodman-Boller equations were not able to provide an acceptable prediction.

Due to their unique microstructure and viscoelastic nature, the mechanical and fatigue behavior of polymers are sensitive to frequency and temperature. Therefore, fatigue models developed for metals may not be suitable for accurately predicting the fatigue life of polymers. In addition, the majority of polymer fatigue studies in the literature have been performed using a crack growth approach, assuming that the material is initially flawed [10]. Only a few researchers focused on obtaining the fatigue lifetime of polymeric materials by means of stress life (S-N) or strain life (ε-N) approaches. However, because of the limited literature available on the fatigue models of polymers, traditional strain/stress based fatigue models, which are extensively used in fatigue life modeling of metals, are employed here to analyze fatigue data for PEEK thermoplastic. The energy based method, which has been shown to be more successful in predicting fatigue life of polymers under different types of control (strain-controlled and load-controlled) [13, 14], is also used to correlate fatigue data in this work.

The objective of this study is to investigate the fatigue behavior of PEEK polymer subjected to fully-reversed uniaxial cyclic loading. The experimental details and results obtained from monotonic tensile and compression tests as well

as strain-controlled and load-controlled fatigue tests conducted at room temperature are presented. Additionally, the effect of test frequency on the cyclic deformation behavior and fatigue life is investigated. A comparison between the fatigue behavior obtained from strain-controlled and load-controlled cyclic tests is made. Three fatigue models, including a strain based model, a strain-stress based model, and an energy based model, are utilized to correlate fatigue data at different frequencies. Finally, conclusions based on experimental observations and analyses performed are made.

2.3 Material and Experimental Procedure

2.3.1 Material and Specimen

The material selected in this study was an unfilled PEEK (TECAPEEK^{TM} by Ensinger) with a melt temperature of 334ºC and a glass transition temperature (T_g) of 143ºC. PEEK rods were machined from bar stock parallel to the extrusion direction to create cylindrical specimens with uniform gage section for tensile and fatigue tests. The specimens had a gage length of 18 mm and a gage diameter of 6.35 mm in accordance with the ASTM E606-04 standard [16] as shown in Fig. 2.1. For the compression tests, cylindrical specimens with a diameter of 12.7 mm and a length of 6.35 mm following the geometric configuration in [17] were used to reduce the probability of buckling. An oil-soluble coolant agent was used during machining to minimize the generated heat. The specimens were carefully polished using sandpapers in the gage section to obtain a smooth surface finish with a minimum surface roughness of approximately 3.4 μm prior being stored in a climate controlled environment (cool dry) [18].

2.3.2 Monotonic Loading

Both monotonic tension and compression tests were performed at ambient temperature and at three strain rates of 0.001/s, 0.01/s, and 0.1/s. Two tests were conducted at each strain rate. Based on the quasi-static tension and compression tests, an average of the duplicate tests at each strain rate level was obtained and the corresponding engineering stress-strain curves were determined. For the compression tests, a moly-paste lubricant was used between the specimens and the compression plates to minimize friction as well as to prevent specimen barreling.

2.3.3 Cyclic Loading

Due to the fact that polymers have low thermal conductivity (i.e., good thermal insulator) and high damping, heat transfer through polymers generally occurs at a lower rate than those with high thermal conductivity [19]. Similar to some materials, some of the input energy in polymers is dissipated as heat during fatigue testing. This results in an initial rise in the temperature, which eventually may be stabilized as the heat transfer between the specimen and its surrounding becomes equal to the heat dissipated through the mechanical loading. In certain cases where the applied stress/strain amplitude or test frequency is sufficiently high, the input energy is continuously dissipated and causes the temperature of the material to gradually increase without reaching stabilization, leading to a thermal softening failure as opposed to a conventional fatigue failure [20]. Therefore, to ensure that failure is due to the mechanical fatigue failure, the temperature of the specimens in this study was carefully monitored throughout testing.

Fully-reversed tension-compression fatigue tests were conducted according to ASTM Standard D7791 12 [21] at ambient laboratory temperature and humidity. For the strain-controlled fatigue tests, constant strain amplitudes ranging from 0.02 mm/mm to 0.04 mm/mm were applied. A sinusoidal waveform was used and the applied frequency ranged from 0.4 Hz to 3 Hz with the intent to maintain the same nominal temperature rise ($\Delta T \approx 50^{o}C$) on the specimen surface in all tests. The temperature on the specimen surface during fatigue test was maintained below the T_g of PEEK ($T_g = 143^{o}C$). The failure criterion was defined as a 50% load drop in all strain-controlled fatigue tests. Three fatigue tests were performed for each prescribed strain amplitude. Runout tests were stopped after a minimum of 10^6 cycles. For the load-controlled fatigue tests, the applied loads were calculated from the stress responses obtained from the strain-controlled fatigue tests at a prescribed strain level. The failure criterion in load-controlled tests was defined as a significant increase in strain amplitude and subsequent complete separation of a specimen. The temperature of the specimen surface on the gage section in all tests was monitored using a laser thermometer (Optris laser thermometer LS LT) [13].

2.4 Experimental Results and Discussions

2.4.1 Monotonic Behavior

The average engineering stress-strain responses were obtained at each strain rate (0.001/s, 0.01/s, and 0.1/s) and at room temperature. The effect of strain rate on the mechanical behavior of the PEEK polymer in tension and compression is given in Figs. 2.2(a) and 2.2(b), respectively. The engineering tensile stress strain responses indicate a ductile behavior for PEEK. As can be seen from Fig. 2.2(a),

the relationship between the stress and strain is initially linear up to the yield point, followed by a period of nonlinear behavior. The specimen then exhibits a significant elongation due to necking deformation and cold drawing that is indicated by the plateau region in the stress strain curves. The necking deformation is the process in which the specimen forms a constriction (i.e., neck) due to localized plastic deformation as the applied load increases [22]. The necking may stabilize, enabling the shoulders of the neck to travel along the specimen, which is called cold drawing [22]. The continuing increase in the plastic deformation beyond the plateau region ultimately led to the strain hardening and fracture of all specimens, except for the specimens subjected to 0.1/s strain rate in which the fracture occurred without prior strain hardening. It should be noted that the yielding point referred to this study is associated with the local maximum nominal stress and the corresponding strain in the engineering stress strain curves prior to the necking deformation. The micromechanical mechanisms underlying the deformation in a ductile fashion of semi-crystalline polymers include the changes of macromolecules in both the amorphous and crystalline regions, the reorganization of the crystalline phase, and the orientation of macromolecules [23]. As the loading increases, there is an unfolding and breaking of molecular chains within the crystalline lamellae and, subsequently, the rearrangement of the lamellae in the crystalline regions to align in the direction of the applied load [24]. As a result, the lamellae is reorganized into a highly oriented fibrillar structure during yielding and the subsequent cold drawing stage [23].

In Fig. 2.2(a), the strain rate dependency can be observed especially in the nonlinear region. With an increasing testing speed (i.e., strain rate), the stress at the yield point increases and the material becomes less ductile with a corresponding decrease in the elongation to failure. As the strain rate increases from 0.001/s to 0.1/s, the tensile stress at the yield point increases by approximately 20% from 105 MPa to 125 MPa and the elongation to failure decreases from 0.27 mm/mm to 0.2 mm/mm. However, the initial tensile modulus of PEEK remains unaffected by strain rates and was measured to be 4.5 GPa, which is in good agreement with material specifications provided by the manufacturer (Ensinger). The increase of the stress at the yield point can be associated with the secondary molecular process (i.e., secondary relaxation) [25, 26]. When a polymer is subjected to a load at a high strain rate and at a temperature below its T_g, its molecular mobility suddenly decreases due to the stiffening molecular chains [25]. Hence, the material behaves in a more brittle fashion as the strain rate increases.

Similar trends were observed for PEEK responses from compression tests, where the strength moderately increases with increasing strain rate as shown in Fig. 1.2(b). The compressive stress-strain responses show a linear behavior with subsequent yielding, strain softening, and strain hardening at all strain rates except for the compression tests at 0.001/s. The absence of strain hardening in the tests performed at the lowest strain rate of 0.001/s is possibly due to the insufficient strain induced crystallization at the slow strain rate [17].

As stated previously, the stiffness in the specimens increases with an increase in the strain rate. Therefore, the strain hardening was observed in

compression tests at higher strain rates, whereas for low strain rate test at 0.001/s, strain hardening was absent. The compressive stress at the yield point increases about 26% due to the decrease in molecular mobility in polymer when the strain rate increases from 0.001/s to 0.1/s. The compressive stress at the yield point was found to be approximately 20% higher than that in tension for all strain rates, which is typically observed in polymers.

2.4.2 Cyclic Behavior

As mentioned previously, a portion of the input energy in the polymeric specimen under cyclic loading is dissipated as heat, which results in the self-heating of the test specimen. Therefore, a set of fatigue tests was conducted at selected frequencies in order to maintain the same nominal temperature rise ($\Delta T \approx 50^0 C$) on the specimen surface. These nominal temperature rise fatigue tests were conducted at 0.02, 0.025, 0.03, 0.035, and 0.04 mm/mm strain amplitudes and the corresponding data are presented in Table 2.1. The data include strain amplitude, $\frac{\Delta\varepsilon}{2}$, test frequency, stress amplitude, $\frac{\Delta\sigma}{2}$, mean stress, σ_m, reversals to failure, $2N_f$, and temperature rise on the surface of the specimen, ΔT. Although the experiments were conducted using uniaxial fully reversed strains (R_ε = -1) waveforms, there was a compressive mean stress in all tests due to the flow strength differential effect, commonly observed in ductile and semi ductile polymers [27]. However, the mean stress values in these tests were varied from test to test and did not significantly affect the fatigue life of PEEK in this study. It should also be noted that the stress

amplitude, $\frac{\Delta\sigma}{2}$, and mean stress, σ_m, presented in Table 2.1 were obtained from the half life cycle.

The cyclic behavior from the fatigue testing at a constant strain amplitude of 0.035 mm/mm and at 0.5 Hz is illustrated in Fig. 2.3. Figures 2.3(a) and 2.3(b) display the constant strain amplitude versus cycle and the corresponding stress measurement, respectively. As reported for polycarbonate (PC) [27], four distinct regions of cyclic stress behavior were also observed in this study as shown in Fig. 2.3(b). These regions are initial, transition, cyclic stability, and crack propagation and fracture. In the initial region, the stress/strain response is unchanged and the magnitude of the peak compressive stress is observed to be slightly larger than that for the tensile stress. The material then reaches the transition stage, where the peak stresses in both tension and compression decreases rapidly as cyclic softening occurs. The softening rate gradually decreases until the stress strain behavior remains constant in the cyclic stability region, which contains the majority of the fatigue cycles.

This is followed by a region of crack propagation in which the magnitude of the peak compressive stress remains essentially unchanged, while the peak tensile stress decreases until the final fracture. The latter region was found to be small for PEEK specimens in this study. The temperature of the specimen surface was monitored as shown in these figures, where it remains constant during the initial region and increases rapidly until it reaches the cyclic stability region. As previously discussed, there are dissipative losses in polymers under cyclic loading conditions that contribute to heat generation, and subsequently, an increase in

specimen temperature. The polymer chains undergo the stretching and reordering as the specimen temperature continues to increase during the transition region. When the specimen temperature is stabilized (i.e., the heat generated is equal to the heat dissipated per cycle), the molecular chains are further aligned and begin to inelastically stretch until reaching the ultimate failure [24]. Additionally, the hysteresis loops for the initial, transition, and cyclic stability regions of strain-controlled fatigue tests at a strain amplitude of 0.035 mm/mm are presented in Fig. 2.3(c). The contrast between the stress-strain responses in different regions at constant frequency is due to the cyclic softening effect, which is more pronounced at higher strain amplitudes. A considerable amount of plastic deformation and the softening effect for PEEK can be seen in Fig. 2.3(c).

A large variation in fatigue behavior under the same test conditions was also observed. For example, the fatigue life of specimens S19, S30, and S31 in Table 2.1, which were all subjected to the strain-controlled tests at a strain amplitude of 0.025 mm/mm and a frequency of 1 Hz, are 475,810, 231,964, and 179,018 reversals, respectively. As shown in Fig. 2.4 which presents the stress responses of specimens S19, S30, and S31, the peak stress of these specimens during the initial region of cyclic softening was approximately 80 MPa in tension and 90 MPa in compression before reducing to approximately 35 MPa in tension and 50 MPa in compression in the cyclic stability region. The number of reversals spent in the initial region of cyclic softening is approximately 300, 700, and 800 for specimens S19, S30, and S31, respectively. Specimen S19, which undergoes the shortest number of cycles in the initial region, exhibits the longest fatigue life when

compared to those of specimens S30 and S31. On the other hand, specimen S31, which experiences the longest number of cycles in the initial region, displays the shortest fatigue life. A similar trend was also observed in all fatigue tests conducted at each strain level. From these observations for the strain-controlled tests, one may conclude that the number of cycles spent in the initial region of cyclic behavior significantly affects the fatigue life of PEEK specimens

Additionally, it should be noted that some polymers, such as ultra-high molecular weight polyethylene, require more loading cycles to reach the cyclic steady state in compression than in tension [28]. Such observation was obtained from the experimental study of the fully-reversed (R_ε = -1) tension compression cyclic straining performed at room temperature. This may be due to the fact that the reorientation of crystalline lamellae and the stretching of non-crystalline region of certain polymers can occur in a faster rate in tension than in compression [28]. However, a comparable number of softening cycles in both tensile and compressive stresses was observed for PEEK, suggesting the morphological rearrangement during uniaxial straining occurs at a similar rate in both tension and compression for this thermoplastic.

The comparison between the stress amplitude versus the number of cycles at strain amplitudes of 0.02, 0.025, 0.03, 0.035, and 0.04 mm/mm is given in Fig. 2.5. As seen, the stress histories of all PEEK specimens exhibit the described initial, transition and cyclic stability regions. The specimens at higher strain amplitudes reach the transition region and the subsequent cyclic stability region faster than those at the lower strain amplitudes. The faster cyclic softening rate with the

increasing strain amplitude was also observed for a thermoset epoxy polymer under fully-reversed uniaxial strain-controlled cyclic loading [29]. As reported in [29], the modulus of elasticity, which was calculated from the stress-strain response at the beginning of each loading cycle, dropped faster at higher strain amplitudes. The magnitude of applied strain in fatigue loading, therefore, affects the cyclic softening rate due to modulus degradation.

To obtain the cyclic stress-strain properties of PEEK, the total strain amplitude, $\frac{\Delta\varepsilon}{2}$, at the stabilized hysteresis loops (i.e., hysteresis loop at half-life) was first separated into elastic strain component, $\frac{\Delta\varepsilon_e}{2}$, and plastic strain component, $\frac{\Delta\varepsilon_p}{2}$. The elastic strain amplitude was calculated using the Hooke's law as:

$$W^T = W^P_{avg} + W^E_{avg} = \kappa\left(N_f\right)^{\gamma} + W_0 \tag{2.5}$$

$$\frac{\Delta\varepsilon_e}{2} = \frac{\Delta\sigma}{2E} \tag{2.6}$$

where $\frac{\Delta\sigma}{2}$ is the stress amplitude and E is modulus of elasticity obtained at half-life. Hence, the plastic strain amplitude was determined by subtracting the elastic strain amplitude from the total strain amplitude as [30]:

$$\frac{\Delta\varepsilon_p}{2} = \frac{\Delta\varepsilon}{2} - \frac{\Delta\sigma}{2E} \tag{2.7}$$

The calculated plastic strain amplitude, $\frac{\Delta\varepsilon_p}{2}$, and the stress amplitude, $\frac{\Delta\sigma}{2}$, at different strain amplitudes from the strain-controlled fatigue test were plotted in log log scale resulting in a linear relationship that can be represented by a power function as [30]:

$$\frac{\Delta\sigma}{2} = K'\left(\frac{\Delta\varepsilon_p}{2}\right)^{n'} \tag{2.8}$$

where K' is the cyclic strength coefficient (the intercept) and n' is the cyclic strain hardening exponent (the slope of the fit). Using Eqs. (2.5)-(2.7), the steady-state cyclic stress strain behavior of PEEK was obtained through the Ramberg-Osgood type relationship that represents the elastic and plastic strain components as [30]:

$$\frac{\Delta\varepsilon}{2} = \frac{\Delta\varepsilon_e}{2} + \frac{\Delta\varepsilon_p}{2} = \frac{\Delta\sigma}{2E} + \left(\frac{\Delta\sigma}{2K'}\right)^{\frac{1}{n'}} \tag{2.9}$$

The summary of the cyclic stress-strain properties of PEEK, which was obtained from the strain-controlled tests with nominal temperature rise at five strain amplitudes, is given in Table 2.2. Additionally, the strain rates performed in the strain-controlled fatigue test in Table 2.1 are within the same order of magnitude as 0.1/s strain rate of the monotonic tests. Hence, the comparison between the cyclic stress-strain curve and the monotonic tensile stress-strain curve at 0.1/s strain rate was generated as displayed in Fig. 2.6. As seen, when compared to the monotonic stress-strain responses, PEEK undergoes a significant cyclic softening.

2.4.2.1 Frequency Effect on Cyclic Behavior

As previously discussed, polymers may exhibit sensitivity to the frequency of cyclic loading due to their viscoelastic nature, which is highly material dependent. It has been reported that the fatigue crack propagation decreases with increasing test frequency in polystyrene, high impact polystyrene, and polymethyl methacrylate (PMMA), while the test frequency does not have any apparent effects on fatigue resistance of some other polymers such as PC, polysulfone, nylon 66,

and polyvinylidene fluoride [10]. Therefore, the effect of loading frequency (i.e., strain rate) on the fatigue behavior of PEEK was also investigated in this study.

Fatigue lives at different frequencies for PEEK specimens are tabulated in Table 2.3 and the strain life diagram under various test frequencies is illustrated in Fig. 2.7, which includes data from Tables 2.1 and 2.3. Numbers in the figure indicate the number of data points on top of each other. At a lower strain amplitude of 0.02 mm/mm, there is a negligible effect of test frequency on the fatigue life of PEEK, as seen in Fig. 2.7. As the frequency increases from 1 Hz to 3 Hz at 0.02 mm/mm strain amplitude, the reversals to failure is observed to slightly decrease from 1,591,982, which is the average life of specimens S20 and S94 (Table 2.3), to 1,114,464, which is the average life of specimens S22, S21, and S50 (Table 2.1). It should be noted that these observations may not fully demonstrate frequency effects on PEEK fatigue behavior with a high level of confidence due to the limited number of experiments performed in this study. Nonetheless, similar effect of frequency on fatigue behavior was also evident in both PP and PO thermoplastics tested at different stress amplitudes and stress ratios [15].

First cycle and half-life hysteresis loops at 1 Hz (specimen S94 in Table 2.3) and 3 Hz (specimen S22 in Table 2.1) and the corresponding temperature increases due to self-heating are presented in Fig. 2.8. The temperature rise in specimens S94 and S22 was observed to be 17ºC and 58ºC, respectively, whereas the dissipated strain energy density calculated at half-life for specimens S94 and S22 were 0.69 MJ/m^3 and 0.61 MJ/m^3, respectively. Therefore, one may conclude that an increase in temperature of these specimens which were subjected to different

test frequencies is mostly due to an increase in the rate of heat generation (i.e., the amount of strain energy density dissipation per second). In addition, a higher cyclic plasticity at a higher loading frequency is noticeable from the evolution of the hysteresis loop as displayed in Fig. 2.8(a). At this strain amplitude, PEEK exhibits higher self-heating and a slightly shorter fatigue life when it is subjected to a faster cyclic loading rate, as seen in Fig. 2.8(b).

The frequency influence on the cyclic behavior of thermoplastics is also highly dependent on the stress/strain level [31]. Based on the experimental results, the opposite frequency effects on PEEK fatigue behavior were observed at other higher strain amplitudes (0.025, 0.03, 0.035, and 0.04 mm/mm), where an increase of test frequency leads to longer fatigue lives, as seen in Fig. 2.7. Again, more confidence in the conclusion regarding the frequency effects on PEEK fatigue behavior can be made by conducting more experiments at each test condition. An increase of the applied frequency in fatigue tests produces a subsequent increase in the strain rate during loading and unloading. Consequently, the stress response of the material tested at a higher test frequency is also expected to increase. Figure 2.9(a) presents the stress strain hysteresis loops for the first and half-life cycles obtained from the test data at a 0.03 mm/mm strain amplitude with frequencies of 0.5 Hz (specimen S28 in Table 2.3) and 1 Hz (specimen S53 in Table 2.3). Although the size of the hysteresis loop measured at half-life cycle of both specimens is not notably different, the stress amplitude of specimen S28 is larger than that of specimen S53. Again, the specimen tested at a higher test frequency generated a

higher self-heating ($\Delta T \approx 66°C$) when compared to that ($\Delta T \approx 36°C$) at a lower test frequency.

In a study of fatigue behavior of a conditioned short glass fiber reinforced polyamide 6, Bernasconi et al. [32] investigated the effects of test frequency, and dissipated strain energy on the rise in temperature at the surface of the specimen due to self-heating. Based on their experimental results, a linear relationship was obtained as [32]:

$$\Delta T = B W_{HL}^{P} f \tag{2.10}$$

where ΔT is the rise in temperature, f is the test frequency, and B is a material constant. The parameter W_{HL}^{P} is the area of the hysteresis loop at the half-life cycle, which also represents the plastic strain energy density dissipated by the specimen. The detailed description of the dissipated energy related to fatigue testing in this study will be discussed in a later section.

Using the linear relation given in Eq. (2.9), the ratio of the rise in temperature to test frequency, $\Delta T/f$, of all strain-controlled fatigue tests reported in both Tables 2.1 and 2.3 was plotted against the plastic strain energy density at the half-life cycle, W_{HL}^{P}, as displayed in Fig. 2.10. The correlation in Fig. 2.10 indicates the combined effects of both test frequency with subsequent temperature rise on the dissipated strain energy density. In general trend, for all strain amplitudes, the increase in test frequency resulted in a higher self-heating in the PEEK specimens. As frequency increases, the heat generated in the specimen due to dissipated strain energy cannot transfer to the surrounding because of shorter time period as well as low thermal conductivity of polymers, which results to the

higher self-heating in the specimen [33]. As observed from Fig 2.10, a good correlation between frequency, temperature rise on the specimen, and strain energy density is obtained with some scatter in the test data at lower frequencies (0.25 Hz and 0.5 Hz).

2.4.2.2 Test Control Effect on Cyclic Behavior

For most metals and some polymers, incremental step deformation tests are generally conducted to obtain the cyclic stress and strain behavior [15]. From these results, the stress life fatigue properties can be used to determine the strain life fatigue properties of a given material. In this study, a series of load-controlled tests were performed to investigate the cyclic deformation and fatigue life of PEEK, which were then compared to those obtained under strain-controlled loading. The applied loads corresponding to stress responses obtained from the strain-controlled tests were utilized to conduct the load-controlled cyclic tests.

The summary of the load-controlled test results with R_σ =-1 is given in Table 2.4. The applied loads for specimens S61, S63, S64, S65, and S66 in Table 2.4 were calculated based on the stress responses obtained from the uniaxial fully-reversed strain-controlled tests at the strain amplitude of 0.03 mm/mm and at a frequency of 0.75 Hz in Table 2.1. Under strain-controlled condition, the fatigue lives ranged from 124,030 to 208,896 reversals with temperature rise ranging from 48°C to 55°C, as presented in Table 2.1. The amplitudes of the stress response are approximately 100 MPa, 65 MPa (average value), and 45 MPa in the initial, transition, and cyclic stability regions of the corresponding strain-controlled tests, respectively. The load-controlled test on specimen S61 was first performed at 0.75

Hz using the applied load corresponding to the tensile stress response during the cyclic stability region (45 MPa). However, the measured strain amplitude was observed to be significantly lower than 0.03 mm/mm with only a 5°C temperature increase. As a result, specimen S61 was able to withstand the prescribed cyclic loading beyond 2,000,000 reversals before the test was terminated.

To account for the stress responses in the three regions of cyclic behavior under the strain-controlled mode, the incremental step fatigue tests under load-controlled condition were performed. Specimen S63 was tested at 0.75 Hz using the following loading profile; 100 MPa for 0 to 80 reversals, 65 MPa for 81 to 1,000 reversals, and 45 MPa for the remaining cycles. Figure 2.11 illustrates the applied stress, strain responses, and the hysteresis loops for specimen S63. The strain responses are also observed to be much lower than 0.03 mm/mm with a temperature rise of only 4°C. Additionally, the evolution of the stress-strain hysteresis loops of specimen S63 presented in Fig. 2.11(c) displays negligible plastic deformation in all the initial, transition, and cyclic stability regions. The test was finally terminated after 2,000,000 reversals.

Additional load-controlled tests were performed using a similar loading profile at reduced test frequencies of 0.4 Hz (specimens S64 and S65) and 0.6 Hz (specimen S66). The rise in temperature, ΔT, of specimens S64-S66 was stabilized at approximately 6°C. However, at a test frequency of 0.4 Hz, both specimens S64 and S65 failed due to cyclic necking at 306 and 172 reversals, respectively. On the other hand, the evolution of the stress-strain hysteresis loops for specimen S66 did not reveal significant plastic deformation, and therefore, the fatigue test was

terminated at 52,810 reversals. Unlike the thermal fatigue failure, which is attributed to the steady increase of self-heating in the material, the cyclic necking described in this study is referred to the failure due to a significant increase in both strain response and surface temperature in the last cycle.

Furthermore, tests were conducted at stress amplitudes ranging from 70 MPa to 80 MPa at various test frequencies. However, all of the specimens (S68-S72) cycled under these load-controlled test conditions did not exhibit a mechanical fatigue failure but rather a failure due to cyclic necking. Figure 2.12 presents the applied stress and strain responses of specimen S68 that was subjected to constant stress amplitude of 80 MPa at 0.5 Hz. Relatively steady strain responses of 0.02 mm/mm were observed throughout the life prior to cyclic necking, where the strain responses abruptly increased to 0.07 mm/mm. Additionally, the stress-strain hysteresis curve at half-life cycle in Fig. 2.12(c) does not display an apparent plastic deformation. An image of specimen S68 that failed due to cyclic necking is shown in Fig. 2.12(d).

It can be concluded from these uniaxial fully-reversed fatigue test results that fatigue behavior of PEEK, such as stress/strain responses, temperature, fatigue life, and failure mode, differs significantly depending on the test control mode (strain-controlled or load-controlled). With given applied stresses corresponding to those attained from the strain-controlled tests, the strain responses under the load-controlled tests are substantially smaller than expected as illustrated in Figs. 2.11 and 2.12. In Table 2.4, it can be seen that the differences between the fatigue lives of specimens S63 S65 with the identical applied load corresponding to the stress

responses obtained from the strain-controlled tests at the strain amplitude of 0.03 mm/mm may be attributed to the test frequency. It is evident that, under load-controlled cyclic tests, an increase in frequency leads to somewhat smaller strain amplitude responses, which subsequently is reflected in a longer fatigue life. However, at a sufficiently high applied load and frequency, PEEK material can exhibit a cyclic necking failure under cyclic loading despite the small increase in the specimen temperature due to the hysteresis heating (i.e., specimens S64 and S65). The similar effect of test frequency on fatigue behavior was also observed at higher stress amplitudes of 80 MPa in specimens S68 to S70 and 70 MPa in specimens S71 and S72. Furthermore, at these stress amplitudes, the temperature rise on the specimens' surfaces were comparatively higher than those of specimens S63-S65. The self-heating in these specimens under load-controlled mode were also observed to increase as test frequency increased.

2.4.3 Fatigue Models

2.4.3.1 Strain Based Approach

The fatigue test data in total strain amplitude, $\frac{\Delta\varepsilon}{2}$, versus reversals to failure, $2N_f$, were used to develop the strain-life fatigue curves. The total strain amplitude can be separated into elastic strain component, $\frac{\Delta\varepsilon_e}{2}$, and plastic strain component, $\frac{\Delta\varepsilon_p}{2}$, from the stabilized hysteresis loops (i.e., hysteresis loop at half-life). These components were plotted (log-log) against the reversals to failure, $2N_f$, in which the

linear relationship between the elastic strain amplitude, $\frac{\Delta\varepsilon_e}{2}$, and fatigue life was obtained using the following equation [30]:

$$\frac{\Delta\varepsilon_e}{2} = \frac{\sigma_f'}{E}(2N_f)^b \tag{2.11}$$

where $\sigma_f'$and b are the fatigue strength coefficient and fatigue strength exponent (slope of the elastic strain-life line), respectively. These parameters were determined by performing a fit using a linear least-squares method, following ASTM standard E739 [34]. Similarly, the plastic strain amplitude, $\frac{\Delta\varepsilon_p}{2}$, as a function of reversals to failure, $2N_f$, was obtained as follow [30]:

$$\frac{\Delta\varepsilon_p}{2} = \varepsilon_f'(2N_f)^c \tag{2.12}$$

where ε_f' is the fatigue ductility coefficient and c is the fatigue ductility exponent (slope of the plastic stain-life line). Therefore, by combining Eqs. (2.10) and (2.11), the total strain amplitude was obtained from the Coffin-Manson relationship as [30]:

$$\frac{\Delta\varepsilon}{2} = \frac{\Delta\varepsilon_e}{2} + \frac{\Delta\varepsilon_p}{2} = \frac{\sigma_f'}{E}(2N_f)^b + \varepsilon_f'(2N_f)^c \tag{2.13}$$

The fatigue parameters in Eqs. (2.10)-(2.12) were calculated from the strain-controlled test at nominal temperature rise (i.e., data in Table 2.1) and presented in Table 2.2. The plots of the elastic, plastic, and total strain amplitude versus reversals to failure for all strain-controlled fatigue tests at nominal temperature and the Coffin-Manson fits are presented in Fig. 2.13(a). As seen, plastic strain amplitudes under uniaxial fully-reversed fatigue tests are greater than

elastic strain amplitudes at all strain levels in this study; thus, the transition fatigue life $2N_t$, which is the number of reversals at the intersection between the elastic and plastic strain lines, is not observed. This observation for PEEK is in contrast to other polymeric materials such as a neat polypropylene and polypropylene elastomer blend, as reported by Mellot et al. [15]. Both materials in [15] were subjected to the fully-reversed load-controlled fatigue tests and the relationships between the strain amplitude and fatigue life were determined from the incremental step cyclic deformation tests. Based on their results, the transient life, $2N_t$, was calculated to be 281 and 3,026 reversals for polypropylene and polypropylene elastomer blend, respectively. For PEEK polymer, the strain amplitude of the fatigue tests in Table 2.1 is primarily governed by the plastic strain as illustrated in the stabilized stress strain hysteresis loops in Fig. 2.13(b), which were obtained from specimens S21, S19, S46, S42, and S24. The size of the hysteresis loop and subsequent plastic strain were observed to be larger with increasing in strain amplitude. The elastic strain amplitude values, which were calculated from the stress range at half-life cycle and the modulus of elasticity, are comparatively similar for all tests as depicted in Figs. 2.13(a) and 2.13(b). Additionally, the predicted fatigue lives from the Coffin-Manson approach were compared to those obtained experimentally from both Tables 2.1 and 2.3 (with and without the frequency effects) as shown in Fig. 2.13(c). In this figure, approximately 77% of total data and 66% of data from the frequency effect tests (i.e., Table 2.3) are within scatter bands of two. The R^2 value of all observed and predicted fatigue lives using the Coffin-Manson approach was calculated to be 0.83. The data that fall outside

of the scatter band are primarily the strain-controlled test with varied frequency (i.e., data reported in Table 2.3).

The poor correlation between the Coffin-Manson fits and the experimental data is possibly due to the significant cyclic softening behavior in PEEK. While the calculated plastic strain values used in the Coffin-Manson expression were obtained from stabilized hysteresis loops that essentially represents the deformation in the cyclic stability region, the cyclic deformation during the initial and transient regions may also contribute to the overall fatigue behavior and life, as previously discussed. Consequently, the elastic and plastic strains obtained from the hysteresis loops at earlier stages of cyclic loading should be incorporated into fatigue analysis. Nonetheless, difficulties may arise when attempting to accurately calculate the elastic and plastic strain components due to the propeller like shape of the stress strain hysteresis loop in the initial cycles, as shown in Fig. 2.3(c).

1.4.3.2 Strain-Stress Based Approach

The experimentally obtained data to study the frequency effect in Table 2.3 revealed that the test frequency significantly affects the stress response as well as the evolution of the stress strain hysteresis loop for all tests at different strain amplitudes. Therefore, using a damage parameter that considers the effects of both stress and strain terms, such as the Smith Watson Topper (SWT) parameter, may improve the fatigue life prediction of PEEK. The SWT damage parameter was originally developed to account for both stress and strain amplitudes as well as mean stress/strain effects. The SWT parameter, which is a product of strain

amplitude, ε_a (or $\frac{\Delta\varepsilon}{2}$), and maximum tensile stress, σ_{max}, has been used extensively and validated with various experimental results in both low and high cycle fatigue for metals [35]. Additionally, the SWT damage parameter has been found to estimate fatigue damage for materials with strong deformation history effects more accurately than the conventional strain-life approach [36].

For the uniaxial fully-reversed fatigue tests reported in Tables 2.1 and 2.3, the SWT parameter was obtained by multiplying the strain amplitude and the maximum stress, σ_{max}. This parameter can then be related to fatigue life as [37]:

$$\varepsilon_a \sigma_{max} = \frac{\left(\sigma_f'\right)^2}{E}(2N_f)^{2b} + \sigma_f'\varepsilon_f' E(2N_f)^{b+c} \tag{2.14}$$

where

$$\sigma_{max} = \sigma_m + \sigma_a \tag{2.15}$$

In Eq. (2.15), σ_m and σ_a are mean stress and stress amplitude, respectively. The correlation of SWT parameter, $\varepsilon_a \sigma_{max}$, and the reversals to failure for the PEEK data under strain-controlled tests with nominal temperature rise (Table 2.1) is presented in Fig. 2.14(a) and the predicted lives using Eq. (2.14) are plotted against the experimentally observed fatigue lives for all the strain-controlled fatigue experiments (Tables 2.1 and 2.3) in Fig. 2.14(b). The $\varepsilon_a \sigma_{max}$ values obtained at each strain amplitude were observed to follow the linear relationship with the fatigue life of PEEK in a log-log plot especially at strain amplitudes of 0.02 mm/mm to 0.035 mm/mm, as seen in Fig. 2.14(a). Under the experimental condition where the nominal temperature rise in the specimens was fixed (i.e. Table

2.1), 59% of fatigue life predictions using the SWT parameter fall within scatter bands of two from experimentally observed fatigue lives, as seen in Fig. 2.14(b). However, a poor correlation of fatigue lives using the SWT approach was observed where only 33% of the frequency effect data (from Table 2.3) are within scatter bands of two. The R^2 value of all observed and predicted fatigue lives using the SWT approach was determined to be 0.77. From the results, it can be seen that the Coffin-Manson equation provides a better correlation between the predictive and experimental fatigue lives when compared to the SWT approach.

Since the SWT parameter represents the combined effects that are associated with only the product of two extreme values (strain amplitude and maximum tensile stress), the model does not necessary capture the shape and size of the hysteresis loop that changes throughout the cyclic loading for PEEK polymer. Additionally, because the shape of the hysteresis loop differs with test frequency even for the same strain amplitudes, the SWT parameter cannot accurately correlate the experimental data generated with various frequencies. Nonetheless, in an attempt to incorporate the cyclic softening effects into the SWT fatigue model, the cumulative SWT parameter (i.e., summation of $\varepsilon_a \sigma_{max}$ values for all cycles) was determined for all strain-controlled tests and correlated to the observed fatigue lives. However, no significant improvement was observed using this approach.

2.4.3.3 Energy Based Approach

Although the SWT parameter that includes both stress and strain terms was considered for PEEK fatigue life prediction, it was not able to provide a good correlation to the experimental data since it only captures the frequency effect based

on only the extreme stress and strain values on the hysteresis loop. As seen in Figs. 2.8(a) and 2.9(a), the shape and size of the hysteresis loop that changes throughout cyclic loading is also significantly affected by the test frequency; therefore, the energy based approach that can capture the shape and size of the hysteresis loop may provide better correlations.

The energy based approach for fatigue life estimation is derived based on the strain energy imposed by the external loading that is further separated into elastic (recoverable) and plastic (irrecoverable) parts. The plastic strain energy density, W^P, dissipated in each cycle of loading, can be defined as the area of hysteresis loop, where the elastic strain energy per unit volume associated with the tensile stress, W^E, can be represented by the positive area under the hysteresis loop.

In the energy based approach, the dissipated energy associated with the irrecoverable plastic deformation is assumed to be proportional to the damage that occurs in each cycle during fatigue process [38]. However, for the life of a material close to its fatigue limit, the corresponding dissipated energy density value becomes very small and is difficult to measure. Therefore, the total strain energy approach was introduced for fully-reversed fatigue tests and the expression for the total strain energy density, W^T, was proposed by including both plastic and elastic strain energy densities as [38]:

$$W^T = W^P + W^E \tag{2.16}$$

In this study, the plastic strain energy density was determined by calculating the area of the hysteresis loop by integration for each cycle, while the elastic strain

energy density was calculated by obtaining the positive area under the hysteresis loop.

Since the majority of PEEK fatigue lives is spent in the cyclic stability region, as illustrated in Fig. 2.3, the plastic and elastic strain energy densities obtained at the half-life cycle in the cyclic stability region were determined and listed in Tables 2.1 and 2.3. The values of the plastic strain energy density, W_{HL}^{P}, and the total strain energy density, W_{HL}^{T},(i.e., sum of both plastic and elastic energy densities) calculated at the half-life cycle were plotted against the reversal to failure for the PEEK data under strain-controlled test with nominal temperature rise (i.e., Table 2.1), as shown in Fig. 2.15(a) and Fig. 2.16(a), respectively. Additionally, the predicted fatigue lives using the plastic and total strain energy densities at the half-life cycle were determined for all strain-controlled fatigue tests (i.e., Tables 2.1 and 2.3) and compared to the experimentally observed fatigue lives as illustrated in Figs. 2.15(b) and 2.16(b), respectively. As seen in these figures, about 77% of all the data and 75% of frequency effect test data are within scatter bands of two. Both R^2 values of all observed and predicted fatigue lives with frequency effect using the plastic and total strain energy densities at the half-life cycle were determined to be 0.87. Due to the minimal differences between Figs. 2.15 and 2.16, one may suggest that the elastic strain energy density has a very small effect on the fatigue behavior of PEEK at the cyclic stability region. A significant plastic strain is typically exists in the hysteresis stress-strain response of PEEK even for the smaller strain amplitude (0.02 mm/mm) tests, as can be seen in Fig. 2.8(a), which

might be the reason that elastic strain energy density does not have a significant effect on the fatigue behavior of PEEK.

In Fig. 2.17(a), the cumulative plastic strain energy density was plotted against the reversals to failure for the strain-controlled experiments reported in Table 2.1. The direct proportionality is observed in this figure. In a study performed by Halford [39], the cumulative plastic energy strain density required for the fatigue failure obtained from more than 1,400 fatigue tests of various types of metals was presented. The results showed that the cumulative plastic strain energy increases with fatigue life irrespective to cycling conditions, test temperature, or initial state of the material [39]. Similar results were observed in this study for PEEK, for which the cumulative plastic strain energy density increased with the increase in fatigue life, as can be seen in Fig. 2.17(a). Figure 2.17(b) displays scatter bands of two for correlation between the predicted fatigue lives using the cumulative plastic strain energy density and the experimentally observed fatigue lives for all the strain-controlled test (Tables 2.1 and 2.3).

Good agreement (R^2 = 0.97) was observed as all of the experimental data with nominal temperature rise and frequency effects are within the scatter band of two as compared to 77%, 59%, and 77% of those using the Coffin-Manson model, SWT damage parameter, and energy based approach using the plastic strain energy density at the half-life cycle, respectively. However, it should be noted that, the transient energy based approach considers sum of all the plastic strain energy density throughout the fatigue life of PEEK. Therefore, the reversals to failure data was embedded in the calculation of the cumulative plastic strain energy density,

which may have, to some degree, contributed to the improved fatigue life predictions. It should be also mentioned that a difficulty in using energy based approaches for fatigue life predictions is requiring a constitutive stress-strain model to estimate the hysteresis stress-strain loop. Some further investigations to calibrate/develop a constitutive model capable of predicting cyclic stress-strain behavior of PEEK at different stages of initial, transition and cyclic stability then may be a necessity.

2.5 Conclusions

In this study, an unfilled PEEK thermoplastic was subjected to a series of experiments including uniaxial monotonic and cyclic tests. Three sets of uniaxial fully-reversed cyclic tests under various control modes were performed. These were (1) strain-controlled tests at five strain amplitudes with adjusted test frequencies to maintain the same nominal temperature on the specimen surface in all tests, (2) strain-controlled tests at various test frequencies to study the effects of loading frequency on cyclic deformation, fatigue life, and the change in temperature, and (3) load-controlled tests with the applied loads corresponding to the stress responses obtained from the strain-controlled tests. Three fatigue models; a strain based (Coffin Manson) model, a strain-stress based (Smith Watson Topper) model, and an energy based model, were employed to predict the fatigue life of PEEK under the strain-controlled tests at various loading frequencies. Based on the effort performed in this study, the following conclusions may be drawn:

1. PEEK exhibited significant cyclic softening in both tension and compression when subjected to the uniaxial strain-controlled cyclic loading. Four distinct regions of cyclic stress behavior were identified. These included initial, transition, cyclic stability, and region of crack propagation. It was observed that the magnitude of the stress responses and the number of cycles in the initial region significantly affected the fatigue lifetime. The specimen that experienced the longer number of cycles in the initial region exhibited the shorter fatigue life when compared to those tested at the same strain amplitude and test frequency.

2. The cyclic softening effect of PEEK was more pronounced under cyclic loading at higher strain amplitudes. By keeping the same nominal temperature on the specimen surface in all tests, the specimens at higher strain amplitudes reached the transition region and the subsequent cyclic stability region faster than those tested at the lower strain amplitudes. The faster cyclic softening rate with the increasing strain amplitude was due to the modulus degradation.

3. The frequency effect on the cyclic behavior of PEEK is highly dependent on the strain amplitude level. Based on the test results, under fully-reversed strain-controlled condition, a minimal frequency effect was observed at a lower strain amplitude of 0.02 mm/mm. At higher strain amplitudes, increasing the test frequency resulted in longer fatigue lives. It should be, however, noted that the experimental data obtained from this study may not demonstrate the effects of test frequency on PEEK fatigue behavior with a high level of confidence due to the limited number of experiments conducted. Further studies are required to correlate frequency, temperature rise on the specimen, and strain energy density with the fatigue life.

4. Unlike most metals, the differences between the fatigue behavior of PEEK under uniaxial fully-reversed load-controlled and strain-controlled cyclic tests were significant. With a given applied stress corresponding to those attained from the strain-controlled tests, the strain responses under the load-controlled tests were substantially smaller than expected. It was evident that, under load-controlled cyclic tests, an increase in frequency led to smaller strain responses, which subsequently reflected a longer fatigue life.

5. Mechanical fatigue failure was not observed in all of the fully-reversed load-controlled tests. Instead, at a sufficiently high applied load and frequency, failure occurred due to cyclic necking that was similar to failure in monotonic testing.

6. Based on the experimental results in this study, it was concluded that the fatigue behavior of PEEK obtained under strain-controlled mode could not be directly related to its behavior under load-controlled fatigue loading. Therefore, it was suggested to evaluate fatigue behavior of PEEK components or structures under the operative control modes for the given application.

7. For the strain based fatigue analysis in this study, values for plastic strain were obtained only from the steady state stage, which represents deformation in cyclically stabilized region. However, the initial and transition regions were found to affect the overall fatigue behavior and total life for PEEK. Therefore, the Coffin-Mansion model may provide a better correlation of fatigue life in polymers if the deformation induced during initial and transition stages is incorporated.

8. Since the Smith-Watson-Topper (SWT) damage parameter, $\varepsilon_a \sigma_{max}$, is associated with only the product of two absolute values (strain amplitude and maximum tensile stress), this fatigue parameter did not necessary capture the shape of the hysteresis loop that changed throughout the cyclic loading for PEEK polymer. The shape of the hysteresis loop also differed with test frequency even for the same strain amplitude. Therefore, the SWT parameter could not well correlate the fatigue data in this study.

9. The transient energy based approach that uses the cumulative plastic strain energy density as the damage parameter provided a better correlation with the PEEK experimental data under strain-controlled mode when compared to the energy based approaches using the plastic and total strain energy densities at the half-life cycle. This is due to the fact that unlike Coffin-Manson and SWT models, the cumulative plastic strain energy density was able to capture the shape of the hysteresis loop for all the cycles including initial, transition, and the cyclic stability regions.

10. Although the energy based approaches were shown to provide better fatigue life predictions than Coffin Manson and SWT models for PEEK, one of the disadvantages of energy based approaches is the fact that they require knowing the cyclic stress-strain behavior of the material. A constitutive cyclic stress-strain model for PEEK is, therefore, required to estimate the hysteresis stress-strain loops at different stages of initial, transition and cyclic stability.

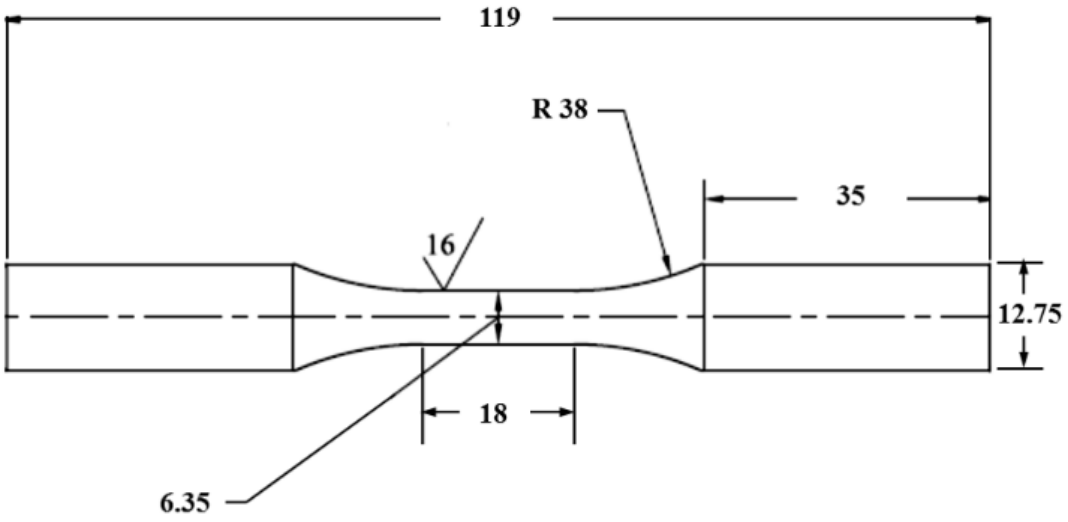

Figure 2.1 Specimen geometry and dimensions for uniaxial monotonic tensile and fatigue tests (dimensions in mm).

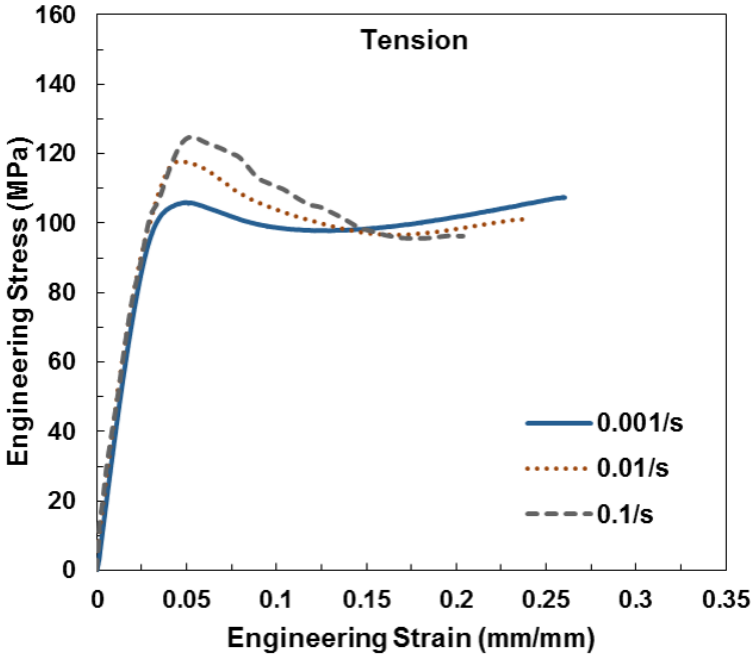

(a)

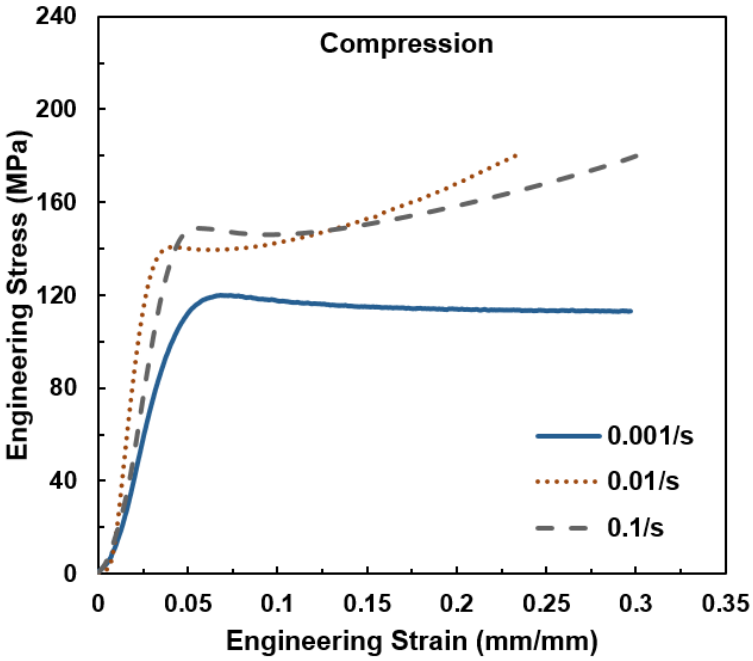

(b)

Figure 2.2 Monotonic stress-strain responses of PEEK in (a) tension and (b) compression with different strain rates and at room temperature.

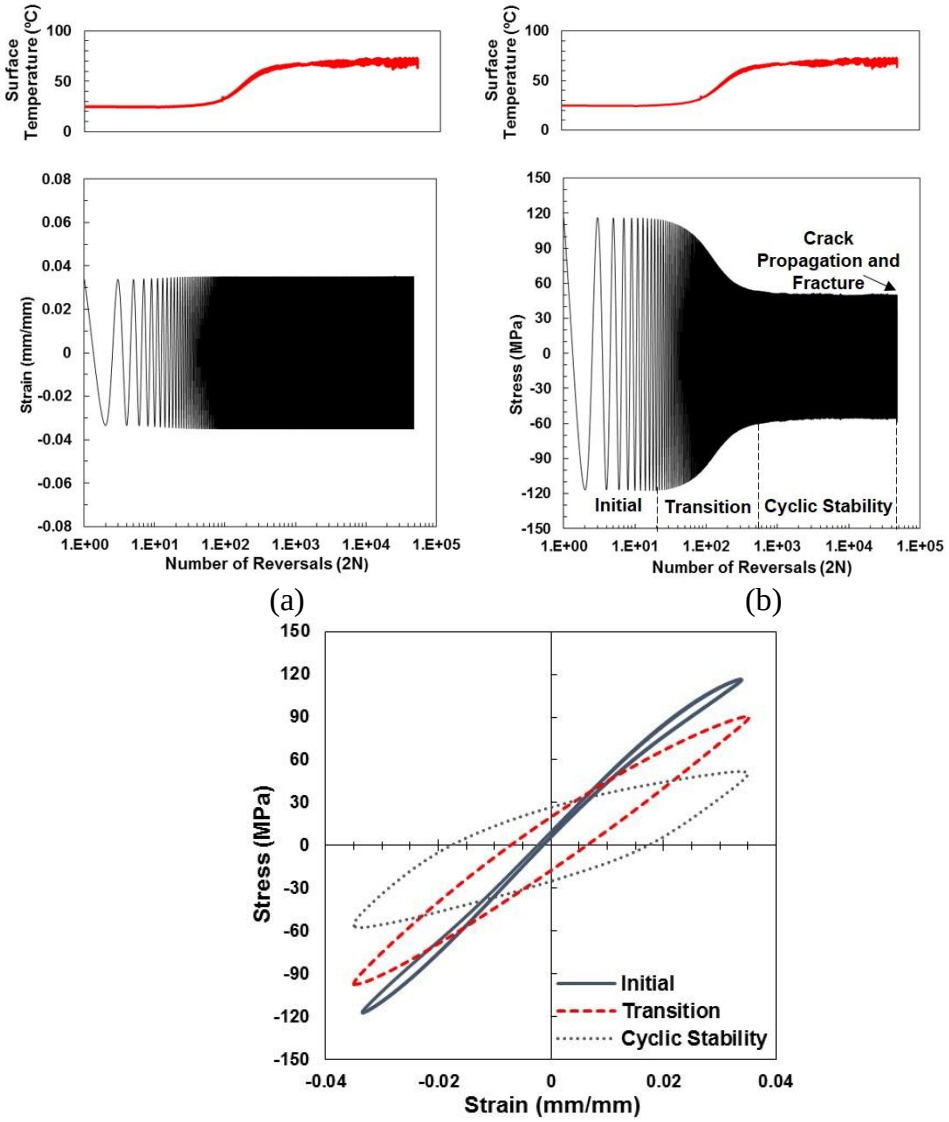

Figure 2.3 Loading history of strain-controlled fatigue tests of PEEK at ε_a = 0.035 mm/mm and 0.5 Hz showing the (a) strain and (b) stress response versus number of reversals (2*N*) and (c) hysteresis loops at different stages of cyclic behavior at room temperature.

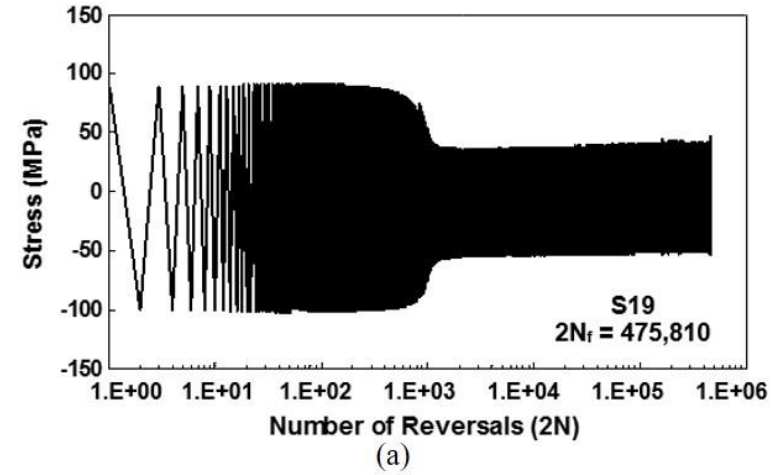

(a)

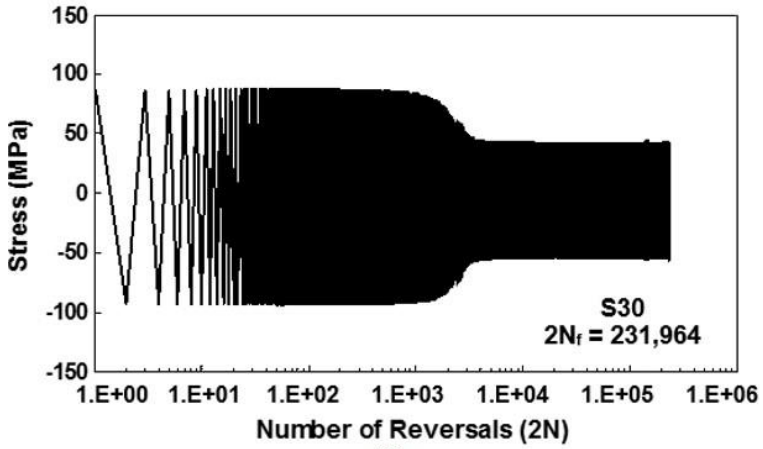

(b)

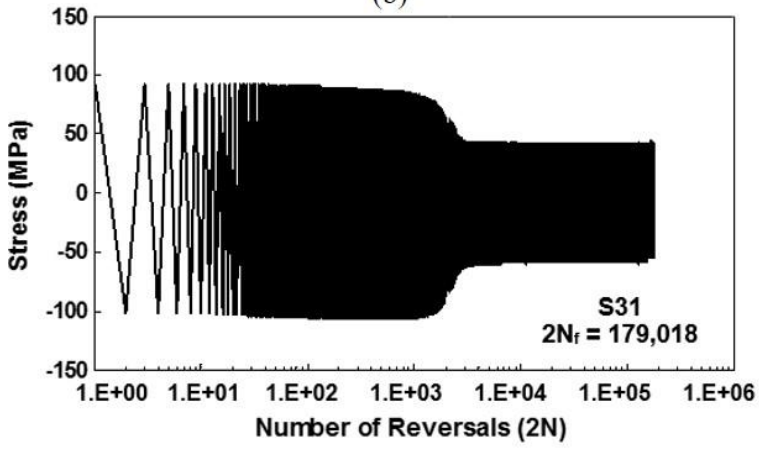

(c)

Figure 2.4 PEEK stress responses of strain-controlled fatigue tests at 0.025 mm/mm strain amplitude and frequency of 1 Hz of specimens (a) S19, (b) S30, and (c) S31 in Table 2.1.

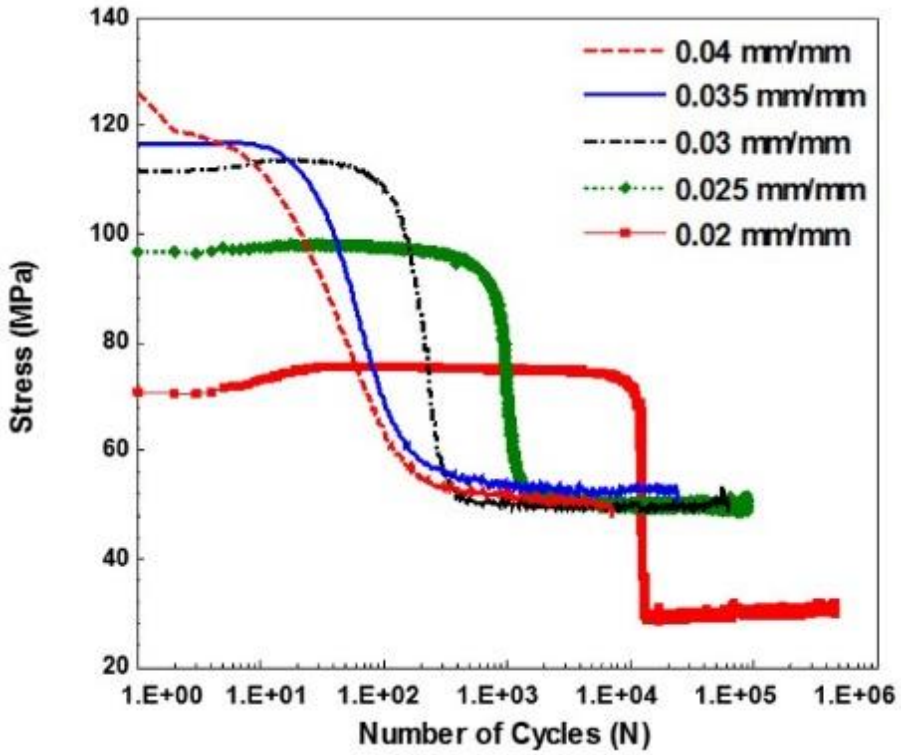

Figure 2.5 Stress amplitude versus number of cycles at different applied strain amplitudes for PEEK fatigue specimens from Table 2.1.

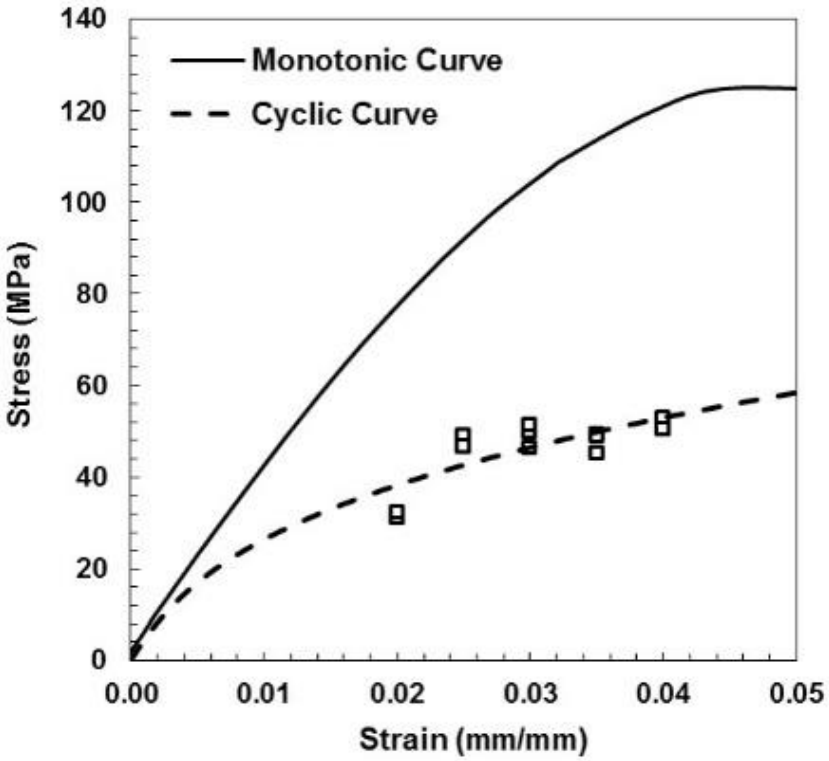

Figure 2.6 Cyclic and monotonic tension stress strain curves for PEEK. The monotonic tensile test data were obtained from the test conducted at 0.1/s strain rate.

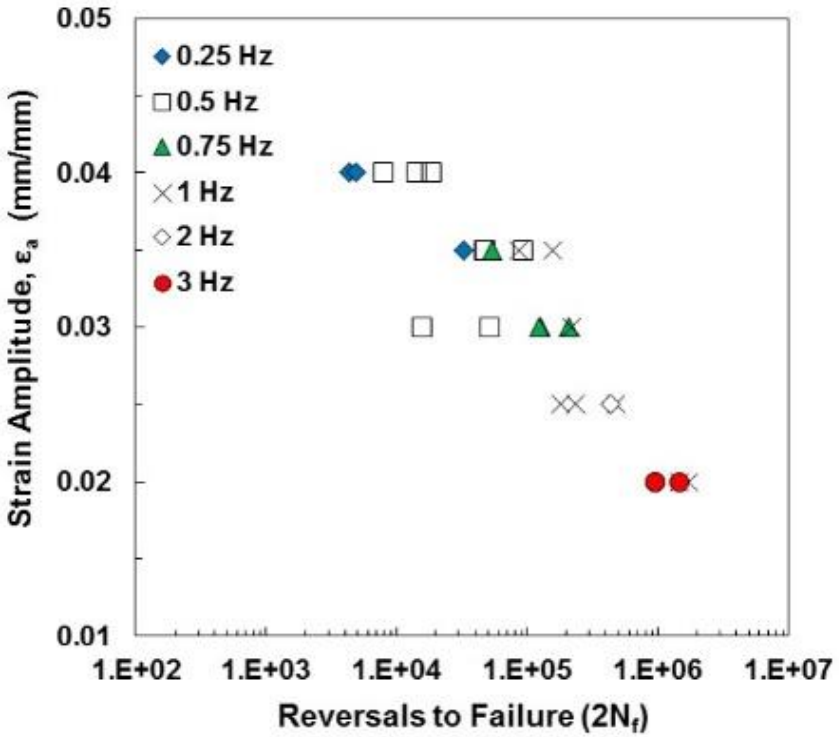

Figure 2.7 Strain-life fatigue behavior of PEEK specimens tested at room temperature and various test frequencies. Numbers in the figure indicate the number of data points on top of each other.

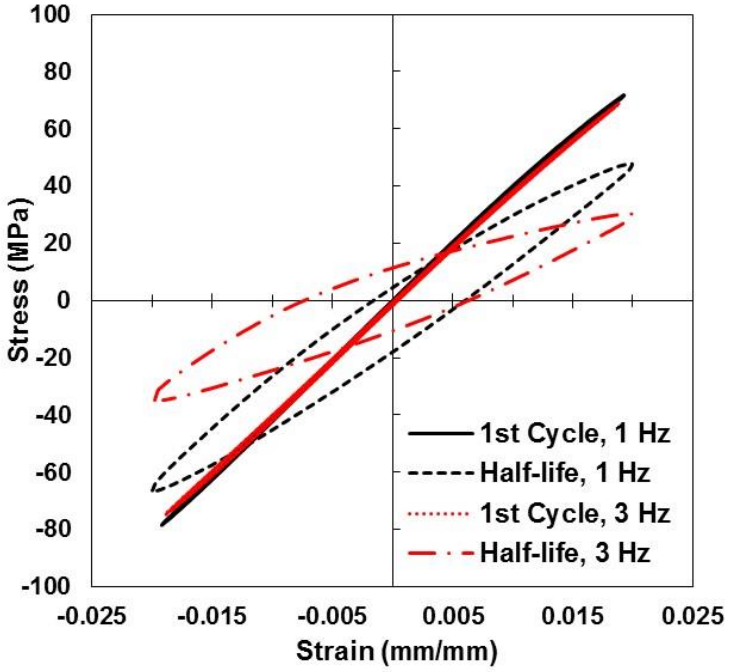

(a)

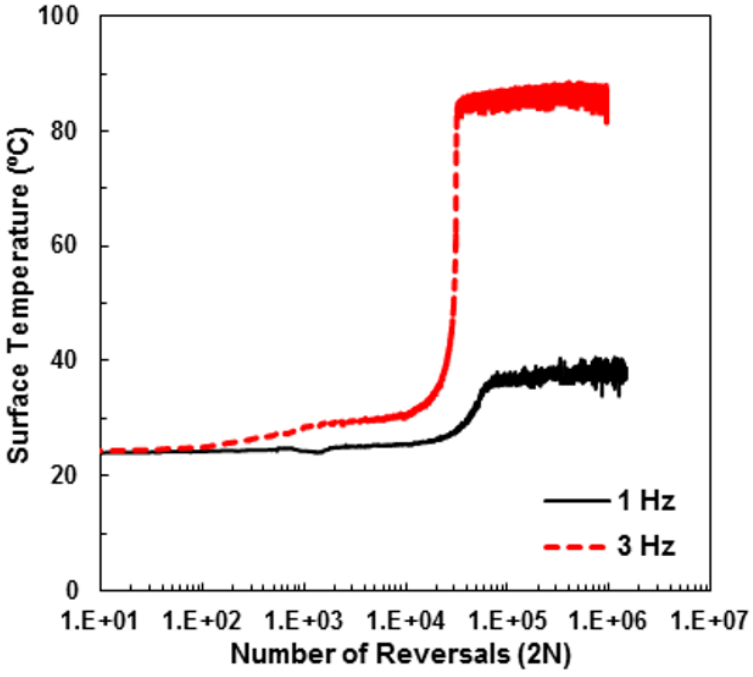

(b)

Figure 2.8 (a) First cycle and half-life cycle hysteresis loops for PEEK tested at 1 Hz (specimen S94) and 3 Hz (specimen S22) with applied strain amplitude of 0.02 mm/mm at room temperature and (b) corresponding temperature increases due to self-heating.

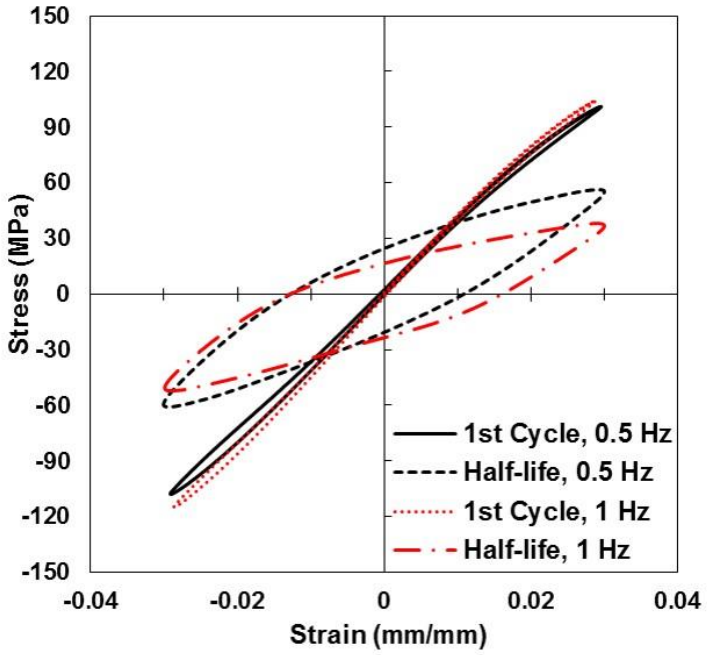

(a)

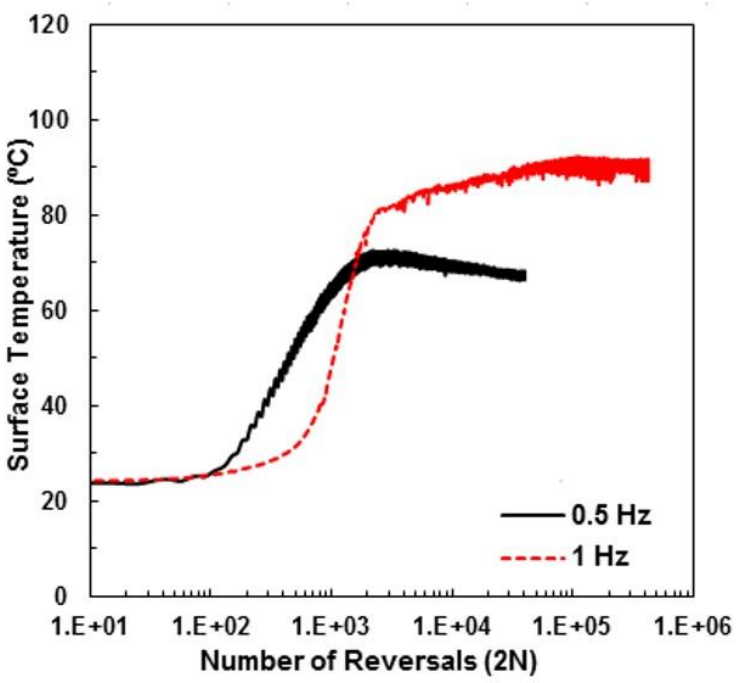

(b)

Figure 2.9 (a) First cycle and half-life cycle hysteresis loops for PEEK tested at 0.5 Hz (specimen S28) and 1 Hz (specimen S53) with applied strain amplitude of 0.03 mm/mm at room temperature and (b) corresponding temperature increases due to self-heating.

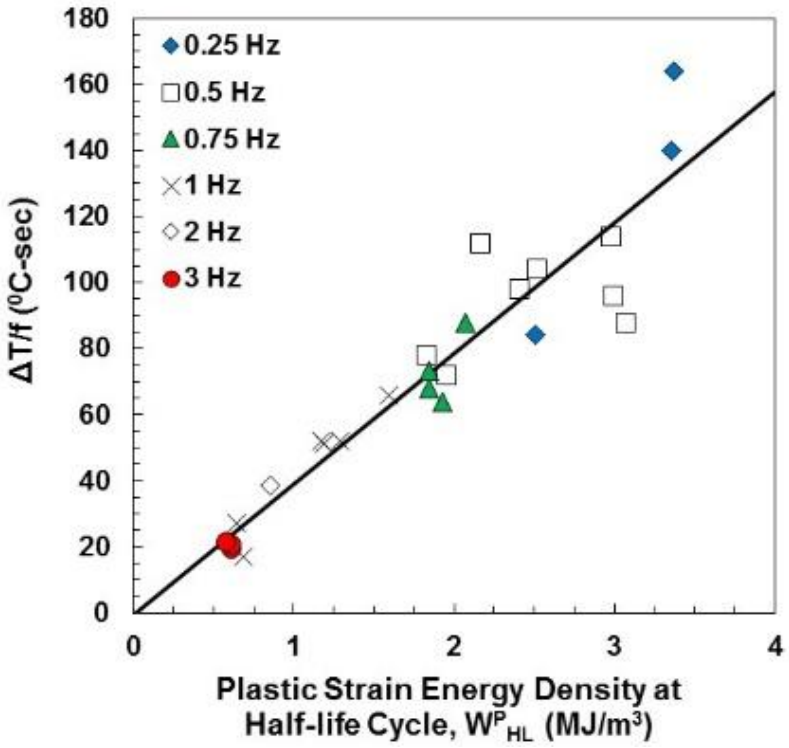

Figure 2.10 The ratio of the rise in temperature to test frequency, $\Delta T/f$, of all strain-controlled fatigue tests versus the plastic strain energy density at half-life (cyclic stability region), W_{HL}^{P}.

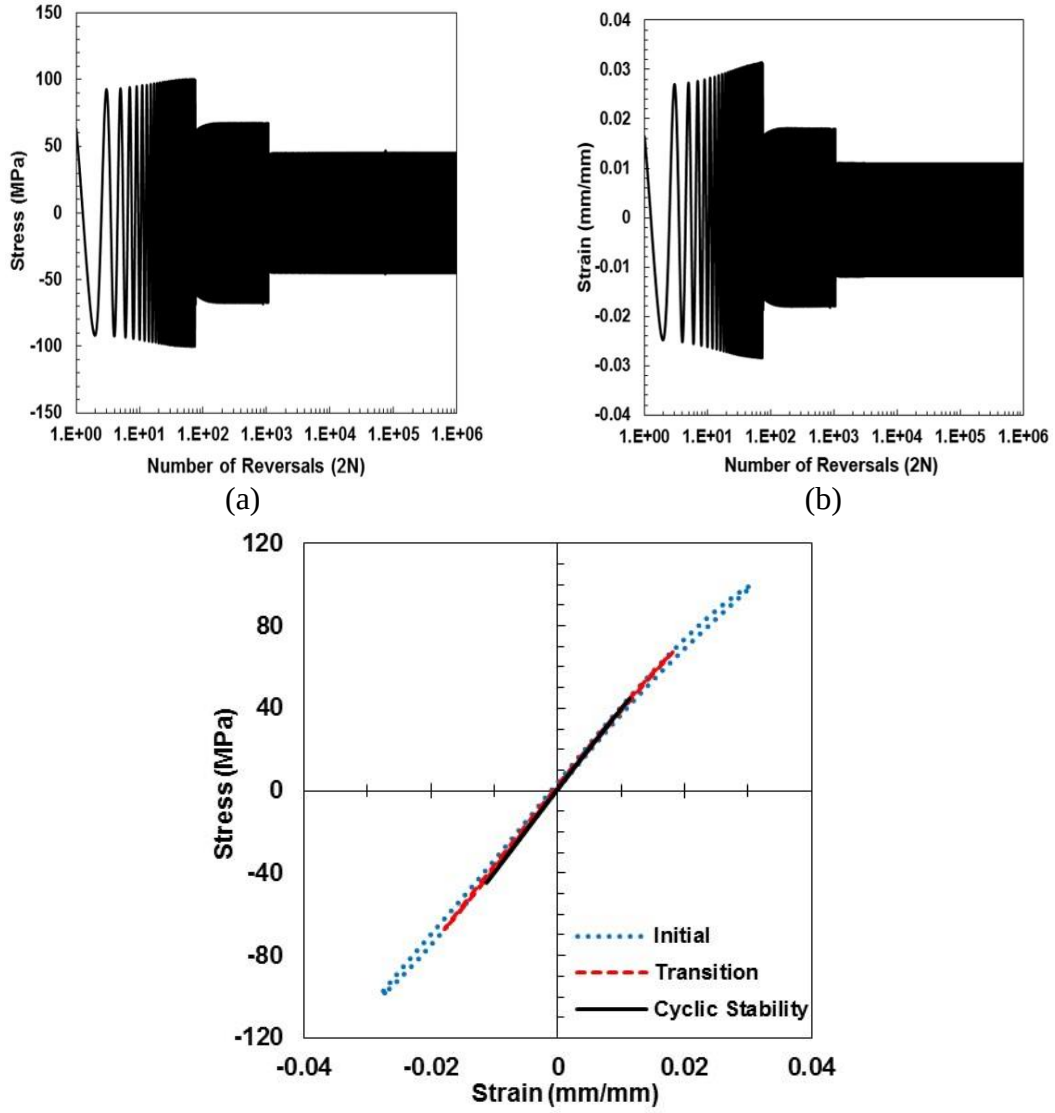

Figure 2.11 Loading history of load-controlled fatigue tests of PEEK (specimen S63 in Table 2.4) at 0.75 Hz showing the (a) stress and (b) strain amplitudes versus number of reversals and (c) hysteresis loops at different regions.

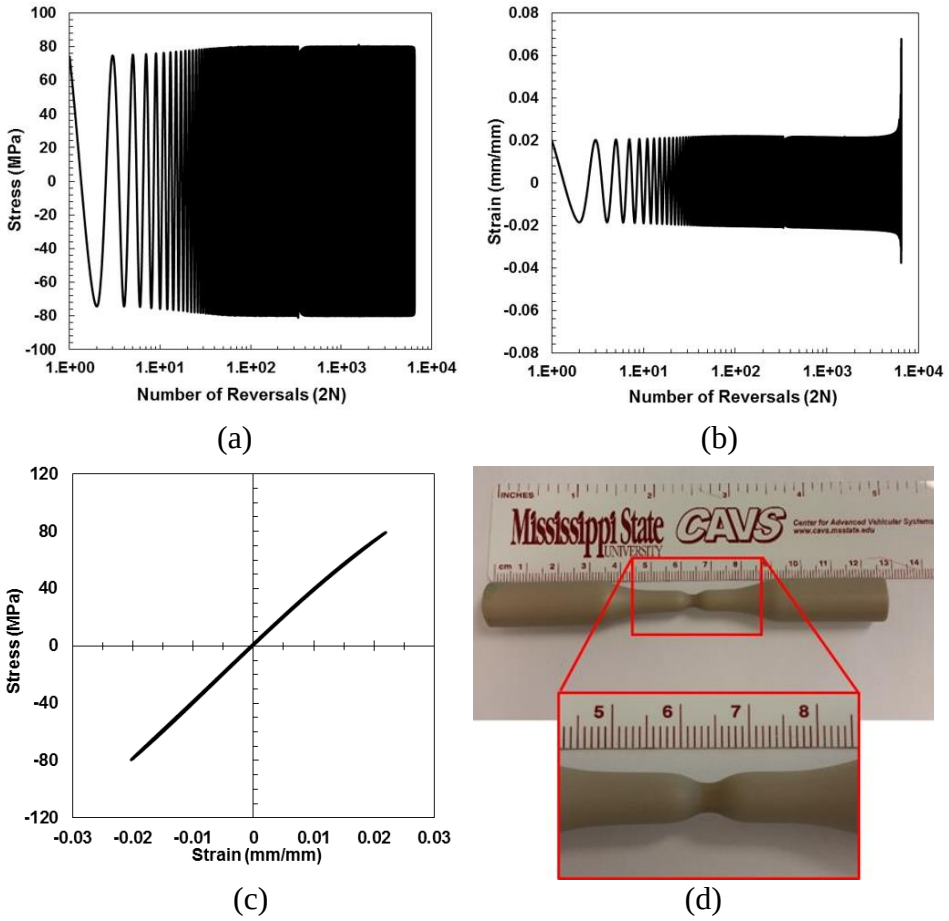

Figure 2.12 Loading history of load-controlled fatigue tests of PEEK (specimen S68 in Table 2.4) at 0.5 Hz showing the (a) stress and (b) strain amplitudes versus number of reversals, (c) hysteresis loop, and (d) cyclic necking image of specimen S68.

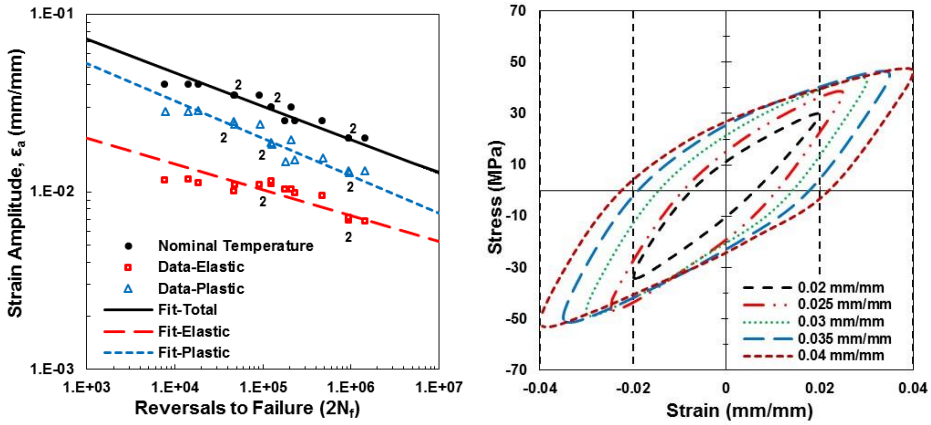

(a) (b)

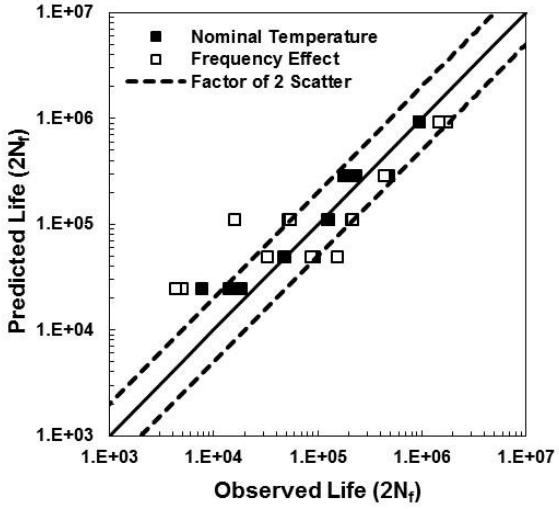

(c)

Figure 2.13 (a) Uniaxial fully-reversed fatigue test data of PEEK in strain amplitude, ε_a, versus reversals to failure, $2N_f$, with nominal temperature rise (Table 2.1) showing elastic, plastic, and total strains and fits, (b) hysteresis stress strain loops at five strain amplitudes, and (c) predicted fatigue lives using the Coffin-Manson model versus experimentally observed fatigue lives for all strain-controlled fatigue data (Tables 2.1 and 2.3). Numbers in the figure indicate the number of data points on top of each other.

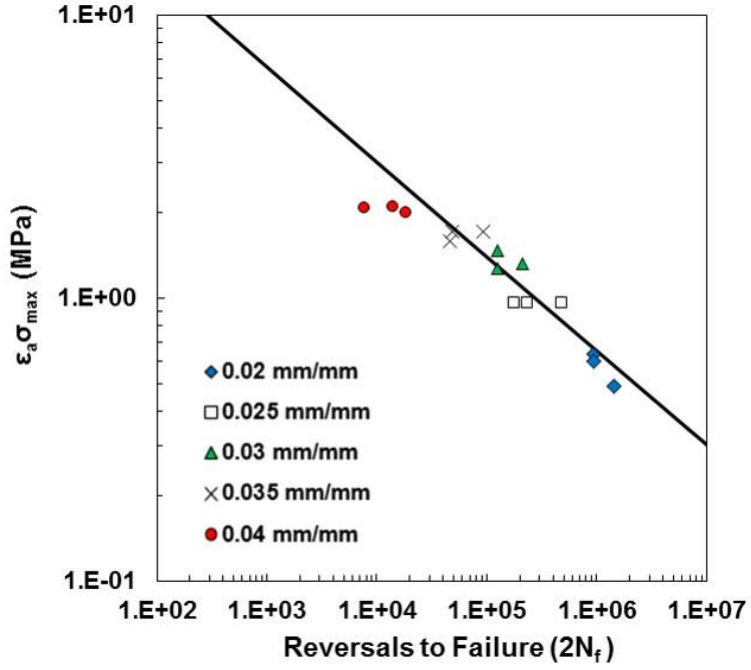

(a)

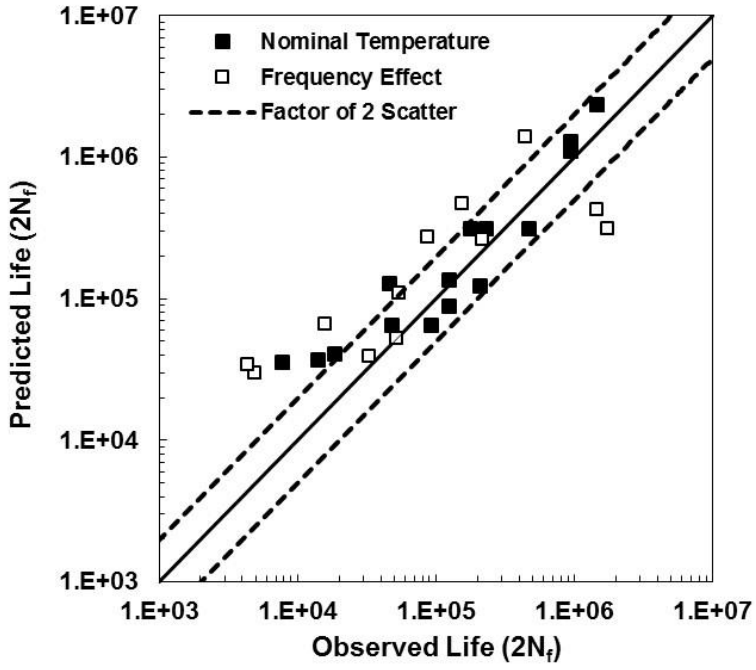

(b)

Figure 2.14 (a) Smith-Watson-Topper (SWT) damage parameter versus reversals to failure, $2N_f$, for the uniaxial fully reversed fatigue tests with nominal temperature rise (Table 2.1), and (b) predicted fatigue lives using the SWT parameter versus experimentally observed fatigue lives for all strain-controlled fatigue data (Tables 2.1 and 2.3)

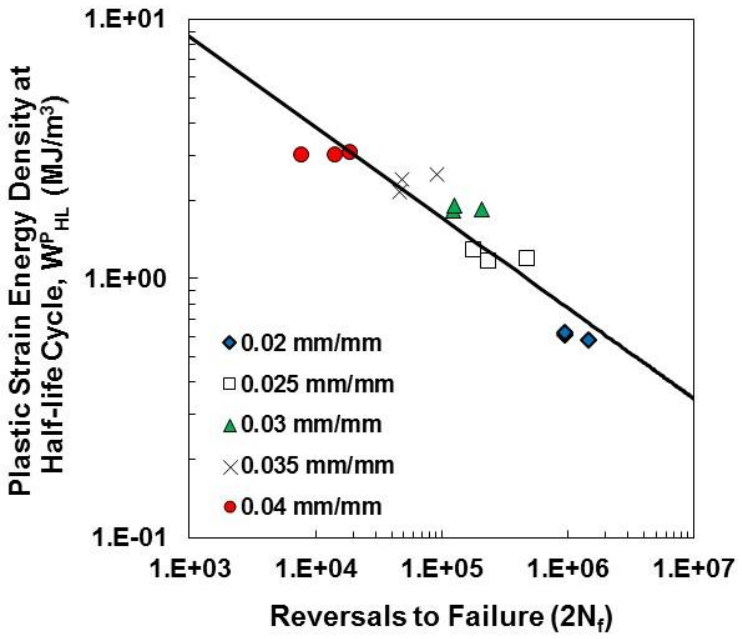

(a)

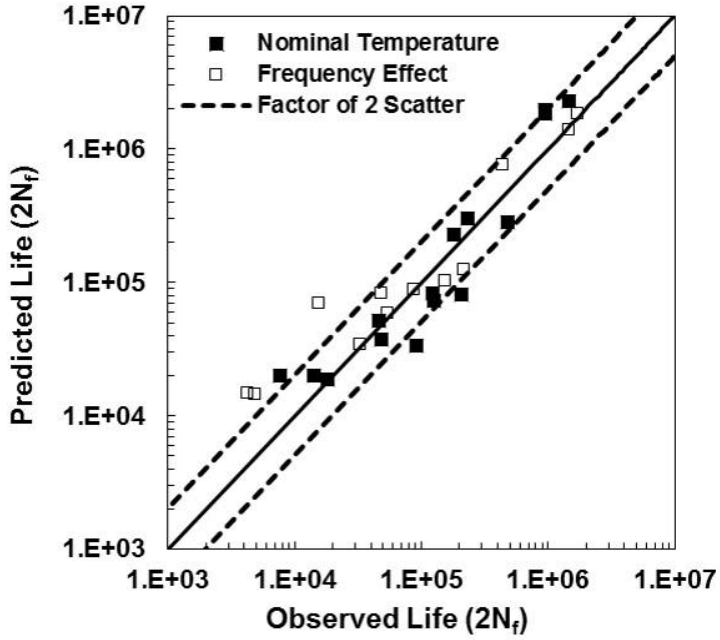

(b)

Figure 2.15 (a) Plastic strain energy density at half-life cycle, W_{HL}^{P}, versus reversals to failure, $2N_f$, for the uniaxial fully reversed fatigue test with nominal temperature rise (Table 2.1), and (b) predicted fatigue lives using this energy based approach versus experimentally observed fatigue lives for all strain-controlled fatigue data (Tables 2.1 and 2.3).

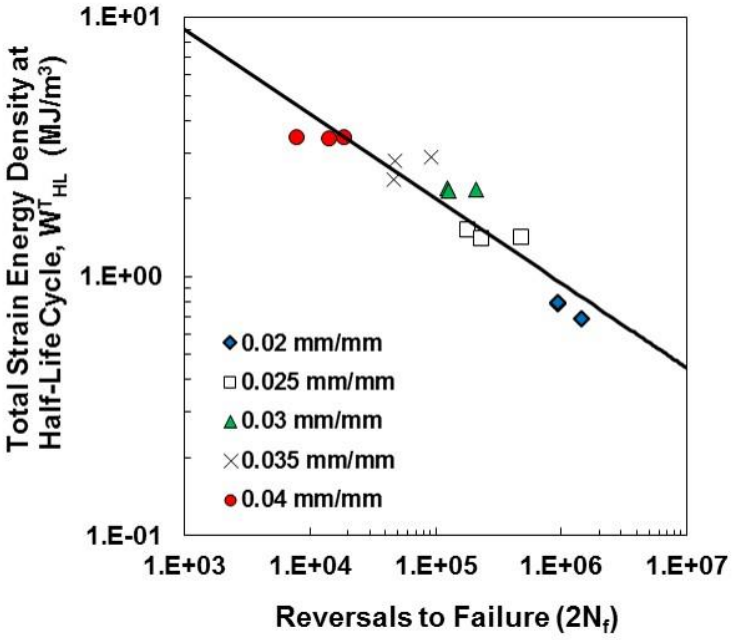

(a)

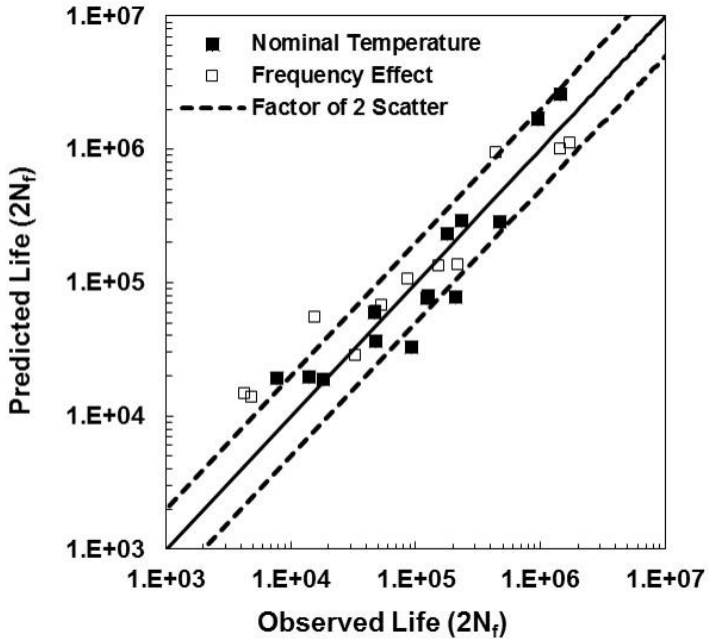

(b)

Figure 2.16 (a) Total strain energy density at half-life cycle, W^T_{HL}, versus reversals to failure, $2N_f$, for the uniaxial fully reversed fatigue test with nominal temperature rise (Table 2.1), and (b) predicted fatigue lives using this energy based approach versus experimentally observed fatigue lives for all strain-controlled fatigue data (Tables 2.1 and 2.3). Numbers in the figure indicate the number of data points on top of each other.

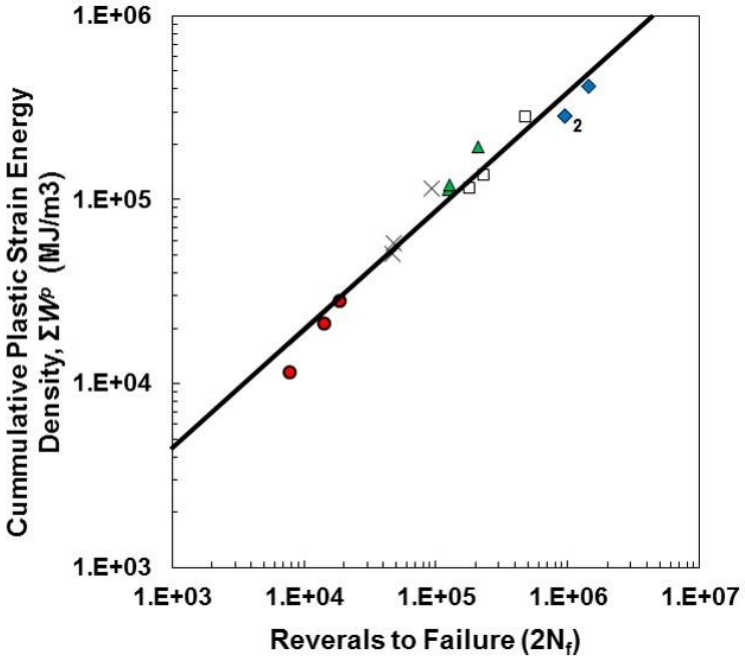

(a)

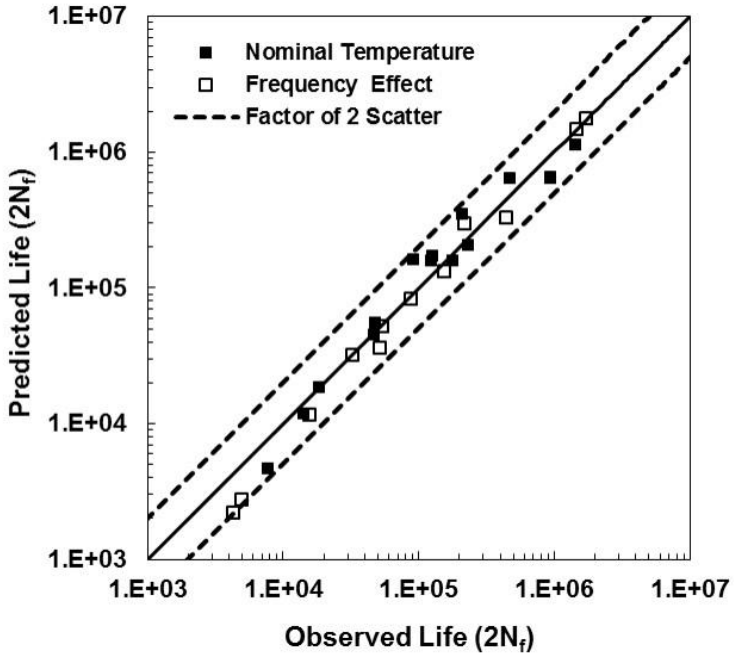

(b)

Figure 2.17 (a) Cumulative plastic strain energy density, $\sum W^P$, versus reversals to failure, $2N_f$, for the uniaxial fully reversed fatigue test with nominal temperature rise (Table 2.1), and (b) predicted fatigue lives using this transient energy based approach versus observed experimentally observed fatigue lives for all strain-controlled fatigue data (Tables 2.1 and 2.3).

Table 2.1 Experimental results for strain-controlled fatigue tests of PEEK at nominal temperature rise.

Specimen ID	$\frac{\Delta\varepsilon^*}{2}$ **(mm/mm)**	**Frequency (Hz)**	$\frac{\Delta\sigma^*}{2}$ **(MPa)**	σ_m* **(MPa)**	$2N_f$ **(Reversals)**	ΔT **(°C)**	$W_{HL}^{P\ *}$ **(MJ/m^3)**	$W_{HL}^{E\ *}$ **(MJ/m^3)**	$\sum W^P$ **(MJ/m^3)**
S50	0.02	3	30.1	-3.7	1,449,114	64	0.58	0.11	412,597
S21			32.2	-4.5	948,248	62	0.62	0.17	286,025
S22			31.0	-1.2	946,032	58	0.61	0.18	285,125
S19	0.025	1	46.8	-12.1	475,810	51	1.19	0.22	282,923
S30			48.9	-11.6	231,964	52	1.17	0.24	134,898
S31			48.3	-16.6	179,018	52	1.29	0.22	114,677
S46	0.03	0.75	46.4	-4.8	208,896	55	1.84	0.32	192,289
S48			51.4	-17.7	125,856	48	1.92	0.23	120,954
S47			49.8	-1.6	124,030	51	1.84	0.34	113,841
S42	0.035	0.5	49.0	-5.0	92,078	52	2.51	0.36	115,738
S43			49.3	-5.5	48,090	53	2.41	0.36	57,887
S35			45.3	-16.6	46,772	56	2.16	0.21	50,463
S24	0.04	0.5	50.3	-5.4	18,454	44	3.07	0.38	28,292
S25			52.9	-7.1	14,172	48	3.01	0.39	21,149
S23			52.1	-4.1	7,766	57	3.02	0.42	11,500

* Measured at half-life cycle

Table 2.2 Cyclic deformation and fatigue properties of PEEK obtained from the nominal temperature rise (Table 2.1) at room temperature.

Properties	**Value**
Cyclic modulus of elasticity, E' (GPa)	2.56
Cyclic yield strength, σ'_y (MPa)	16
Cyclic strength coefficient, K' (MPa)	275
Cyclic strain hardening exponent, n'	0.46
Fatigue strength coefficient, σ'_f (MPa)	246
Fatigue ductility coefficient, ε'_f	0.23
Fatigue strength exponent, b	-0.15
Fatigue ductility exponent, c	-0.21

Table 2.3 Experimental results for strain-controlled fatigue tests of PEEK to study the test frequency effects.

Specimen ID	$\frac{\Delta\varepsilon}{2}$ **(mm/mm)**	**Frequency (Hz)**	$\frac{\Delta\sigma^*}{2}$ **(MPa)**	σ_m* **(MPa)**	$2N_f$ **(Reversals)**	ΔT **(°C)**	$W_{HL}^{P\ *}$ **(MJ/m^3)**	$W_{HL}^{E\ *}$ **(MJ/m^3)**	$\sum W^P$ **(MJ/m^3)**
S20	0.02	1	57	-19	1,723,898	27	0.62	0.28	550,116
S94			55	-23	1,460,066	17	0.69	0.26	489,564
S55	0.025	2	31	-16	437,176	77	0.84	0.11	185,860
S26	0.03	0.5	60	-3.3	51,472	39	1.83	0.51	43,781
S28			57	-6.8	15,716	36	1.95	0.47	21,096
S53		1	41	-13.0	216,650	66	1.59	0.2	172,375
S59	0.035	0.25	46	-1.75	32,076	21	2.51	0.5	40,919
S34		0.75	61	-12.1	53,968	66	2.07	0.2	55,798
S4		1	37	-26	155,206	N/A	1.7	0.12	102,174
S8			38	-20	86,514	N/A	1.8	0.17	75,820
S56	0.04	0.25	59	-11.8	4,924	42	3.37	0.44	8,300
S95			58	-15	4,306	35	3.36	0.4	7,197

Table 2.4 Experimental results for load-controlled fatigue tests of PEEK.

Specimen ID	$\frac{\Delta\sigma}{2}$ **(MPa)**	**Frequency (Hz)**	$\frac{\Delta\varepsilon^*}{2}$ **(mm/mm)**	ε_m^* **(mm/mm)**	$2N_f$ **(Reversals)**	ΔT **(°C)**
S65	100-45**	0.4	0.031	0.0100	172***	6
S64	100-45**	0.4	0.029	0.0060	306***	6
S66	100-45**	0.6	0.011	0.0053	> 52,810	6
S63	100-45**	0.75	0.011	-0.00009	> 2,000,000	4
S61	45	0.75	0.011	-0.0004	> 2,000,000	5
S68	80	0.5	0.020	-0.0005	6,444***	21
S69	80	0.75	0.021	-0.0005	7,404***	24
S70	80	1.5	0.021	0.0002	9,716***	24
S71	70	1	0.020	-0.0010	95,830***	40
S72	70	2	0.020	0.0020	109,294***	44

* Measured at half-life cycle, ** Step test, *** Specimen failed due to necking

CHAPTER 3 MEAN STRAIN EFFECTS ON CYCLIC DEFORMATION AND FATIGUE BEHAVIOR OF POLYETHER ETHER KETONE (PEEK)

(Polymer Testing, 2016, 55, 69-77)

3.1 Abstract

In this study, the fatigue behavior of polyether ether ketone (PEEK) thermoplastic was investigated under uniaxial strain-controlled cyclic loading condition with various mean strains (R_ε = 0, 0.2, and 0.25). The mean stress responses of PEEK from all mean strain fatigue tests were found to be fully relaxed. As a result, minimum mean strain effect on fatigue behavior of PEEK was observed. Fractography analyses utilizing a scanning electron microscope were performed on PEEK specimens under tensile mean strain cyclic loading. Two distinct stages of fatigue process, including the crack initiation and the physically small crack growth, were observed on all the fracture surfaces. Moreover, two types of inclusions, unmelted particles and void-like defects, were identified to be the cause of crack initiation. Void-like defects were found to have more detrimental effects on fatigue life of PEEK when compared to particles of similar size. The effect of inclusions on fatigue behavior of PEEK was observed to be more significant than that of the tensile mean strain.

3.2 Introduction

With the advancement in the field of polymer science and engineering, new generation of polymers with tailored properties have been developed to meet specific requirements for various applications. Polymeric materials generally offer a variety of unique characteristics including relatively high strength, good chemical and corrosion resistance, lubricity, ease of processing, and cost effectiveness. In addition, due to a relative high strength to weight ratio, polymers are considered as ideal candidates for structural components in automotive and aerospace industries where light-weighting is required to improve the fuel efficiency [1].

Polyether ether ketone (PEEK), a semi-crystalline, high-performance engineered thermoplastic is the material of interest in this study. Due to its excellent dimensional stability and mechanical properties under extreme conditions, PEEK and its composites are widely used in oil and gas applications as compressor valve plates, seals and gaskets, pipes, etc. [3]. Moreover, selected grades of PEEK polymer are designed to conform to the strict requirements of the Food and Drug Administration to be used in a wide range of biomedical components, from sterilization equipment and temporary dentistry implants to long-term orthopedic implants [2, 40]. As the majority of these PEEK components are typically subjected to cyclic loading, the fatigue characterization of the material is therefore a necessity.

Unlike fatigue in metallic materials, the fundamental understanding underlying the fatigue process in polymers has not been fully realized. This may be due in part to the complexities of polymer structure, which poses a challenge in

obtaining the overall failure processes and their correlation with loading conditions [41]. The problem is compounded by the facts that the fatigue behavior of polymers are sensitive to material variables, such as the crystalline morphology as well as loading variables, including frequency, waveform, temperature, etc. [42]. The dependency on time and frequency is inherent to polymeric materials due to their viscoelastic nature. However, despite the growing use of polymeric materials, only a small number of experimental investigations have been performed to study the fatigue behavior of polymers under mean stress/strain conditions.

Sauer et al. [43] conducted a series of load-controlled fatigue experiments on polystyrene (PS) to obtain the effect of tensile mean stress by varying the alternating stress ratio, *A*, which is a ratio of alternating stress (or stress amplitude) to mean stress. The alternating stress ratios were adjusted using two approaches; increasing the mean stress while keeping the stress amplitude constant, and varying both the stress amplitude and mean stress with fixed maximum stress value. For a constant stress amplitude, shorter fatigue lives were observed for PS as tensile mean stress increased. On the other hand, for a constant maximum stress, increase of tensile mean stress and decrease of alternating stress resulted in longer fatigue lives. In some cases, the average fatigue life of PS was reported to be three or four times greater than that obtained from the fully-reversed cyclic loading at the same maximum stress value [43]. This may be explained by more influential effect of stress amplitude as compared to mean stress on the fatigue behavior of PS. The presence of tensile mean stress has been also observed to have detrimental effects

on fatigue life of other polymers, including acetal [44], epoxy [45], polyoxymethylene [14], and polypropylene (PP) [15].

Fewer studies have been conducted on polymers to obtain their fatigue behavior under strain-controlled condition with a presence of mean strain. Tao and Xia [13, 29] investigated mean strain effects on fatigue life of an epoxy polymer subjected to uniaxial strain-controlled cyclic loading. For the same strain amplitude, the fatigue life of epoxy decreased with increase of mean strain to strain amplitude ratio. Mean stress relaxation was also observed during initial loading cycles in all tests [13]. Chen and Wong [46] studied the fatigue behavior of nylon 6 and PP under nonzero mean strain cyclic tests at various temperatures (e.g. -40ºC, 25ºC, 65ºC, and 125ºC). They reported the tensile mean strain to reduce the fatigue resistance of both investigated polymers at all test temperatures [46].

As mentioned earlier, fatigue behavior of polymers is highly sensitive to loading, material, and environment variables. In this study, an experimental investigation has been conducted to obtain the fatigue behavior of PEEK thermoplastic subjected to strain-controlled cyclic loadings with various mean strains (ratios of minimum to maximum strain, R_ε, of 0, 0.2, and 0.25).The experimental program, including the material description and fatigue test setup, are presented. The effects of mean strain on cyclic deformation and fatigue life of PEEK are then discussed. Fractography results displaying crack initiation sites, inclusions responsible for crack initiation, as well as crack propagation characteristics of PEEK specimens are also presented. Finally, conclusions and recommendations are made based on the experimental observations in this study.

3.3 Material and Experimental Procedure

Neat PEEK polymer (TECAPEEK™ by Ensinger Inc.) with a glass transition temperature of 143°C and a melt temperature of 343°C was selected in this study. Round specimens with uniform gage section were machined from 12.8 mm diameter extruded PEEK rod using an oil based coolant to reduce heat buildup on specimens. The dimensions and geometry for specimens, as presented in Fig. 2.1, were designed in conformance with ASTM E606/E606M standard [16] with gage section diameter and length of 6.35 mm and 18 mm, respectively. The specimens were further polished in several stages to remove machining marks, resulting in an average surface finish of 3.4 μm in the gage section. The polished specimens were stored in a cool-dry climate-controlled environment prior testing.

In this study, uniaxial strain-controlled fatigue experiments were conducted on PEEK specimens using constant amplitude loading with various R_ε values. Previous studies [18, 42] observed significant plastic deformation in PEEK specimens when subjected to cyclic loading; therefore, strain-controlled tests, which can better characterize the fatigue behavior of a material that exhibits localized plastic deformation as compared to force controlled tests, were performed in this study. Experimental results also indicated that the fatigue behavior of PEEK polymer obtained under strain-controlled condition could not be directly correlate to its behavior under force-controlled condition. As a result, the fatigue behavior of PEEK should be evaluated depending on the loading condition for a given application, many of which are under cyclic deformation.

Moreover, it has been reported that PEEK polymer exhibits self-heating when subjected to cyclic loading due to its low thermal conductivity and high damping characteristics [18, 42]. Consequently, there is a conversion of input energy into heat that causes an initial rise in the specimen temperature, which may be stabilized when the heat generated equals to the heat transferred to surrounding environment. However, in certain test conditions when the specimen is subjected to a high strain/stress amplitude and/or test frequency, the temperature rise in the specimen, ΔT, does not stabilize; thus, leading to a thermal failure. Therefore, ΔT was monitored throughout testing to avoid thermal failure and ensure mechanical fatigue failure in all specimens.

All fatigue tests were conducted in accordance with ASTM D7791-12 standard [21] at ambient laboratory temperature (~23ºC) and humidity (~50% humidity) using a closed loop servo-hydraulic load frame with a 25 kN load cell. The grip sections of specimens were secured to the load frame using hydraulically operated wedge grips. Tests were performed using a sinusoidal waveform. Axial strain was measured using a mechanical extensometer with 15 mm gage length. The failure criterion was defined as 50% load drop and runout tests were stopped at 10^6 cycles. At least two tests were conducted for each prescribed test condition. A portable laser thermometer (Optris laser thermometer LS LT) was used to monitor the surface temperature of the specimen gage section.

Constant amplitude uniaxial strain-controlled fatigue tests were conducted at strains ranging from zero to 0.06 mm/mm at three R_ε values (0, 0.2, and 0.25). The following tensile mean stain values were used; 0.02, 0.025, and 0.03 mm/mm

for R_ε = 0 (pulsating tension) tests, 0.03 mm/mm for R_ε = 0.2 tests, and 0.0375 mm/mm for R_ε = 0.25 tests. The representations of different strain cycles for these tests are illustrated in Fig. 3.1. Test frequencies ranging from 0.5 Hz to 1.5 Hz were selected to maintain similar strain rate and temperature rise (ΔT) on the surface of the specimen gage section. In addition, fracture surfaces of specimens subjected to constant amplitude loading with mean strains were examined using a scanning electron microscope (SEM). Specimens were first cut, mounted, and sputter coated with a thin layer of gold for SEM analysis. The fracture surfaces were inspected to obtain microstructural inclusion factors (i.e. particles, voids, etc.) for crack initiation and evidence of propagation.

3.4 Experimental Results and Discussions

3.4.1 Cyclic Deformation and Fatigue Behavior

In this section, the effects of tensile mean strain on cyclic deformation and fatigue behavior of PEEK are discussed. The experimental data from constant amplitude fatigue tests with mean strains are summarized in Table 3.1, which includes strain amplitude, ε_a, mean strain, ε_m, test frequency, f, strain ratio, R_ε, stress amplitude, σ_a, mean stress, σ_m, reversals to failure, $2N_f$, and the rise in temperature on the specimen gage surface, ΔT. The stress amplitude, σ_a, and mean stress, σ_m, listed in this table, were obtained from the half-life cycle.

The temperature rise in polymer under cyclic loading is due to the self-heating resulting from low thermal conductivity and high damping characteristics, which has been discussed in Chapter 2. The frequency effect on the fatigue behavior

of PEEK with zero mean strain was investigated previously [42]. For tests with non-zero mean strains performed in the present study, test frequencies were adjusted for each combination of strain amplitude and strain ratio to maintain relatively constant strain rate and temperature rise on the specimen's gage section in all tests

The rise in temperature, cyclic deformation, and hysteresis stress-strain responses of PEEK under R_ε = 0 and ε_a = 0.025 mm/mm at 1 Hz condition (specimen S78) are presented in Fig. 3.2(a). The fatigue life of approximately 320,000 reversals and ΔT of 46ºC are obtained for specimen S78. Unlike the cyclic softening for PEEK under fully-reversed (R_ε = -1) fatigue tests, where four distinct regions of stress responses (i.e. initial, transition, cyclic stability, and final failure) were observed [42], the cyclic softening for PEEK with R_ε = 0 was not noticeably evident. The four regions of cyclic softening can be illustrated in Fig. 3.2(b) for specimen S31 subjected to R_ε = -1 and ε_a= 0.025 mm/mm at 1 Hz test condition [42]. Additionally, the stress range during testing for specimen S78 only reduced from approximately 120 MPa to 90 MPa, as compared to its fully-reversed counterpart at similar strain amplitude in Fig. 3.2(b), which had a reduction in stress range from 180 MPa to 90 MPa and a comparable ΔT value of 52 ºC [42].

As presented in Fig. 3.2(a), PEEK thermoplastic under pulsating strain loading exhibited significant mean stress relaxation immediately upon the initial cycling. The mean stress continuously relaxed as cycling progressed and became fully relaxed at approximately 2,000 reversals (less than 1% of total life). Similar behavior was observed in all mean strain tests, where the mean stress response was

fully-relaxed in a relatively short time period compared to the total life and the mean stress as well as stress range thereafter held stable for the remaining life. The increasing in the size of the hysteresis loops in this figure indicates the increasing amount of plastic deformation with continued straining up to cyclic stability region. Evolution of the hysteresis loop also indicates the mean stress relaxation phenomenon as the value of mean stress decreases from 58 MPa at initial region to 33 MPa at the transition region, and finally stabilizes to nearly zero at the cyclic stability region. On the other hands, small compressive mean stress (~ -17 MPa) was observed at the cyclic stability region for specimen S31 tested under R_ε = -1 and ε_a = 0.025 mm/mm test condition in [42], as can be noticed in Fig. 3.2(b). It should be noted that the shape of the hysteresis loops for specimens with zero mean strain are generally symmetric throughout the cyclic process (Fig. 3.2(b)), while the initial irregular shape of the hysteresis loops of specimens with tensile mean strain become more symmetric as the number of cycle increases (Fig. 3.2(a))

Using the PEEK fatigue data with mean strains (i.e. data in Table 3.1), the mean stress values were plotted against number of reversals in Fig. 3.3 to investigate the effect of strain amplitude on the stress relaxation rate. Figure 3.3(a) shows the mean stress evolution for PEEK specimens S83, S88, and S81, which were all tested under R_ε = 0 condition with strain amplitudes of 0.02, 0.025, and 0.03 mm/mm, respectively. As seen in Fig. 3.3(a), the initial mean stress (i.e. up to approximately 200 reversals) relaxed faster for the specimen subjected to a larger strain amplitude. At around 200 reversals, the mean stress values for all specimens

in Fig. 3.3(a) reduced to nearly 10% of the mean stress magnitude of the initial loading cycles.

The mean stress continued to decrease, but at a much lower rate, and eventually were fully-relaxed at approximately 2,000 reversals. As a result, one may conclude that, while the rate of relaxation increases by increasing strain amplitude, the mean stress of PEEK relaxes to a stable value close to zero under strain-controlled condition with non-zero mean strain, independent of the strain amplitude level. A similar observation was also reported for an epoxy polymer, where the rate of mean stress relaxation increased with increasing strain amplitude under constant strain ratio [13].

To obtain the effect of strain ratio on the mean stress relaxation, the mean stress of specimens subjected to various R_ε values, but at comparable strain amplitudes, were plotted against number of reversals, $2N$. Figure 3.3(b) presents the mean stress evolution of specimens S83, S91, S99, which were tested under R_ε = 0, 0.2, and 0.25, respectively. The R_ε = 0 and 0.2 experiments were conducted at ε_a = 0.02 mm/mm, while R_ε = 0.25 test was performed at ε_a = 0.025 mm/mm. It was observed that, while almost fully-relaxed mean stress was achieved around 2,000 reversals for all test conditions, the initial mean stress relaxation rate was higher for larger R_ε values at comparable strain amplitudes. The strain-life fatigue behavior of PEEK specimens tested under constant amplitude condition with various mean strains is presented in Fig. 3.4. In addition, the fully-reversed (R_ε = -1) PEEK data [42] are included in this figure. As seen, fatigue lives for PEEK with various mean strains (R_ε = 0, 0.2, and 0.25) were observed to be within a factor of

three of those under fully-reversed (R_ε = -1) loading conditions. For examples, the average lives of PEEK specimens tested at 0.02 mm/mm were 1,114,464 reversals for R_ε = -1 [42], 682,324 reversals for R_ε = 0 (specimens S86, S76, and S83 in Table 2.1), and 712,567 reversals for R_ε = 0.2 (specimens S92, S91, and S89 in Table 2.1). The small effect of tensile mean strain on fatigue behavior of PEEK observed in this study may be attributed to the fully-relaxed mean stress response, as illustrated in Figs. 3.2 and 3.3.

Furthermore, as seen in Fig. 3.4, slightly shorter or longer fatigue lives for PEEK with a presence of mean strain were observed. For example, shorter fatigue lives were noticed for specimens subjected to 0.02 mm/mm and 0.03 mm/mm with tensile mean strain when compared to specimens under fully-reversed loading condition at comparable strain amplitudes. On the other hand, some beneficial effect of tensile mean strain was obtained for specimens tested at 0.025 mm/mm. As a result, one may conclude that the presence of tensile mean strain may not necessary result in shorter fatigue lives for PEEK.

Although the rate of cyclic softening (amount of cyclic softening per cycle) may be slightly different, it should be noted that similar level of cyclic softening and hysteresis stress-strain responses at the cyclic stability region for specimens with zero and non-zero mean strain were observed, as previously illustrated in Fig. 3.2. In addition, it has been shown in [42] that the number of cycles spent in the initial region of cyclic softening may affect the fatigue life of PEEK specimens, where the PEEK specimen with greater number of cycles in the initial region of cyclic softening exhibited the shortest fatigue life when compared to those

subjected to the identical test condition. It can be noticed that specimens with tensile mean strain, as shown in Fig. 3.2, typically have shorter number of cycles in the initial region of cyclic softening when compared to those without mean strain. In addition, some tensile mean stress, which is generally detrimental to fatigue life, can be observed during the initial cycles. Therefore, the combination of these two (number of cycles in the initial region of cyclic softening and the presence of tensile mean stress) may result the specimens with tensile mean strain to exhibit slightly shorter or longer fatigue lives as compared to the fully-reversed ones.

The combined effects of frequency and rise in temperature on dissipated strain energy was investigated for the uniaxial strain-controlled fully-reversed (R_ε = -1) test in an earlier study [42]. Similar approach is conducted in the present work to obtain the relationship between frequency, f, rise in temperature, ΔT, and dissipated plastic strain energy density at half-life cycle, W_{HL}^P, for PEEK specimens subjected to cyclic loading in presence of mean strains. The energy parameter W_{HL}^P was measured by determining the area of hysteresis stress-strain loop at half-life cycle using an integration method. A linear relationship expressed by Eq. (3.1) was proposed by Bernasconi and Kulin [32] for short glass fiber reinforced polyamide 6:

$$\frac{\Delta T}{f} = B W_{HL}^P \tag{3.1}$$

where B is a material constant and W_{HL}^P, reported in Table 3.1 for all constant amplitude fatigue tests, is the plastic strain energy density represented by the area of the hysteresis loop at half-life cycle. Using the linear relation expressed by Eq.

(3.1), the ratio of rise in temperature to the test frequency, $\Delta T/f$, is plotted against the dissipated plastic strain energy at half-life cycle, W_{HL}^{P}, in Fig. 3.5(a) for all the specimens under constant amplitude fatigue loading with mean strains (i.e. data in Table 3.1). The fully-reversed (R_ε = -1) fatigue data from [42], which include both nominal temperature rise tests as well as those conducted to study the frequency effect, are also included in this figure. As seen, while better correlation is obtained for tests with lower $\Delta T/f$ values, some scatter is noticeable at higher $\Delta T/f$ values (i.e. higher strain amplitude tests). Nonetheless, an acceptable correlation, indicated by the R^2 = 0.89 between $\Delta T/f$ and W_{HL}^{P}, can be realized in this figure for all tests with zero and non-zero mean strains and at different frequencies.

A different approach to correlate the temperature rise in specimen under cyclic loading to test frequency, proposed by Krause [47], was also employed in this study. Krause's model was initially developed for glass fiber reinforced laminates [47] and recently has been validated for reinforced and unreinforced PP, as well as PP blended with 25 wt% elastomer and filled with 30% magnesium silicate [33]

Based on this model, the ratio of temperature rise in the specimen to cycling frequency can be expressed as:

$$\frac{\Delta T}{f} = C\sigma_a(\varepsilon_a)^2 \tag{3.2}$$

where C is a material constant. Using the data in Table 3.1, the correlation for $\Delta T/f$ and $\sigma_a(\varepsilon_a)^2$ is presented in Fig. 3.5(b) for all fatigue data with tensile mean strain. Similar to Fig. 3.5(a), PEEK fatigue data reported in [42] for fully-reversed (R_ε = -

1) condition with various frequencies are also included in this figure. Although some scatter is noticeable at higher $\Delta T/f$ values, a reasonable correlation, expressed by $R^2 = 0.84$, is obtained. Based on the results shown in Fig. 3.5, one may suggest that fatigue prediction models utilizing energy based approaches may be suitable for PEEK polymer subjected to mean strain cyclic loading.

3.4.2 Fractography Analysis

The fractography analysis was conducted on fatigue specimens subjected to various R_ε values to determine microstructural inclusions responsible for fatigue crack initiation, as well as to observe crack propagation behavior of PEEK. Under fully-reversed ($R_\varepsilon = -1$) cyclic loading, two distinct stages of fatigue process were observed for PEEK polymer [18]. These include (1) crack initiation stage, which consists of crack incubation (i.e. nucleation period of a crack) and microstructural small crack (MSC), and (2) physically small crack (PSC) stage

The fracture surface of specimen S86 subjected to 0.02 mm/mm and $R_\varepsilon = 0$ loading condition is illustrated in Fig. 3.6, which also represents a typical fatigue fracture surface observed for all PEEK specimens with mean strains (i.e. specimens in Table 3.1). Both crack initiation and PSC stages are noticeable in this figure. In addition, Simsiriwong et al. observed two different types of inclusions, including particles (i.e. unmelted particles) and void-like defects as respectively displayed in Figs. 3.6 and 3.7 of their paper [18], to be responsible for crack initiation in PEEK. Similar inclusions were also found to be responsible for fatigue crack initiation in specimens with tensile mean strains in this study. For specimen S86 in Fig. 3.6, a

subsurface particle with the approximated size of 34 μm, determined from the square root of the projected area of the particle as described in [48], caused the crack initiation. Figure 3.7 displays SEM images of the fracture surface of specimens S86 ($2N_f$ = 475,726 reversals), S76 ($2N_f$ = 696,398 reversals), and S83 ($2N_f$ = 874,850 reversals), which were all subjected to pulsating cyclic loading (R_ε = 0) with 0.02 mm/mm strain amplitude. The crack initiation site (i.e. incubation + MSC region) was also identified for each specimen and the area of crack initiation site was obtained from SEM images using an image processing software. Fatigue crack in all specimens in Fig. 3.7 was initiated from a subsurface particle of a similar size

As seen in this figure, the particle responsible for crack initiation in specimens S86, S76, and S83 located at approximately 746, 589, and 225 μm away from the surface, respectively. The crack initiation site in specimens S86, S76, and S83 was also determined to be approximately 0.41, 0.26, 0.048 mm^2, respectively. From this observation, it appears that the location of the particle relative to the specimen surface may influence the size of the initiation site (i.e. the farther the distance from the particle to the specimen surface, the larger the area of the crack initiation site). In addition, it may be concluded from Fig. 3.7 that, under the same test condition, specimens with inclusions furthest away from the outer surface yielded larger crack initiation sites and shorter fatigue lives. Furthermore, cracks in the MSC region of these specimens were observed to be on an inclined plane and propagated toward the surface of specimens prior transitioning to the loading plane in the PSC region.

Figure 3.8 presents SEM images of fracture surfaces of specimens S76, S91, and S90, which were tested at 0.02 mm/mm with R_ε = 0, 0.02 mm/mm with R_ε = 0.2, and 0.025 mm/mm with R_ε = 0.25, respectively. In addition, the fracture surface of specimen subjected to R_ε = -1 in [18] at 0.02 mm/mm strain amplitude is also displayed in this figure. It can be observed that, although the presence of mean strain did not significantly affect the fatigue behavior of PEEK, the size of the crack initiation site in PEEK specimens generally decreased with an increase in strain ratio, R_ε. The crack initiation site in specimens with tensile mean strain were observed to be subsurface, which is in contrast to most specimens under fully-reversed (R_ε = -1) condition reported in [18], where the crack initiation typically occurred at the specimens' surface. The particles responsible for crack initiation in the specimens in Fig. 3.8 were also found to be at a greater distance away from the specimen surface as the strain ratio, R_ε, increased. In an attempt to explain such observations for specimens in Fig. 3.8 under different strain ratios, the surface roughness of all of these specimens was measured. An increase in the surface roughness was noticed as the strain ratio, R_ε, increased. This may indicate that, despite the fact that specimens in Fig. 3.8 appear to have the preferential crack nucleation at or near the surface, the surface roughness (intrusion/extrusion mechanism) may not be the cause of fatigue failure in PEEK polymer.

The effect of crack initiation factor (i.e. particles or void-like defect) size on fatigue life for all specimens with tensile mean strain and in fully-reversed [42] condition is presented in Fig. 3.9. The size of crack initiation factors shown in Fig.

3.9 is categorized by the diameter: 1-10 μm, 11-15 μm, 16-20 μm, 21-30 μm, and 31-40 μm. Solid and hollow features in this figure represent particles and void-like defects, respectively. It should be noted that the fatigue cracks in most PEEK specimens with non-zero mean strain initiated from particles, while only a few specimens had void-like defects that caused the crack initiation. As seen in Fig. 3.9, for all the combinations of R_ε values and strain amplitude levels, PEEK fatigue lives decreased with an increase in size of inclusion factors. Moreover, specimens with void as crack initiation factor exhibited much lower fatigue resistance than those with particles of similar size. Such observation indicated that voids had more influence on PEEK fatigue behavior when compared to particles. Figure 3.9 also reveals that the scatter in fatigue lives of PEEK is largely attributed to the size and type of inclusion responsible for crack initiation, while minimal effect of tensile mean strain was observed. As a result, one can conclude that the effect of the size/type of the crack initiation factors on fatigue life of PEEK may be more significant than the mean strain effect.

Although the formation of inclusions within the material, such as voids or unmelted particles that are typically introduced during the manufacturing process, is unavoidable, there are some manufacturing techniques that may potentially reduce the inclusions in polymers. Some examples include using high curing pressure to avoid air entrapment during the curing process, utilizing preform mold with less complex geometry, as well as optimizing the flow rate of the resin, mold temperature, and resin injection temperature [49]. By minimizing the presence of inclusions, fatigue performance of PEEK polymer may be improved.

3.5 Conclusions

In this study, uniaxial strain-controlled tests with various strain ratios were utilized to study the mean strain effect on fatigue behavior of a neat PEEK thermoplastic Based on the experimental results, the following conclusions can be drawn:

1. PEEK exhibited significant mean stress relaxation under uniaxial strain-controlled loading with tensile mean strains. The mean stress for tests at R_ε = 0, 0.2, and 0.25 was observed to be fully-relaxed and minimally affect the PEEK fatigue life.

2. The mean stress relaxation rate for PEEK significantly depends on the strain amplitude and R_ε value. It was observed that the mean stress relaxation rate was initially higher for tests subjected to larger strain amplitudes and/or a larger R_ε values (i.e. larger mean strains).

3. Unlike those without mean strain, PEEK subjected to cyclic loading with tensile mean strain did not clearly exhibit the multiple stages of cyclic softening behavior, most likely due the concurrent mean stress relaxation in the material. The initial irregular shape of hysteresis stress-strain loops of specimens with mean strains were observed to become more symmetric as the number of cycle increased.

4. For all fatigue tests with zero and non-zero mean strains, a linear relationship can be assumed between the ratio of the temperature rise in the specimen gage section (due to cyclic loading) to the test frequency, $\Delta T/f$, and (1) the dissipated plastic strain energy density, W_{HL}^{P}, or (2) $\sigma_a(\varepsilon_a)^2$. As a result, energy based fatigue models may be suitable to correlate PEEK data under cyclic loading with and without mean strains at different test frequencies.

5. The fractography analysis revealed two fatigue stages observed on the fracture surface of PEEK specimens under tensile mean strain cyclic loading. These are crack initiation stage that consists of crack incubation and microstructurally small crack (MSC), as well as physically small crack (PSC) growth stage. Two types of inclusions, including particles and void-like defect, were found to be responsible for crack initiation in PEEK specimens. Moreover, the incubating inclusions in most specimens under fully-reversed loading were observed to be on the outer surface, while they appeared to be subsurface inclusions for specimens under non-zero mean strains.

6. At comparable strain amplitudes and strain ratios, presence of a larger inclusion (particles or void-like defects) generally resulted in a shorter fatigue life of the PEEK specimen. Furthermore, specimens with void-like defects, serving as the source of crack initiation, were found to have shorter fatigue lives as compared to the specimens containing particles of similar size.

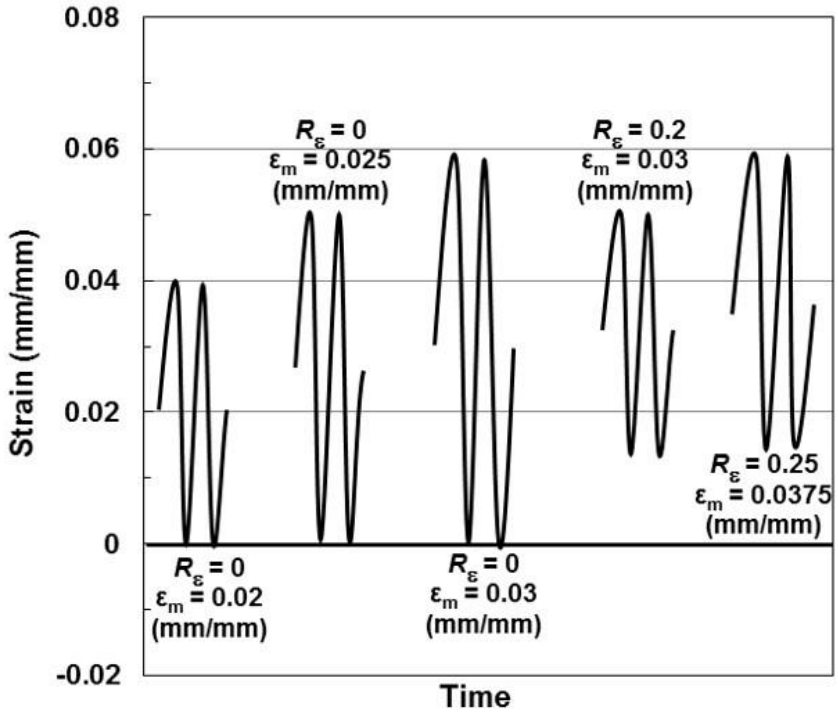

Figure 3.1 Representation of different strain cycles used for mean strain fatigue tests for PEEK thermoplastic in this study.

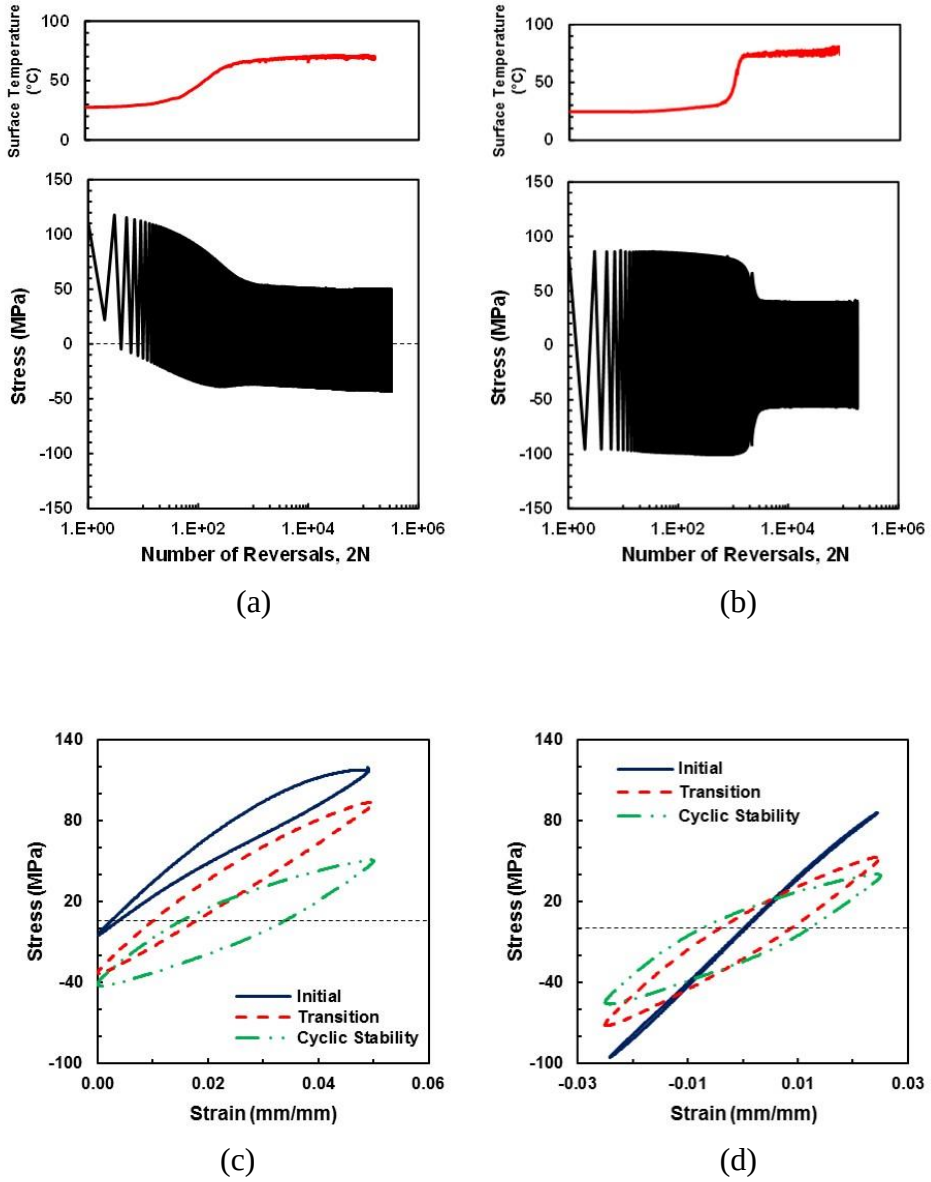

Figure 3.2 Surface temperature, stress responses and hysteresis loops at different stages of cyclic deformation of fatigue tests at ε_a= 0.025 mm/mm and 1 Hz for (a) specimen S78 with R_ε = 0 and (b) specimen S31 with R_ε = -1 [42]

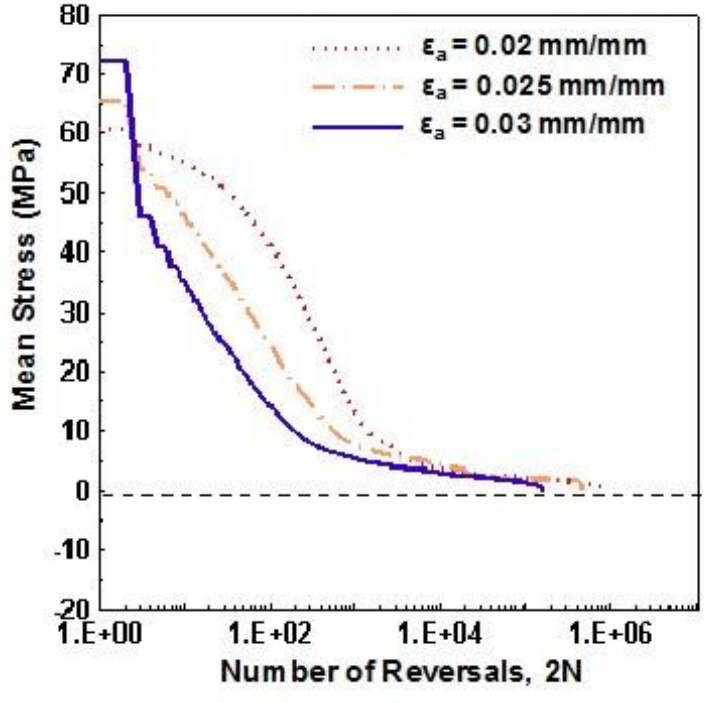

(a)

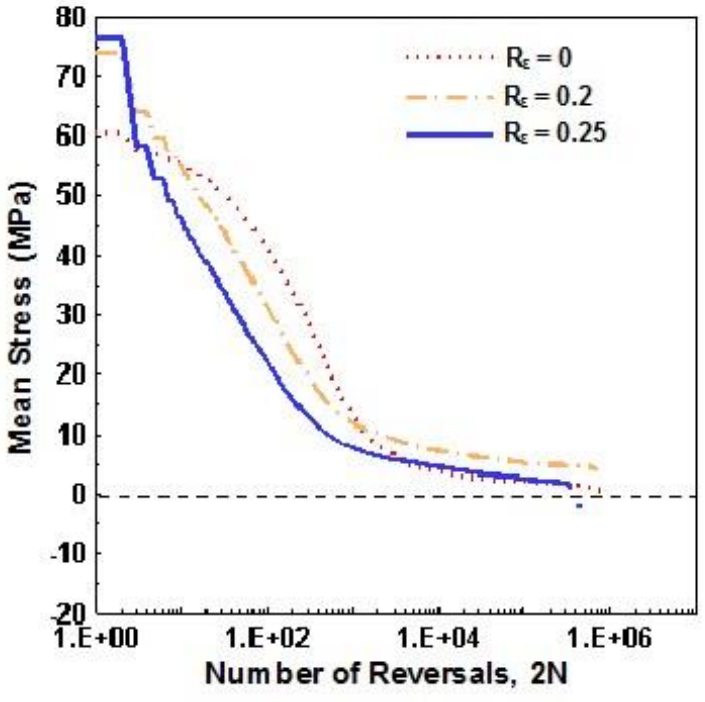

(b)

Figure 3.3 Mean stress versus number of reversals of PEEK fatigue specimen for (a) tests at various strain amplitudes and R_ε = 0, and (b) tests at 0.02 mm/mm and various R_ε values.

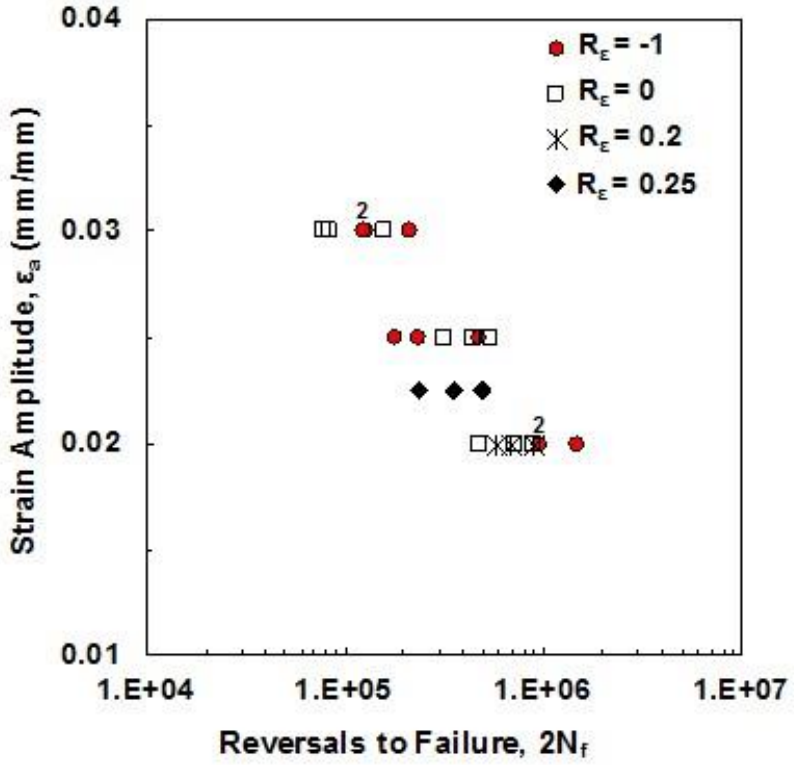

Figure 3.4 Strain-life fatigue behavior of PEEK specimens under strain-controlled fully-reversed (R_ε = -1) [42] and tensile mean strains (R_ε = 0, 0.2, and 0.25) cyclic loadings in Table 2.1.

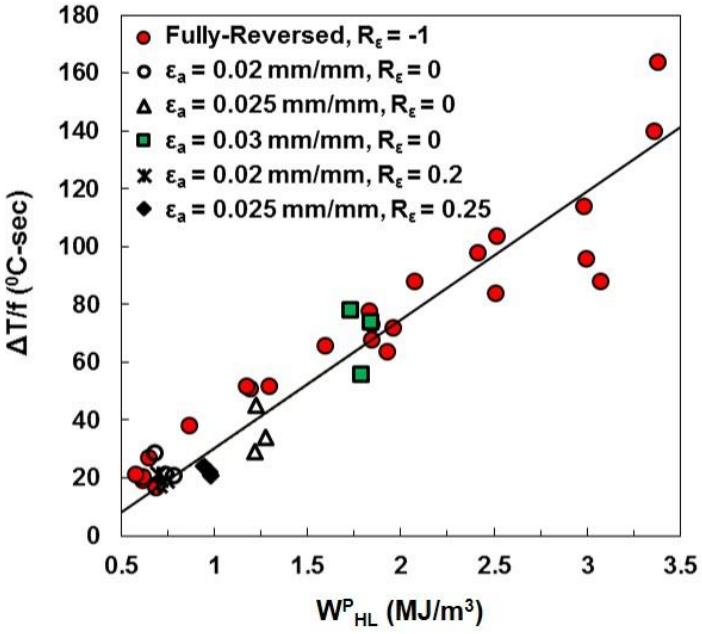

(a)

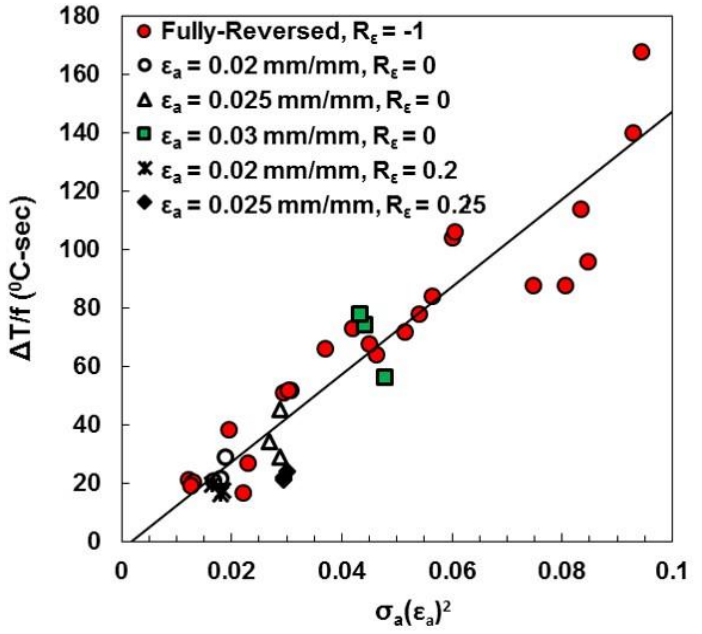

(b)

Figure 3.5 (a) The ratio of the rise in temperature to test frequency, ΔT/f, versus the plastic strain energy density at half-life (cyclic stability region), W_{HL}^P, and (b) the ratio of ΔT/f versus $\sigma_a(\varepsilon_a)^2$for strain-controlled fatigue data with and without tensile mean strains.

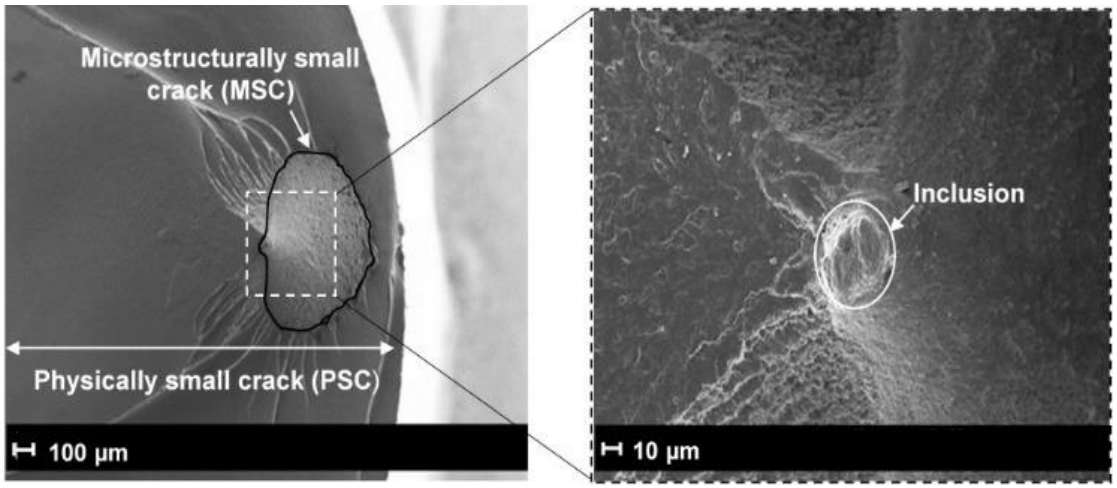

Figure 3.6 SEM images of the fracture surface of PEEK specimen S86 tested at 0.02 mm/mm strain amplitude with $R_\varepsilon = 0$, showing (a) an overview of fatigue failure stages including crack initiation, microstructurally small crack (MSC), and physically small crack (PSC), and (b) the inclusion caused the crack initiation.

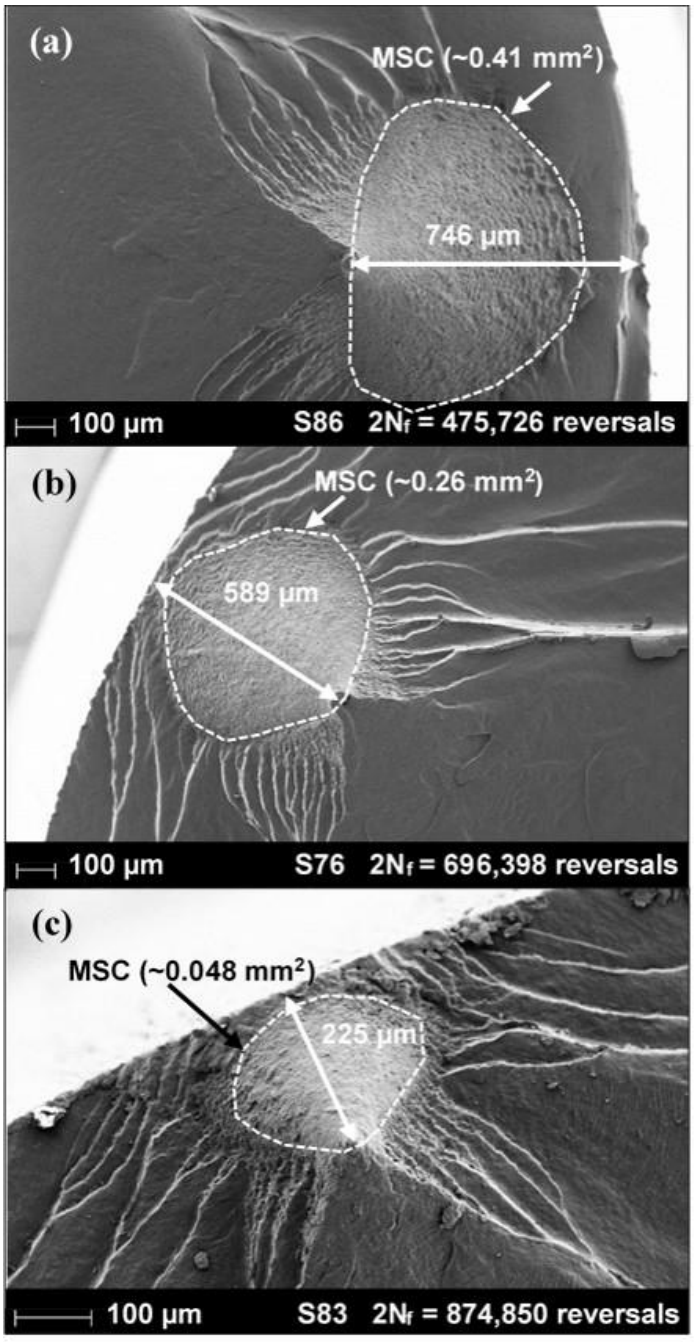

Figure 3.7 Fracture surfaces of fatigue specimen (a) S86, (b) S76, and (c) S83, showing the variations of the location of micro-particles responsible for the crack initiation, and the size of microstructurally small crack (MSC) region. All specimens were subjected to 0.02 mm/mm strain amplitude and $R_\varepsilon = 0$ test condition.

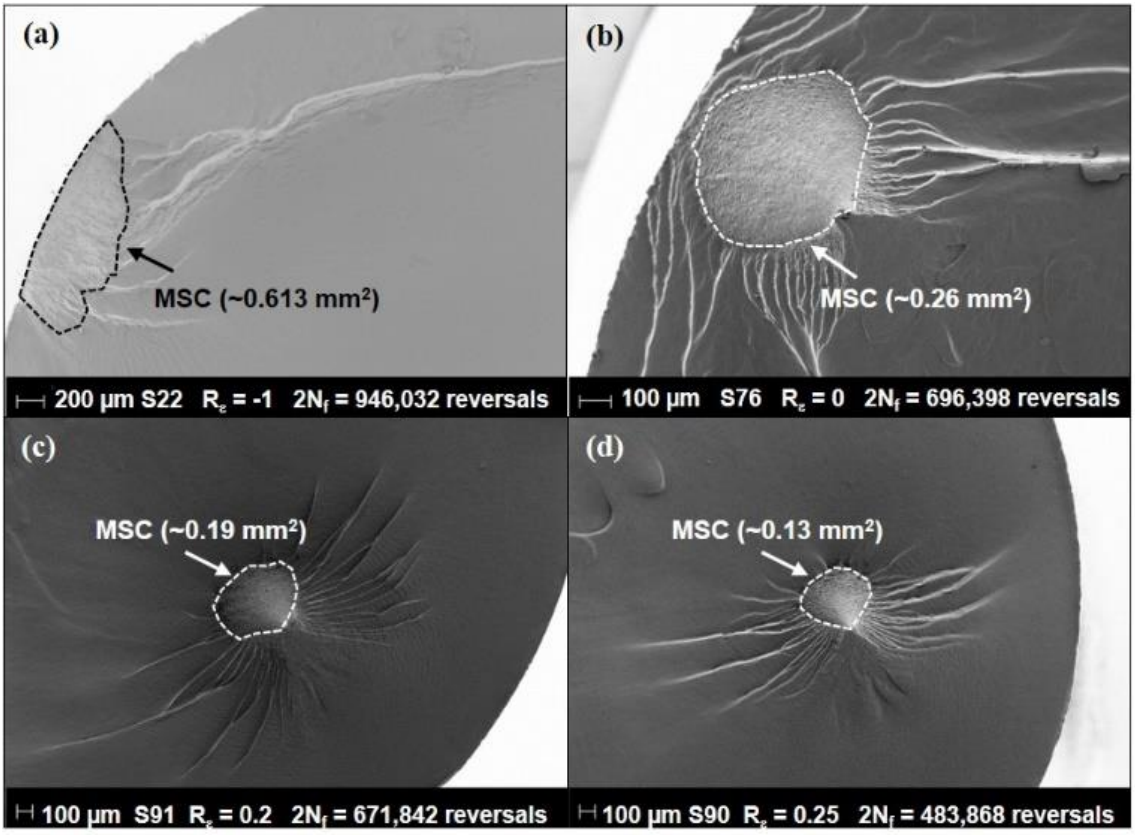

Figure 3.8 Fracture surfaces of fatigue specimen (a) S22 under R_ε = -1 and ε_a = 0.02 mm/mm [42], (b) S78 under R_ε = 0 and ε_a = 0.02 mm/mm, (c) S91 under R_ε = 0.2 and ε_a = 0.02 mm/mm, and (d) S90 under R_ε = 0.25 and ε_a = 0.025 mm/mm, showing the effect of strain ratio on the size of microstructurally small crack (MSC) region.

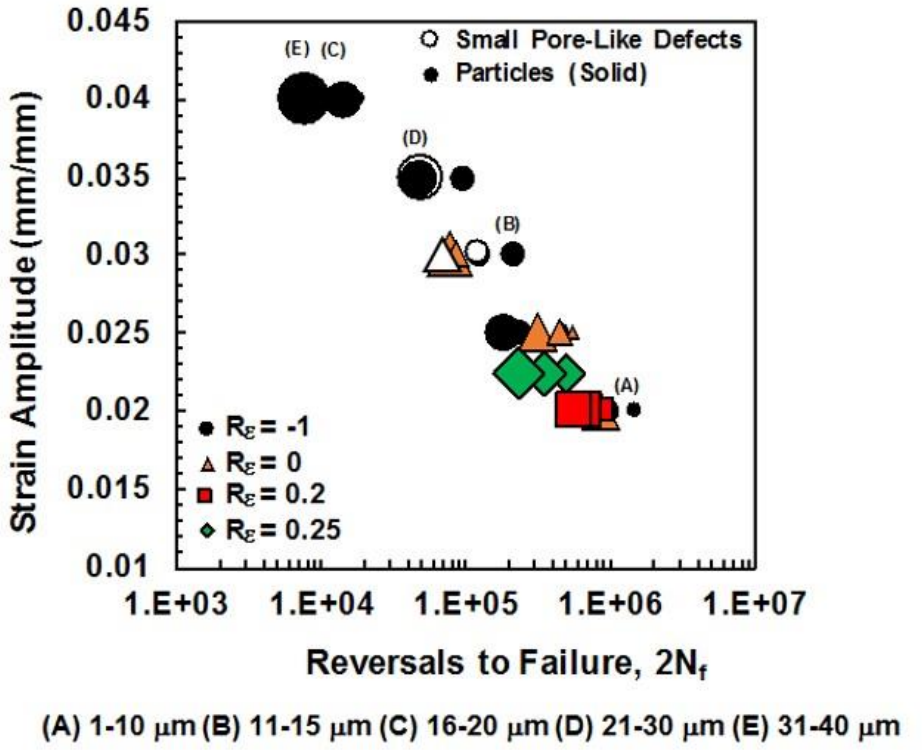

Figure 3.9 Strain amplitude versus reversals to failure for PEEK subjected to constant amplitude fully-reversed (R_ε = -1) [42] and mean strain tests (R_ε = 0, 0.2, and 0.25), showing the effect of size and type of inclusion responsible for crack initiation on the fatigue behavior.

Table 3.1 Experimental results for PEEK polymer subjected to uniaxial strain-controlled fatigue loading with mean strains.

Specimen ID	ε_a (mm/mm)	ε_m (mm/mm)	Frequency (Hz)	R_ε Value	σ_a^* (MPa)	σ_m^* (MPa)	$2N_f$ (Reversals)	ΔT (°C)	ΔW_{HL}^P (MJ/m^3)
S86	0.02	0.02	1.5	0	42	-1.98	475,726	31	0.78
S76					47	7.71	696,398	43	0.68
S83					45	0.98	874,850	32	0.74
S78	0.025	0.025	1		46	4.11	318,690	45	1.2
S88					46	1.59	443,580	29	1.2
S84					43	-0.80	535,546	34	1.3
S85	0.03	0.03	0.5		49	2.51	77,892	37	1.9
S87					53	-0.95	83,096	28	1.8
S81					48	1.40	155,458	39	1.7
S92	0.02	0.03	1.5	0.2	45	2.50	578,224	24	0.69
S91					41	4.56	671,842	29	0.74
S89					46	7.50	887,634	26	0.71
S97	0.025	0.0375	1	0.25	47	1.92	231,896	22	0.98
S99					47	2.03	347,108	21	0.98
S90					48	3.84	483,868	24	0.95

*Measured at half-life cycle

CHAPTER 4 LOAD HISTORY AND SEQUENCE EFFECTS ON CYCLIC DEFORMATION AND FATIGUE BEHAVIOR OF A THERMOPLASTIC POLYMER

(Polymer Testing, 2016, 56, 99-109)

4.1 Abstract

In this study, the effect of load history and sequence on the cyclic deformation and fatigue behavior of polyether ether ketone (PEEK) thermoplastic was experimentally investigated. Various uniaxial strain-controlled multi-block fatigue tests were conducted, including (1) fully-reversed (R_ε = -1) two-, three-, and four-block loadings with adjusted frequencies to maintain a nominal temperature rise on the specimen gage surface, (2) fully-reversed two-block loading to study the frequency effect, and (3) pulsating tension (R_ε = 0) two-block loading to investigate the combine effect of pre-loading and mean stress/strain on cyclic deformation and fatigue behavior of PEEK. For all fatigue tests under fully-reversed (R_ε = -1) multi-block loadings, cyclic stability of PEEK specimens was achieved at approximately the same reversals and with similar stress amplitudes as those without pre-loading under identical test condition. Additionally, for tests with R_ε= -1, pre-loading was found to have a significant beneficial effect on PEEK fatigue resistance irrespective to the load sequence (i.e. high-low or low-high). However, no obvious load history and sequence effect on fatigue behavior of PEEK was observed for pulsating

tension (R_ε = 0) block loading tests. Experimental results also revealed that increasing test frequency generally leads to higher fatigue lives.

4.2 Introduction

Polymeric materials have been extensively used in various applications, from common household products to advanced prosthetic hip devices. This is due to their unique advantageous characteristics, such as high strength to weight ratio, ease of processing, and tailorability, allowing the material properties to be altered to meet specific requirements by utilizing a wide range of additives such as fillers, reinforcements, stabilizers, and plasticizers [11]. Despites these advantages, the mechanical behavior of most polymers is known to be complex and depend significantly on time, temperature, and loading rate, specifically when it is influenced by the presence of some fluctuating loads (i.e. fatigue) [50]. Since polymers and polymer-based materials (i.e. polymer matrix composites) are often used for load-bearing purposes where cyclic loadings are typically experienced, an adequate understanding of their fatigue resistance and in service performance is necessary.

Unlike the relatively advanced, state-of-the-art understanding of progressive damage evolution processes in metals under cyclic loading, those in polymeric materials, including crazing and shear banding, as well as fatigue crack initiation and propagation, are not yet well understood [51]. Only a small number of studies have been conducted to obtain their correlations to material structure, material composition, and loading conditions [18, 42, 52-57]. The problem is also compounded by the fact that realistic loading conditions in most applications

typically involve non-constant amplitude loading. As a result, additional loading variables, including level of mean force (or mean deformation), presence of periodic overloading, and load interaction/sequence, etc., should be taken into consideration in analysis and design of these structures and components.

To circumvent the high cost and time-consuming nature of realistic loading experiments, a number of laboratory test methods have been developed to simulate non-constant amplitude service histories. Among them, block testing with multiple high-low and low-high sequences has been widely utilized to obtain the effects of load history and sequence on the material's mechanical behavior under cyclic loading [30]. However, in spite of the growing use of polymers in structural applications, very few studies involving fatigue testing with block loading on polymers have been conducted. Eftekhari et al. [58] performed load-controlled two-block cyclic tests with both zero and nonzero mean stresses to evaluate the effects of load sequence and periodic overload histories on notched and un-notched polypropylene (PP) polymer specimens. They concluded that, similar to the observation for metals, less detrimental effect on fatigue life of both types of PP specimens was observed for low-high loading as compared to high-low loading. In addition, a factor of 2.5 reduction in fatigue life was reported for PP in presence of periodic overload.

The objective of this study is to experimentally investigate the effects of mean strain, frequency, as well as load history and sequence on the fatigue behavior of a thermoplastic polymer subjected to block loading. The material of interest in this study is polyether ether ketone (PEEK), an engineering grade, high

performance polymer. PEEK thermoplastic has gained popularity in various structural and nonstructural applications due to its highly stable chemical structure that results in exceptional chemical, high temperature, and hydrolysis resistance [59]. Furthermore, PEEK polymer possesses processing versatility, allowing parts to be manufactured by various techniques, such as extrusion, compression molding, injection molding, thermoforming [60], or additive manufacturing [61]. Common applications that utilize PEEK polymer include aerospace, automotive, oil and gas, and biomedical [60].

In this study, the fatigue behavior of PEEK polymer is evaluated under different types of strain-controlled multi-block cyclic loading. The loading conditions examined in this study include (1) fully-reversed (ratios of minimum to maximum strain, R_ε, of -1) two, three-, and four-block loadings with adjusted frequencies to maintain a nominal temperature rise on the specimen gage surface, (2) fully-reversed two-block loading to study the frequency effect, and (3) pulsating tension ($R_\varepsilon = 0$) two-block loading to investigate the effect of pre-loading in presence of mean strain/stress. The experimental program, entailing the material, specimen geometry, and test procedure, is presented. The experimental results regarding the effects of load sequence on cyclic deformation and fatigue life of PEEK with various strain ratios and test frequencies are given and discussed, followed by conclusions and recommendations.

4.3 Material and Experimental Procedures

In this study, a series of experiment was performed on unfilled PEEK polymer (TECAPEEK™ by Ensinger Inc.) with a glass transition and melt temperatures of 143°C and 343°C, respectively. To prepare the fatigue specimens, extruded PEEK rod was machined to round specimens with uniform gage section of 6.35 mm in diameter and 18 mm in length, using an oil based coolant to minimize heat buildup on specimens. The dimensions and geometry of the specimens were designed in accordance to ASTM E606-04 standard [16] and can be found in [53]. The specimens were further polished to achieve an average surface finish of 3.4 µm in the gage section.

Fatigue tests were conducted in conformance to ASTM D7791-12 standard [21] at ambient laboratory temperature (~23ºC) with relative humidity of ~45%. All tests were performed using an MTS closed-loop servo-hydraulic load frame with a 25 kN load cell. A mechanical extensometer with 15 mm gage length and sinusoidal waveform was utilized. Runout tests were stopped at 10^6 cycles. In addition, the surface temperature of the specimens' gage section was monitored using a portable laser thermometer. The purpose of the temperature monitoring throughout testing was to ensure that specimens underwent mechanical failure and not the failure due to excessive temperature rise on the specimen during cycling (i.e. self-heating), resulting from inherent high damping and low thermal conductivity characteristics of polymers. Such failure due to self-heating in PEEK polymer under cyclic loading has been reported in [62, 63].

PEEK specimens were subjected to strain-controlled low-high (L-H) and high-low (H-L) block loading at R_ε values of -1 and 0. Two sets of experiments were conducted under R_ε = -1 test condition. Experiments were first performed using the frequencies at each level that were similar to those used in [42], which were selected to maintain a nominal temperature rise on the specimen surface, ΔT, in fully-reversed constant amplitude fatigue tests. Therefore, any tests conducted using these frequencies will be referred to as "tests with nominal temperature rise" throughout this paper. The second set of block loading fatigue tests with R_ε = -1 were conducted using various frequencies to study the effect of test frequency on PEEK specimens under block loading. The applied frequencies for these tests are identical to those conducted in [42], which were used to study the effect of test frequency on fatigue behavior for PEEK subjected to constant amplitude fully-reversed cyclic loading. For R_ε = 0 test condition, the applied frequencies at each strain amplitude level were similar to those used for constant amplitude tests with mean strains in [53].

The number of cycles applied in the first loading block was approximately equal to half of the average fatigue lives at the same level that was reported in [42, 53]. Following the initial loading, the specimens were subjected to subsequent loading block until failure. In R_ε = -1 tests, 0.02 or 0.03 mm/mm was selected as the lower strain amplitude and 0.04 mm/mm was taken as the higher strain amplitude. Similarly, for tests with R_ε = 0, 0.02 and 0.03 mm/mm were taken as the lower and higher strain amplitudes, respectively.

The strain histories for fatigue tests with two-block loading (i.e. L-H and H-L) with R_ε = -1 are presented in Figs. 4.1(a) and 4.1(b), respectively. Similar strain histories with zero minimum strain were used for two-block loading fatigue tests at R_ε = 0 condition. Additionally, three- and four-block loading tests with R_ε = -1 were also conducted to further study the fatigue behavior and cyclic deformation of PEEK under zero mean strain, multi-block loading. The L-H-L and H-L-H strain histories for three-block loading tests are illustrated in Figs. 4.1(c) and 4.1(d), respectively, while the four-block loading, H-L-H-L, is displayed in Fig. 4.1(e).

4.4 Experimental Results and Discussions

The effect of loading sequence on cyclic deformation and fatigue behavior of PEEK specimens subjected to multi-block loading is presented in this section. In addition, mean strain and frequency effects on cyclic deformation and fatigue behavior of PEEK under multi-block loading are discussed.

4.4.1 Fully-Reversed Block Loading with Nominal Temperature Rise

The results obtained from the two-block loading fatigue tests under fully-reversed strain cycles, using the frequencies similar to those presented in an earlier work [42] or the constant amplitude conditions, are summarized in Table 4.1. The data in Table 4.1 include the strain amplitude, ε_a, cyclic frequency, f, temperature rise on the specimen gage surface, ΔT, and reversals to failure, $2N_f$. The stress amplitude, σ_a, and mean stress, σ_m, values obtained at half-life cycle (i.e. stabilized cycle) are also given in this table. It should be reminded that test frequencies employed for these tests were selected to maintain a similar nominal temperature

rise on the gage section of the specimen, ΔT. In Table 4.1, the test data associated to the first and second loading blocks are denoted by subscripts 1 and 2, respectively.

The stress response for tests with H-L loading for specimen S105 and L-H loading for specimen S109 from Table 4.1 are presented in Figs. 4.2 and 4.3, respectively. Fully-reversed strain amplitude of 0.04 mm/mm at 0.5 Hz was taken as the high load and fully-reversed strain amplitude of 0.03 mm/mm at 0.75 Hz was chosen as the low load. As expected, cyclic stress responses in the first loading block for both H-L (first 6,000 reversals) and L-H (first 100,000 reversals) loadings, shown in Figs. 4.2(a) and 4.3(a), were similar to those observed in [42] for the fully-reversed constant amplitude cyclic tests at the same strain amplitude and frequency, where distinct stages of stress responses, including initial, transition, and cyclic stability were observed.

Furthermore, the stress response of the second loading block is compared to that obtained from the test conducted using an identical strain amplitude and frequency, but without pre-loading in [42]. This can be seen in Figs. 4.2(b) and 4.2(c) for H-L loading (specimen S105), and Figs. 4.3(b) and 4.3(c) for L-H loading (specimen S109). By comparing Figs. 4.2(b) and 4.2(c), it can be noticed that the stress response of specimen S105 in the second loading block did not distinctly display the initial stage of cyclic softening and immediately decreased upon cycling into transition stage. Similar behavior can be also seen for specimen S109 with L-H loading, as illustrated in Fig. 4.3(b). Overall, higher stress amplitudes (~ 15% higher) at the initial cycles of the specimens without pre-loading were observed as

compared to those with pre-loading. It has been reported that the duration of the initial region of cyclic softening for polymers significantly depends on the initial state of material microstructure as well as the applied strain/stress amplitude [27]. During the initial stage of cyclic softening, some molecular rearrangement may occur which can cause the movement and formation of mobile defects (i.e. voids) in polymeric materials. The materials will begin to soften (i.e. enter the transition stage of cyclic softening) when the mobile defect population reaches its critical value.

Some polymers, such as nylon and acrylonitrile butadiene styrene, do not exhibit an initial stage of cyclic softening under constant amplitude cyclic loading, which is believed to be associated to the presence of a larger mobile defect population in the initial material state [27]. As a result, an absence of the initial stage of cyclic softening in PEEK specimens with pre-loading may be explained by an increased mobile defects as compared to the virgin material. However, despite the differences in the initial cyclic deformation, the stress response of PEEK specimens with pre-loading irrespective of loading sequence (i.e. L-H or H-L) was stabilized at approximately the same loading cycle as the specimens without pre-loading. Furthermore, the pre-loading effect on the stress amplitude at the cyclic stability region was not noticeable.

Fatigue lives obtained from the second loading block (i.e. data in Table 1) were compared to the experimental results from the constant amplitude fully reversed tests (i.e. without any pre-loading) with nominal temperature rise [42], as presented in Fig. 4.4. Numbers in this figure represents the number of data points

lie on top of each other. Although the damage caused by the first loading block is approximated to be 50% of the overall fatigue tolerance of the material, PEEK specimens exhibited significantly longer fatigue lives by pre-loading with either lower or higher strain amplitudes, when compared to those without any pre-loading. For example, the average fatigue life for specimens subjected to 0.04 mm/mm at 0.5 Hz without pre-loading was 13,464 reversals [42], while the average fatigue life for PEEK specimens under fully-reversed 0.04 mm/mm strain amplitude (specimens S103, S109, and S106 in Table 4.1) increased to 45,585 reversals after being subjected to a prior loading block of 0.03 mm/mm strain amplitude for 100,000 reversals. Similarly, in the case of 0.03 mm/mm at 0.75 Hz, the average fatigue life (specimens S105, S102, and S108) increased from 152,927 reversals without pre-loading [42] to 389,495 reversals when a loading block with strain amplitude of 0.04 mm/mm was first applied for 6,000 reversals.

Although some compressive mean stresses are noticeable in two-block loading tests in Table 4.1, PEEK specimens under constant amplitude loading also exhibited some compressive mean stresses, but at slightly less values [42]. Furthermore, while specimen S123 in Table 4.1 exhibited a tensile mean stress at half-life cycle, it had a longer fatigue life (>2,000,000 reversals) than specimen S101 (1,370,000 reversals) with some compressive mean stress. Therefore, the presence of compressive mean stress may not be the main contributor to the increased fatigue resistance observed in PEEK thermoplastic when subjected to pre-loading.

Under cyclic loading, polymeric materials may experience some microstructural rearrangements that consist of the realignments and entanglements of individual polymer molecules, leading to a molecular directional hardening [10]. A small increase (~ 1%) in density for polycarbonate and nylon polymers was reported after being subjected to fully-reversed strain-controlled cyclic loading at room temperature [64]. Hence, a decrease in the material's internal free volume may possibly affect the fatigue behavior of PEEK with pre-loading. Further microstructural investigations, however, are needed to better understand the mechanisms involved in the fatigue failure of PEEK polymer with and without pre-loading.

The next set of fatigue experiment with nominal temperature rise was conducted using three- (H-L-H and L-H-L) and four-block (H-L-H-L) loadings with zero mean strain (R_ε = -1). Strain amplitudes of 0.04 mm/mm at 0.5 Hz and 0.03 mm/mm at 0.75 Hz were chosen as the high and low loads, respectively. The experimental details and results for three- and four-block tests are presented in Table 4.2.

The stress response for specimen S126, which was subjected to three-block H-L-H loading is presented in Fig. 4.5. As expected, the overall cyclic deformation for the first two loading blocks shown in Fig. 4.5(a) was similar to that of the specimen with H-L loading (i.e. specimen S105 in Fig. 4.2(a)). Furthermore, the initial stage of cyclic deformation (i.e. the stage with constant stress response prior to transitioning to the cyclic stability stage) was not evident in either the second (Fig. 4.5(b)) or the third (Fig. 4.5(c)) loading blocks. Specimen S126 in the third

loading block (Fig. 4.5(c)) underwent a similar number of cycles (~1,000 reversals) to the specimen without pre-loading before achieving cyclic stability. Minimum effect of pre-loading was also observed on the stabilized mean stress and stress amplitude values in the third loading block, when compared to the cyclic stability stage of fully-reversed constant amplitude 0.04 mm/mm strain amplitude test without pre-loading in [42].

Regardless of the damage caused by the first two blocks in the specimen under three-block loading, which is close to the overall fatigue tolerance of the material, significant increase in the number of reversals to failure of the last loading block was observed for these specimens as compared to those without pre-loading, as illustrated in Fig. 4.4. For example, the average life of PEEK specimens at strain amplitude of 0.03 mm and 0.75 Hz without pre-loading was reported to be 152,927 reversals [42]. However, the number of reversals for the third loading block of specimen S127 increased to 239,800 after pre-loading by two-block loading of 100,000 reversals at 0.03 mm/mm strain amplitude and 20,000 reversals at 0.04 mm/mm strain amplitude. Similar improvement in fatigue life under 0.04 mm/mm fully-reversed strain amplitude at 0.5 Hz from 13,464 without pre-loading [42] to 44,098 reversals after two-block of H-L pre-loading was observed for specimen S126 in Table 4.2.

Similarly, despite the fact that the overall cumulative damage exceeds 100% of the material's fatigue tolerance based on the constant amplitude case, the beneficial effect of pre-loading on PEEK fatigue life in the last loading block was observed for the specimen subjected to four-block loading. This can be seen for the

specimen tested at the strain amplitude of 0.03 mm/mm at 0.75 Hz under fully-reversed condition, where an increase in fatigue life from 153,927 reversals without pre-loading [42] to 237,786 reversals after three-block of H-L-H pre-loading for specimen S128 in Table 4.2 was obtained. Again, it should be emphasized that further investigations at lower-length scales are needed to understand the mechanisms involved in fatigue failure of polymers to explain the beneficial effects of pre-loading on fatigue resistance of PEEK.

4.4.2 Fully-Reversed Block Loading to Study Frequency Effects

Table 4.3 contains the experimental results from the fully-reversed fatigue tests under two-block loading with frequencies lower than those used in the previous test conditions (i.e. data in Table 4.1). The stress response of specimen S114 in Table 4.3 under H-L loading sequence is shown in Fig. 4.6(a). For this test, 0.04 mm/mm strain amplitude at 0.25 Hz was considered as the high load and 0.03 mm/mm strain amplitude at 0.5 Hz was taken as the low load. When comparing the stress response for the first loading block (first 2,000 reversals) of specimen S114 to that of specimen 105 (first 6,000 reversals with ε_a= 0.04 mm/mm and f = 0.5 Hz) in Fig. 4.2(a), the stress amplitudes in the initial region of cyclic response are comparable, while slightly higher stress amplitude (~ 23% higher) in the stabilized cyclic region was observed for specimen S114 with lower frequency. Such observation, where an increase in test frequency resulted in a lower stabilized stress amplitude, was also reported for PEEK polymer in [42].

In addition, the stress responses for the second loading block under H-L test (specimen S114) and constant amplitude test with an identical loading condition

(i.e. 0.03 mm/mm strain amplitude at 0.5 Hz) [42] are presented in Figs. 4.6(b) and 4.6(c), respectively. Again, no initial region of cyclic response was observed for specimen with pre-loading. However, the stress amplitude in the initial cycles for the second loading block (Fig. 4.6(b)) was lower (~ 40%) than that of the specimen without pre-loading (Fig. 4.6(c)). Nonetheless, the stress amplitudes at the cyclic stability region for both cases were observed to be comparable.

Similarly, specimens S111 and S113 in Table 4.3, which were subjected to L-H loading with lower test frequencies, exhibited no initial region of cyclic softening in the second loading block. The initial stress amplitude in the second loading block of these specimens was also much lower than the one for the specimen without pre-loading in [42], while the stress amplitudes at the cyclic stability region were observed to be comparable.

Fatigue lives obtained from the second loading block for specimens listed in Table 4.3 are plotted in Fig. 4.7. The test data under constant amplitude loading at similar strain amplitude and test frequency without pre-loading [42] are also included in this figure. As seen, fatigue lives of the second loading block increased significantly for specimens subjected to pre-loading (i.e. either H-L or L-H) when compared to those under constant amplitude loading. The average fatigue life of PEEK without pre-loading at 0.03 mm/mm strain amplitude and 0.5 Hz was 33,594 reversals [42]. However, when PEEK was first subjected to the prior higher strain amplitude of 0.04 mm/mm at 0.25 Hz, the average fatigue life for the second loading block of specimens S124 and S114 were 191,104 reversals.

Similar increase in fatigue lives were also observed for specimens with pre-loading at a lower strain amplitude. Therefore, it can be concluded that, under uniaxial fully-reversed strain-controlled cyclic loading regardless of the loading frequency, the fatigue behavior of PEEK polymer demonstrates a strong strain history dependence, which needs to be taken into consideration by an appropriate cumulative damage parameter.

In addition, it is worth mentioning that the frequency effect on fatigue behavior of PEEK under fully-reversed constant amplitude loading was observed to be highly dependent on strain level [42]. At smaller strain amplitude (i.e. 0.02 mm/mm), an increase in test frequency led to shorter fatigue lives of PEEK. In contrast, at higher strain amplitudes (i.e. 0.025-0.04 mm/mm), an increase in frequency resulted in longer fatigue lives. In this study, a similar trend of frequency effect on fatigue behavior of PEEK was observed under fully-reversed block loading to the ones under constant amplitude loading at 0.03 and 0.04 mm/mm, where a decrease in frequency reduced the fatigue resistance of this polymer.

4.4.3 Pulsating Tension Block Loading

The results obtained from pulsating tension (R_ε = 0) two-block loading fatigue experiments, using the frequencies similar to those presented in [53] for the constant amplitude conditions with R_ε = 0, are summarized in Table 4.4. For these tests, 0.03 mm/mm strain amplitude at 0.5 Hz and 0.02 mm/mm strain amplitude at 1.5 Hz were taken as the high and low loads, respectively. The overall stress response for specimen S116 under H-L loading in Table 4.4 is presented in Fig. 4.8(a). Additionally, the stress response of the second loading block of specimen

S116 and the stress response of specimen subjected to pulsating tension loading (R_ε = 0) without pre-loading (i.e. constant amplitude condition) at similar strain amplitude and frequency [53], are displayed in Figs. 4.8(b) and 4.8(c), respectively. As seen in Fig. 4.8(b), although there was some compressive mean stress at initial cycles of the second loading block for specimen S116, it gradually relaxed from -22.5 MPa to -1.5 MPa. On the other hand, tensile mean stress (55 MPa) was initially observed in Fig. 4.8(c) for the PEEK specimen without pre-loading prior to becoming stabilized at approximately -5 MPa.

Fully-relaxed mean stresses in Figs. 4.8(b) and 4.8(c) were achieved at similar number of reversals, and stress amplitudes at the cyclic stability region in both specimens were also comparable. Similar behavior was observed for all the specimens under pulsating tension L-H loading condition in Table 4.4.

The strain-life fatigue data of the second loading block from block loading tests with R_ε = 0 (i.e. specimens in Table 4.4), as well as the fatigue data for constant amplitude pulsating tension (R_ε = 0) loadings in [53], are compared in Fig. 4.9. As seen, the pre-loading minimally affected fatigue life of PEEK and generally resulted in slightly shorter lives when compared to those without pre-loading. For example, specimen S116 in Table 4.4 failed at 645,088 reversals after pre-loading with a higher strain amplitude for 60,000 reversals. The number of reversals to failure of specimen S116 is similar to the average fatigue life of specimens subjected to pulsating tension constant amplitude loading with ε_a = 0.02 mm/mm without pre-loading, which was reported to be 682,324 reversals in [53]. Therefore, the significant beneficial effect of pre-loading on fatigue lives was primarily

observed for the specimens under fully-reversed cyclic loading and not pulsating tension loading.

4.5 Conclusions

A series of uniaxial strain-controlled cyclic tests under various multi-block loading conditions were employed in this study to investigate the load sequence effects on fatigue behavior of a neat PEEK thermoplastic. The fatigue tests conducted in this study include multi-block fully-reversed loading with various frequencies and multi-block loading with mean strains. Based on the experimental results, the following conclusions and recommendations can be made:

1. In general, PEEK specimens with fully-reversed (R_ε = -1) pre-loading (with higher or lower strain amplitude) did not exhibit the initial stage of cyclic softening. The cyclic stability of the pre-loaded specimens was achieved at approximately the same reversals as those without pre-loading under identical test condition. Furthermore, the stress amplitudes at the cyclic stability region were also comparable. Such cyclic deformation behavior was observed for all specimens under two-, three-, or four-block loading with R_ε = -1.

2. Pre-loading for specimens under fully-reversed (Rε = -1) condition was found to have a significant beneficial effect on PEEK fatigue resistance irrespective to the load sequence (i.e. high-low or low-high).

3. Similar to fatigue tests without pre-loading for higher strain amplitudes (i.e. $\varepsilon_a \geq 0.025$ mm/mm), increasing the test frequency resulted in longer fatigue lives in both low-high and high-low loading block tests.

4. Load history and sequence minimally affected fatigue behavior of PEEK under pulsating tension condition ($R\varepsilon = 0$). Only some slight decreases in fatigue lives of specimens under block-loading (high-low or low-high with $R\varepsilon = 0$) were observed as compared to those under constant amplitude loading.

5. The experimental results in this study revealed a distinctive fatigue behavior of PEEK under multi-block loading. However, due to the unavailability of published studies in polymer fatigue involving both upper-length scale non-constant (i.e. variable) amplitude loading and lower-length scale micro/nanostructure analysis, the mechanisms causing such behaviors are not fully realized. Therefore, there is a need for further fatigue related multi-scale studies to better understand the underlying fatigue damage mechanisms of polymers.

While the present work deals with the experimental investigation to obtain the effect of load history and sequence on PEEK fatigue behavior, the knowledge gained based on this study can be used to develop appropriate cumulative fatigue damage models that are essential for life prediction of polymeric components under realistic service loadings.

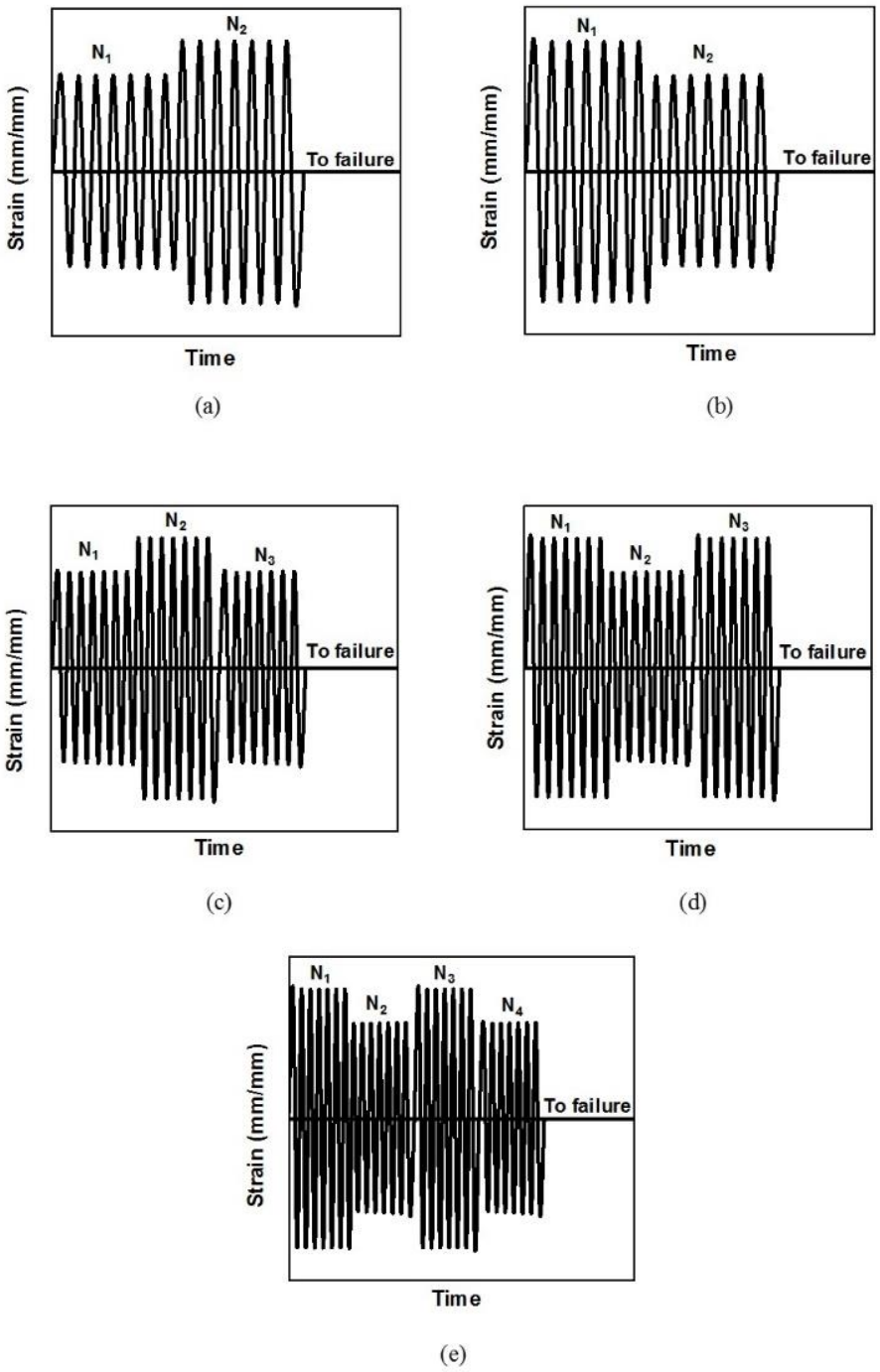

Figure 4.1 Loading history for multi-block loading fatigue tests with R_ε = -1 including (a) two-block L-H, (b) two-block H-L, (c) three block L-H-L, (d) three block H-L-H, and (e) four-block H-L-H-L.

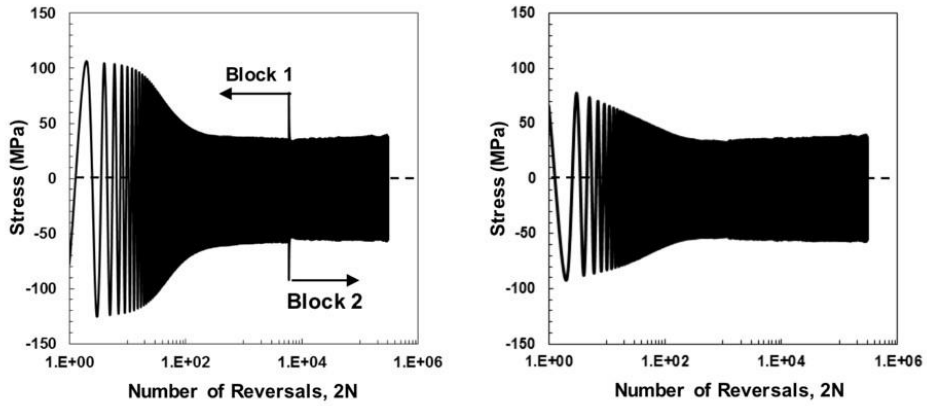

(a) (b)

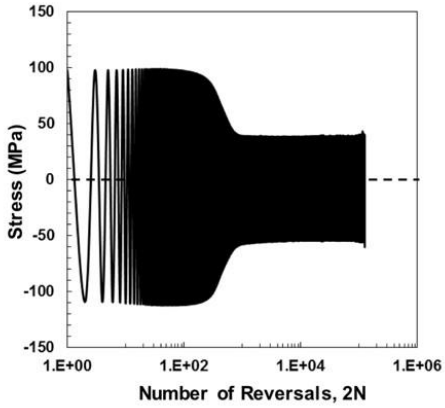

(c)

Figure 4.2 (a) Overall PEEK stress response of specimen S105 subjected to fully-reversed strain-controlled H-L block loading (ε_{a1} = 0.04 mm/mm at 0.5 Hz and ε_{a2} = 0.03 mm/mm at 0.75 Hz), as well as the comparison between the stress responses of (b) the second loading block of specimen S105 and (c) the specimen subjected to constant amplitude loading of 0.03 mm/mm at 0.75 Hz without pre-loading reported in [42].

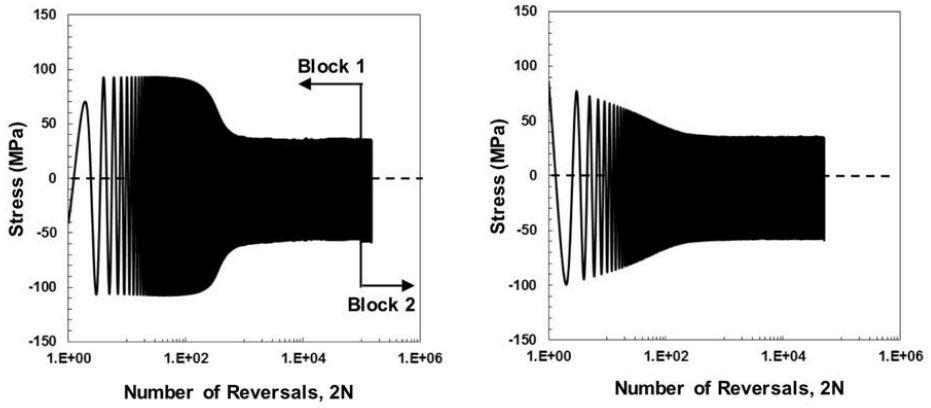

(a) (b)

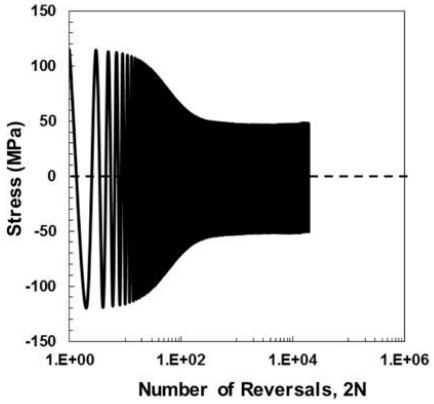

(c)

Figure 4.3 (a) Overall PEEK stress response of specimen S109 subjected to fully-reversed strain-controlled L-H block loading (ε_{a1} = 0.03 mm/mm at 0.75 Hz and ε_{a2} = 0.04 mm/mm at 0.5 Hz), as well as the comparison between the stress responses of (b) the second loading block of specimen S109 and (c) the specimen subjected to constant amplitude loading of 0.04 mm/mm at 0.5 Hz without pre-loading, reported in [42].

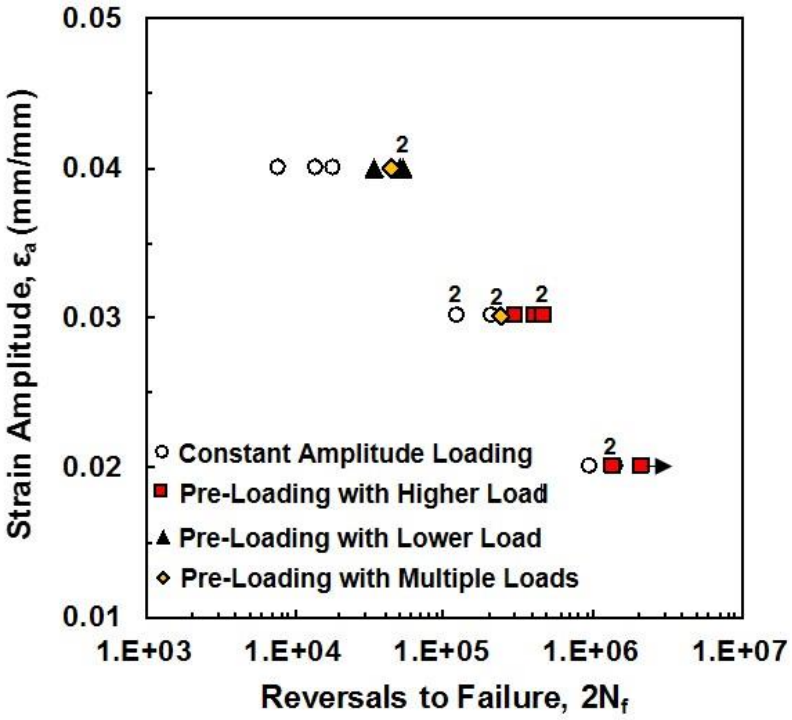

Figure 4.4 Comparison of fatigue lives obtained from the last loading block for two- (Table 4.1), three-, and four-block loading tests (Table 4.2) along with the fatigue results from the fully-reversed constant amplitude strain-controlled tests without any pre-loading [42], all with nominal temperature rise.

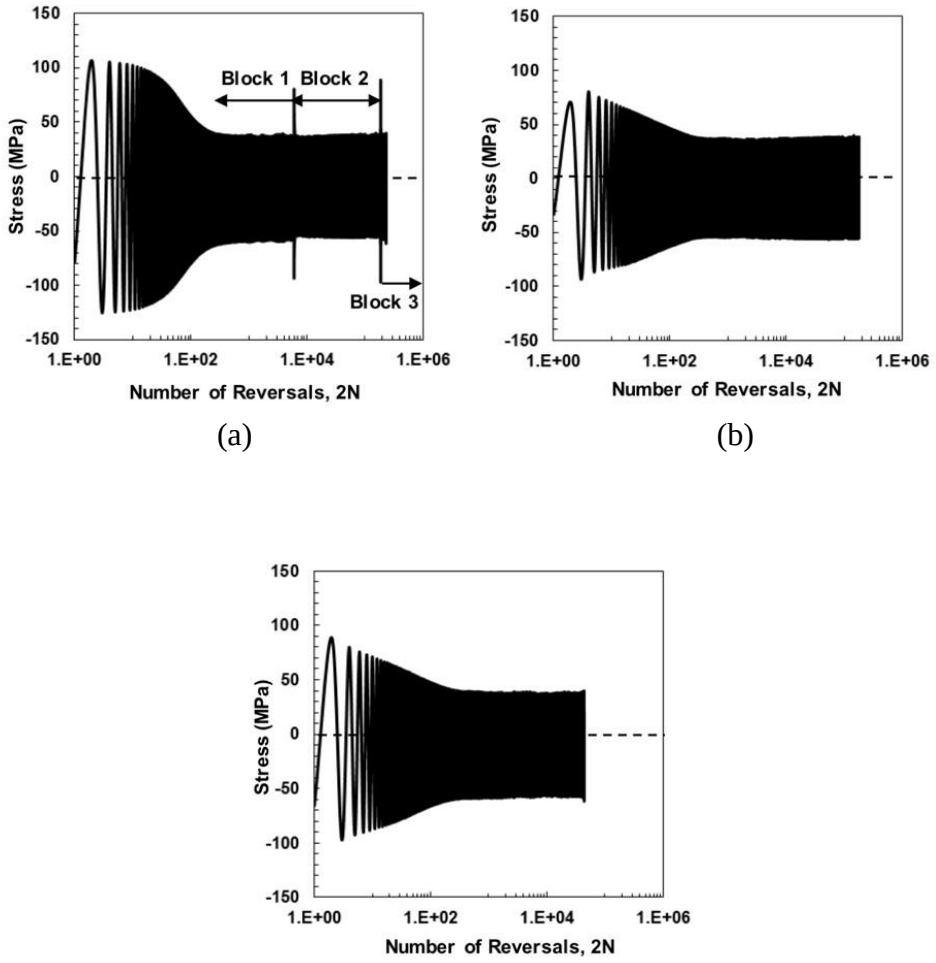

Figure 4.5 (a) Overall PEEK stress response of specimen S126 subjected to fully-reversed strain-controlled H-L-H block loading (ε_{a1}= 0.04 mm/mm at 0.5 Hz, and ε_{a2} = 0.03 mm/mm at 0.75 Hz, ε_{a3} = 0.04 mm/mm at 0.5 Hz), as well as the stress response of (b) the second loading block at ε_a = 0.03 mm/mm, 0.75 Hz, and (c) the third loading block at ε_a = 0.04 mm/mm, 0.5 Hz.

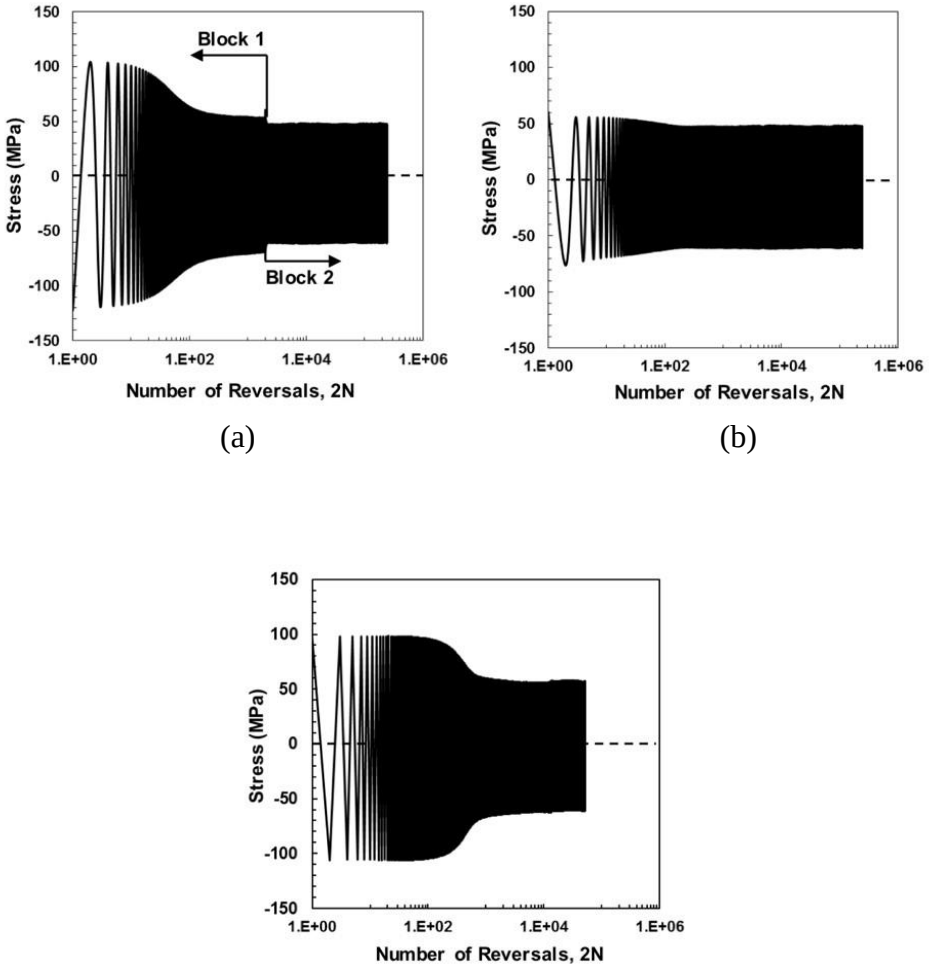

Figure 4.6 (a) Overall PEEK stress response of specimen S114 subjected to fully-reversed strain-controlled H-L block loading (ε_{a1}= 0.04 mm/mm at 0.25 Hz, and ε_{a2} = 0.03 mm/mm at 0.5 Hz), as well as the comparison between the stress responses of (b) the second loading block of specimen S114 and (c) the specimen subjected to constant amplitude loading of 0.03 mm/mm at 0.5 Hz without pre-loading, reported in [42].

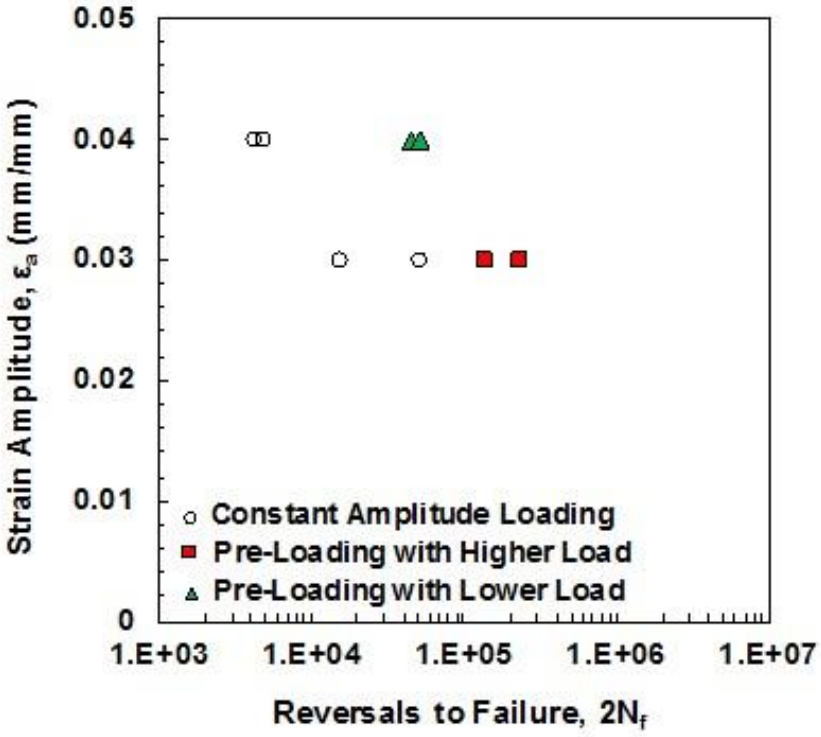

Figure 4.7 Comparison of fatigue lives obtained from the second loading block of H-L and L-H tests (Table 4.3) with the fatigue results from the fully-reversed constant amplitude strain-controlled tests without pre-loading [42], both from the frequency effect study.

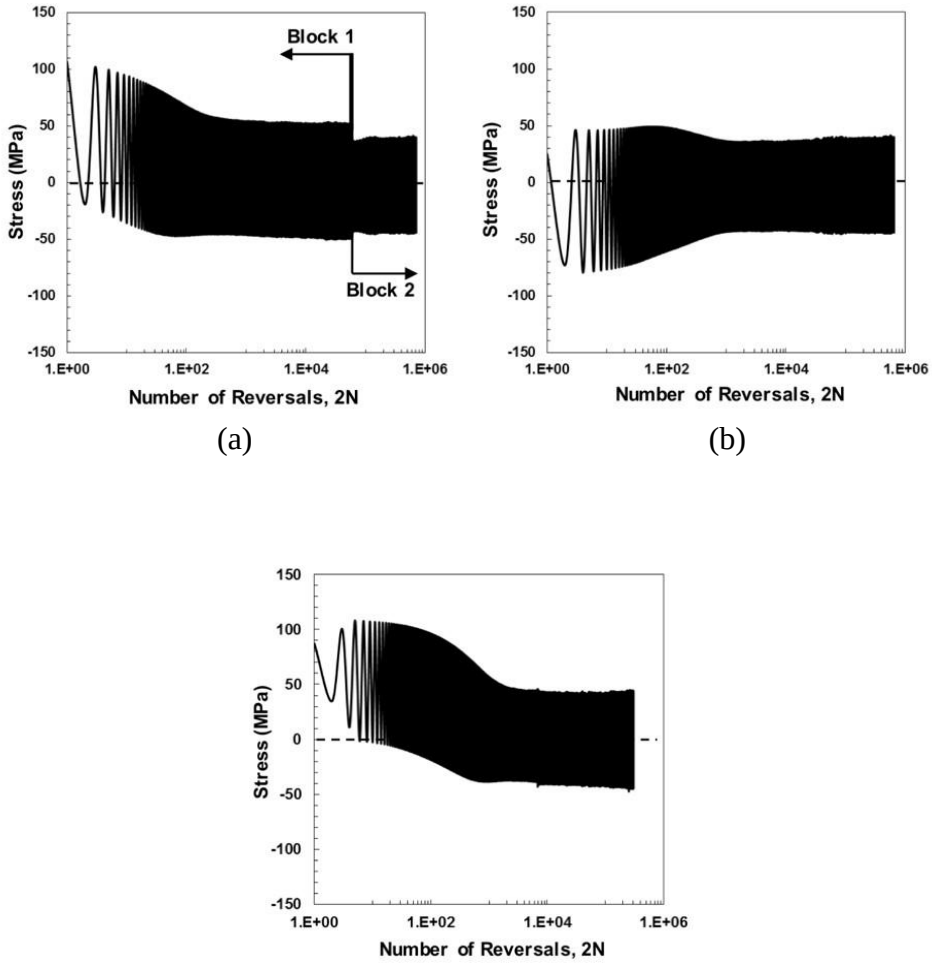

Figure 4.8 (a) Overall PEEK stress response of specimen S116 subjected to strain-controlled H-L block loading with mean strain, $R_\varepsilon = 0$ (ε_{a1}= 0.03 mm/mm at 0.5 Hz, and ε_{a2} = 0.02 mm/mm at 1.5 Hz), as well as the comparison between the stress responses of (b) the second loading block of specimen S116 and (c) the specimen subjected to constant amplitude loading of 0.02 mm/mm at 1.5 Hz with $R_\varepsilon = 0$ without pre-loading in [53].

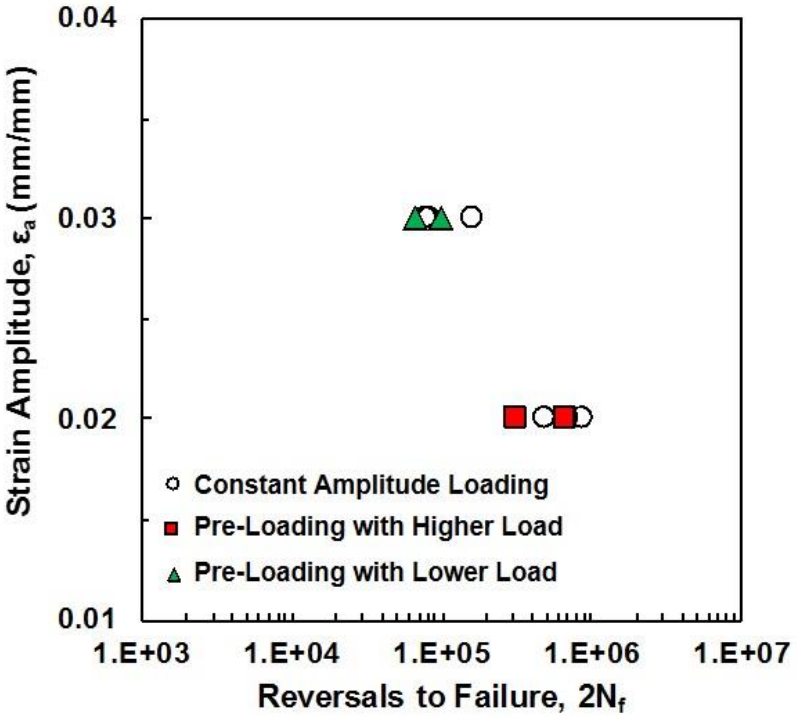

Figure 4.9 Comparison of fatigue lives obtained from the second loading block of H-L and L-H tests with $R_\varepsilon = 0$ (Table 4.4) with the fatigue results from the constant amplitude pulsating tensile loading tests ($R_\varepsilon = 0$) without pre-loading [53].

Table 4.1 Experimental results for uniaxial fully-reversed (R_ε = -1) strain-controlled fatigue tests of PEEK with two-block loading with adjusted frequencies to maintain a nominal temperature rise on the specimens.

Specimen ID	$\boldsymbol{\varepsilon_{a1}/\varepsilon_{a2}}$ **(mm/mm)**	$\boldsymbol{f_1/f_2}$ **(Hz)**	$\boldsymbol{\Delta T_1/\Delta T_2}$ **(°C)**	$\boldsymbol{2N_1/2N_2}$ **(Reversals)**	$\boldsymbol{\sigma_{a1}/\sigma_{a2}}^*$ **(MPa)**	$\boldsymbol{\sigma_{m1}/\sigma_{m2}}^*$ **(MPa)**
High-Low						
S123	0.04/0.02	0.5/3	20/36	6,000/2,130,352#	49/30	14/16
S101			31/37	6,000/1,371,616	47/30	-12/-9
S105	0.04/0.03	0.5/0.75	26/28	6,000/296,276	49/47	-11/-9
S102			28/27	6,000/412,318	47/47	-12/-10
S108			31/30	6,000/459,890	51/49	-12/-10
Low-High						
S103	0.03/0.04	0.75/0.5	27/31	100,000/33,542	51/51	-10/-11
S109			29/31	100,000/50,136	47/48	-10/-11
S106			22/29	100,000/53,076	50/49	-10/-11

*Measured at half-life cycle

Runout test

Table 4.2 Experimental results for uniaxial fully-reversed (R_ε = -1) strain-controlled fatigue tests of PEEK with three- and four-block loadings with adjusted frequencies to maintain a nominal temperature rise on the specimens.

Specimen ID	**$\varepsilon_{a1}/\varepsilon_{a2}/\varepsilon_{a3}$ (mm/mm)**	**$f_1/f_2/f_3$ (Hz)**	**$\Delta T_1/\Delta T_2/\Delta T_3$ (°C)**	**$2N_1/2N_2/2N_3$ (Reversals)**	**$\sigma_{a1}/\sigma_{a2}/\sigma_{a3}$* (MPa)**	**$\sigma_{m1}/\sigma_{m2}/\sigma_{m3}$* (MPa)**
High-Low-High						
S126	0.04	0.5	22	6,000	51	-11
	0.03	0.75	26	180,000	47	-9
	0.04	0.5	21	44,098	59	10
Low-High-Low						
S127	0.03	0.75	30	100,000	47	-7
	0.04	0.5	32	20,000	48	-9
	0.03	0.75	31	239,800	46	-10
Specimen ID	**$\varepsilon_{a1}/\varepsilon_{a2}/\varepsilon_{a3}/\varepsilon_{a4}$ (mm/mm)**	**$f_1/f_2/f_3/f_4$ (Hz)**	**$\Delta T_1/\Delta T_2/\Delta T_3/\Delta T_4$ (°C)**	**$2N_1/2N_2/2N_3/2N_4$ (Reversals)**	**$\sigma_{a1}/\sigma_{a2}/\sigma_{a3}/\sigma_{a4}$* (MPa)**	**$\sigma_{m1}/\sigma_{m2}/\sigma_{m3}/\sigma_{m4}$* (MPa)**
High-Low-High-Low						
S128	0.04	0.5	26	6,000	47	-10
	0.03	0.75	26	180,000	46	-8
	0.04	0.5	31	20,000	48	-8
	0.03	0.75	29	237,786	47	-6

*Measured at half-life cycle

Table 4.3 Experimental results for uniaxial fully-reversed (R_ε = -1) strain-controlled fatigue tests of PEEK with two-block loading for frequency effect study.

Specimen ID	$\varepsilon_{a1}/\varepsilon_{a2}$ (mm/mm)	f_1/f_2 (Hz)	$\Delta T_1/\Delta T_2$ (°C)	$2N_1/2N_2$ (Reversals)	σ_{a1}/σ_{a2}* (MPa)	σ_{m1}/σ_{m2}* (MPa)
High-Low						
S124	0.04/0.03	0.25/0.5	9/15	2,000/140,582	64/55	14/15
S114			37/30	2,000/241,626	64/55	-8/-7
Low-High						
S111	0.03/0.04	0.5/0.25	17/14	30,000/46,000	54/61	-10/-11
S113			17/14	30,000/53,434	55/61	-7/-7

*Measured at half-life cycle

Table 4.4 Experimental results for uniaxial pulsating tension (R_ε = 0) strain-controlled fatigue tests of PEEK with two-block loading.

Specimen ID	**$\varepsilon_{a1}/\varepsilon_{a2}$ (mm/mm)**	**f_1/f_2 (Hz)**	**$\Delta T_1/\Delta T_2$ (°C)**	**$2N_1/2N_2$ (Reversals)**	**σ_{a1}/σ_{a2}* (MPa)**	**σ_{m1}/σ_{m2}* (MPa)**
High-Low						
S120	0.03/0.02	0.5/1.5	14/16	60,000/312,756	55/44	24/19
S116			21/31	60,000/645,088	52/42	1/-3
Low-High						
S121	0.02/0.03	1.5/0.5	20/18	300,000/65,032	45/54	24/24
S118			26/31	300,000/99,310	44/53	-0.2/1

*Measured at half-life cycle

CHAPTER 5 FATIGUE MODELING OF POLYETHER ETHER KETONE (PEEK) UNDER MEAN STRAIN AND MULTI-BLOCK LOADINGS

(International Journal of Fatigue, 2017, 100, 429-443)

5.1 Abstract

The applicability of several fatigue damage models for polyether ether ketone (PEEK) under mean strain and variable amplitude multi-block loadings is evaluated. The models utilized in this study are assessed against experimental data for PEEK under various cyclic loading conditions, including (1) constant amplitude loading with non-zero mean strains, (2) two-block loading with zero and non-zero mean strains, and (3) three- and four-block loading with zero mean strain. Several fatigue models, including a strain based, a strain-stress based, and an energy based, are employed to correct for the effect of mean strain and stress on fatigue behavior of PEEK. Among these models, the energy based approach, which considers the deformation response of the material throughout its entire life, better correlates the PEEK experimental data in the presence of mean strain. For specimens under block loading, three different damage accumulation models are employed to evaluate their applicability for PEEK. These include the Linear Damage Rule, as well as the non-linear Damage Curve Approach and Hashin-Rotem model. Additionally, a Direct Cumulative Damage (DCD) approach using an energy based parameter is also employed to account for the load history and sequence effect on PEEK fatigue behavior. The DCD method is found to provide acceptable fatigue life predictions for PEEK under multi-block loading with various strain ratios and frequencies.

5.2 Introduction

Polyether ether ketone (PEEK), a high-performance thermoplastic polymer, has been widely used in various applications, such as aerospace, automotive, and biomedical, due to its excellent mechanical properties, high dimensional stability, as well as good chemical and wear resistance. In addition to being commonly used in bearing and sealing applications, PEEK is being increasingly adopted as an alternative implant material, considering its acceptable resistance to damage from hydrolysis, radiation, and lipid exposure (i.e. *in vivo* degradation) [2].

The mechanical properties of PEEK can also be tailored, enabling the material to be conformed to specific requirements of a given application. For example, the modulus of elasticity of PEEK can be altered to closely match that of cortical bones by reinforcing the material with carbon fiber, allowing more uniform stress distribution between the bone and the implant material [65]. Successful clinical studies of PEEK have been reported for dental implants [66] and spinal cages used in cervical spinal fusion [67], while there is also a growing interest in a number of PEEK-based orthopedic components, such as fracture fixation plate [68] and hip joint endoprosthesis [2].

Despite the increasing demand for polymer-based components in aforementioned applications, there are only a limited number of works [13-15, 18, 33, 69] related to the mechanical behavior of polymers under cyclic (fatigue) loading. Additionally, cyclic loading under realistic service conditions is generally complex in nature and seldom involves constant amplitude cycles. Therefore, the effects of loading history and sequence, resulting from the changes in stress/strain amplitude, stress/strain ratio, test frequency, etc., on cyclic deformation and fatigue life must be considered in a component design. The

damage accumulated in a material under such loading should also be carefully quantified using appropriate and reliable methodologies.

Considerable efforts have been made in the past decades to develop cumulative fatigue damage and life prediction models for metals and their alloys as discussed in a comprehensive review paper by Fatemi and Yang [70]. However, despite the growing use of polymers, not many studies regarding the cumulative fatigue damage of neat (unfilled) polymers can be found in the literature, and their fatigue behavior under non-constant (i.e. variable) amplitude cyclic loading is not yet fully understood. Nonetheless, a number of experimental studies have indicated that fatigue and fracture behavior of polymer matrix composites (PMCs) are generally governed by micro-mechanical response of the matrix material and its interface with reinforcing fillers [71]. Therefore, the damage process in PMCs under cyclic loading typically initiates from cracks in the polymer matrix [8].

The Palmgren-Miner Linear Damage Rule (also referred to as LDR or Miner's rule) has been commonly used to quantify the cumulative fatigue damage in PMCs. In [72], a series of tension-tension load-controlled fatigue tests using high-low (H-L) and low-high (L-H) block loading were conducted on short glass fiber-reinforced styrene maleic anhydride. The data was analyzed using the LDR, expressed by Eq. (5.1) [72].

$$D = \sum \frac{N_i}{N_{f_i}} \tag{5.1}$$

where D is the cumulative damage or the sum of all damage induced in the specimen from each cycle. In Eq. (5.1), N_i is the number of cycles at a stress level of i and N_{f_i} is the total number of cycles to failure at the same stress level, which is obtained from the stress-life (S-N) curve under constant amplitude load-controlled test. The LDR predicts failure when

the value of D approaches unity. Using Eq. (5.1), cumulative damage values ranging from 0.40 to 1.14 were obtained for all tests in [72].

The fatigue process in short fiber reinforced composites can also be described as a two-stage process as defined in [73]. The fatigue damage in the first stage concentrated near the fiber's end and caused the crack propagation up to approximately 1 mm in the material. The process in the second stage, where the fatigue damage is concentrated at the crack tip, resulted in crack length from 1 mm to final fracture. As a result, a two-stage LDR was proposed by combining the damage induced in each stage using the LDR, and validated for short carbon fiber-reinforced PEEK under rotating-bending cyclic block loading [73].

Zago and colleagues [74, 75] proposed a non-linear cumulative damage model for short glass fiber-reinforced copolyamide subjected to block loading that consisted of random load cycles. Moreover, a cumulative damage rule using the residual strength as the damage parameter was introduced by Yao and Himmel [76], and validated for glass/epoxy cross-ply laminates and carbon fiber-reinforced composites.

Due to its simplicity, the LDR is still commonly used to determine fatigue damage accumulation under variable amplitude loading conditions. As previously discussed, reasonable cumulative damage predictions for different types of PMCs were obtained utilizing original [72] and modified [73-76] LDRs. On the other hand, it has been recently shown that the energy based fatigue models provide satisfactory life predictions for PEEK under various uniaxial strain-controlled constant amplitude loadings [42]. Therefore, a cumulative damage approach with an energy based damage parameter may provide

reasonable fatigue life predictions for PEEK under block loading (or variable amplitude loading).

In this study, an analytical investigation is carried out to obtain appropriate fatigue life prediction models for PEEK polymer subjected to different cyclic loading conditions based on the experimental results presented in the previous studies [53, 77, 78], where neat PEEK polymer was subjected to a series of cyclic loadings, including constant amplitude loading with non-zero mean strains, and multi-block (two-, three-, and four-block) loading with various strain ratios and frequencies. In the present study, a strain based model, a strain-stress based model, and an energy based fatigue model are employed to predict fatigue lives for PEEK polymer under constant amplitude loading with non-zero mean strains. For block loading fatigue tests, the LDR and several established non-linear cumulative damage models, with either strain amplitude or strain energy density as the damage parameter, are utilized to evaluate their applicability for fatigue life predictions for PEEK. Furthermore, an alternative method for cumulative damage prediction utilizing an energy based parameter is employed and validated against experimental data. Finally, some conclusions based on prediction models are presented.

5.3 Fatigue Modeling for Mean Strain Condition

In this section, three types of fatigue models, including the Coffin-Manson model, the Smith-Watson-Topper (SWT) model, and an energy based fatigue model, are used to predict the fatigue behavior of PEEK polymer in the presence of mean strain/stress. The strain based Coffin-Manson model and the strain-stress based SWT model are employed in this study since they have been commonly used in both low and high cycle fatigue for metals. On the other hand, the energy based approach was previously shown to provide

reasonable fatigue life predictions for PEEK under uniaxial fully-reversed strain-controlled cyclic loading at various frequencies [42]; therefore, its capability in predicting fatigue lives of PEEK in the presence of mean strain is also examined here.

The experimental data used in the fatigue life modelling was obtained from the uniaxial strain-controlled cyclic loading tests conducted to study the effects of tensile mean strain on the fatigue behavior of PEEK polymer. The strain-controlled fatigue tests were conducted at R_ε (ratios of minimum to maximum strain) values of 0, 0.2, and 0.3 with strain values ranging from 0 to 0.06 mm/mm. The test frequencies were varied to maintain a nominal rise in temperature throughout all the fatigue tests. A detail description of experimental setup, fatigue data, and the results obtained from the study of effects of tensile mean strain on the fatigue behavior of PEEK are published in [53].

5.3.1 Strain Based Approach

For the strain based Coffin-Manson model, the total strain amplitude, $\frac{\Delta\varepsilon}{2}$, from the stabilized hysteresis loop (i.e. hysteresis loop at half-life) can be separated into elastic and plastic strain components, represented by $\frac{\Delta\boldsymbol{\varepsilon_e}}{\mathbf{2}}$ and $\frac{\Delta\boldsymbol{\varepsilon_p}}{\mathbf{2}}$, respectively. These components at the half-life cycle were determined using Eqs. (5.2) and (5.3), respectively [30].

$$\frac{\Delta\varepsilon_e}{2} = \frac{\Delta\sigma}{2E} \tag{5.2}$$

$$\frac{\Delta\varepsilon_p}{2} = \frac{\Delta\varepsilon}{2} - \frac{\Delta\sigma}{2E} \tag{5.3}$$

where $\frac{\Delta\sigma}{2}$ is the stress amplitude obtained at the half-life cycle and E is the modulus of elasticity. The elastic and plastic strain amplitudes were determined using Eqs. (5.2) and (5.3), based on the experimental data for PEEK under fully-reversed loading (R_ε = -1) with

nominal rise in temperature (i.e. tests with adjusted frequencies to maintain a similar nominal temperature rise on the gage section of the specimen) presented in [42]. These elastic and plastic strain components were plotted against the reversals to failure, $2N_f$, to obtain a linear relationship in log-log scale between each strain component and fatigue life as [30]:

$$\frac{\Delta\varepsilon_e}{2} = \frac{\sigma_f'}{E}(2N_f)^b \tag{5.4}$$

$$\frac{\Delta\varepsilon_p}{2} = \varepsilon_f'(2N_f)^c \tag{5.5}$$

where σ_f', ε_f', b, and c are the fatigue strength coefficient, ductility coefficient, strength exponent, and ductility exponent, respectively. These fatigue parameters were obtained using a linear least square fit method following the ASTM standard E739-10 [34] as reported in [42]. By summing Eqs. (5.4) and (5.5), the total strain amplitude is determined as [30]:

$$\frac{\Delta\varepsilon}{2} = \frac{\Delta\varepsilon_e}{2} + \frac{\Delta\varepsilon_p}{2} = \frac{\sigma_f'}{E}(2N_f)^b + \varepsilon_f'(2N_f)^c \tag{5.6}$$

The experimental results and the Coffin-Manson fit for PEEK polymer under constant amplitude fully-reversed (R_ε = -1) fatigue loading with nominal rise in temperature [42] are displayed in Fig. 5.1(a). In addition, the experimental data for tests with non-zero mean strains (R_ε = 0, 0.2, and 0.25) with nominal temperature rise from the earlier work [53], tabulated in Table 5.1, are also superimposed in this figure. As seen, a reasonable correlation was obtained for all tests with various R_ε values. Additionally, the predicted fatigue lives using the Coffin-Manson model, based on fully-reversed data, were compared to the experimental data for all constant amplitude loading tests with nominal temperature

rise as depicted in Fig. 5.1(b). It can be seen that all the data, except the zero mean strain data at 0.04 mm/mm strain amplitude, are within scatter bands of two with $R^2 = 0.76$.

As displayed in Fig. 5.1(b), the Coffin-Manson model based on zero mean strain ($R_\varepsilon = -1$) test data alone was able to moderately correlate PEEK fatigue lives with non-zero mean strains. Such observation can be attributed to the mean stress relaxation phenomenon as reported by Shrestha et al. [53], in which the presence of tensile mean strains in PEEK resulted in an initial tensile mean stress prior to it becoming fully-relaxed in a relatively short time period as compared to the total life. Despite these facts, it has been demonstrated in [53] that the change in shape and size of hysteresis stress-strain loop throughout various cyclic softening stages (i.e. initial, transition, and cyclic stability) may influence the fatigue life of PEEK polymer. Since the Coffin-Manson model only utilizes the elastic and plastic strain amplitudes at the half-life cycle, it may not be the most suitable fatigue model for PEEK under various strain ratios (zero and non-zero mean strains), as illustrated in Fig. 1(b).

5.3.2 Strain-Stress Based Approach

In the SWT fatigue model, the mean strain/stress effect can be corrected by including the maximum tensile stress, σ_{max}, within the damage parameter as [37]:

$$\varepsilon_a \sigma_{max} = \frac{\left(\sigma_f'\right)^2}{E}(2N_f)^{2b} + \sigma_f'\varepsilon_f'(2N_f)^{b+c} \tag{5.7}$$

where

$$\sigma_{max} = \sigma_m + \sigma_a \tag{5.8}$$

Here, ε_a is the strain amplitude and $2N_f$ is the number of reversals to failure. The mean stress, σ_m, and stress amplitude, σ_a, are obtained from the stabilized hysteresis loop (i.e.

half-life cycle). These stress components for constant amplitude fatigue tests with various tensile mean strains (R_ε = 0, 0.2, and 0.25) and nominal temperature rise [53] are summarized in Table 5.1. The fatigue coefficients and exponents in this model are obtained using Eqs. (5.4) and (5.5) and based on fully-reversed data with nominal temperature rise [42].

The correlation between the SWT damage parameter, $\varepsilon_a\sigma_{max}$ (i.e. the left hand side of Eq. (5.7)), and the corresponding experimentally observed reversals to failure, $2N_f$, for all tests with tensile mean strains (i.e. data in Table 5.1) is displayed in Fig. 5.2(a). The fully-reversed (R_ε = -1) PEEK data with nominal rise in temperature [42] are also included in this figure. Again, the scatter appears to be mostly for the fully-reversed (R_ε = -1) data at 0.04 mm/mm strain amplitude. In Fig. 5.2(b), PEEK fatigue lives are determined using Eq. (5.7), based on fully-reversed data, and plotted against the experimentally observed fatigue lives along with the scatter bands of two. As depicted in Fig. 5.2(b), 12 out of 30 fatigue data for PEEK with zero and non-zero mean strains are outside of the scatter bands. The predicted fatigue lives for specimens with mean strains are generally underestimated (i.e. conservative predictions), while the life predictions for zero mean strain condition using the SWT model are slightly overestimated. A poor correlation indicated by R^2 = 0.65 was obtained using the SWT model, as seen in Fig. 5.2(b).

The presence of the stress component in the fatigue parameter appears to have a detrimental effect on the fatigue life prediction of PEEK, as compared to the strain based model (i.e. the Coffin-Manson model). When plotting σ_{max} versus $2N_f$ for all tests with zero and non-zero mean strains, a large scatter in data was observed, which may explain the inadequacy of the SWT model to capture the mean strain effect for PEEK polymer. In addition, PEEK

exhibited both stress relaxation and cyclic softening under mean strain test condition, resulting in the hysteresis stress-strain loop to evolve, specifically at the beginning of the test [53]. Therefore, the SWT model may not be an appropriate model to account for the mean strain/stress effect on the fatigue behavior of PEEK as it only employs the stress and strain responses at half-life cycle and does not take the variation of cyclic deformation at different stages of the fatigue behavior into account.

5.3.3 Energy Based Approach

The imposed strain energy, resulting from an external loading, can generally be divided into two parts: a recoverable elastic strain energy and an irrecoverable plastic strain energy [38]. The dissipated plastic strain energy density, ΔW^P, is defined by the area of the hysteresis stress-strain loop, while the tensile elastic strain energy density, ΔW^{E+}, is defined here as the positive area under the hysteresis loop. In the energy based approach, the irrecoverable plastic strain energy density, ΔW^P, has been used as a damage parameter for fully-reversed or nearly fully-reversed fatigue tests. However, ΔW^P is generally not sensitive to stress relaxation or ratchetting behavior [38] and may not be suitable for fatigue tests with mean strain/stress. Additionally, for high cycle fatigue tests or tests at small strain amplitudes, ΔW^P becomes very small and may be difficult to calculate. Therefore, the total strain energy density, ΔW^T, which is defined as the sum of tensile elastic and plastic strain energy densities, has been proposed as a damage parameter [79], which can be used for both high cycle and low cycle fatigue [38]. The energy based model with ΔW^T for fatigue life prediction has been successfully employed for various materials under mean strain/stress loading [12, 80].

As the majority of PEEK fatigue lives is spent in the cyclic stability region [42, 53], the total strain energy density calculated at the half-life cycle, ΔW_{HL}^{T}, can be considered as a damage parameter, which is given as:

$$\Delta W_{HL}^{T} = \Delta W_{HL}^{P} + \Delta W_{HL}^{E+} \tag{5.9}$$

where ΔW_{HL}^{P} and ΔW_{HL}^{E+} are the plastic and tensile elastic strain energy densities obtained at the half-life cycle, respectively. These values for constant amplitude fatigue tests with mean strains conducted in [53] were determined by an integration method and listed in Table 5.1.

Figure 5.3(a) presents the data for uniaxial strain-controlled fatigue tests with zero (R_ε = -1) mean strain and nominal temperature rise [42], showing the plot of ΔW_{HL}^{T} versus $2N_f$ and the corresponding power function that was fitted to the data. In addition to the data for fully-reversed test condition, the data of specimens under non-zero mean strains (R_ε = 0, 0.2, 0.25) with nominal temperature rise [53] is also included in this figure. As seen, an acceptable correlation of the fatigue life data is obtained. In Fig. 5.3(b), the predicted fatigue lives using the correlation based on fully-reversed data are plotted against the experimentally observed fatigue lives. All fatigue lives under cyclic loading with R_ε values of 0.2 and 0.25 are within scatter bands of two, while 3 out of 9 fatigue life data under pulsating tension loading (R_ε = 0) and 3 out of 15 data points under fully-reversed loading (R_ε = -1) are merely outside the scatter bands. Nonetheless, better fatigue life predictions using the energy based model employing ΔW_{HL}^{T} are obtained as denoted by R^2 = 0.78 when compared to the strain based Coffin-Manson model (R^2 = 0.76) and the strain-stress based SWT model (R^2 = 0.65).

The cumulative total strain energy density, $\sum W^T$, [39, 81] is also considered in this study to account for both mean stress relaxation that results in vertical shifting in the stress-strain hysteresis loops as well as the cyclic softening effects that significantly incurred during the initial cycling, as discussed in [53]. The value of $\sum W^T$ is determined from the following:

$$\sum W^T = \sum W^P + \sum W^{e+} \tag{5.10}$$

where $\sum W^P$ and $\sum W^{e+}$ are the cumulative plastic and tensile elastic strain energy densities, respectively, which represent the sum of plastic and tensile elastic strain energy densities for all cycles. The $\sum W^T$ values for all constant amplitude loading tests with mean strains are calculated and tabulated in Table 5.1.

Using the experimental results from [42], $\sum W^T$ values for tests with fully-reversed cyclic loading (R_ε = -1) and nominal temperature rise are obtained and plotted against the corresponding reversals to failure, $2N_f$, as shown in Fig. 5.4(a). A power function, as illustrated in this figure, was utilized to fit the fully-reversed data. In addition, the fatigue data with various mean strains (R_ε = 0, 0.2, and 0.25) [53] and nominal temperature rise are also included in Fig. 5.4(a). Using the power fit on the fully-reversed data in Fig. 5.4(a), the predicted fatigue lives are calculated and plotted against the experimentally observed fatigue lives for all uniaxial strain-controlled test with and without mean strains, as shown in Fig. 5.4(b). As seen, all the data points are within scatter bands of two and a satisfactory correlation (R^2 = 0.88) is obtained using the energy based fatigue model with $\sum W^T$ as the damage parameter, when compared to those of the strain based Coffin-Manson model (R^2 = 0.76), the strain-stress based SWT model (R^2 = 0.65), and the energy based model using ΔW_{HL}^T (R^2 = 0.78). Therefore, it is evident that the energy based

model utilizing $\sum W^T$ may be an appropriate model to correlate fatigue data of PEEK under strain-controlled loading conditions in presence of mean stresses and strains. It also has to be noted that, as the value of $\sum W^T$ is obtained by summing total strain energy density from all of the individual cycles as shown in Eq. (5.10), the value of $\sum W^T$ will increase with the increase in number of cycles. Hence, the fatigue life curve obtained using the energy based method with $\sum W^T$ as a damage parameter has a positive slope. On the other hand, in the case of strain- and strain-stress based models, the value of the damage parameter is taken from a single cycle at the steady state region (mid-life cycle) resulting to a constant value of the damage parameter and fatigue life curve with a negative slope.

Unlike the strain based and strain-stress based approaches, the energy based approach, using either $\sum W^T$ or ΔW_{HL}^T as the damage parameter, takes the shape and size of the hysteresis loop into account. Thus, it inherently incorporates the stress and strain responses from the entire loading cycle, and not only at the extreme points (i.e. maximum and/or minimum values). Moreover, the energy based approach with $\sum W^T$ considers the evolution of cyclic responses of the material, such as mean stress relaxation, cyclic softening, change in the stress response due to self-heating, etc. However, it should be noted that the number of cycles to failure is inherently included in the $\sum W^T$ parameter (i.e. a specimen with longer life would have a larger $\sum W^T$ value, and vice versa), which may have attributed to much improved fatigue life predictions using this energy based fatigue model to some degree.

5.4 Fatigue Modeling for Block Loading Condition

The applicability of several cumulative fatigue damage approaches for PEEK specimens under multi-block loading condition with zero and non-zero mean strains at

various frequencies is evaluated in this section. Three cumulative fatigue damage models, including the LDR, the Damage Curve Approach (DCA), and the Hashim-Rotem (H-R) model, are employed. Moreover, due to the satisfactory life predictions using $\sum W^T$ for specimens under constant amplitude loading in the previous section, a Direct Cumulative Damage (DCD) method based on this energy parameter is also considered.

The validity of the selected cumulative damage models is evaluated using the experimental data for PEEK polymer under various uniaxial strain-controlled multi-block (i.e. variable amplitude) loading conditions. The experimental results employed in this study were obtained using the following test conditions [77]:

I. fully-reversed (R_ε = -1) two-block loading with nominal temperature rise (i.e. data in Table 5.2),
II. fully-reversed (R_ε = -1) two-block loading to study the frequency effect (i.e. data in Table 5.3),
III. pulsating tension (R_ε = 0) two-block loading with nominal temperature rise (i.e. data in Table 5.4), and
IV. fully-reversed (R_ε = -1) three- and four-block loadings with nominal temperature rise (i.e. data in Table 5.5).

The fatigue tests under two-block loading were conducted using either high-low (H-L) or low-high (L-H) loading sequence, while three-block loading experiments were performed using high-low-high (H-L-H) or low-high-low (L-H-L) sequence. Finally, high-low-high-low (H-L-H-L) loading was used for four-block loading fatigue tests [77].

5.4.1 Established Cumulative Fatigue Damage Models

Three cumulative damage models, including the LDR, the DCA, and the H-R model, are employed to assess their applicability for PEEK polymer. In this section, a brief overview of the selected models is presented and their accuracy in predicting the cumulative damage, using either a strain or energy based parameter, for PEEK under multi-block loadings are discussed.

According to the Palmgren-Miner LDR, which is the most widely used and commonly accepted for fatigue life prediction of a variety of materials, the damage induced in each loading block, D_i (i.e. damage produced by N_i cycles for a specific loading block of i), is added linearly to predict fatigue failure, which occurs when the cumulative damage, D, approaches unity as [82]:

$$D = D_1 + D_2 + \cdots + D_k = \frac{N_1}{N_{f1}} + \frac{N_2}{N_{f2}} + \cdots + \frac{N_k}{N_{fk}} = 1 \qquad (5.11)$$

where i = 1, 2,…, k represents the number of loading blocks, and N_{fi} is the number of cycles to failure at particular strain or stress level applied in the loading block i. The damage D_i can be defined as a cycle ratio or a fraction of life that is removed from the material. Depending on the damage parameter chosen, N_{fi} can be obtained from the fatigue data under constant amplitude loading.

In addition to the LDR, many non-linear damage accumulation models have been proposed [70]. Among them, the DCA [82] and the H-R model [83] have been employed extensively for fatigue damage predictions of metallic materials [70]. By recognizing that the major manifestation of fatigue damage is crack growth, which typically involves various processes from dislocation agglomeration to micro-cracks coalescence, Manson

and Hartford empirically proposed the DCA to account for the processes associated to crack growth in the material. According to this approach, the instantaneous crack length, *a*, can be approximated using the following relation [82]:

$$a = a_0 + (a_f - a_0)\left(\frac{N_a}{N_f}\right)^{BN_f{}^{\alpha}} \tag{5.12}$$

where a_0 and $a_f$are the initial and final crack lengths. The parameter N_a represents the number of cycles required to reach a crack length of *a*, while *B* and α are material constants. The damage accumulation is then defined as the ratio of instantaneous to final crack length, $D = a/a_f$. For variable amplitude block loadings, the cumulative damage can be represented by [82]:

$$D = \left\{\left[\left(\frac{N_1}{N_{f1}}\right)^{\left(\frac{N_{f1}}{N_{f2}}\right)^{\alpha}} + \frac{N_2}{N_{f2}}\right]^{\left(\frac{N_{f2}}{N_{f3}}\right)^{\alpha}} + \cdots + \left(\frac{N_{k-1}}{N_{f(k-1)}}\right)\right\}^{\left(\frac{N_{f(k-1)}}{N_{fk}}\right)^{\alpha}} + \frac{N_k}{N_{f(k)}} = 1 \tag{5.13}$$

In Eq. (5.13), the subscripts, 1, 2,…, *k*-1, *k*, are the sequence number of loading block, and the material parameter α = 0.4 is commonly used for most metallic materials [82]. Additionally, both the DCA and the LDR were recently employed to calculate fatigue damage in notched and un-notched polypropylene (PP) polymer subjected to load-controlled two-block loadings and periodic overloads [58]. The DCA with the material parameter α = 0.2 was found to provide better damage predictions for both notched and un-notched PP specimens when compared to the LDR.

Lastly, Hashin and Rotem [83] proposed a cumulative damage model based on the stress-life convergence approach. In their work, a set of isodamage curves, which

correspond to the residual lifetimes of the material under arbitrary cyclic loading, was suggested. Each damage curve is considered to be unique and governed by the initial loading condition (i.e. stress amplitude, the number of applied cycles, etc.). When the residual lifetime of the material is zero, the damage curve essentially becomes the stress-life curve. Hanshin and Rotem also speculated two types of convergences for the damage curves to either pass through the static strength points (i.e. the fatigue strength at $N_f = 1$) or ultimately converge to the endurance limit for the material. Based on the H-R model, the equation governing the fatigue failure of a material subjected to two-block cyclic loading is expressed as [83]:

$$D = \left(\frac{N_1}{N_{f1}}\right)^{\frac{\log(N_{f2})}{\log(N_{f1})}} + \frac{N_2}{N_{f2}} = 1 \tag{5.14}$$

The H-R model can be further generalized for variable amplitude loading as discussed in [83].

Theses cumulative damage models with strain amplitude as a damage parameter are first employed for PEEK specimens under two-, three-, and four-block loadings. The damage accumulation values are determined using Eqs. (5.11), (5.13), and (5.14) in which N_i represents the number of cycles applied in each loading block, and N_{fi} is obtained from the best fit (i.e. the Coffin-Manson fit in Fig. 5.1(a)) on strain-life data for constant amplitude fully-reversed (R_ε = -1) loading with nominal temperature rise. The values of cumulative damage, D, using the three cumulative damage models based on strain amplitude are listed in Tables 5.2-5.5 for the test conditions I-IV, respectively.

To illustrate the applicability of the selected cumulative damage models, N_1/N_{f1} is plotted against N_2/N_{f2} for all two-block loading tests (i.e. test conditions I-III) using

the strain based approach, as shown in Figs. 5.5(a) and 5.5(b) for H-L and L-H loading, respectively. The ratio N_1/N_{f1} corresponds to the damage induced in the initial block, while N_2/N_{f2} represents the remaining damage tolerance. The LDR prediction lines, which are the straight lines intersecting unity on both x- and y-axes, the damage prediction curves based on the DCA (Eq. (5.13)), and the H-R model (Eq. (5.14)), as well as lines/curves representing the factor of two for each damage line/curve, are displayed in these figures. It should be noted that the damage prediction lines/curves in these figures are the thicker ones and the lines/curves representing the factor of two are the thinner ones. As seen, by utilizing the LDR, the DCA, and the H-R model with a strain based parameter, unsatisfactory and very conservative damage predictions are obtained for the majority of both H-L and L-H loadings under test conditions I and II. On the other hand, relatively reasonable predictions can be noticed in Fig. 5.5 for all four PEEK specimens subjected to loading condition III.

In addition, energy based fatigue models inherently incorporate the shape and size of the hysteresis stress-strain response of the material, and were shown in the previous section to provide acceptable fatigue life predictions for PEEK under various strain ratios. Therefore, the cumulative fatigue damage based on the total strain energy density at half-life, ΔW_{HL}^{T}, is considered here as well. In this approach, the value of N_{f_i} for each loading block is obtained from ΔW_{HL}^{T}- life curve fit in Fig. 5.3(a). Once N_{f_i} is determined, the cumulative damage values, D, are calculated using Eqs. (5.11), (5.13), and (5.14) for the LDR, the DCA, and the H-R model, respectively, and listed in Tables 5.2-5.5 for the test conditions I-IV.

The plots similar to Fig. 5.5 are generated for the employed cumulative damage models with ΔW_{HL}^{T} as a damage parameter and presented in Fig. 5.6. Again, the thicker line/curves represent the damage prediction line/curves, while the thinner ones correspond to the factor of two for each damage prediction approach. As seen, the energy based LDR, DCA, and H-R model are not able to accurately predict the damage accumulation in PEEK specimens subjected to variable amplitude block loading. Again, with an exception for H-L loading in test condition III, very conservative predictions are obtained in Figs. 5.6(a) and 5.6(b) for H-L and L-H loading, respectively.

Typically, for most metals in H-L loading, micro-cracks can initiate during the higher loading level and continue to grow during the lower loading level. On the other hand, in L-H loading, the possibility of cracks to initiate during the lower loading level is generally limited; hence, longer fatigue lives are often observed for L-H loading as compared to H-L loading. In addition, the corresponding cumulative damage using the LDR is generally less than one when the material is subjected to H-L loading sequence, and greater than one for L-H loading sequence [30]. However, for all the test conditions in this study, cumulative damage values of greater than one ($D > 1$) were mostly obtained using either the strain- or energy based LDR, as seen in Tables 5.2-5.5. Calculating higher cumulative damage values, especially for loading conditions I and III, can be attributed to the significant increase in fatigue life for PEEK when it is subjected to pre-loading, irrespective to the loading sequence.

The LDR yields conservative damage predictions ($1.7 < D < 3.14$ for strain based and $3.81 < D < 4.30$ for energy based) for loading condition II in Table 3 irrespective to the loading sequence, as seen in Figs. 5.5 and 5.6. Conservative predictions using the LDR

can be attributed to the fact that the LDR assumes the damage accumulates in a linear fashion and is not capable of incorporating the load history and sequence effects. Hence, the LDR may not be appropriate for capturing the beneficial effect of pre-loading on fatigue life of PEEK when subjected to fully-reversed strain loading (i.e. loading conditions I and II), as reported in [77]. On the other hand, for tests conducted under pulsating tension loading (i.e. loading condition III), pre-loading effect on fatigue life was not noticeable as reported in [77]. This may explain an acceptable correlation of the fatigue data under pulsating tension ($R_\varepsilon = 0$) block loading (i.e. loading condition III) using the LDR.

Moreover, for the loading condition I in Table 5.2 in which PEEK specimens were subjected to two-block loading with nominal temperature rise, lower cumulative damage values using either the strain- or energy based LDR can be generally obtained for all specimens subjected to L-H loading, as compared to those under H-L loading with identical strain amplitude and frequency. Higher cumulative damage and more conservative predictions for H-L loading may be due to the more influence of pre-loading on fatigue life (i.e. greater increase in fatigue life) for specimens subjected to H-L loading as compared to the L-H loading. As seen in Figs. 5.5(a) and 5.6(a), the majority of the H-L data for loading condition I are further to the right side of the predictions lines as compared to the L-H data, indicating more conservative predictions using the LDR for H-L loading.

The DCA and the H-R model employed in this study were originally proposed to alleviate the shortcomings with the linear damage predictions for L-H loading by assuming longer fatigue lives for such loading conditions. However, for L-H loading in Tables 5.2-5.4, no significant increase in the damage accumulation is calculated based on the DCA and the H-R model as compared to the LDR. In addition, since these non-linear damage

models also presume shorter fatigue lives for H-L loading, they typically provide more conservative predictions for H-L loading when compared to the LDR. Hence, higher cumulative damage values using the DCA and the H-R model as compared to the LDR are generally obtained for specimens subjected to H-L loading as tabulated in Tables 5.2-5.4. It is evident that, for specimens under test condition III whose lives were minimally affected by the load history and sequence, the damage predictions using the DCA and H-R model are fairly similar to the LDR. One also can generally notice less accurate damage predictions using the energy based LDR, DCA, and H-R models as compared to the strain based ones. In summary, these models are found to be unsuitable for damage predictions of PEEK polymer under variable amplitude loading blocks.

5.5 The Direct Cumulative Damage (DCD) Method

Due to the shortcomings of the LDR and the selected non-linear approaches in predicting the damage accumulation in PEEK polymer, the Direct Cumulative Damage (DCD) method based on the cumulative total strain energy density parameter, $\sum W^T$, is employed in this study. In the DCD approach, the best fit in Fig. 5.4(a) is used as the reference curve that relates $\sum W^T$ to PEEK fatigue life for each loading block. This reference curve represents the cumulative total strain energy density required to cause the specimen's failure and is capable of taking the loading history and sequence effect into account. In this method, the cumulative damage of a specimen under multi-block cyclic loading may be determined using the following simple relation:

$$D = \frac{N_t}{N_f} = 1 \tag{5.15}$$

where the failure is deemed to occur when *D* equals to unity. In Eq. (5.15), N_t is the overall fatigue life of a specimen (i.e. summation of number of cycles from all loading block). The predicted life, N_f, represents the number of cycles, which corresponds to the total summation of $\sum W^T$ from all loading blocks on the reference curve. For example, $\sum W^T$ for two-block loading was determined by combining $\sum W_1^T$ and $\sum W_2^T$, which represents the cumulative total strain energy density in the first and second loading blocks, respectively. This $\sum W^T$ value is then used to calculate fatigue life using the equation in Fig. 5.4(a).

The cumulative damage values obtained using the DCD method for specimens under loading conditions I-IV are listed in Tables 5.2-5.5, respectively. As seen in these tables, all cumulative damage values using the DCD method are very close to a factor of two from unity, ranging from 0.45 to 1.44. Furthermore, the ratios N_1/N_f versus N_2/N_f were plotted for all data with two-block loading, as displayed in Fig. 5.7(a). In addition, for three-block loading, $N_1/N_f + N_2/N_f$ is plotted against N_3/N_f, while for four-block loading, $N_1/N_f + N_2/N_f + N_3/N_f$ is plotted against N_4/N_f, as illustrated in Fig. 5.7(b). For test conditions I - III, the DCD method yields satisfactory predictions for the data with L-H loading, while it slightly underestimates the damage in the first block of H-L loading, as seen in Fig. 5.7(a). As a result, the damage induced in the initial block for the H-L loading using the DCD method appear to be significantly lower than the remaining cycle ratios. Nonetheless, much better correlations within a factor of two can be noticed in Figs. 5.7(a) and 5.7(b) for all test conditions using the DCD method. For PEEK specimen, which exhibits various cyclic deformation behavior, including cyclic softening and stress relaxation when subjected to various test conditions (i.e. zero or non-zero mean strain, different test frequencies, pre-loading, etc.), the cumulative total strain energy density

inherently takes into account the evolution of stress-strain responses of the material as well as the damage accumulated throughout the life time of the specimen.

The cumulative fatigue damage obtained using the strain based LDR, the energy based LDR, and the DCD method for PEEK specimens subjected to loading conditions I-IV are presented in Fig. 5.8(a)-5.8(d), respectively. In general, the LDR, with either strain amplitude or ΔW_{HL}^{T} as the damage parameter, provide more conservative damage predictions for PEEK polymer as compared to the DCD method. The strain based LDR and energy based LDR significantly overestimated the accumulated damage particularly under test conditions I, II, and IV regardless of loading sequence. Nonetheless, for the test condition III (i.e. data in Table 5.4) with minimum load history and sequence effects on fatigue life of PEEK, they were able to provide reasonable results with $0.91 \leq D \leq 1.42$ based on the strain based approach and $1.42 \leq D \leq 2.70$ based on the energy based approach.

In addition, the cumulative damage values obtained using the DCA and the H-R model with either a strain or energy based parameter, and the DCD method are compared in Figs. 5.9(a)-5.9(d) for loading conditions I-IV, respectively. As seen, while the employed non-linear models had a tendency to overestimate the fatigue damage for PEEK polymer, the DCD method, considering the cumulative total strain energy density of all cycles to capture the load history and sequence effects, provided the best results among all methods considered in this study.

Furthermore, to illustrate the capability of using $\sum W^{T}$ as a damage parameter for PEEK polymer under non-constant (i.e. variable) amplitude loading, $\sum W^{T}$ for all specimens in Table 2-5 are plotted against $2N_f$ in Fig. 5.10(a). The $\sum W^{T}$ value for each

specimen was determined by combining the cumulative total strain energy density from all loading blocks. In addition to the fatigue data under variable amplitude loading, the data for PEEK specimens subjected to different constant amplitude cyclic loading conditions is superimposed in this figure. This includes (1) fully-reversed (R_ε = -1) loading with nominal temperature rise [42], (2) fully-reversed (R_ε = -1) loading with various frequencies to study the frequency effect [42], and (3) mean strain (R_ε = 0, 0.2, and 0.25) loading with nominal temperature rise (i.e. data in Table 5.1) [53].

As depicted in Fig. 5.10(a), an excellent correlation between $\sum W^T$ and fatigue lives for all loading conditions is obtained. It should be pointed out that the y-intercept on the $\sum W^T$- life curve in this figure is approximately 21 MJ/m^3, which is comparable to the total strain energy density of 26 MJ/m^3 that was obtained from the quasi-static tensile test of PEEK polymer at the strain rate of 0.1 s^{-1} [42]. Using the relationship established in Fig. 5.4(a) based on fully-reversed data, fatigue lives for all PEEK specimens were calculated and plotted against the experimentally observed lives in Fig. 5.10(b). As seen from this figure, all the fatigue life predictions are within scatter bands of two from experimentally observed ones with R^2 = 0.92, which is an indicative of the effectiveness of $\sum W^T$ as a fatigue damage parameter for PEEK polymer under constant or variable amplitude loadings with various strain ratios and frequencies.

5.6 Conclusions

The applicability of various fatigue models to account for the mean strain and load history/sequence effects for PEEK polymer was investigated. The analysis presented in this study was based on the experimental data from a series of uniaxial strain-controlled test under various constant and non-constant amplitude loading conditions [53, 77]. Three

fatigue models; the strain based Coffin-Manson model, the strain-stress based Smith-Watson-Topper (SWT) model, and two models based on the strain energy density were examined to correlate the constant amplitude fatigue life data with zero and non-zero mean strains.

The cumulative damage in specimens under variable amplitude block loading conditions was determined using the Linear Damage Rule (LDR), as well as the non-linear Damage Curve Approach (DCA) and Hashim-Rotem (H-R) model, in conjunction with either the strain amplitude or the total strain energy density at half-life, ΔW_{HL}^{T}. A Direct Cumulative Damage (DCD) approach with the cumulative total strain energy density, $\sum W^{T}$, as the damage parameter was also employed to predict fatigue damage for PEEK under various multi-block loading conditions. Based on the analyses presented in this study, the following conclusions can be made:

1. Since PEEK polymer exhibited mean stress relaxation in the presence of mean strain, and minimal effect of mean strain on PEEK fatigue life was observed, the strain based Coffin-Manson model was found to correlate the mean strain data reasonably well.
2. Contrary to the expectation, the SWT model, which involves both stress and strain terms in its damage parameter, was not able to provide accurate fatigue life predictions for test data with mean strain.
3. In contrast to the energy based model based on the total strain energy density at half-life, ΔW_{HL}^{T}, the model based on the cumulative total strain energy density, $\sum W^{T}$, satisfactorily correlated the fatigue data with zero and non-zero mean strains. Such result can be attributed to the fact that the energy model utilizing

$\sum W^T$ was able to capture the changes in shape and size of the hysteresis stress-strain loop resulting from cyclic softening and mean stress relaxation throughout the lifetime of the specimen.

4. The LDR with either the strain amplitude or the total strain energy density at half-life, ΔW_{HL}^T, overestimated the cumulative damage in PEEK specimens subjected to fully-reversed cyclic loading, which exhibited significant load history effect. However, acceptable predictions were obtained for specimens subjected to pulsating tension two-block loading, where a minimal load history and sequence effect was observed.
5. The non-linear Damage Curve Approach and the Hashim-Rotem model, with either strain- or energy based parameter, were not able to accurately capture the beneficial effect of pre-loading on PEEK fatigue resistance. As a result, they overestimated the fatigue damage under variable amplitude loading blocks.
6. Regardless of loading conditions (zero or non-zero mean strains) and sequence (high-low or low-high), the Direct Cumulative Damage (DCD) approach based on $\sum W^T$, was able to take into consideration the loading history/sequence effects on PEEK fatigue behavior and provide an acceptable predictive capability under variable amplitude loading at various frequencies.

It was shown in this study that the energy based approach with $\sum W^T$ as the damage parameter was able to correlate PEEK fatigue lives under constant and variable amplitude loadings, with zero and non-zero mean strains and at various frequencies. However, one difficulty in employing this model is the need for having the cyclic deformation response of the polymer.

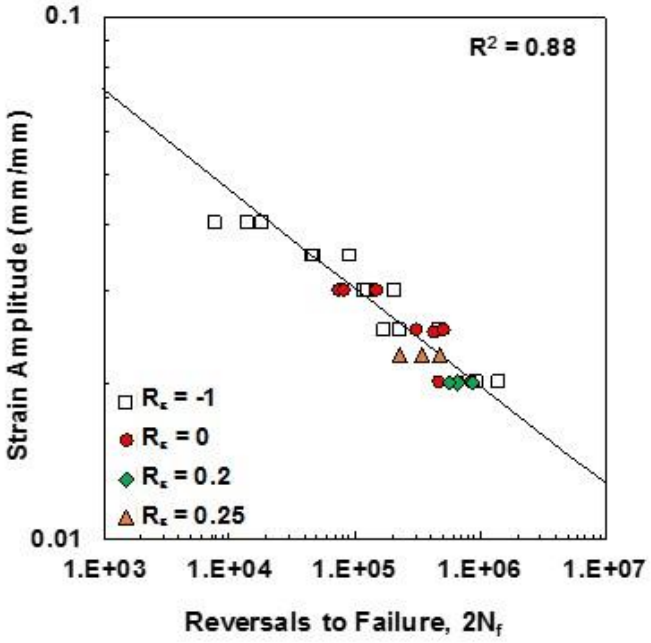

(a)

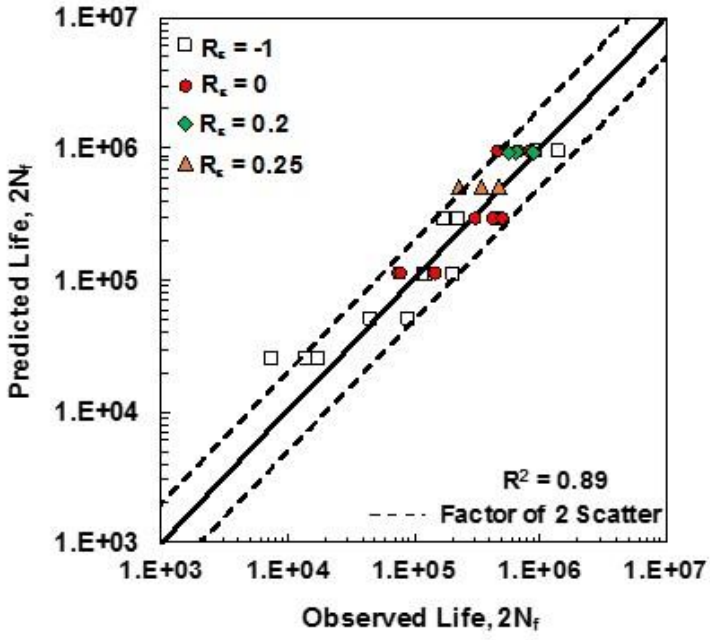

(b)

Figure 5.1 (a) Strain amplitude versus reversals to failure, $2N_f$, for PEEK under uniaxial strain-controlled constant amplitude fatigue tests with zero [42] and non-zero [53] mean strains with nominal rise in temperature, and (b) predicted fatigue lives using the Coffin-Manson model versus experimentally observed fatigue lives.

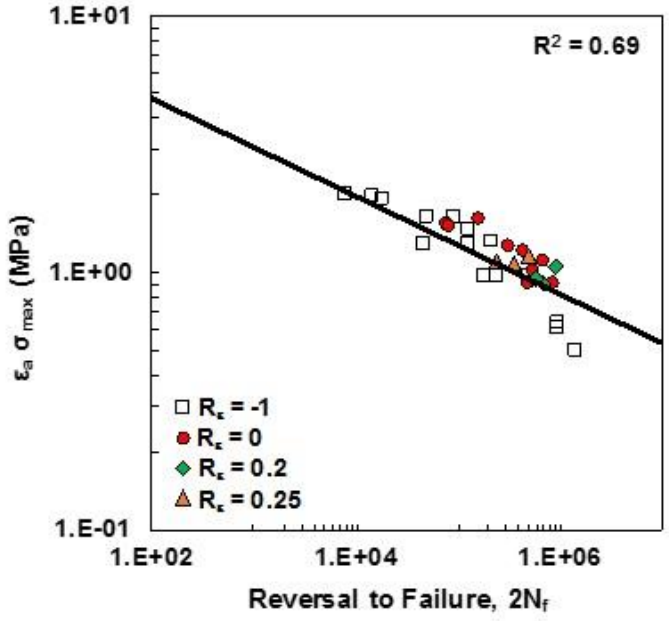

(a)

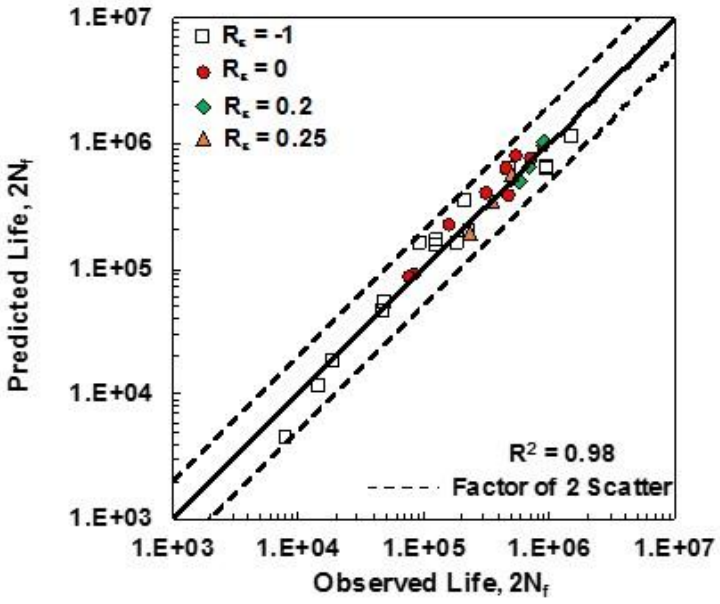

(b)

Figure 5.2 (a) Smith-Watson-Topper (SWT) damage parameter versus reversals to failure, $2N_f$, for PEEK under uniaxial strain-controlled constant amplitude fatigue tests with zero [42] and non-zero [53] mean strains with nominal rise in temperature, and (b) predicted fatigue lives using the SWT parameter versus experimentally observed fatigue lives.

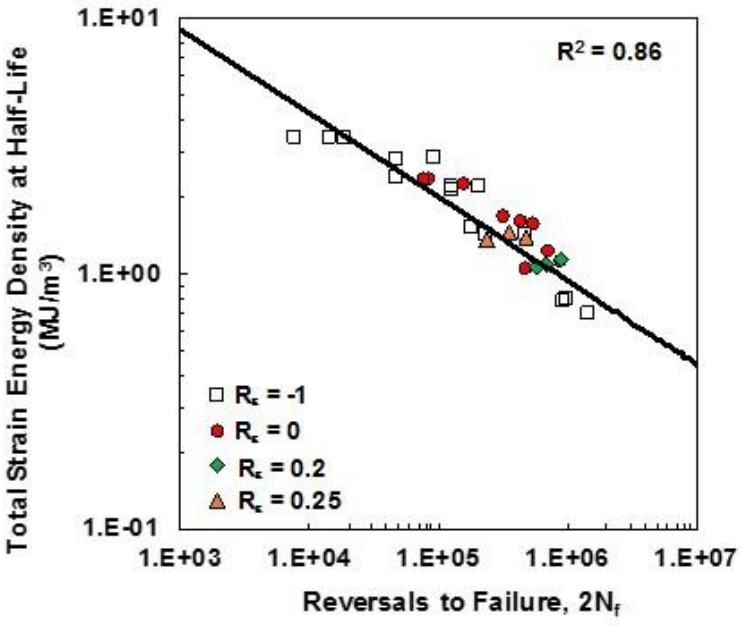

(a)

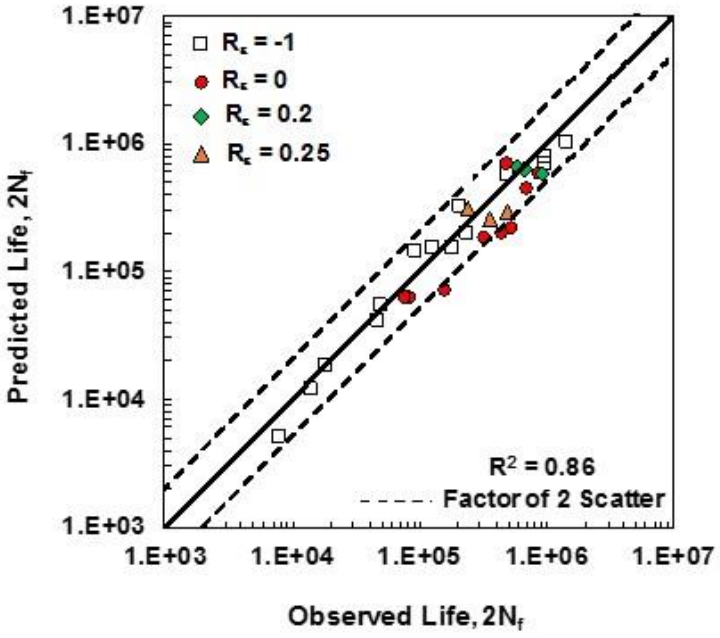

(b)

Figure 5.3 (a) Total strain energy density at half-life, ΔW_{HL}^{T}, versus reversals to failure, $2N_f$, for PEEK under uniaxial strain-controlled constant amplitude fatigue tests with zero [42] and non-zero [53] mean strains with nominal rise in temperature, (b) predicted fatigue lives using energy based approach with ΔW_{HL}^{T} versus experimentally observed fatigue lives.

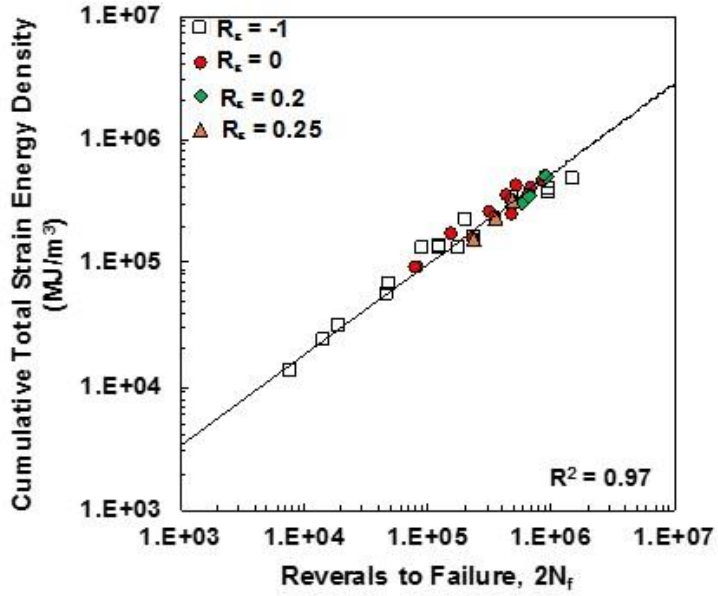

(a)

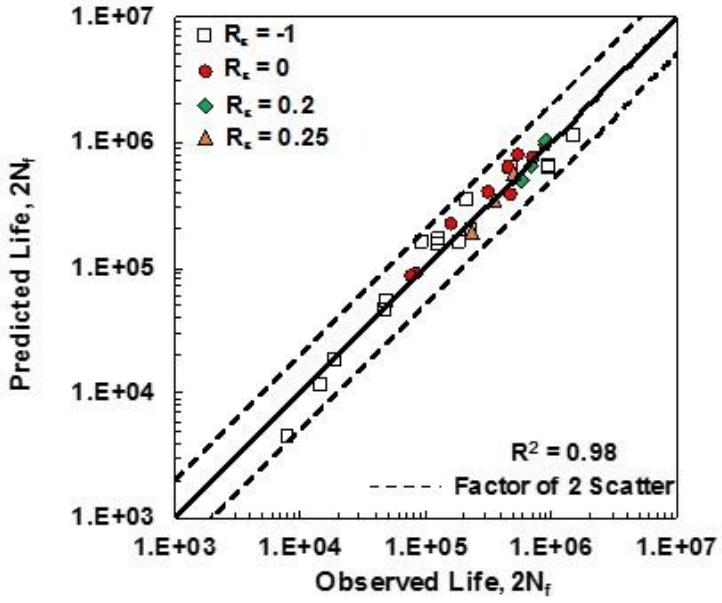

(b)

Figure 5.4 (a) Cumulative total strain energy density, $\sum W^T$, versus reversals to failure, 2Nf, for PEEK under uniaxial strain-controlled constant amplitude fatigue tests with zero [42] and non-zero [53] mean strains with nominal rise in temperature, (b) predicted fatigue lives using energy based approach with $\sum W^T$ versus experimentally observed fatigue lives.

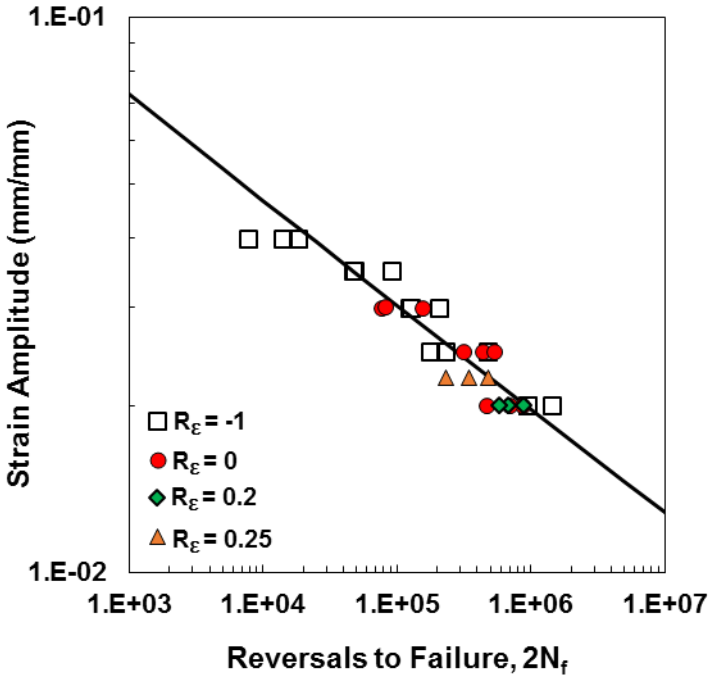

(a)

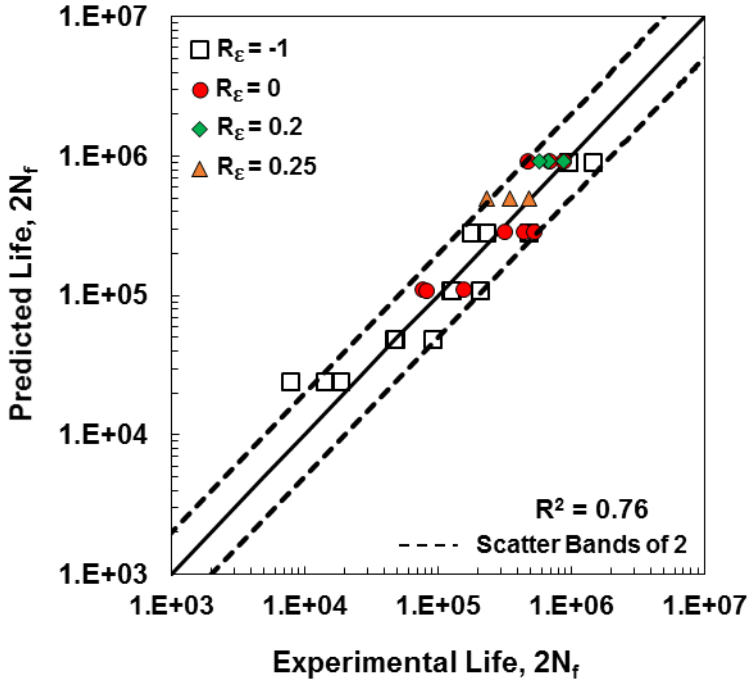

(b)

Figure 5.5 (a) Strain amplitude versus reversals to failure, $2N_f$, for PEEK under uniaxial strain-controlled constant amplitude fatigue tests with zero [42] and non-zero [53] mean strains with nominal rise in temperature, and (b) predicted fatigue lives using the Coffin-Manson model versus experimental fatigue lives.

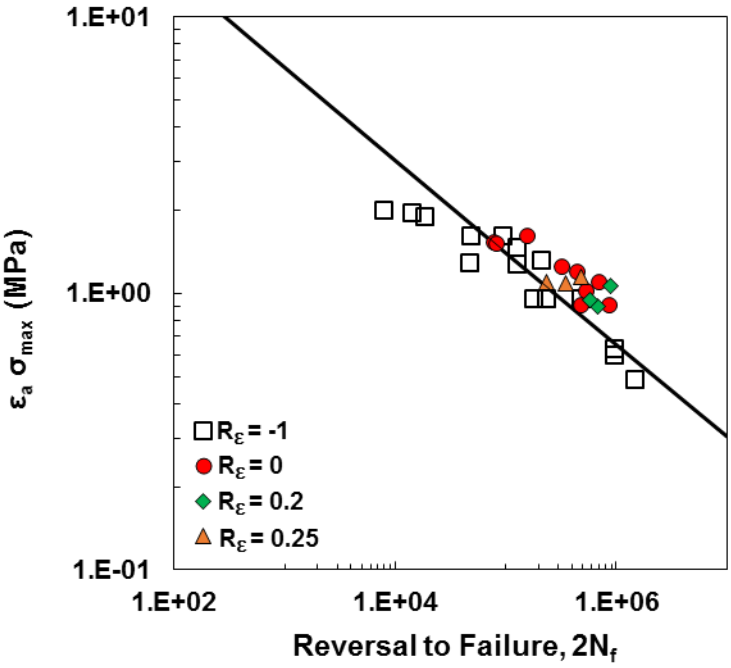

(a)

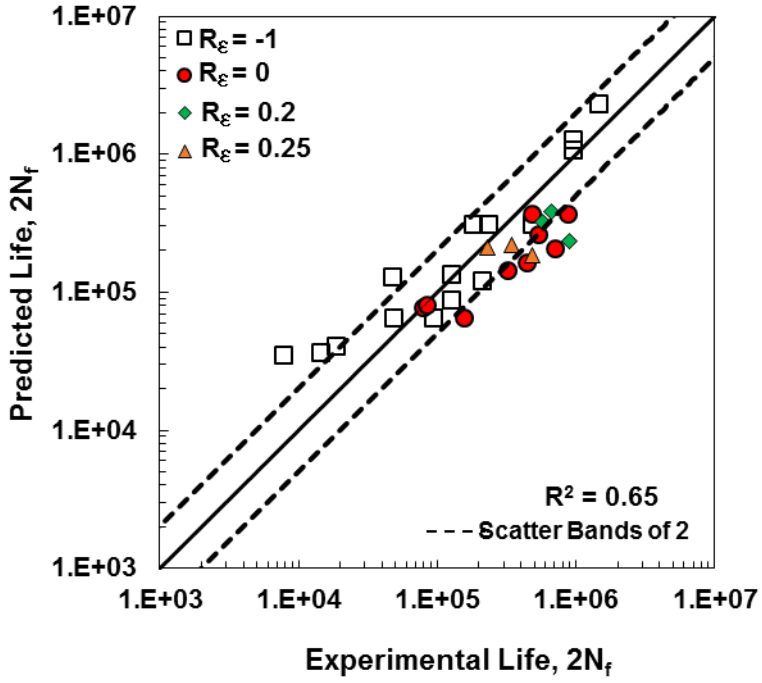

(b)

Figure 5.6 (a) Smith-Watson-Topper (SWT) damage parameter versus reversals to failure, $2N_f$, for PEEK under uniaxial strain-controlled constant amplitude fatigue tests with zero [42] and non-zero [53] mean strains with nominal rise in temperature, and (b) predicted fatigue lives using the SWT parameter versus experimental fatigue lives.

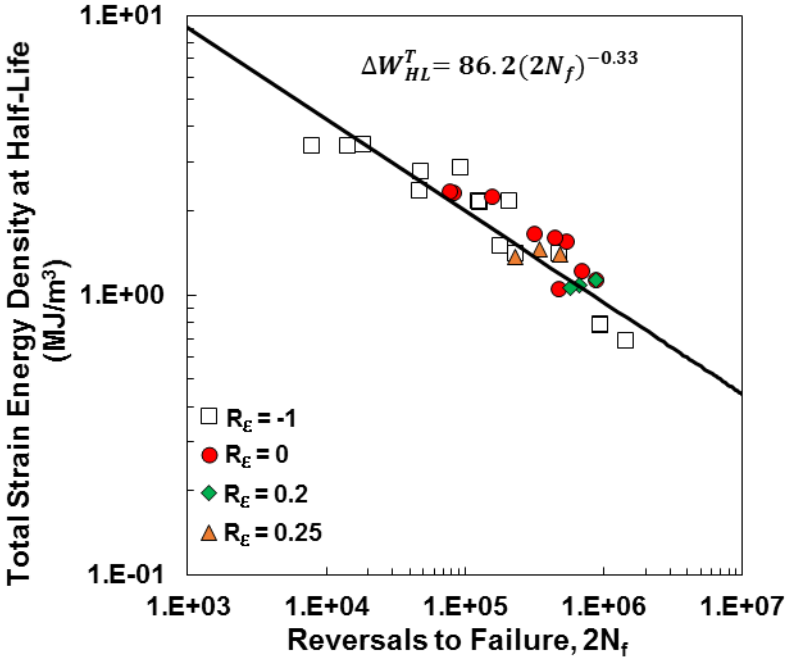

(a)

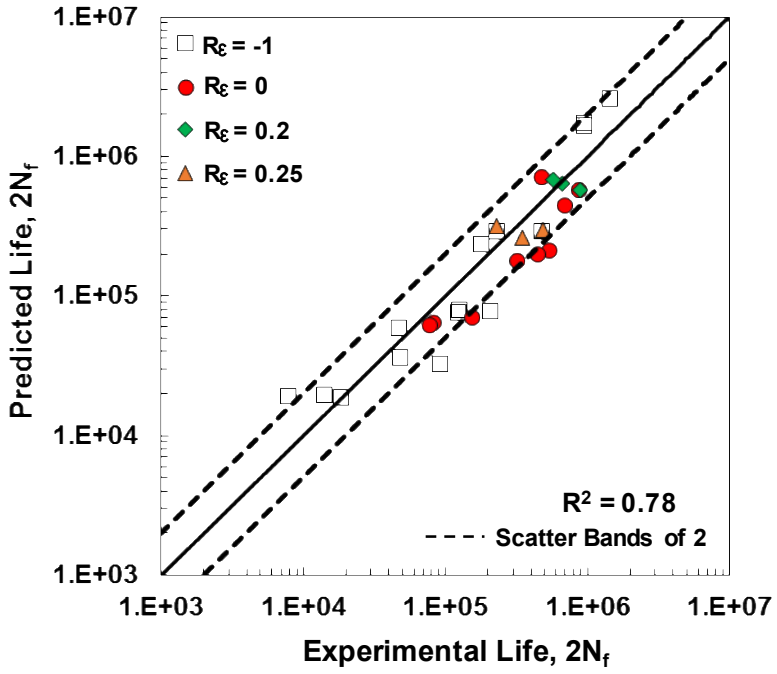

(b)

Figure 5.7 (a) Total strain energy density at half-life, ΔW_{HL}^{T}, versus reversals to failure, 2Nf, for PEEK under uniaxial strain-controlled constant amplitude fatigue tests with zero [42] and non-zero [53] mean strains with nominal rise in temperature, and (b) predicted fatigue lives using energy based approach with ΔW_{HL}^{T} versus experimental fatigue lives.

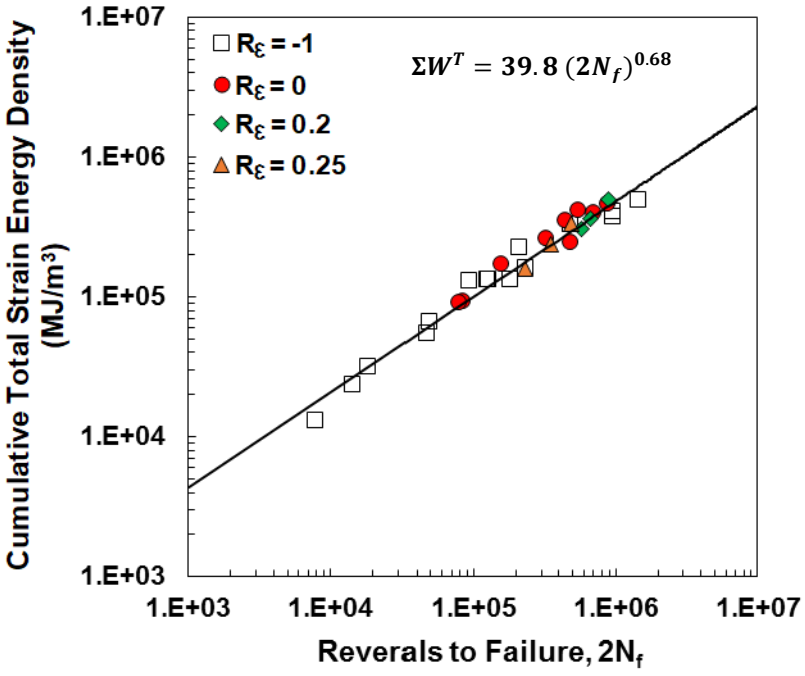

(a)

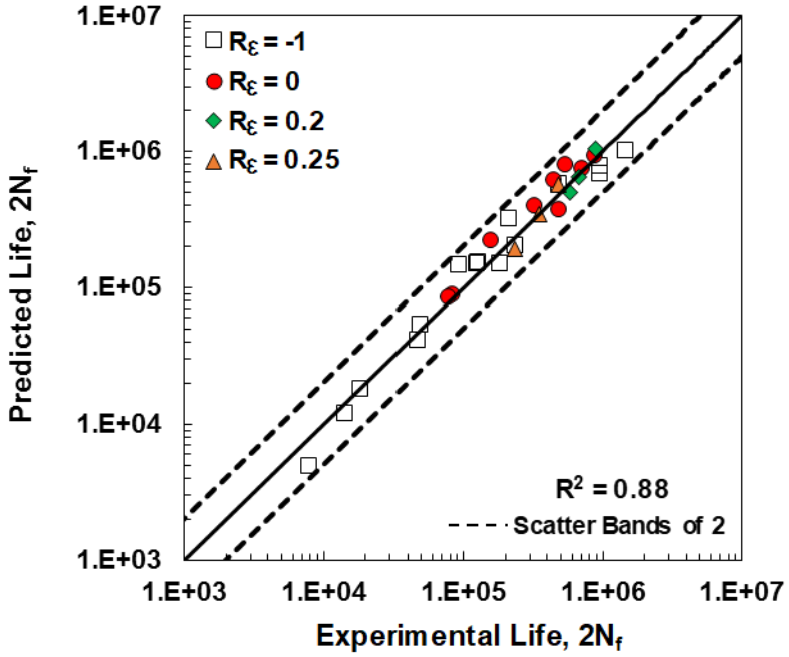

(b)

Figure 5.8 (a) Cumulative total strain energy density, ΣW^T, versus reversals to failure, $2N_f$, for PEEK under uniaxial strain-controlled constant amplitude fatigue tests with zero [42] and non-zero [53] mean strains with nominal rise in temperature, and (b) predicted fatigue lives using energy based approach with ΣW^T versus experimental fatigue lives.

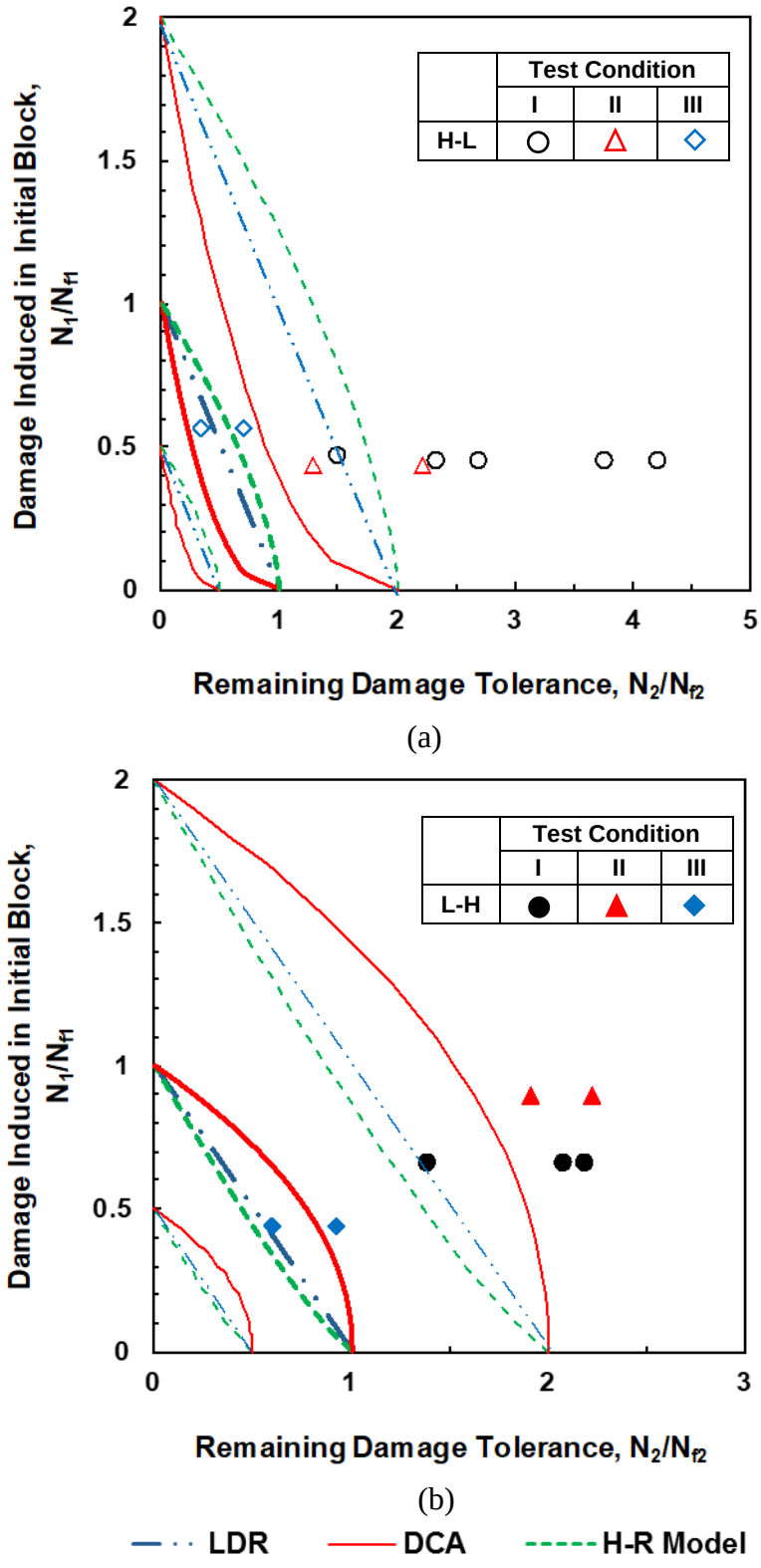

Figure 5.9 Cycle ratios obtained using various established cumulative damage models with a strain based parameter for test conditions I, II, and III with (a) H-L loading and (b) L-H loading along with scatter bands of two.

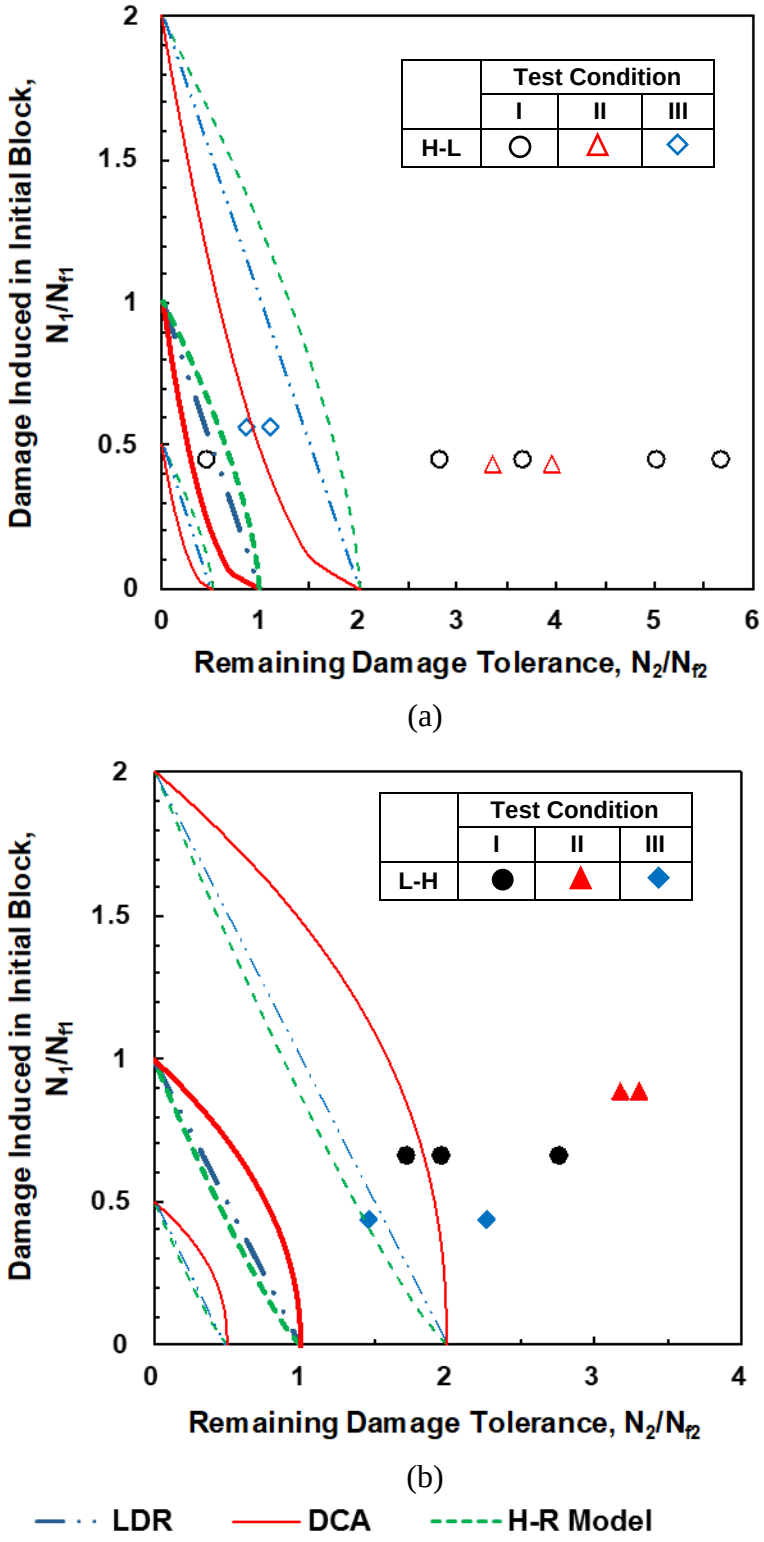

Figure 5.10 Cycle ratios obtained using various established cumulative damage models with an energy based parameter, ΔW_{HL}^{T}, for test conditions I, II, and III with (a) H-L loading and (b) L-H loading along with scatter bands of two.

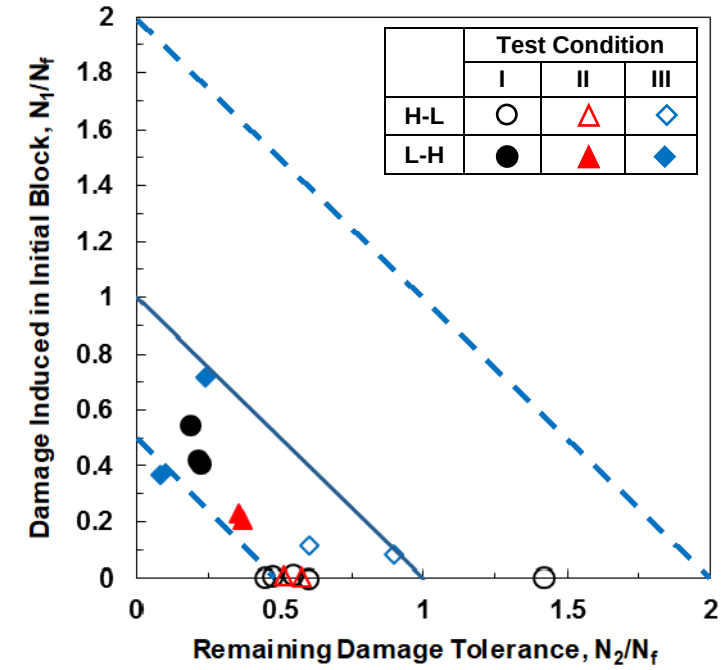

(a)

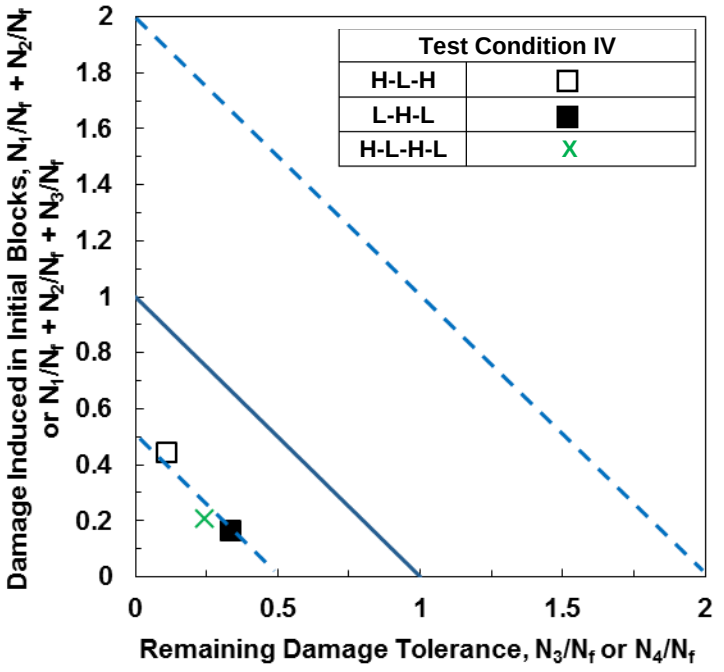

(b)

Prediction line Scatter bands of 2

Figure 5.11 Cycle ratios in (a) two-block loading (test conditions I-III), and (b) three- and four-block loading (test condition IV) experiments obtained using the Direct Cumulative Damage (DCD) method, with $\sum W^T$.

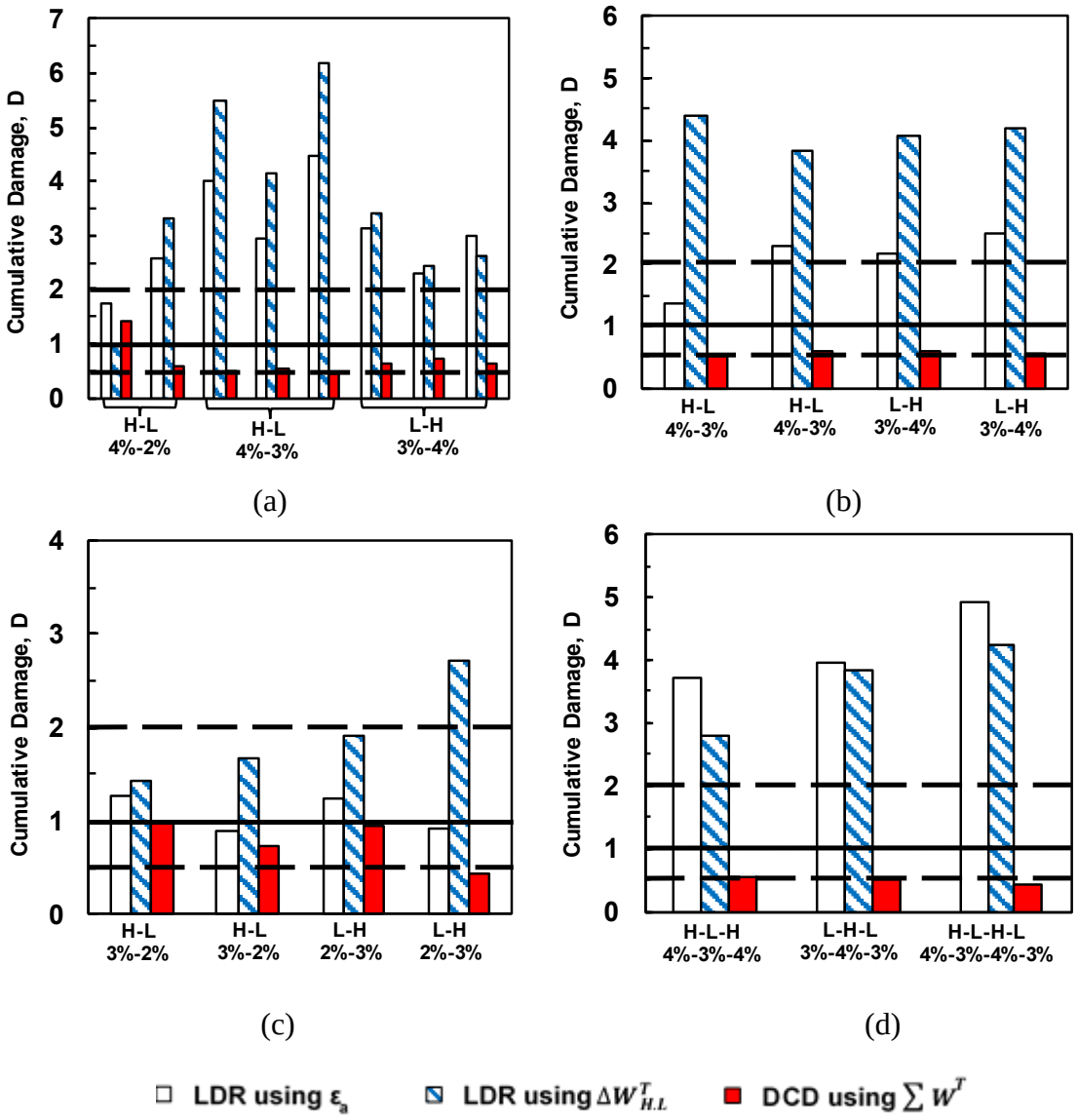

Figure 5.12 Bar charts showing the comparisons of the cumulative damage using the strain based LDR, the energy based LDR, and the DCD method for PEEK polymer under (a) two-block loading with zero mean strain and nominal temperature rise (test condition I), (b) two-block loading with zero mean strain to study the frequency effect (test condition II), (c) two-block pulsating tension loading with nominal temperature rise (test condition III), and (d) three- and four- block loading with zero mean strain and nominal temperature rise (test condition IV).

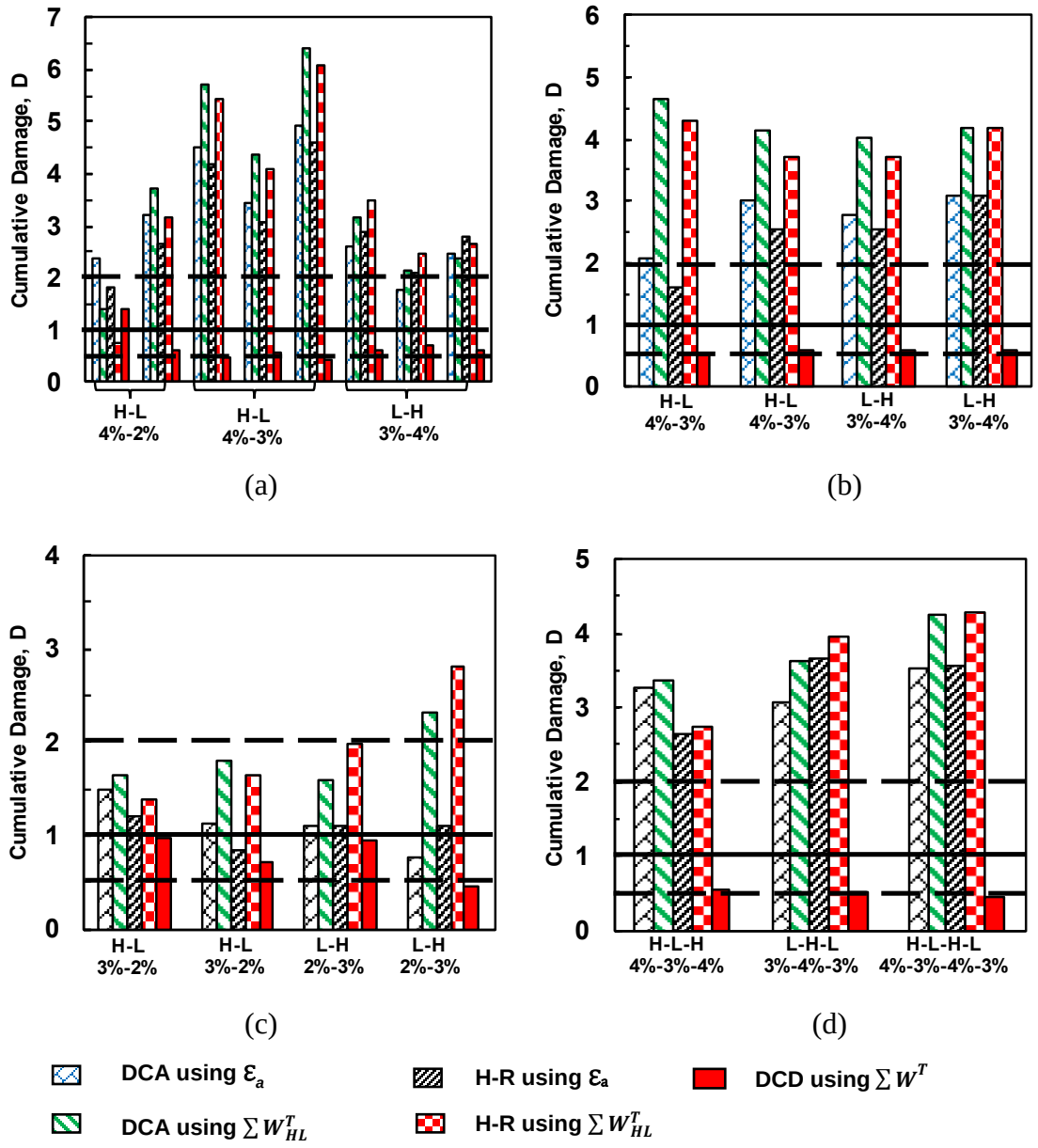

Figure 5.13 Bar charts showing the comparisons of the DCA and the H-R model using either a strain- or energy- based parameter, and the DCD method for PEEK polymer under (a) two-block loading with zero mean strain and nominal temperature rise (test condition I), (b) two-block loading with zero mean strain to study the frequency effect (test condition II), (c) two-block pulsating tension loading with nominal temperature rise (test condition III), and (d) three- and four- block loading with zero mean strain and nominal temperature rise (test condition IV).

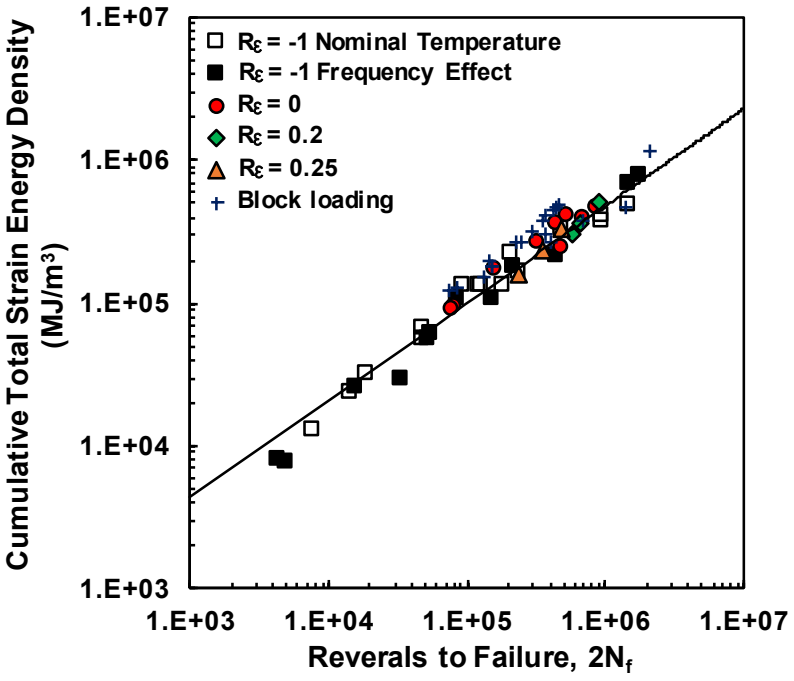

(a)

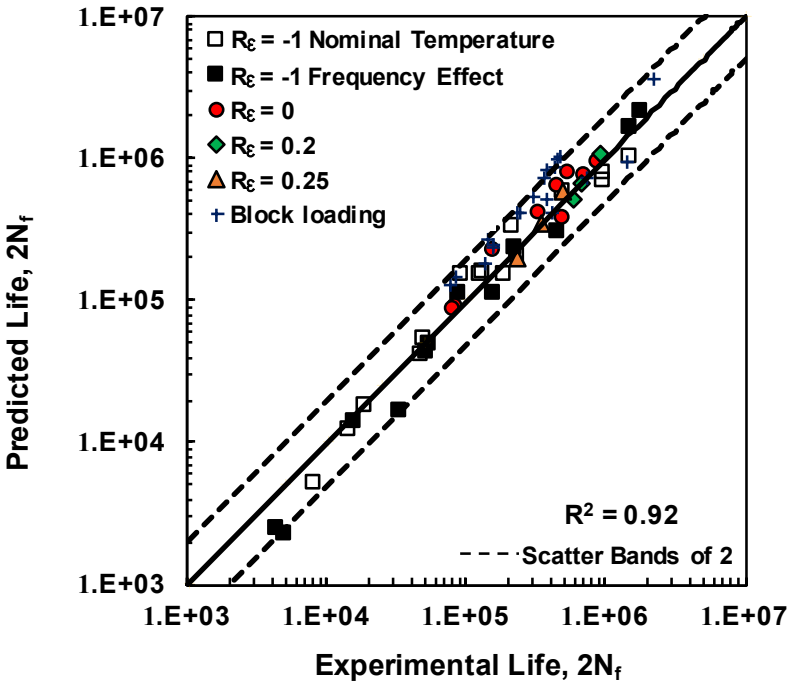

(b)

Figure 5.14 (a) Cumulative total strain energy density, ΣW^T, versus reversals to failure, $2N_f$, for PEEK under different test conditions, showing the reference curve for the Direct Cumulative Damage (DCD) method, and (b) predicted fatigue lives using the energy based approach with ΣW^T versus experimental fatigue lives.

Table 5.1 Experimental results [53] for PEEK polymer and the corresponding energy densities for uniaxial constant amplitude strain-controlled fatigue tests with mean strains.

Specimen ID	ε_a (mm/mm)	ε_m (mm/mm)	Frequency (Hz)	R_ε Value	σ_a^* (MPa)	σ_m^* (MPa)	$2N_f$ (Reversals)	ΔT (°C)	ΔW_{HL}^P (MJ/m^3)	ΔW_{HL}^E (MJ/m^3)	$\sum W^T$ (MJ/m^3)
S86	0.02	0.02	1.5	0	42	-1.98	475,726	31	0.78	0.27	248,987
S76					47	7.71	696,398	43	0.68	0.54	400,771
S83					45	0.98	874,850	32	0.74	0.39	467,617
S78	0.025	0.025	1		46	4.11	318,690	45	1.2	0.42	262,781
S88					46	1.59	443,580	29	1.2	0.38	352,939
S84					43	-0.80	535,546	34	1.3	0.28	417,132
S85	0.03	0.03	0.5		49	2.51	77,892	37	1.9	0.49	91,105
S87					53	-0.95	83,096	28	1.8	0.52	93,544
S81					48	1.40	155,458	39	1.7	0.51	173,921
S92	0.02	0.03	1.5	0.2	45	2.50	578,224	24	0.69	0.37	304,513
S91					41	4.56	671,842	29	0.74	0.34	360,697
S89					46	7.50	887,634	26	0.71	0.42	501,458
S97	0.025	0.0375	1	0.25	47	1.92	231,896	22	0.98	0.39	158,243
S99					47	2.03	347,108	21	0.98	0.48	236,173
S90					48	3.84	483,868	24	0.95	0.45	330,107

*Measured at half-life cycle

Table 5.2 Experimental results [77] and calculated cumulative damages for uniaxial fully-reversed (Rε = -1) strain-controlled fatigue tests of PEEK with two-block loading with adjusted frequencies to maintain the nominal temperature rise on the specimens (i.e. test condition (I)).

Specimen ID	$\varepsilon_{a1}/\varepsilon_{a2}$ (mm/mm)	f_1/f_2 (Hz)	ΔT (°C)	$2N_1/2N_2$ (Reversals)	σ_{a1}/σ_{a2}* (MPa)	σ_{m1}/σ_{m2}* (MPa)	LDR using ε_a		LDR using ΔW_{HL}^T		DCD Method using $\sum W^T$
							D_1/D_2	D	D_1/D_2	D	
High-Low											
S123	0.04/0.02	0.50/3	20 36	6,000/2,130,352#	49/30	14/16	0.44/1.4	1.8	0.44/2.1	2.5	0.74
S101			31 37	6,000/1,371,616	47/30	-12/-9	0.44/0.9	1.5	0.44/0.3	0.72	1.6
S105	0.04/0.03	0.5/0.75	26 28	6,000/296,276	49/47	-11/-9	0.44/3.7	4.1	0.44/4.1	4.6	0.59
S102			28 27	6,000/412,318	47/47	-12/-10	0.44/5.1	5.5	0.44/5.6	6.1	0.53
S108			31 30	6,000/459,890	51/49	-12/-10	0.42/5.7	6.1	0.44/5.59	6	0.51
Low-High											
S103	0.03/0.04	0.75/0.5	27 31	100,000/33,542	51/51	-10/-11	0.65/3.4	4	0.65/2.6	3.3	0.72
S109			29 31	100,000/50,136	47/48	-10/-11	0.65/5.1	5.7	0.65/2.8	3.4	0.64
S106			22 29	100,000/53,076	50/49	-10/-11	0.65/5.4	6	0.65/4.1	4.7	0.63

*Measured at half-life cycle
#Runout

Table 5.3 Experimental results [77] and calculated cumulative damages for uniaxial fully-reversed (Rε = -1) strain-controlled fatigue tests of PEEK with two-block loading with adjusted frequencies to maintain the nominal temperature rise on the specimens (i.e. test condition (I)).

Specimen ID	$\varepsilon_{a1}/\varepsilon_{a2}$ (mm/mm)	f_1/f_2 (Hz)	ΔT (°C)	$2N_1/2N_2$ (Reversals)	σ_{a1}/σ_{a2}* (MPa)	σ_{m1}/σ_{m2}* (MPa)	LDR using ε_a		LDR using ΔW_{HL}^T		DCD Method using $\sum W^T$
							D_1/D_2	D	D_1/D_2	D	
High-Low											
S123	0.04/0.02	0.50/3	20 36	6,000/2,130,352#	49/30	14/16	0.44/1.4	1.8	0.44/2.1	2.5	0.74
S101			31 37	6,000/1,371,616	47/30	-12/-9	0.44/0.9	1.5	0.44/0.3	0.72	1.6
S105	0.04/0.03	0.5/0.75	26 28	6,000/296,276	49/47	-11/-9	0.44/3.7	4.1	0.44/4.1	4.6	0.59
S102			28 27	6,000/412,318	47/47	-12/-10	0.44/5.1	5.5	0.44/5.6	6.1	0.53
S108			31 30	6,000/459,890	51/49	-12/-10	0.42/5.7	6.1	0.44/5.6	6	0.51
Low-High											
S103	0.03/0.04	0.75/0.5	27 31	100,000/33,542	51/51	-10/-11	0.65/3.4	4	0.65/2.6	3.3	0.72
S109			29 31	100,000/50,136	47/48	-10/-11	0.65/5.1	5.7	0.65/2.8	3.4	0.64
S106			22 29	100,000/53,076	50/49	-10/-11	0.65/5.4	6	0.65/4.1	4.7	0.63

*Measured at half-life cycle
#Runout

Table 5.4 Experimental results [77] and calculated cumulative damages for uniaxial fully-reversed (Rε = -1) strain-controlled fatigue tests of PEEK with two-block loading for frequency effect study (i.e. test condition (II)).

Specimen ID	$\boldsymbol{\varepsilon_{a1}/\varepsilon_{a2}}$ **(mm/mm)**	$\boldsymbol{f_1/f_2}$ **(Hz)**	$\boldsymbol{\Delta T}$ **(°C)**	$\boldsymbol{2N_1/2N_2}$ **(Reversals)**	$\boldsymbol{\sigma_{a1}/\sigma_{a2}}$* **(MPa)**	$\boldsymbol{\sigma_{m1}/\sigma_{m2}}$* **(MPa)**	**LDR using $\boldsymbol{\varepsilon_a}$**		**LDR using $\boldsymbol{\Delta W_{HL}^T}$**		**DCD Method using $\boldsymbol{\sum W^T}$**
							D_1/D_2	**D**	**D_1/D_2**	**D**	
High-Low											
S124	0.04/0.03	0.25/0.5	9	2,000/140,582	64/55	14/15	0.43/1.7	2.2	0.43/5.2	5.6	0.53
			15								
S114			37	2,000/241,626	64/55	-8/-7	0.43/3	3.4	0.43/3.9	4.3	0.61
			30								
Low-High											
S111	0.03/0.04	0.5/0.25	17	30,000/46,000	54/61	-10/-11	0.89/4.6	5.5	0.89/4.9	5.8	0.56
			14								
S113			17	30,000/53,434	55/61	-7/-7	0.89/5.4	6.3	0.89/3.9	4.8	0.56
			14								

*Measured at half-life cycle

Table 5.5 Experimental results [77] and calculated cumulative damages for uniaxial pulsating tension (Rε = 0) strain-controlled fatigue tests of PEEK with two-block loading (i.e. test condition (III)).

Specimen ID	$\boldsymbol{\varepsilon_{a1}/\varepsilon_{a2}}$ **(mm/mm)**	$\boldsymbol{f_1/f_2}$ **(Hz)**	$\boldsymbol{\Delta T}$ **(°C)**	$\boldsymbol{2N_1/2N_2}$ **(Reversals)**	$\boldsymbol{\sigma_{a1}/\sigma_{a2}}^*$ **(MPa)**	$\boldsymbol{\sigma_{m1}/\sigma_{m2}}^*$ **(MPa)**	**LDR using** $\boldsymbol{\varepsilon_a}$		**LDR using** $\boldsymbol{\Delta W_{HL}^T}$		**DCD Method using** $\boldsymbol{\sum W^T}$
							$\boldsymbol{D_1/D_2}$	**D**	$\boldsymbol{D_1/D_2}$	**D**	
High-Low											
S120	0.03/0.02	0.5/1.5	14	60,000/312,756	55/44	24/19	0.57/0.2	0.77	0.57/0.96	1.5	0.76
			16								
S116			21	60,000/645,088	52/42	1/-3	0.56/0.4	0.98	0.57/0.62	1.2	1.1
			31								
Low-High											
S121	0.02/0.03	1.5/0.5	20	300,000/65,032	45/54	24/24	0.44/0.8	1.2	0.44/3.1	3.5	0.5
			18								
S118			26	300,000/99,310	44/53	-0.19/0.88	0.44/1.2	1.6	0.44/1.7	2.1	1
			31								

*Measured at half-life cycle

Table 5.6 Experimental results [77] and calculated cumulative damages for uniaxial fully-reversed (Rε = -1) strain-controlled fatigue tests of PEEK with three- and four-block loadings (i.e. test condition (IV)).

Specimen ID	$\varepsilon_{a1}/\varepsilon_{a2}/\varepsilon_{a3}$ (mm/mm)	$f_1/f_2/f_3$ (Hz)	ΔT (°C)	$2N_1/2N_2/2N_3$ (Reversals)	$\sigma_{a1}/\sigma_{a2}/\sigma_{a3}$* (MPa)	$\sigma_{m1}/\sigma_{m2}/\sigma_{m3}$* (MPa)	LDR using ε_a		LDR using ΔW_{HL}^T		DCD Method using $\sum W^T$
							$D_1/D_2/D_3$	D	$D_1/D_2/D_3$	D	
High-Low-High											
S126	0.04	0.5	22	6,000	51	-11	0.44	5.4	0.44	3.6	0.58
	0.03	0.75	26	180,000	47	-9	0.46		0.46		
	0.04	0.5	21	44,098	59	10	4.4		2.7		
Low-High-Low											
S127	0.03	0.75	30	100,000	47	-7	0.65	4.1	0.65	4.1	0.54
	0.04	0.5	32	20,000	48	-9	0.44		0.44		
	0.03	0.75	31	239,800	46	-8	3		3		
Specimen ID	$\varepsilon_{a1}/\varepsilon_{a2}/\varepsilon_{a3}/\varepsilon_{a4}$ (mm/mm)	$f_1/f_2/f_3/f_4$ (Hz)	ΔT (°C)	$2N_1/2N_2/2N_3/2N_4$ (Reversals)	$\sigma_{a1}/\sigma_{a2}/\sigma_{a3}/\sigma_{a4}$* (MPa)	$\sigma_{m1}/\sigma_{m2}/\sigma_{m3}/\sigma_{m4}$* (MPa)	LDR using ε_a		LDR using ΔW_{HL}^T		DCD Method using $\sum W^T$
							$D_1/D_2/D_3/D_4$	D	$D_1/D_2/D_3/D_4$	D	
High-Low-High-Low											
S128	0.04	0.5	26	6,000	47	-10	0.44	4.3	0.44	4.6	0.5
	0.03	0.75	26	180,000	46	-8	0.46		0.46		
	0.04	0.5	31	20,000	48	-8	0.45		0.45		
	0.03	0.75	29	237,786	47	-6	2.9		3.2		

*Measured at half-life cycle

CHAPTER 6 MULTIAXIAL FATIGUE BEHAVIOR AND MODELING FOR A THERMOPLASTIC

6.1. Abstract

In this study, the fatigue behavior of a semi crystalline thermoplastic, polyether ether ketone (PEEK), is investigated under fully-reversed strain-controlled pure torsion as well as multiaxial loading. Multiaxial axial-torsion tests were conducted under two different conditions; proportional in phase (IP) and non-proportional 90° out of phase (OP) loading. The values of equivalent stress and strain amplitudes calculated using von Mises criterion was used to compare the fatigue lives obtained from different fatigue tests including uniaxial, multiaxial, and torsion loading. The stress responses under torsion, uniaxial, and IP and OP multiaxial loadings were investigated to understand the cyclic deformation behavior of PEEK polymer under different loading and its effects on fatigue lives. Results showed that under similar equivalent strain amplitudes, specimens subjected to OP multiaxial loading exhibited higher rise in temperature at the surface of the specimen, higher stress response, and shorter fatigue lives compared to IP multiaxial loading. Fatigue life models based on von Mises equivalent strain amplitude and cumulative total strain energy density were employed to correlate the fatigue data of PEEK under different types of loading. The energy based model with cumulative total strain energy density as the damage parameter was found to provide a reasonably well correlation of both uniaxial and multiaxial fatigue data with the 97% of predicted lives falling within the scatter bands of two from experimentally obtained fatigue lives.

6.2. Introduction

With the development in the field of polymer science and engineering, polymeric materials have transitioned from a low cost alternative to metals in simple static applications to materials of interest for fabricating structural components with dynamic load bearing capabilities. Properties such as high strength to weight ratio, resistance to chemical and wear degradations, as well as ease of processing and cost effectiveness make new generation, high strength engineering thermoplastics an ideal choice for various applications in automotive, aerospace, and bio-medical industries [1] . The state of stresses and strains at the critical location of the structural components used in majority of the applications is typically repetitive and are multiaxial in nature. The multiaxial stresses can be resulting from multidirectional external loading and/or stress concentrations [84]. Therefore, understanding the fatigue behavior of polymeric materials to establish their reliability under multiaxial cyclic loading condition is crucial.

Unlike metals, for which uniaxial and multiaxial fatigue behaviors under both constant and variable amplitude loadings are well investigated, studies dealing with the fatigue behavior of polymeric materials under cyclic and especially under multiaxial cyclic loadings are limited in the literature. Tao and Xia [85] studied the fatigue behavior of an Epoxy polymer subjected to strain-controlled pure torsion and proportional axial-torsion loadings with tensile mean strains. Obtained fatigue data was then correlated using stress, strain, and energy based models. Among all the fatigue models utilized, stress- and energy based models were reported to provide the best correlation of the fatigue life data obtained from uniaxial, pure torsion, and axial-torsion tests. The stress based model considered Stassi equivalent stress, while for the energy based model, the total strain energy density at half-life was used as the damage parameter.

Wang et al. [86] conducted a study on the fatigue behavior of micro-tube PEEK specimens under uniaxial, pure torsion, as well as proportional in phase (IP) and non-proportional out of phase (OP) axial-torsion multiaxial loadings. Different types of critical plane approaches such as Fatemi-Socie, Smith-Watson-Topper, and Chen-Xu-Huang were utilized to correlate the experimental data. Results showed that the Chen-Xu-Wang model, which considers the maximum shear strain plane as the critical plane, provided better fatigue life predictions as compared to other fatigue life models.

Mars and Fatemi conducted a thorough investigation on the fatigue behavior of filled natural rubber subjected to displacement-twist controlled uniaxial, pure torsion, proportional axial-torsion IP, and non-proportional axial-torsion OP multiaxial loadings [87-89]. The study on the effects of multiaxial stresses on the fatigue crack nucleation and growth of filled natural rubber, first presented in [87], indicated that the fatigue cracks nucleated and grew perpendicular to the plane of maximum principal strain. Moreover, theoretical aspects of most commonly used approaches for the analysis of crack nucleation behavior of rubber were presented in [88]. These approaches included traditional equivalence criteria such as maximum principal strain, strain energy density, octahedral shear strain, and cracking energy density. The study also emphasized that the analysis method adopted for metallic materials may not be consistently accurate for the fatigue analysis of rubber materials due to the fundamental differences in their failure mechanisms.

Equivalence criteria presented in [88] were then employed to analyze the fatigue life of natural filled rubber subjected to compression-torsion, pure torsion, tension-torsion, and pure tension loadings [89]. The compression-torsion and tension-torsion tests were conducted under variety of proportional and non-proportional loading conditions. Results

showed that among various classical equivalence criteria, the maximum principal strain provided the best correlation of the multiaxial data. In addition, the cracking energy criterion, the combination of energy based and critical plane approaches, was also resulted in a good correlation of fatigue data for the natural filled rubber subjected to multiaxial loading.

Klimkeit et al. [90], studied the fatigue behavior of two different types of polymeric materials: first a blend of polybutylene terephthalate and polyethylene terephthalate and second polyamide 66, both of which were reinforced with glass fiber. Force-controlled fatigue tests were conducted on tubular specimens under uniaxial, pure torsion, and combined axial-torsion loadings. Under uniaxial and torsion loading the cracking behavior was seen to be influenced by the microstructure as the orientation of the fibers corresponded with orientation of the crack, which was along the plane of maximum shear stress. In the case of combined axial-torsion loading, the crack propagation was reported to be along the plane of maximum principal stress although it did not correspond to the orientation of fibers. Three different classical fatigue models based on the maximum principal stress, von Mises stress, and strain energy density were employed to correlate the fatigue data of the two polymer-based composite materials, and the energy based model was found to better correlate the fatigue data.

Amjadi and Fatemi [91] studied the multiaxial fatigue behavior of various types of polymers including neat high density polyethylene (HDPE), polypropylene (PP), Polyamide 66 (PA66), along with short glass fibers reinforced PA 66 (PA66-G30). Force-controlled fatigue tests were conducted under uniaxial, torsion, and combined axial-torsion IP and OP multiaxial loadings. Fatigue cracks in the majority of loading conditions were

reported to initiate and grow along the plane of maximum shear stress. However, only in the case of IP multiaxial loading, the cracks were seen to initiate along the maximum shear stress plane but grow along the plane of maximum normal stress. Among employed fatigue life models, von Mises approach correlated the fatigue lives of uniaxial, torsion, and IP multiaxial loading, while it was not able to predict the detrimental effect of OP multiaxial loading. On the other hand, the stress version of Fatemi-Socie damage parameter was seen to better correlate the fatigue data as compared to the classical von Mises model.

In the current study, polyether ether ketone (PEEK), a semi-crystalline thermoplastic is chosen as a material of interest. Due to their high melting and glass transition temperature, this engineering thermoplastic exhibits superior mechanical properties in a wide range of temperatures. As a result, PEEK polymers are used as the matrix of composite systems [3, 92, 93] . Mechanical properties of PEEK polymers can be tailored by adding different types of filler materials to meet the requirements of a specific application. For instance, mechanical properties of PEEK implants can be altered to match the elastic modulus of cortical bones by introducing carbon fiber fillers, which enable uniform distribution of stresses between the bone and the implant [2, 3] . In the majority of applications, PEEK and its composites are subjected to the more realistic multiaxial cyclic loading throughout their service lifetime. Therefore, the fatigue behavior and failure mechanisms of PEEK polymer under multiaxial loading conditions need to be fully characterized before they can be reliably utilized in structural components under cyclic loading.

The deformation and fatigue behavior of PEEK polymer subjected to pure torsion, as well as multiaxial proportional IP and non-proportional 90° OP axial-torsion loading are

investigated and compared with the data generated previously under uniaxial loading. Detailed description on the material used and different loading types including IP, OP, and pure torsion are presented in experimental setup following the introduction. Deformation behavior represented by the stress responses obtained under strain-controlled torsion and multiaxial loading and its comparison to the ones obtained from the uniaxial fatigue testing in [42] are presented and discussed. Two different fatigue models are employed to correlate the fatigue life of PEEK under multiaxial as well as axial and torsion loading conditions and results are presented. Finally, important conclusions drawn for the observed multiaxial deformation and fatigue behaviors as well as modeling results are summarized

6.3 Material and Experimental Procedures

6.3.1 Material and specimens

Neat PEEK polymer (TECA PEEK by Ensigner Inc.) with melting temperature of 334°C and glass transition temperature of 143°C, supplied in the form of extruded rods with the diameter of 25 mm, was used in the current study. PEEK rods were further machined using a computer numerical controlled (CNC) lathe into a thin-walled tubular specimens with a gage length of 32 mm, outside diameter (OD) of 12.7 mm, and inside diameter (ID) of 10.6 mm following ASTM Standard E2207 [94], as shown in Fig. 6.1. Adequate coolant was used continuously during the machining of the specimens to eliminate the effect of heat generated due to the machining process. Fatigue specimens were further polished using different grit sand papers to remove any machining marks on both inside and outside surfaces. Due to the small wall thickness and ease in removal of thermoplastics, special care was taken during the machining process to obtain best possible surface finish and to minimize post machining polishing steps.

6.3.2 Cyclic loading

All of the axial-torsion and pure torsion fatigue tests were conducted under strain-controlled, fully-reversed ($R\varepsilon = -1$) loading condition using an MTS close-loop servo-hydraulic test frame with axial and torsional load capacity of 10 kN and 100 N-m, respectively. An Epsilon axial-torsion extensometer was used to control as well as measure both axial and shear strain amplitudes applied on the gage section of the specimens. A sinusoidal waveform with three different types of strain paths, including IP and OP with ratio of axial, ε, to shear, γ, strain amplitudes of $\lambda = \frac{1}{\sqrt{3}}$ as well as pure torsion loading with $\lambda = 0$ were used to study the effect of loading path on the fatigue behavior of PEEK polymer. Schematics showing the axial and shear strains under IP, OP, and torsion loadings are presented in Figs. 6.2(a), 6.2(b), and 6.2(c), respectively.

As polymeric materials are poor conductor of heat and are viscoelastic in nature, the temperature on the gage section of the specimen can rise upon fatigue loading and can affect the resulting fatigue life [42] . The change in temperature is known to be affected by the cyclic strain rate, adjusted by the test frequency in this study. The equivalent strain amplitude for multiaxial and torsion tests was calculated using von Mises equation and the test frequency was set to be similar to the equivalent uniaxial tests in [42]. The test frequencies in [42] were adjusted to maintain similar rise in temperature on the gage section of the uniaxial specimens and to obtain somewhat similar average cyclic strain rates for all fatigue tests. Rise in temperature on the gage section of each specimen was also monitored using a laser thermometer through the entire duration of the fatigue test. The failure criterion was defined as a 50% drop in the value of either load or torque as compared to

the ones at the mid-life of the specimen, and the fatigue tests that exceeded 10^6 cycles were stopped and considered as run-outs.

6.4 Cyclic Deformation Behavior

To study the behavior of PEEK under multiaxial cyclic loading, axial and shear stress amplitudes were obtained at the mid-life cycle for each test. The values of equivalent strain and stress amplitudes were then calculated based on von Mises relationships given as [95]:

$$\bar{\varepsilon}_a = \frac{\Delta\bar{\varepsilon}}{2} = \frac{1}{\sqrt{2}\,(1+\bar{\nu})}\sqrt{2(\varepsilon_a)^2\,(1+\bar{\nu})^2 + \frac{3}{2}\,(\gamma_a)^2} \tag{6.1}$$

$$\bar{\sigma}_a = \frac{\Delta\bar{\sigma}}{2} = \sqrt{(\sigma_a)^2 + 3(\tau_a)^2} \tag{6.2}$$

where, $\bar{\varepsilon}_a$, $\bar{\sigma}_a$, ε_a, σ_a, γ_a, and τ_a, are the equivalent strain, equivalent stress, axial strain, axial stress, shear strain, and shear stress amplitudes, respectively. For the multiaxial loading conditions, transverse strain amplitude, ε_{a_tr} is considered to be a function of axial strain amplitude and equivalent Poisson's ratio, $\bar{\nu}$, represented by $\varepsilon_{a\_tr} = -\bar{\nu}\varepsilon_a$. Furthermore, the equivalent Poisson's ratio is calculated using:

$$\bar{\nu} = \frac{\nu_e \Delta\varepsilon_e + 0.5\,\Delta\varepsilon_p}{\Delta\varepsilon_p} \tag{6.3}$$

where ν_e is elastic Poisson's ratios and $\frac{\Delta\varepsilon_e}{2}$, $\frac{\Delta\varepsilon_p}{2}$, and ε_a are elastic, plastic, and total strain amplitudes, respectively. For the PEEK polymer, value of ν_e was found to be 0.4 [86].

Since all the fatigue tests in the current study were conducted under strain-controlled loading, the axial and shear strains on the surface of the specimen were directly measured from the extensometer reading. The axial stress, which is uniform throughout the gage section of the specimen, was calculated based on the axial load obtained from the data

acquisition system and the surface area at the gage section of the specimen. While the axial strain at the mid-section of the specimen was assumed to be similar to the axial strain on the surface, the shear stress and strain values were determined at the mid-section of the specimen using [96] :

$$\tau_{a\_mid} = \frac{T_a}{r_{mid}A} \tag{6.4}$$

$$\gamma_{a\_mid} = \gamma_{a\_surf}\left(\frac{r_{mid}}{r_{surf}}\right) \tag{6.5}$$

where τ_{a_mid} is the shear stress amplitude at the mid-section of the specimen, T_a is the torque amplitude, r_{mid} is the mid-section radius and r_{surf} is the surface radius of the gage, *A* is the cross-section area of the gage section and γ_{a_mid} and γ_{a_surf} are the shear strain amplitude at mid-section and surface of the gage of the tubular specimen, respectively.

It is important to note that the fatigue cracks typically initiate from the surface of the specimen, where the value of shear stress/strain are higher compared to the ones calculated at the mid-section of the specimen. In order to determine the shear stress at the surface of the specimen, first the constitutive equivalent stress and strain relation is determined from the mid-section shear stress and strain amplitudes using a Ramberg-Osgood type equation. The equivalent strain amplitude in the initial region was considered for the analysis because not all the tests under multiaxial loading reached to the steady state region, which will be discussed further in later sections. The equivalent total strain amplitude, calculated from Eq. (6.1), at the initial stage of stress response was first separated into equivalent elastic and plastic strain amplitude. The equivalent elastic strain, $\frac{\Delta\bar{\varepsilon}_e}{2}$, is calculated using the Hooke's law, which is given as:

$$\frac{\Delta\bar{\varepsilon}_e}{2} = \frac{\bar{\sigma}_a}{E} \tag{6.6}$$

where $\bar{\sigma}_a$ is the equivalent stress amplitude and E is the Young's modulus. Considering equivalent total strain amplitude as the sum of equivalent elastic and plastic strain amplitudes, the equivalent plastic strain amplitude, $\frac{\Delta\bar{\varepsilon}_p}{2}$ is then determined as:

$$\frac{\Delta\bar{\varepsilon}_p}{2} = \bar{\varepsilon}_a - \frac{\bar{\sigma}_a}{E} \tag{6.7}$$

Further, the relation between calculated equivalent plastic strain amplitude with equivalent stress amplitude can be represented by a power law as [30] :

$$\bar{\sigma}_a = K' \left(\frac{\Delta\bar{\varepsilon}_p}{2}\right)^{n'} \tag{6.8}$$

where K' is the cyclic strength coefficient, taken as the intercept and n' is the cyclic strain hardening coefficient considered as the slope of the fitted line. Finally, using Eqs. (6.6) – (6.8), the equivalent strain-stress amplitudes relationship can be represented by a Ramberg-Osgood type equation given as [30]:

$$\bar{\varepsilon}_a = \frac{\Delta\bar{\varepsilon}_e}{2} + \frac{\Delta\bar{\varepsilon}_p}{2} = \frac{\bar{\sigma}_a}{E} + \left(\frac{\Delta\bar{\sigma}}{2K'}\right)^{\frac{1}{n'}} \tag{6.9}$$

Cyclic equivalent stress-strain amplitudes data and fitted curves for IP and OP multiaxial loading based on Eq. (6.9) is shown in Fig. 6.3. As seen, the cyclic stress-strain curve for OP multiaxial loading is slightly higher than that of IP multiaxial loading. This may suggest that the PEEK polymer exhibits some non-proportional cyclic hardening, which has been also reported for various metallic materials [97, 98] and for some polymeric materials [99]. While shorter fatigue lives under OP multiaxial loading have been reported even for materials with no non-proportional cyclic hardening [100, 101], the

extra hardening can potentially affect the fatigue behavior of PEEK under OP multiaxial loading.

Once the constitutive equivalent stress-strain relationship using mid-section shear stress and strain amplitudes is established, the surface equivalent strain amplitude is then calculated using the surface shear strain amplitudes taken from the extensometer reading using Eq. (6.1). Based on the value of equivalent strain amplitude at the surface, the surface equivalent stress amplitude is then determined from the Ramberg-Osgood equation given in Eq. (6.9) and Fig. 6.3. Finally, using the surface equivalent stress amplitude, the surface shear stress amplitude can be determined using Eq. (6.2), where the axial stress obtained from the test is considered to be constant throughout the section. Using Eqs. (6.1) – (6.9) , the values of ε_a, Υ_{a_surf}, σ_a obtained from mid-life and first cycle, τ_{a_mid}, γ_{a_mid}, $\bar{\varepsilon}_{\text{a\_mid}}$, and $\bar{\sigma}_{\text{a\_mid}}$ are calculated and along with the rise in temperature, ΔT, and reversals to failure, $2N_f$, are listed in Table 6.1.

From previous studies under strain-controlled uniaxial loading condition, PEEK polymer, similar to many other polymers, exhibited cyclic softening phenomenon with three distinct stages of stress response; initial, transition, and steady state [27, 42]. Constant and relatively high value of stress for first few number of reversals represented the initial stage, which was followed by the abrupt drop in the stress response during the transition stage resulting from breaking of polymeric chains as well as increase in temperature due to viscoelastic nature of polymeric materials. Finally, upon further straining, the stress response attained a constant value at the steady stage region until the specimen failure [27, 42]. Furthermore, all the three stages of cyclic behavior were distinctly observable in all the uniaxial fatigue tests performed in previous studies, with the majority of the fatigue life

being spent at the steady state region (~ <95% of the total fatigue life) for all values of stress amplitudes. Previous studies have shown that the incorporation of deformation behavior and stress-strain relationship at each of the stages in the fatigue life model was critical to obtain a decent correlation of fatigue life data [42, 53, 77, 102] . Therefore, cyclic deformation behavior represented by the axial and shear stress responses for PEEK polymer under IP and OP multiaxial loadings are presented and compared with the results observed from the uniaxial fatigue tests in this section.

To compare the variation in cyclic deformation behavior, stress responses, including axial stress, σ, shear stress, τ, and equivalent stress, $\bar{\sigma}$ are shown, respectively, in Figs. 6.4(a), 6.4(b), and 6.4(c) for specimen S16 subjected to IP multiaxial loading with an equivalent strain amplitude of 0.025 mm/mm (with mid-section σ_a = 55 MPa and τ_a = 1.19 MPa). The stress response obtained for a specimen subjected to strain amplitude of 0.025 mm/mm under uniaxial loading [42] is also presented in Fig. 6.4(d). The axial stress response and equivalent stress response are noticeably very similar in the IP multiaxial tests (see Figs. 6.4(a) and 6.4(c)), which may be attributed to the shear stress being relatively small compared to the axial stress, although axial to shear strain ratio of $\lambda = \frac{1}{\sqrt{3}}$ was considered for all multiaxial fatigue tests. However, even under almost identical equivalent strain amplitudes, the cyclic softening behavior observed under IP multiaxial loading (see Figs. 6.4(a), 6.4(b), and 6.4(c)) is significantly different to the one under uniaxial loading (see Fig. 6.4(d)). Comparing these figures, the initial, transition, and steady state regions of stress response are not clearly observable under IP multiaxial loading and it seems that the majority of the life is spent in the initial stage of the cyclic stress response.

Another important observation from Fig. 6.4 that needs to be mentioned is the lower value of axial stress at the initial region of the stress response for the IP specimen in Fig. 6.4(a) compared to the specimen under uniaxial loading in Fig. 6.4(d). Although the equivalent strains in Fig. 6.4(a) and 6.4(d) are similar, the axial strain under IP multiaxial loading is lower compared to uniaxial loading, which may have resulted in lower value of axial stress. This difference in the value of axial stress may indicate that at the initial region, axial stress is more influenced by the axial strain and not the combined effect of axial and shear strains. To further evaluate this observation, axial stress at the initial region for specimens subjected to IP and OP multiaxial loading presented in Table 6.1 were compared to that under uniaxial loading published in [103] with similar axial strain amplitudes. Result showed that under similar axial strains, of the axial stresses at the initial stage of multiaxial and uniaxial loading were similar.

As it can be seen in Figs. 6.4(a) and 6.4(b), axial and shear stress responses under IP multiaxial loading follow a similar trend in cyclic behavior and simultaneously transform from one stage of cyclic deformation to the next stage. This behavior was observed in all of the specimens subjected to multiaxial loading. In addition, the percentage reduction in the axial and shear stress amplitudes in initial and steady state regions were also observed to be similar in all of the multiaxial tests. For instance, the percentage reduction in the value of axial stress and shear stress between initial and steady state region was calculated to be respectively 20% and 19% for specimen S16 in Fig. 6.4.

Although the stress responses were seen to follow a similar trend from the comparison of Figs. 6.4(a) and 6.4(b), the values of axial and shear stresses were significantly different. Under identical loading condition including equivalent strain

amplitude and loading type, the value of shear stress was calculated to be much lower as compared to the axial stress response. It is also worth mentioning that for most metallic materials, the ratio of axial to shear stress is approximately 1.7 under a strain-controlled loading with $\lambda = \frac{1}{\sqrt{3}}$. However, for the PEEK polymer under multiaxial loading in the current study, the ratio of axial to shear stress was calculated to be ~ 42.15.

Axial stress responses obtained for IP multiaxial tests conducted at equivalent strain amplitudes of 0.025, 0.030, and 0.040 mm/mm are presented in Figs. 6.5(a), 6.5(b), and 6.5(c), respectively. In all of the plots presented in Fig. 6.5, the x-axis (i.e. number of reversals) are in linear scale and not in logarithmic scale. A distinct variation in the stress response is clearly evident among the specimens subjected to different equivalent strain amplitudes. For specimen S16 (Fig. 6.5(a)) and S30 (Fig. 6.5(c)) subjected to the equivalent strain amplitudes of 0.025 and 0.040 mm/mm, the majority of the fatigue life was spent in the transition region (~58% for S16 and ~ 61% for S30). On the other hand, for specimen S23 (Fig. 6.5(b)) subjected to the equivalent strain amplitude of 0.030 mm/mm, the stress response was dominated by the steady state region, which comprised of ~83% of the total fatigue life. Although the majority of the stress response for specimen S23 was spent in the steady state region, in general the stress responses under IP multiaxial loading varied to those observed from the uniaxial fatigue tests (Fig. 6.4(d)), in which ~99% of the total fatigue life was spent in the steady state region [42, 77].

Similar to the IP multiaxial loading, axial, shear, and equivalent stress responses obtained for specimen S17 subjected to OP multiaxial loading with equivalent strain amplitude of 0.020 mm/mm are presented in Figs. 6.6(a), 6.6(b), and 6.6(c), respectively. Analogous to the IP multiaxial loading, the shear stress values were seen to be much

smaller than the axial stresses at all strain levels tested in this study. As a result, equivalent and axial stress responses were seen to be almost identical, as evident from Figs. 6.6(a) and 6.6(c) as well as from Table 6.1. The deformation behavior represented by the axial and shear stress responses were also seen to follow a similar trend as both transitioned from initial to transition, and later to steady state regions at the same number of reversals. Furthermore, the percentage drop in the value of axial and shear stress at initial and steady state region for specimen S17 was determined to be 66% and 71%, respectively. The similarity between the stress drop from initial to steady state region of axial and shear channels was seen in all OP multiaxial tests.

In order to compare the deformation behavior obtained from uniaxial and multiaxial tests, the stress response obtained from uniaxial loading at strain amplitude of 0.020 mm/mm [42] is presented in Fig. 6.6(d). As can be seen, although all three stages (i.e. initial, transition, and steady state) were evident and the majority of the fatigue lives were spent in steady state region in both OP multiaxial and uniaxial loading, the number of reversals spent in each of the stages were significantly different. In the case of uniaxial loading, the specimen spent a longer number of reversals in the initial region, while in the case of OP multiaxial loading, the specimen spent less time in the initial region and entered the transition region after a couple of hundred reversals of loading.

Axial stress response obtained for specimens S18, S17, and S26 subjected to OP multiaxial loading with equivalent strain amplitudes of 0.015, 0.020, and 0.025 mm/mm are shown in Figs. 6.7(a), 6.7(b), and 6.7(c), respectively. Similar to Fig. 6.5, the x-axis (i.e. number of reversals) in Fig.6.7 is in linear scale and not in logarithmic scale. At lower equivalent strain amplitude of 0.015 mm/mm (S18 in Fig. 6.7(a)), axial stress remained

constant throughout the fatigue test, whereas for the specimen subjected to the equivalent strain amplitude of 0.020 mm/mm (S17 in Fig. 6.7(b)), the majority of the fatigue life (i.e. ~ 95%) was spent at the steady state region; only 5% of the fatigue life for S17 specimen was spent in the transition region and almost no initial stage was noticed. However, under higher equivalent strain amplitude of 0.025 mm/mm (S26 Fig. 6.7(c)), 69% of the fatigue life was spent under transition region and only 25% of the total fatigue life was spent at the steady state region. This observation was similar to the one noticed in Fig. 6.5 for IP multiaxial loading, in which the majority of fatigue live was also spent in initial, steady state, and transition region respectively, under low, mid, and high equivalent strain amplitudes.

Significantly different stress responses were observed for specimens subjected to IP and OP multiaxial loading under identical equivalent strain amplitude of 0.025 mm/mm and frequency shown in Figs. 6.5(a) and 6.7(c), respectively. Under IP multiaxial loading, specimen spent longer period of time in the initial region (approximately 14% of the fatigue life), while specimen reached the transition region at 5% of the fatigue life under OP multiaxial loading. Furthermore, the reduction in the stress response (i.e. percentage drop in the stress value) from initial to the steady state region was calculated to be higher in the case of OP multiaxial loading (~69% for specimen S26), as compared to the IP multiaxial loading (~20% for specimen S16) under a similar equivalent strain amplitude of 0.025 mm/mm Furthermore, the rise in temperature on the gage section of the specimen was observed to be higher for specimen S26 ($\Delta T = 40^\circ$ C) compared to S16 ($\Delta T = 26^\circ$ C), as listed in Table 6.1.

In order to also compare the effect of multiaxial load path (i.e. IP versus OP) on the cyclic deformation behavior, the stress responses obtained for IP and OP multiaxial tests with similar axial and shear strains were compared using Fig. 6.5(b) (ε_a = 0.021 mm/mm, γ_a = 0.037 mm/mm) and Fig. 6.7(b) (ε_a = 0.020 mm/mm, γ_a = 0.035 mm/mm), respectively. Even under similar value of axial and shear strain amplitudes, the specimen subjected to OP multiaxial loading (S17 in Fig. 6.7(b)) reached the transition region in a lower number of reversals (~ 200 reversals) as compared to the specimen S23 in Fig. 6.5(b) and under IP multiaxial loading (~ 2900 reversals). Stress response also revealed a higher percentage drop in the value of stress from initial to steady state region in OP multiaxial test (~ 66%) compared to that seen in IP multiaxial test (~ 28%). Therefore, reaching the steady state region in shorter number of reversals as well as higher drop in stress between initial and steady state region under multiaxial OP multiaxial loading, whether they are compared based on equivalent strain amplitudes or axial/shear strain amplitudes, may indicate that the OP multiaxial loading has a more detrimental effect on the fatigue strength as compared to the IP multiaxial loading.

As mentioned earlier, a significant variation was observed in the axial stress response between uniaxial and multiaxial loading. This variation may also be related to the differences in the specimen geometry, which can influence the rise in temperature at the gage section of the specimen and eventually affect the cyclic softening behavior. Uniaxial fatigue tests are conducted using solid specimen, while multiaxial tests are conducted on thin-walled tubular specimens. As a result, under identical strain amplitude, the temperature at the gage section of the specimen may increase in a faster rate and reach the steady state temperature at lower number of reversals under the multiaxial state of loading

(thin-walled specimen). To further analyze this observation, the number of reversals needed for the rise in temperature to attain steady state were compared between specimens subjected to uniaxial and OP multiaxial loading at strain amplitude of 0.025 mm/mm and frequency of 1 Hz. In the case of uniaxial specimen, the rise in temperature was seen to stabilize around 4,112 reversals, while for the OP multiaxial specimen, the rise in temperature was seen to stabilize at ~ 1,200 reversals.

Similar comparison was also conducted between uniaxial and IP multiaxial loading under identical equivalent strain of 0.030 mm/mm and test frequency of 0.75 Hz. In contrast to OP multiaxial loading, the rise in temperature for specimen under IP multiaxial loading was seen to stabilize at a higher number of reversals (~23,228 reversals) compared to uniaxial loading (~1,630 reversals). However, it should be noted that the rise in temperature and stress response in the case of multiaxial loading maybe primarily governed by the applied axial strain than shear strain. Hence, the number of reversals required for the specimen under IP multiaxial loading (with axial strain amplitude of 0.021 mm/mm) was compared with the uniaxial loading under 0.020 mm/mm strain amplitude. Interestingly, similar to the OP multiaxial loading, the rise in temperature at the gage section of the specimen under IP multiaxial loading was seen to reach steady state at lower number of reversals (~ 23,228 reversals) compared to uniaxial loading (~48,000 reversals).

Shear stress response obtained for pure torsion loading under shear strain amplitude of 0.069 mm/mm and equivalent strain amplitude of 0.040 mm/mm is shown in Fig 6.8. Under pure torsion loading, the shear stress amplitude remained constant throughout the fatigue test and temperature at the gage section of the specimen remained similar to the room temperature as well. Under identical equivalent strain amplitude of 0.040 mm/mm,

specimens subjected to pure torsion loading ($2N_f$ = 739,900 reversals) was seen to exhibit significantly better fatigue resistance compared to uniaxial ($2N_f$ = 20,314 reversals) as well as IP multiaxial loading ($2N_f$ = 1,211 reversals). In addition, for equivalent strain amplitudes lower than 0.040 mm/mm, no failure was observed under torsion loading up to 2,000,000 reversals; therefore, tests were terminated and marked as run-outs. This may indicate that the damage induced by pure torsion loading may be significantly smaller compared to the one induced by axial loading. However, when combined with the axial loading, the deformation induced by the shear strain may result in some additional detrimental effects on the fatigue resistance, causing the specimens subjected to combined axial-torsion loading to exhibit shorter fatigue lives as compared to uniaxial loading with the same value of equivalent as well as axial strain amplitudes.

6.5 Fatigue Behavior and Modelling

6.5.1. Fatigue behavior under multiaxial loading

In general, materials subjected to IP multiaxial loading have been reported to exhibit higher fatigue resistance compared to those under OP multiaxial loading. Similar results were observed in the case of PEEK polymer, as the fatigue life of specimens tested under IP multiaxial loading were seen to be comparably higher than those tested under OP multiaxial loading. Under identical values of equivalent strain amplitudes as well as similar axial and shear strain amplitudes, specimens subjected to IP multiaxial loading were seen to have lower rise in temperature at the surface of the specimens and much longer fatigue lives compared to those for specimens subjected to OP multiaxial loading in Table 6.1.

For instance, specimen S16 subjected to IP multiaxial loading with equivalent strain amplitude of $\bar{\varepsilon}_a$ = 0.025 mm/mm lasted for 321,684 reversals and the temperature in the

gage section was seen to increase by 26°C. However, specimen S25 subjected to identical equivalent strain amplitude of 0.025 mm/mm under OP multiaxial loading lasted for only 1,730 reversals, while the rise in temperature at the gage section was measured to increase by 41°C. Similarly, fatigue life of specimen S06 subjected to IP multiaxial loading with axial strain amplitude of ε_a = 0.021 mm/mm and shear strain amplitude of γ_a = 0.037 mm/mm was observed to be higher ($2N_f$ = 165,718 reversals) and the rise in temperature at the gage section was seen to be lower (ΔT = 19° C) when compared to specimen S05 under OP multiaxial loading with ε_a = 0.020 mm/mm, γ_a = 0.035 mm/mm, resulting in $2N_f$ = 69,910 reversals and ΔT = 54° C. This is also very interesting because axial stress under IP multiaxial loading is significantly larger than the one under OP multiaxial loading (54 MPa for IP (S06) versus 28 MPa (S05)) and shear stresses are very small in both specimens.

From the cyclic stress-strain curve shown in Fig. 6.3, which was based on the stresses obtained from the initial region of stress responses, PEEK polymer exhibited some level of non-proportional cyclic hardening behavior, which may also have some detrimental effect on the fatigue live of OP specimens. More importantly, the number of reversals spent in the initial region prior to reaching transition region was observed to be higher in IP multiaxial tests compared to the OP multiaxial tests. The transition region can be is associated with breaking of polymeric bonds, permanent deformation, and rise in temperature due to self-heating [24, 27, 42]. Therefore, such results may signify that OP multiaxial loading may have a higher detrimental effect on the deformation behavior of PEEK polymers, which consequently results in shorter fatigue lives.

6.5.2. Fatigue modelling under uniaxial and multiaxial loading

Under multiaxial loadings, the cyclic behavior represented by the stress responses for PEEK polymer was seen to be significantly different when compared to the ones seen under uniaxial loading. As a result, fatigue life models capable of correlating the fatigue data of PEEK polymers under uniaxial loading may or may not be appropriate to accurately predict their fatigue life under more realistic multiaxial state of loading. In the current study, two different types of fatigue life models, one based on octahedral shear strain theory (i.e. von Mises model) and other one based on cumulative total strain energy density were employed to correlate fatigue life. The main goal of this study is to identify a fatigue life model capable of correlating the fatigue data of PEEK polymer under both uniaxial [42, 102] and multiaxial loadings. It is also important to point out that surface equivalent stress and strain amplitudes were observed to be very similar to the mid-section equivalent stress and strain amplitudes. As a result, the calculations for the damage parameters in the current study were conducted using mid-section shear stress, shear strain, equivalent stress, and equivalent strain.

6.5.2.1. Octahedral shear strain theory

One of the most commonly used strain based method to incorporate the combined effect of axial and torsion loading is the octahedral shear strain theory also known as von Mises model. To investigate the ability of this method to correlate fatigue data under various multiaxial loadings, equivalent strain amplitude calculated using Eq. 6.1 was plotted against corresponding fatigue lives and is presented in Fig. 6.8(a). Strain amplitude versus fatigue lives obtained from the uniaxial test with nominal rise in temperature at the surface of the specimen along with the Coffin-Manson fit, which are discussed in detail

and is published in [42] was also included in Fig. 6.8(a). These uniaxial data and fit serve as the baseline for fatigue life predictions under multiaxial loading.

For both metals and polymers, it has been well established that under identical equivalent stress/strain amplitudes, the OP multiaxial loading has often higher detrimental effect on the fatigue life when compared to proportional IP multiaxial loading [30, 84, 91, 101, 104]. Hence, a distinct separation between the fatigue data of IP and OP multiaxial loading may suggest that the employed octahedral shear strain theory (von Mises) was not able to accurately consider higher amount of damage induced during the OP multiaxial loading compared to the IP multiaxial loading. The short coming of von Mises classical model to correlate the fatigue data of both metallic and polymeric materials under OP multiaxial loading has also been reported in other studies [84, 91]. Interestingly, at lower strain amplitude of 0.025 mm/mm and 0.030 mm/mm, similar fatigue lives were observed for tests conducted under IP multiaxial and uniaxial fatigue loading, while the IP multiaxial loading was seen to be more detrimental at a higher equivalent strain amplitude of 0.040 mm/mm.

Predicted fatigue lives calculated based on the Coffin-Manson fit obtained from uniaxial strain-controlled fatigue test presented in detail in [42] are plotted against experimentally observed fatigue lives for uniaxial and multiaxial loading in Fig. 6.8(b). As the figure shows, all the fatigue life predictions under the OP multiaxial loading and the once for IP multiaxial loading at a higher equivalent strain amplitude are outside the factor of two scatter bands from experimentally obtained fatigue lives. Therefore, to accurately correlate the fatigue data of the PEEK polymer under various loading conditions, one may

need to understand the damage mechanism and cyclic deformation behavior and incorporate them in the fatigue model

6.5.2.2. Cumulative total strain energy density approach

Previous studies conducted on the fatigue behavior of PEEK subjected to uniaxial strain-controlled cyclic loading have shown that the overall shape and size of hysteresis loop need to be considered by employing energy based models in order to correlate the fatigue life data generated under various strain rates, mean stresses and variable amplitude loading [42, 102]. In the energy based approaches, the input energy is divided into two parts, the irrecoverable plastic strain energy density and recoverable elastic energy density. The area inside the hysteresis loop is considered as the plastic strain energy density, ΔW^p, while tensile area under the hysteresis loop is taken as the elastic strain energy density, ΔW^{E+}, which are shown in the schematic in Fig. 6.9.

In general, the irrecoverable plastic strain energy density is considered as the primary factor resulting to causing damage in the material. However, in some cases, such as tests conducted under tensile mean stress loading or at lower strain amplitudes (i.e. where the value of plastic strain energy is difficult to determine due to small or no plastic deformation), total strain energy density, ΔW^T, which is considered as the sum of both plastic and tensile portion of elastic strain energy density is reported to better correlate the fatigue life data.

$$\Delta W^T = \Delta W^p + \Delta W^{E+} \tag{6.10}$$

Overall fatigue life of PEEK polymer subjected to different types of uniaxial strain-controlled fatigue loading, including constant amplitude tests with and without mean strain and variable amplitude block loading tests conducted at different frequencies, was seen to

be affected by the fraction of fatigue life spent at different stages of stress response i.e. initial, transition, and steady state regions [42, 53, 77]. As a result, a fatigue model capable of incorporating the damage induced during each of these stages of deformation was found to correlate the fatigue data of PEEK polymer under uniaxial strain-controlled loading [102]. It is also important to mention that unlike uniaxial loading, majority of the fatigue life under multiaxial loading was not always spent in the steady state region. Therefore, considering the damage induced during different stages of deformation for PEEK under multiaxial loading may be even more critical than uniaxial loading.

For incorporating damage accumulated through different stages of deformation, cumulative total strain energy density calculated by adding total strain energy density for all cycles, is considered as the damage parameter in this study. In addition, under multiaxial loading, the damage induced by the combination of axial and torsion loading can affect the final fatigue life and is essential to be considered. As a result, the total axial strain energy density was first determined using Fig. 6.9 and Eq. (6.10) from the axial stress-strain hysteresis loops. Finally, values of total axial strain energy density from each of the cycles were then added together for calculating the cumulative total axial strain energy density, given as:

$$\sum W_{axial}^{T} = \sum W_{axial}^{P} + \sum W_{axial}^{E+} \tag{6.11}$$

where $\sum W_{axial}^{T}$ is the cumulative total strain energy density, $\sum W_{axial}^{P}$ is the cumulative plastic and $\sum W_{axial}^{E+}$ is the cumulative tensile elastic strain energy density obtained from axial stress-strain hysteresis loops. Similarly, from the shear stress-strain data, first the total shear strain energy density for each cycle was calculated, which were then added together to determine the cumulative total shear strain energy density given as:

$$\sum W_{shear}^{T} = \sum W_{shear}^{P} + \sum W_{shear}^{E+} \quad (6.12)$$

where $\sum W_{shear}^{T}$ is the cumulative total strain energy density, $\sum W_{shear}^{P}$ is the cumulative plastic, and $\sum W_{shear}^{E+}$ is the cumulative tensile elastic strain energy density obtained from torsion stress-strain hysteresis loop. Finally, the cumulative total strain energy density, W_{MA}^{T} for specimen under multiaxial loading is then calculated as:

$$\sum W_{MA}^{T} = \sum W_{axial}^{T} + \sum W_{shear}^{T} \quad (6.13)$$

The cumulative total strain energy density represents the all of energy dissipated during the entire fatigue life of a specimen due to both axial and shear loading. Furthermore, the value of tensile elastic and plastic strain energy densities under both axial and shear loading was determined from the actual hysteresis loop and were not based on equations. Hence, any effect of loading paths on the dissipated strain energy density will also affect the hysteresis loop, which as a result will be incorporated during the calculation of cumulative axial and shear strain energy densities. Therefore, in the current study, the cumulative total strain energy density was calculated by adding cumulative total axial and shear strain energy densities each determined using axial stress-strain and shear stress-strain hysteresis loops for both IP and OP multiaxial loadings.

Figure 6.10(a) presents cumulative total strain energy density versus fatigue life for torsion, IP and OP multiaxial loading along with fatigue data obtained from uniaxial nominal rise in temperature tests gathered from [102]. Using the cumulative total strain energy density as the damage parameter provided a good correlation for the fatigue data from IP and OP multiaxial loading with the uniaxial fatigue data indicated by the R^2 value of 0.97. The proposed model was not able to correlate the fatigue data obtained under torsion loading; however, fatigue failure was only obtained for one specimen under torsion

loading. The rest of the specimens under torsion loading at lower strain levels reached 10^6 cycles and considered as run-outs, as indicated by red arrows in Fig. 6.10 (a). Furthermore, predicted fatigue lives based on uniaxial data with nominal temperature rise are compared with experimentally observed fatigue lives for IP and OP multiaxial data in Fig. 6.10(b) along with scatter bands of two. As can be seen from this figure, fatigue lives of IP and OP multiaxial specimens are predicted well based on the cumulative total strain energy density damage parameter and the curve fitted to the uniaxial fatigue data with nominal temperature rise. Significantly better correlation of fatigue data in Fig 6.10 can be attributed to the fact that cumulative total strain energy density could incorporate the damage accumulated throughout the fatigue life of the specimen during different stages of cyclic deformation under both uniaxial as well as multiaxial loading and also reflect the detrimental effects of OP multiaxial loading.

Finally, Fig. 6.11 presents the predicted fatigue lives for various types of uniaxial constant amplitude tests with and without mean strains at different frequencies [42], variable amplitude block loading tests [102], and IP and OP multiaxial tests, generated in this study, using cumulative total strain energy density versus experimentally obtained fatigue lives. It is important to note that all prediction in Fig 6.11 under different loading conditions were made based on the cumulative total strain energy density versus fatigue life data obtained for PEEK specimens subjected to uniaxial fully-reversed strain-controlled loading with frequency adjusted to maintain a nominal temperature rise on the surface of the specimen. As can be seen from the figure, the employed damage parameter based on the cumulative total strain energy density was able to correlate all of the fatigue data within a factor of three scatter, with 97% of the fatigue data falling within the scatter

bands of two. Therefore, capturing and incorporating the damage induced during different stages of cyclic deformation, regardless of the loading condition, seem to be the key for an accurate fatigue life prediction for the PEEK polymer, and perhaps other polymeric materials subjected to fatigue loading.

6.6 Conclusions

In the current study, the effect of pure torsion loading along with two different types of multiaxial loading (i.e. proportional in phase (IP) and not-proportional 90° out of phase (OP)) on the cyclic deformation behavior and fatigue resistance of PEEK polymer was investigated. Based on the results obtained from the cyclic deformation and fatigue behavior, two different types of fatigue life models, including strain based and energy based approaches were employed to correlate the fatigue life data of PEEK under multiaxial as well as uniaxial loading using a single master curve. Based on the experimental results and discussions presented, the following conclusions can be drawn:

1. Under multiaxial loading condition, the stress response exhibited by PEEK polymer could be distinguished into initial, transition, and steady state regions similar to the ones observed under uniaxial loading condition. However, compared to uniaxial fatigue loading, under multiaxial loading, majority of the fatigue lives for PEEK polymer was not always spent in the steady state region but varied based on the applied equivalent strain amplitude.
2. At similar equivalent or axial strain amplitudes, PEEK polymer exhibited lower fatigue resistance and higher rise in temperature at the surface of the specimen under non-proportional 90° out of phase loading compared to when the material was subjected to proportional in phase loading.

3. Classical octahedral shear strain theory based von Mises model could not correlate the fatigue data of PEEK polymer under multiaxial loading, which can be attributed to the inability of this model to incorporate detrimental effects of OP multiaxial loading on the fatigue behavior.
4. The fatigue life model based on cumulative total strain energy density, which is able to incorporate the damage induced by the combined effects of axial and torsion loading during different stages of cyclic deformation, was found to provide better correlation of multiaxial fatigue data of PEEK.
5. Fatigue lives predicted based on the cumulative total strain energy density as the damage parameter were observed to be within the factor of two of the experimentally obtained fatigue lives for 97% of the fatigue data and within the factor of three for all of the fatigue data generated under different types of uniaxial and multiaxial loading conditions. The predicted fatigue lives were determined from cumulative total strain energy density versus fatigue lives curve constructed using uniaxial strain-controlled fatigue data with nominal rise in temperature.

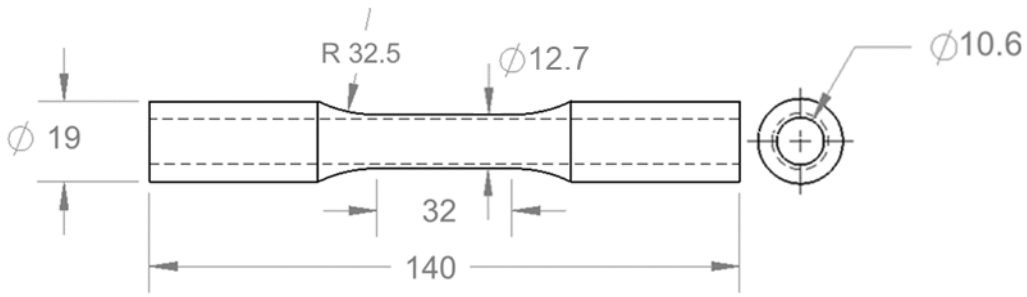

Figure 6.1 Geometry and dimensions of thin-walled fatigue specimens used for multiaxial and pure torsion tests (all dimensions are in mm) designed based on ASTM E2207 [94].

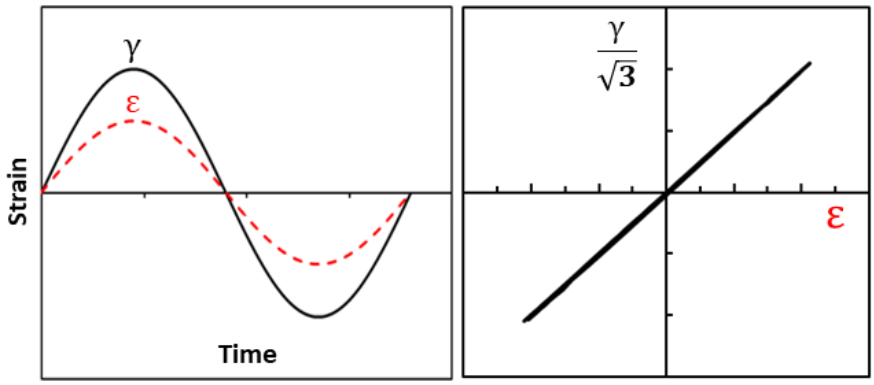

(a)

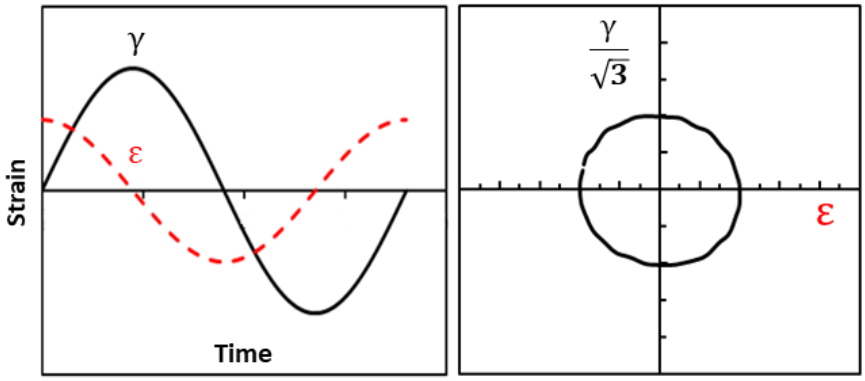

(b)

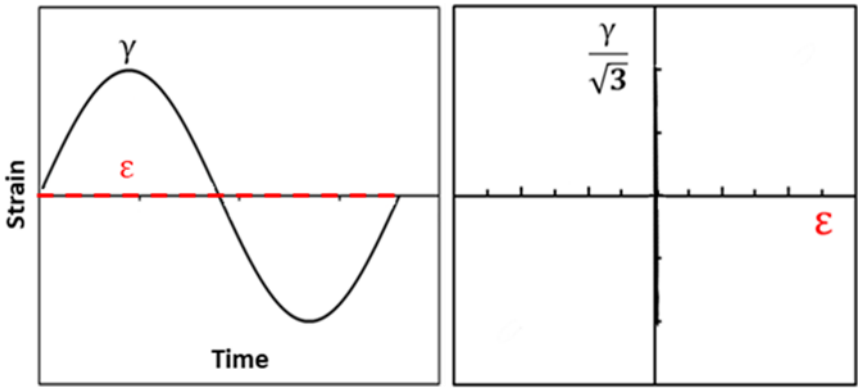

(c)

Figure 6.2 Schematics describing the relationship between axial and shear strains in (a) proportional in phase (IP), (b) non-proportional 90° out of phase (OP), and (c) torsion loadings.

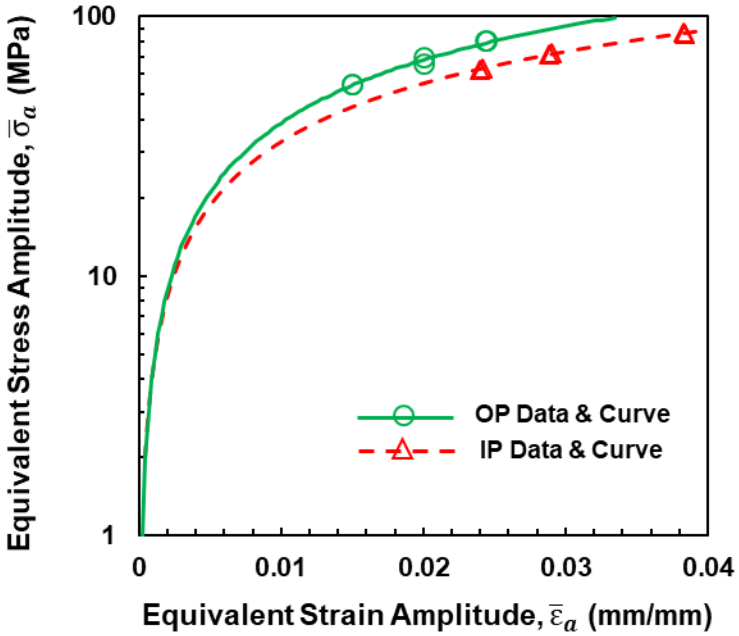

Figure 6.3 Cyclic equivalent stress-strain amplitude curve and data for PEEK subjected to IP and OP multiaxial loading.

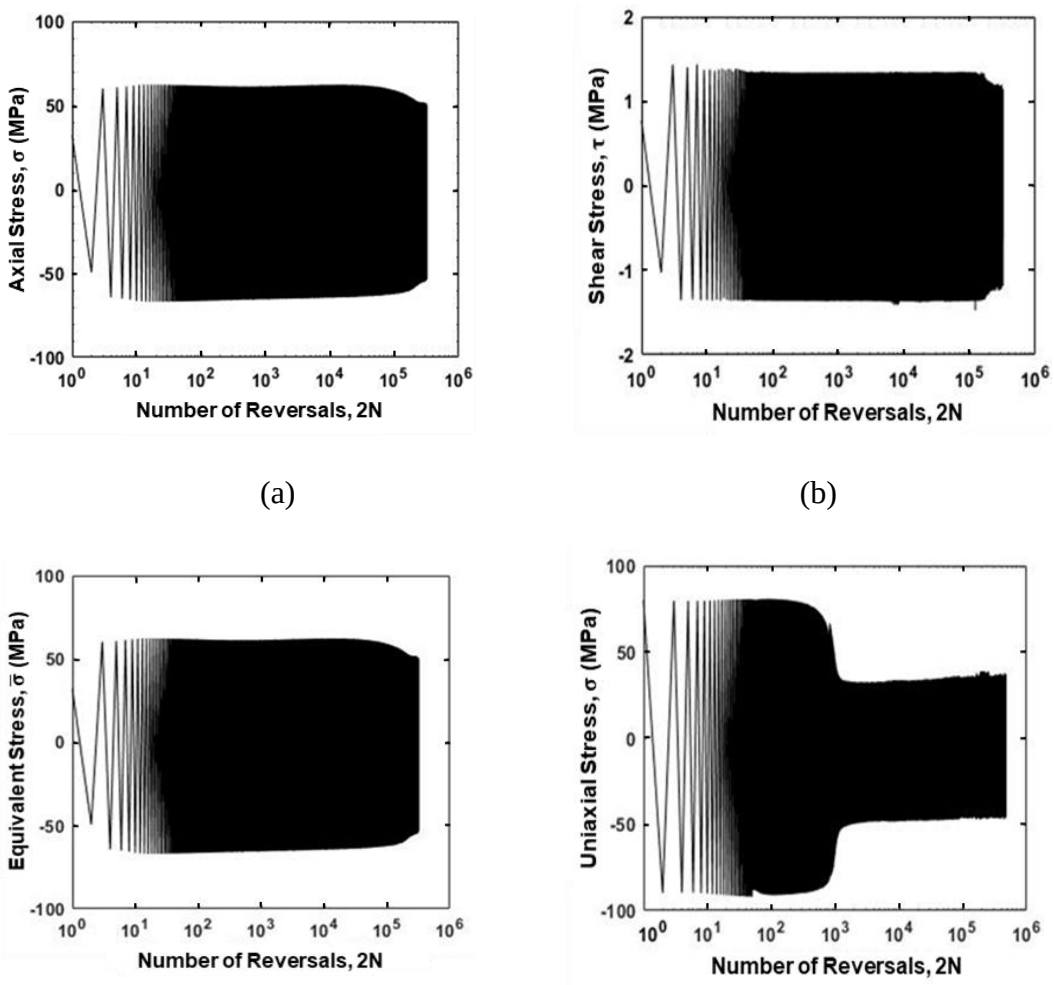

Figure 6.4 Cyclic deformation behavior represented by (a) axial stress response, (b) shear stress response and (c) equivalent stress response for a specimen under multiaxial IP loading at the equivalent strain amplitude of $\bar{\varepsilon}_a$= 0.025 mm/mm (S16) along with (d) the stress response for a specimen under uniaxial loading [42] at strain amplitude of ε_a = 0.025 mm/mm.

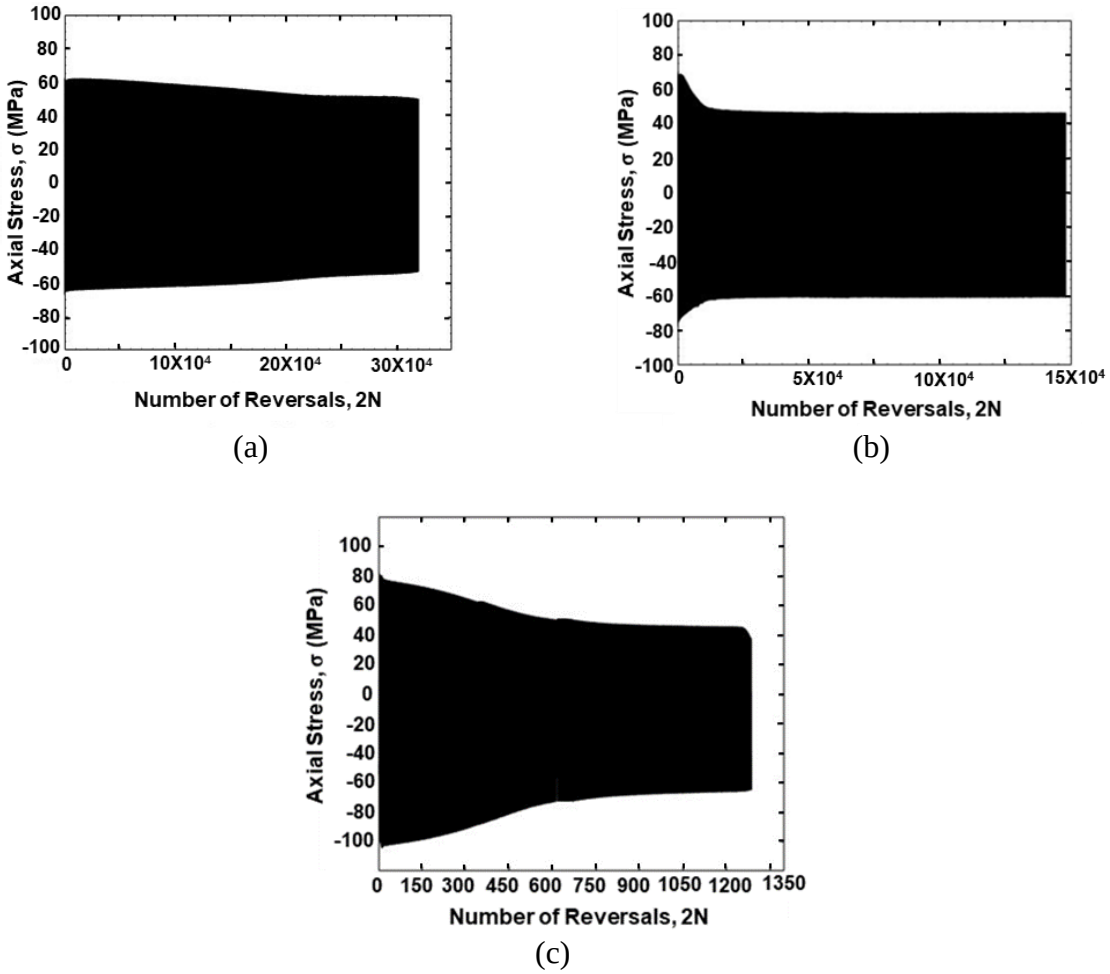

Figure 6.5 Axial stress responses for specimens under IP multiaxial loading at equivalent strain amplitudes of (a) $\bar{\varepsilon}_a$= 0.025 mm/mm (S16), (b) $\bar{\varepsilon}_a$= 0.030 mm/mm (S23), and (c) $\bar{\varepsilon}_a$= 0.040 mm/mm (S30) showing different regions of cyclic deformation. In all of the cases, the x-axis (i.e. number of reversals) is in linear scale and not in logarithmic scale.

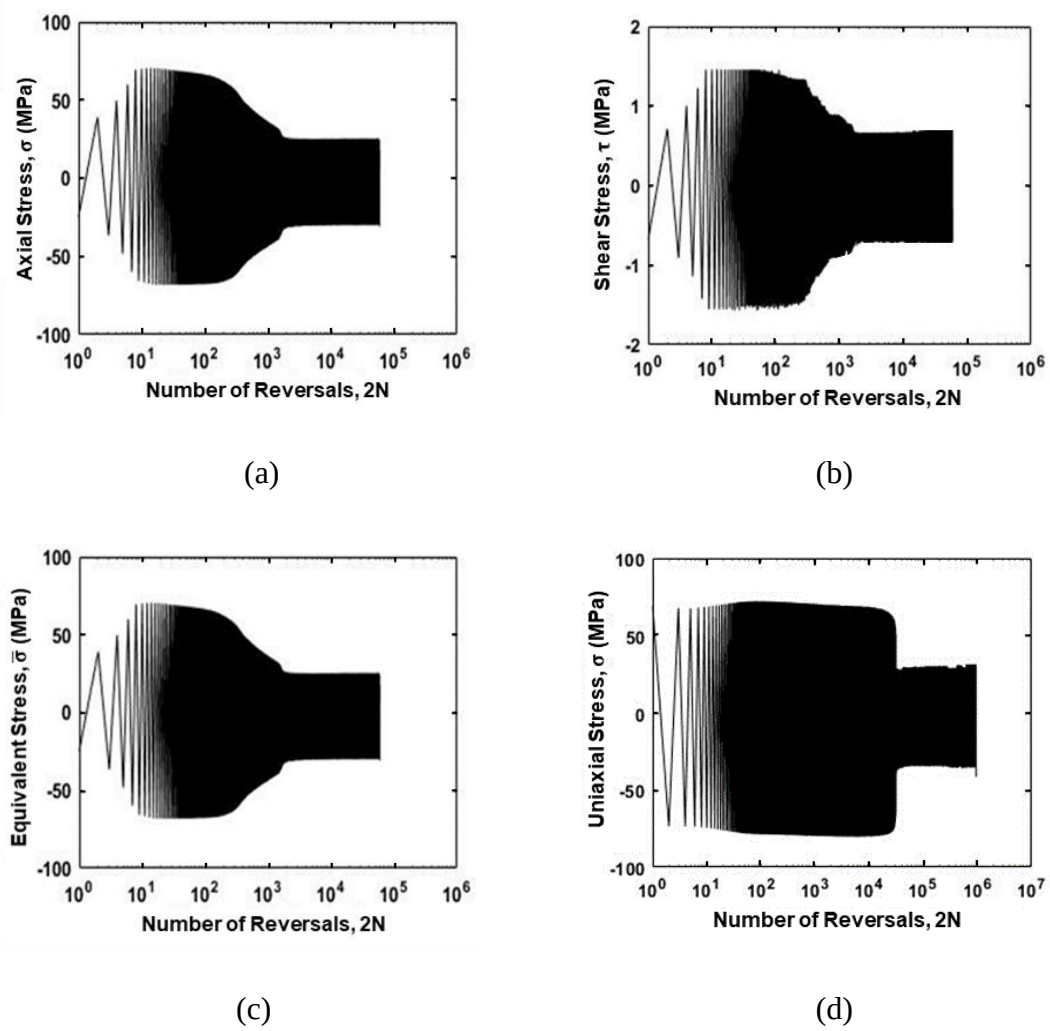

Figure 6.6 Cyclic deformation behavior represented by (a) axial stress response, (b) shear stress response and (c) equivalent stress response for a specimen under multiaxial OP loading at equivalent strain amplitude of $\bar{\varepsilon}_a$= 0.020 mm/mm (S17) along with (d) the stress response for a specimen under uniaxial loading [42] at the strain amplitude of ε_a = 0.020 mm/mm.

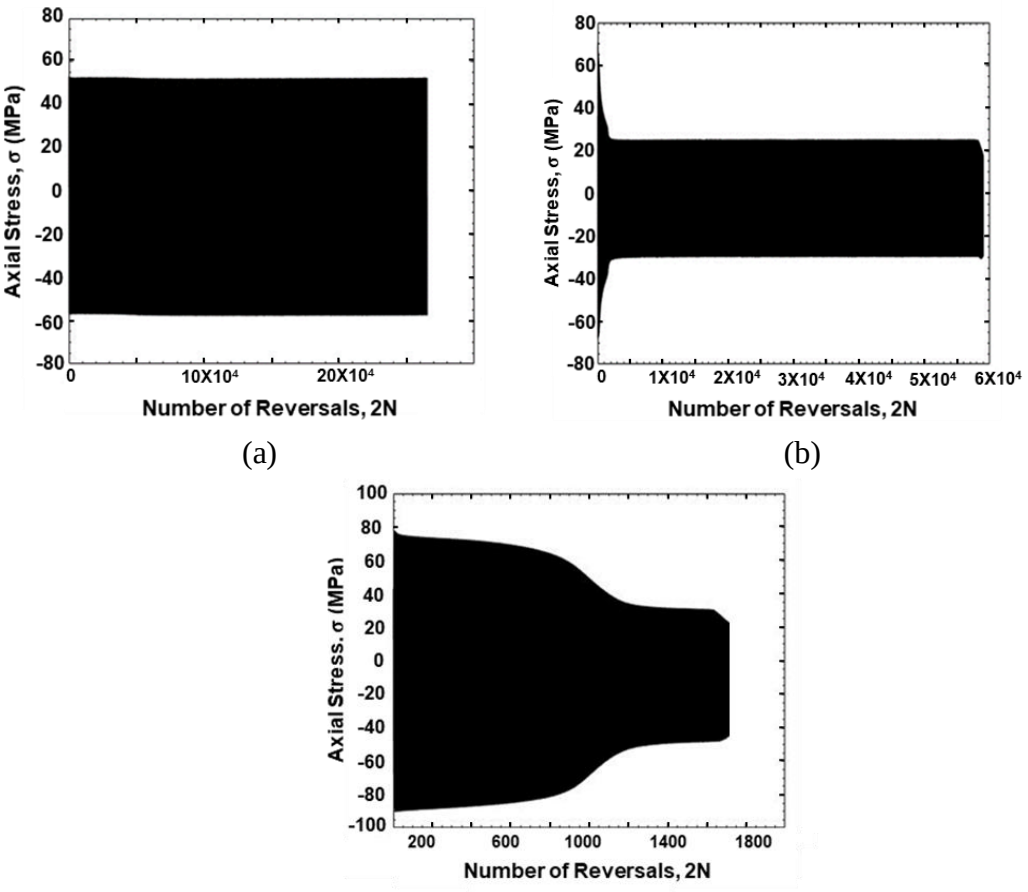

Figure 6.7 Axial stress responses for specimens under OP loading at equivalent strain amplitudes of (a) $\bar{\varepsilon}_a$= 0.015 mm/mm (S18), (b) $\bar{\varepsilon}_a$= 0.020 mm/mm (S17), and (c) $\bar{\varepsilon}_a$= 0.025 mm/mm (S26) showing different regions of cyclic deformation. In all of the cases, the x-axis (i.e. number of reversals) is in linear scale and not in logarithmic scale.

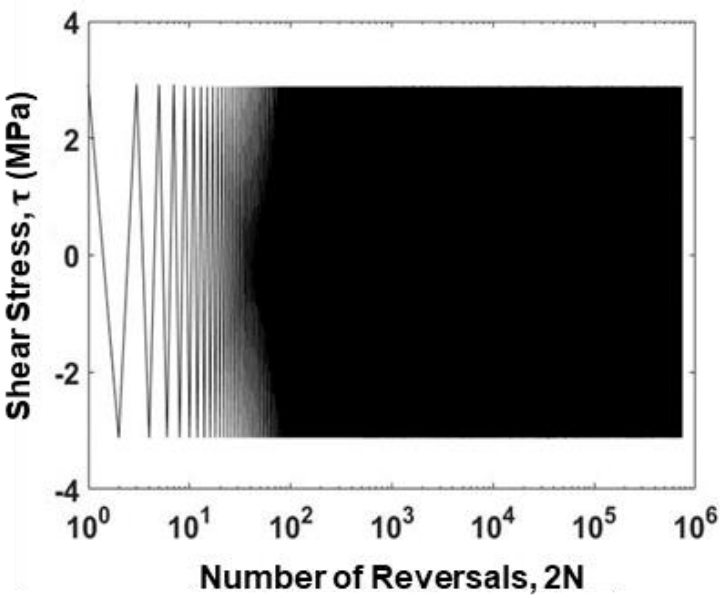

Figure 6.8 Shear stress responses for specimens S33 under torsion loading at equivalent strain amplitudes of $\bar{\varepsilon}_a$ = 0.04 mm/mm and shear strain amplitude of 0.069 mm/mm.

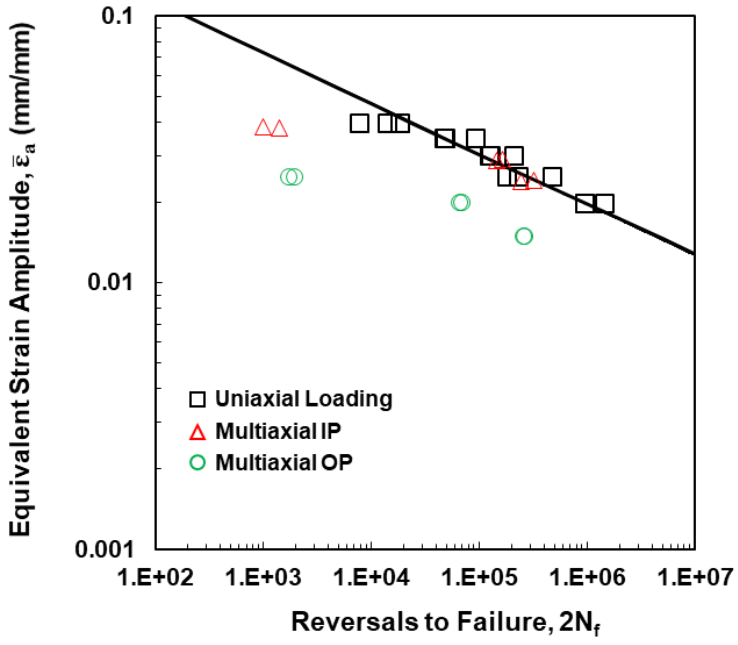

(a)

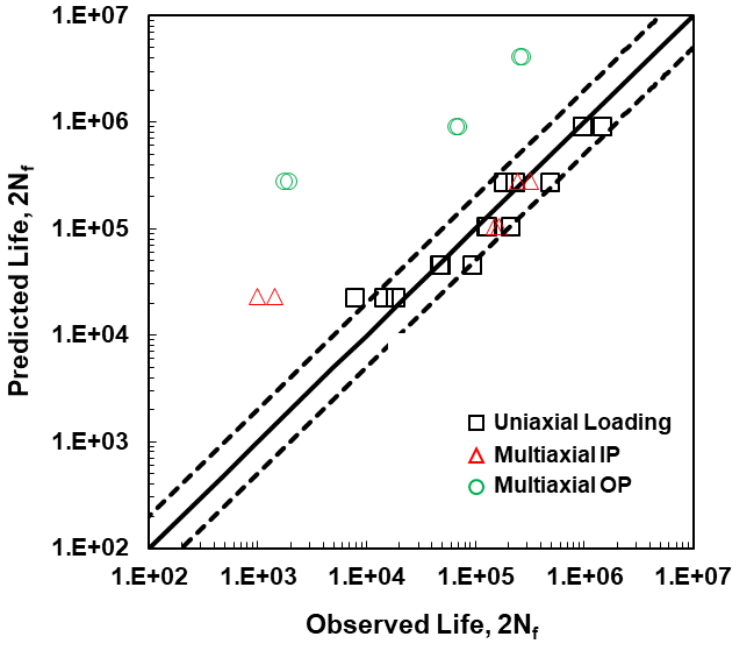

(b)

Figure 6.9 Plots showing (a) equivalent strain amplitude calculated using von Mises approach versus the fatigue lives and (b) predicted versus experimentally observed fatigue lives for tests conducted under multiaxial [Table 6.1] and uniaxial loading conditions [42].

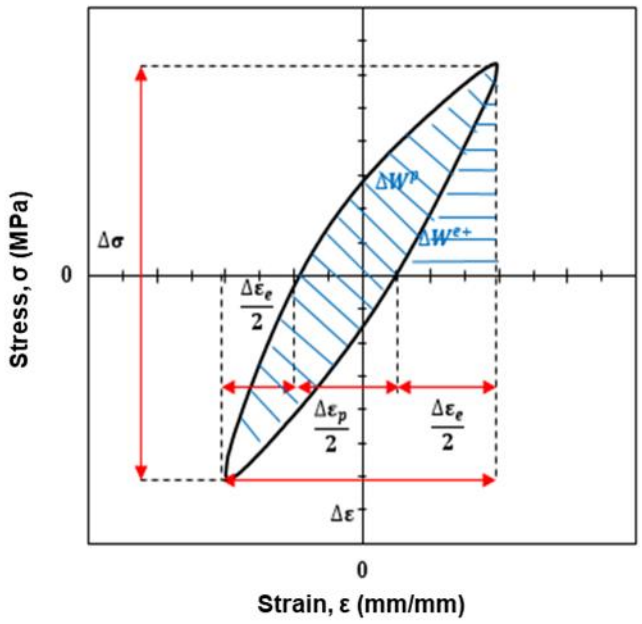

Figure 6.10 Schematic showing elastic and plastic components of energy based approaches.

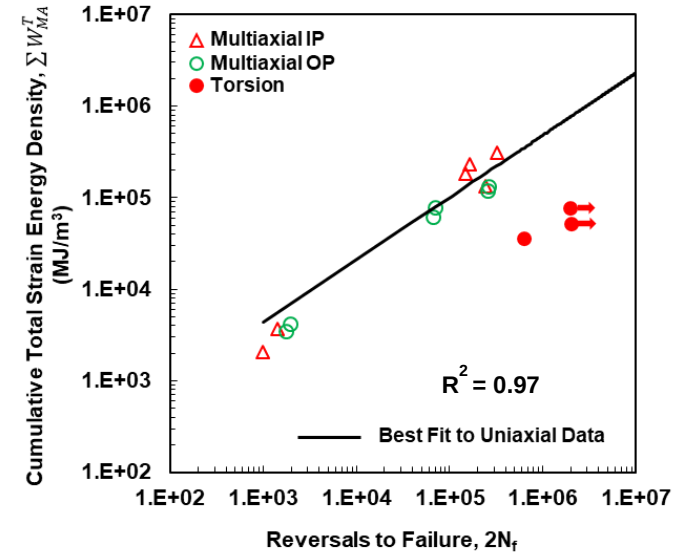

(a)

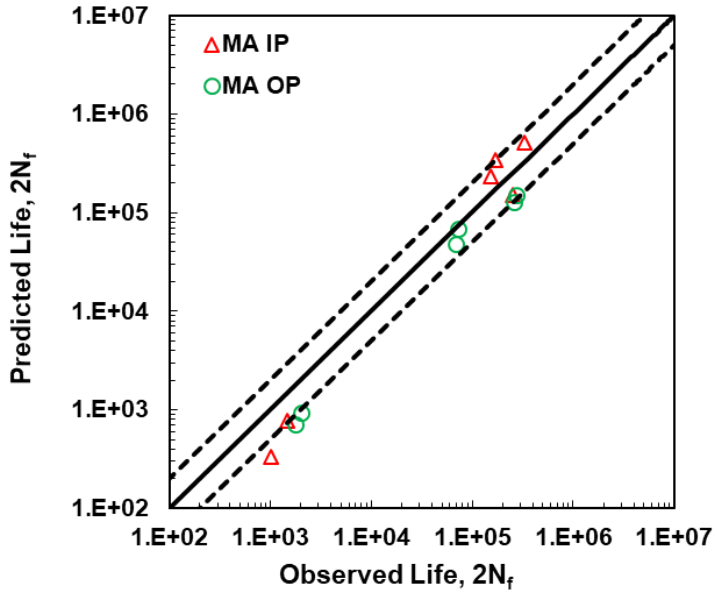

(b)

Figure 6.11 Plots showing (a) cumulative total strain energy density versus fatigue lives subjected to torsion, IP and OP multiaxial loading and (b) predicted fatigue lives calculated based on best fit to uniaxial fatigue data with nominal rise in temperature. The torsion data were not included for calculating the R^2 value.

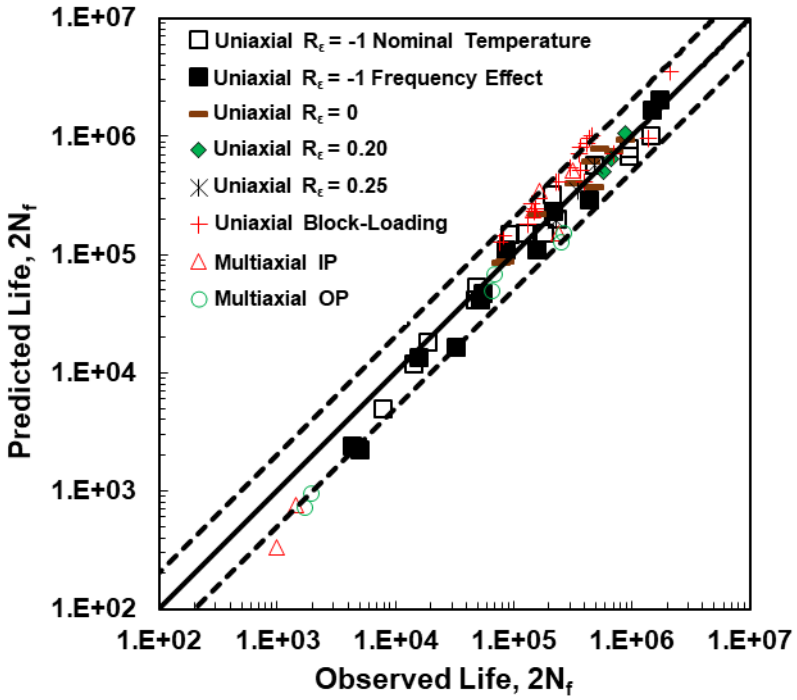

Figure 6.12 Predicted fatigue lives versus experimentally observed fatigue lives for PEEK specimen subjected to various types of uniaxial and multiaxial loadings [42, 102] based on cumulative total strain energy density. Only the curve fit to the uniaxial fatigue data with nominal temperature rise was used for all the predictions.

Table 6.1 Fatigue test results under torsion as well as in phase (IP) and 90° out of phase (OP) multiaxial loading conditions.

Specimen I.D.	**Loading**	**ε_a (mm/mm)**	**γ_{a_surf} (mm/mm)**	**σ_a * (MPa)**	**σ_a# (MPa)**	**τ_{a_mid} * (MPa)**	**$\bar{\varepsilon}_{a\_mid}$ (mm/mm)**	**$\bar{\sigma}_{a\_mid}$ (MPa)**	**ΔT (°C)**	**$2N_f$ (reversals)**
S16	IP	0.017	0.031	55	63	1.19	0.024	55	26	321,684
S34				58	63	1.26	0.024	58	30	243,268
S06		0.021	0.037	54	73	1.19	0.028	54	19	165,718
S23				53	72	1.18	0.028	53	24	147,758
S30		0.028	0.049	57	88	1.30	0.038	57	30	1,428
S31				54	88	1.22	0.038	54	29	994
S10	OP	0.015	0.026	54	52	1.13	0.014	54	6	255,298
S18				54	53	1.12	0.014	54	6	266,170
S05		0.020	0.035	28	66	0.76	0.019	28	54	69,910
S17				27	65	0.78	0.019	27	51	66,194
S26		0.025	0.044	59	75	1.60	0.024	59	40	1,944
S25				54	76	1.75	0.024	54	41	1,730
S20	Torsion	0	0.043	0	0	2.11	0.025	3.7	3	>2,000,000
S32		0	0.052	0	0	2.33	0.030	4.1	1	>2,000,000
S33		0	0.069	0	0	3.00	0.040	5.2	1	739,900

*Values taken from the mid-life cycle

#Values taken from the first cycle

CHAPTER 7 SUMMARY AND POTENTIAL FUTURE WORK

7.1 Summary and Major Conclusions

High strength engineering thermoplastics with acceptable mechanical properties and wear resistance are being extensively used in various applications in aerospace, biomedical, and automotive industries. In such applications, these components are commonly subjected to cyclic loading conditions for a long period of time. As a result, the cyclic deformation behavior of polymeric materials under different types of fatigue loading conditions needs to be thoroughly understood to enable their reliable use in structural components for load bearing applications. Furthermore, a majority of fatigue models, that are currently used to correlate the fatigue life of polymeric materials, were originally developed for metallic materials. Therefore, there is a need to either assess and modify available fatigue models or develop new predictive fatigue modeling tools specifically for polymeric materials considering the fact that the mechanical behavior and microstructural features of polymers are significantly different than those of metals.

In this study, the fatigue behavior of an unfilled Polyether Ether Ketone (PEEK) thermoplastic under monotonic tension, compression, and various types of uniaxial and multiaxial fatigue loading conditions were investigated. Based on the understanding of the deformation behavior obtained under different loading conditions, the ability of an energy based model to correlate the fatigue data of PEEK generated from different types of fatigue loading is then investigated. The effects of fully-reversed, tensile mean strain, block, and multiaxial loadings on the deformation behavior of PEEK obtained from strain-controlled

fatigue tests were presented, respectively, in Chapters 2, 3, 4, and 6. In addition, various strain-, strain-stress-, and energy based fatigue models were employed to correlate the fatigue life data in Chapters 2, 5, and 6.

PEEK exhibited significant cyclic softening in both tension and compression when subjected to the uniaxial strain-controlled cyclic loading. Four distinct regions of cyclic stress behavior were identified, namely initial, transition, cyclic stability, and crack propagation. It was observed that the magnitude of stress responses and the number of cycles in the initial region were significantly influential to the fatigue lifetime. The specimen that experienced a longer number of cycles in the initial region exhibited shorter fatigue lives when compared to those tested at the same strain amplitude and test frequency having a shorter number of cycles in the initial region. Additionally, it was found that the frequency effect on the cyclic behavior of PEEK was highly dependent on the strain amplitude level. Based on the test results, under fully-reversed strain-controlled condition, a minimal frequency effect was observed at a lower strain amplitude of 0.02 mm/mm. At higher strain amplitudes, however, increasing the test frequency resulted in longer fatigue lives.

Unlike most metals, significant differences between the fatigue behaviors of PEEK under uniaxial fully-reversed force- and strain-controlled cyclic tests were observed. Based on the experimental results in this study, it was concluded that the fatigue behavior of PEEK obtained under strain-controlled mode could not be directly related to its behavior under force-controlled loading. For the strain based fatigue analysis in this study, values for plastic strain were obtained only from the steady state stage, which represents deformation in cyclically stabilized region. However, the initial and transition regions were

found to affect the overall fatigue behavior and total life for PEEK. Therefore, it was concluded that a fatigue model that incorporates the deformation behavior during initial and transition stages could have provided better correlation of fatigue life data for polymers.

Since the Smith-Watson-Topper (SWT) damage parameter, $\varepsilon_a \sigma_{max}$, is associated with only the product of two absolute values (i.e. strain amplitude and maximum tensile stress), this fatigue parameter may not necessarily capture the shape of the hysteresis loop that changed throughout the cyclic loading for PEEK polymer. The shape of the hysteresis loop also differed with test frequency even for the same strain amplitude. Therefore, the SWT parameter could not well correlate the fatigue data either. The transient energy based approach that uses the cumulative plastic strain energy density as the damage parameter provided a better correlation with the PEEK experimental data under strain-controlled mode. This is due to the fact that unlike Coffin-Manson and SWT models, the cumulative plastic strain energy density can capture the shape of the hysteresis loop for all the deformation stages including initial, transition, and the cyclic stability.

Uniaxial strain-controlled tests with various strain ratios were utilized to study the mean strain effect on the fatigue behavior of a neat PEEK polymer. PEEK exhibited significant mean stress relaxation under uniaxial strain-controlled loading with tensile mean strains. The mean stress for tests at R_ε = 0, 0.2, and 0.25 was observed to be fully relaxed and minimally affect the PEEK fatigue life. Unlike those without mean strain, the PEEK specimens subjected to cyclic loading with tensile mean strain did not clearly exhibit the multiple stages of cyclic softening behavior, which was attributed to the concurrent mean stress relaxation in the material. The initial irregular shape of hysteresis stress-strain

loops of specimens with mean strains were observed to become more symmetric as the number of cycles increased.

The analysis on the fracture surfaces of the PEEK specimens under tensile mean strain cycling loading revealed two fatigue stages including crack initiation and physically small crack (PSC) growth. In addition, the former stage consisted of crack incubation and microstructurally small cracks (MSCs). Two types of inclusions, including particles and void-like defects, were found to be responsible for crack initiation in the PEEK specimens. At comparable strain amplitudes and strain ratios, presence of a larger inclusion (particles or void-like defects) generally resulted in shorter fatigue lives for PEEK specimens. Furthermore, specimens with void-like defects, serving as the source of crack initiation, were found to have shorter fatigue lives as compared to the specimens containing particles of similar size.

A series of uniaxial strain-controlled cyclic tests under various multi-block loading conditions were employed in this study to investigate the load sequence effects on fatigue behavior of a neat PEEK polymer. The fatigue tests conducted in this study included multi-block fully-reversed loading with various frequencies and multi-block loading with mean strains. In general, PEEK specimens with fully-reversed (R_ε = -1) pre-loading (with higher or lower strain amplitudes) did not exhibit the initial stage of cyclic softening behavior. The cyclic stability of the pre-loaded specimens was achieved at approximately the same reversals as those without pre-loading under identical test conditions. Furthermore, the stress amplitudes at the cyclic stability region were also comparable. Such cyclic deformation behavior was observed for all specimens under two-, three-, or four-block loading with R_ε = -1. Pre-loading for specimens under fully-reversed (R_ε = -1) condition

was found to have a significant beneficial effect on the PEEK fatigue resistance irrespective of the load sequence (i.e. high-low or low-high). The experimental results in this study revealed a distinctive fatigue behavior of PEEK under multi-block loading.

Applicability of various fatigue models to account for the mean strain and load history/sequence effects for PEEK polymer was investigated. Since PEEK polymer exhibited mean stress relaxation behavior in the presence of mean strain and minimal effect of mean strain on PEEK fatigue life was observed, the strain based fatigue model was found to correlate mean strain data for PEEK polymer reasonably well. Contrary to the expectation, the SWT model, which involved the fatigue parameter with both stress and strain terms, was not able to provide accurate life predictions for test data with mean strains. The energy based model based on the cumulative total strain energy density, $\sum W^T$, satisfactorily correlated the fatigue data with zero and non-zero mean strains. Such results can be attributed to the fact that the energy based model utilizing $\sum W^T$ was able to capture the changes in the shape and size of the hysteresis stress-strain loops resulting from cyclic softening and mean stress relaxation throughout the lifetime of the specimen.

The linear damage rule (LDR) with either the strain amplitude or the total strain energy density at half-life, ΔW_{HL}^T, overestimated the cumulative damage in PEEK specimens subjected to fully-reversed cyclic loading, which exhibited significant load history effects. The non-linear Damage Curve Approach and the Hashim-Rotem model, with either strain or energy based parameters, were not able to accurately capture the beneficial effect of pre-loading on the PEEK fatigue resistance. As a result, they overestimated the fatigue damage under variable amplitude loading blocks. Regardless of loading conditions (zero or non-zero mean strains) and sequence (high-low or low-high),

the Direct Cumulative Damage (DCD) approach based on cumulative total strain energy density, $\sum W^T$, was able to take into consideration the loading history/sequence effects on PEEK fatigue behavior and provide an acceptable predictive capability under variable amplitude block loading at various frequencies.

Effect of pure torsion loading along with two different types of multiaxial loading (i.e. proportional in phase (IP) and not-proportional 90° out of phase (OP)) on the cyclic deformation behavior and fatigue resistance of PEEK polymer was investigated. Under multiaxial loading condition, the stress response exhibited by PEEK polymer could be distinguished into initial, transition, and steady state regions similar to the ones observed under uniaxial loading condition. However, compared to uniaxial fatigue loading, under multiaxial loading, majority of the fatigue lives for PEEK polymer was not always spent in the steady state region but varied based on the applied equivalent strain amplitude. At similar equivalent or axial strain amplitudes, PEEK polymer exhibited lower fatigue resistance and higher rise in temperature at the surface of the specimen under non-proportional 90° out of phase loading compared to when the material was subjected to proportional in phase loading.

Based on the results obtained from the cyclic deformation and fatigue behavior, two different types of fatigue life models, including strain based and energy based approaches were employed to correlate the fatigue life data of PEEK under multiaxial as well as uniaxial loading using a single master curve. Classical octahedral shear strain theory based von Mises model could not correlate the fatigue data of PEEK polymer under multiaxial loading, which can be attributed to the inability of this model to incorporate detrimental effects of OP multiaxial loading on the fatigue behavior. The fatigue life model

based on cumulative total strain energy density, which is able to incorporate the damage induced by the combined effects of axial and torsion loading during different stages of cyclic deformation, was found to provide better correlation of multiaxial fatigue data of PEEK.

Fatigue lives predicted based on the cumulative total strain energy density as the damage parameter were observed to be within the factor of two of the experimentally obtained fatigue lives for 97% of the fatigue data and within the factor of three for all of the fatigue data generated under different types of uniaxial and multiaxial loading conditions. The predicted fatigue lives were determined from cumulative total strain energy density versus fatigue lives curve constructed using uniaxial strain-controlled fatigue data with nominal rise in temperature

The generated understanding on the cyclic deformation behavior and the proposed fatigue life model in this study can be used as a tool to develop multiscale energy approaches for polymer fatigue life predictions, which will provide a new means to design polymeric parts in various applications such as aerospace, automotive, biomedical, etc. The design of polymeric parts and assemblies with application-specific fatigue resistance using the proposed approach will reduce prototype testing and verification time, leading to a faster product launch by reducing the experimentations. In automotive industries, it will lead to the development of polymeric automotive structures with prolonged fatigue life, making it possible to fulfill the ultimate goal of reducing the weight in the U.S. automobile and truck fleet, thereby significantly improving the fuel economy.

The proposed tools for fatigue life prediction will also be beneficial to the design of polymer matrix composites that have been increasingly used in the aerospace structures

as well as the design of polymeric based components used in biomedical applications, such as bone anchors, spinal cages, and total hip replacement, etc. This research will also enhance our knowledge of polymer fatigue processes and damage under various loading conditions. The knowledge gained from this research will form the basis of our understanding for the structure-property relationships of polymers. The outcome of this research has been and will be disseminated among the technical community to propel the understanding of polymer fatigue.

7.2 Possible Future Studies

Results obtained from the block loading tests shown in the current study indicated that the fatigue behavior of PEEK polymer was affected significantly by load history and sequence, especially under fully-reversed loading, while the effect was minimal under pulsating tension loadings. In addition, this study showed the effect of load history and sequence on the cyclic deformation behavior of PEEK under variable amplitude loading. However, to fully characterize the mechanical and fatigue properties of PEEK, the effect of random variable amplitude loading on the cyclic deformation behavior, and consequently, on the fatigue resistance also needs to be understood. In addition, appropriate cycle counting methods, as well as the applicability of the energy based model using cumulative total strain energy density as the damage parameter to correlate the fatigue life data of PEEK under random variable amplitude loading, also need to be investigated.

The cracks that were seen on the surface of the PEEK specimens under multiaxial loading were oriented in specific directions, which indicates that the cracks in thermoplastics do not grow randomly, but may initiate and grow on a preferred plane. The orientation of these cracks was also seen to vary based on the applied load path (i.e. IP,

OP, or pure torsion). These valuable insights can be used to determine the critical failure planes for PEEK polymer, which is also the basis of various types of critical plane approaches such as Brown-Miller, Smith-Watson-Topper, Fatemi-Socie, etc. As these fatigue life approaches were designed based on the failure mechanism of different types of metals, they need to be examined for polymeric materials to check their applicability. Therefore, a better understanding of the failure mechanisms based on the results presented in this study can aid to determine applicable critical plane approaches or make the appropriate changes if necessary to better predict the fatigue life of polymeric materials. In addition, the effect of different types of multiaxial paths on the cyclic deformation behavior as well as failure mechanisms needs to be understood to determine the robustness of the proposed cumulative total strain energy density fatigue model. Furthermore, some studies investigating the cyclic deformation and fatigue behavior under the more realistic variable amplitude multiaxial loading need to be conducted to enable the use of the proposed approaches in engineering design of polymer in fatigue critical applications.

The cyclic deformation behavior presented in this study under different types of uniaxial and multiaxial fatigue loading condition was studied in macroscopic level. However, relationship between the cyclic deformation behavior and resulting microstructural changes such as rearrangement and degradation of polymeric chains, variation in the crystallinity, etc. under fatigue loading should also be well understood. An understanding of the relationships between the microstructural features and fatigue behavior is essential to develop more fatigue resistant polymers and minimize the need for the long and exhausting fatigue testing. In addition, the fatigue model with cumulative strain energy density as the damage parameter is based on the stress-strain hysteresis loop,

which at this study is obtained from the fatigue test. However in the absence of testing equipment, a constitutive cyclic stress–strain model for polymers to estimate the hysteresis stress–strain loops at different stages of initial, transition and cyclic stability for different fatigue loading conditions is necessary to accurately predict the fatigue life.

PEEK polymer is also being used as matrix in fiber reinforced composite materials. Although the cracks in composite materials are reported to initiate from the matrix, the interaction between the cracks and reinforced fibers can affect the resulting fatigue behavior. In addition, the effect of different loading condition for composites may vary significantly compared to that seen for neat polymeric materials due to the reinforced fibers and potentially more anisotropic behavior. However, based on the fatigue behavior observed for neat PEEK polymer in this study, the effect of different load variables including, loading mode, cyclic strain rate, mean strain/stress, block-loading, and multiaxial load paths on the fatigue behavior and life should be investigated for the PEEK based composites to exploit their full potential for fatigue-critical applications.

CHAPTER 8 REFERENCES

[1] I.M. Ward, J. Sweeney, Mechanical properties of solid polymers, John Wiley & Sons2012.

[2] S.M. Kurtz, J.N. Devine, PEEK biomaterials in trauma, orthopedic, and spinal implants, Biomaterials 28(32) (2007) 4845-4869.

[3] D. Jones, D. Leach, D. Moore, Mechanical properties of poly (ether-ether-ketone) for engineering applications, Polymer 26(9) (1985) 1385-1393.

[4] F. El Halabi, J. Rodriguez, L. Rebolledo, E. Hurtós, M. Doblaré, Mechanical characterization and numerical simulation of polyether–ether–ketone (PEEK) cranial implants, Journal of the mechanical behavior of biomedical materials 4(8) (2011) 1819-1832.

[5] D.J. Kelsey, G.S. Springer, S.B. Goodman, Composite implant for bone replacement, Journal of composite materials 31(16) (1997) 1593-1632.

[6] K. Liao, Performance characterization and modeling of a composite hip prosthesis, Experimental Techniques 18(5) (1994) 33-38.

[7] A. Corvelli, P. Biermann, J. Roberts, Design, analysis, and fabrication of a composite segmental bone replacement implant, Journal of advanced materials 28(3) (1997) 2-8.

[8] R.M. Jones, Mechanics of composite materials, CRC press2014.

[9] L. Sawyer, D.T. Grubb, G.F. Meyers, Polymer microscopy, Springer Science & Business Media2008.

[10] R.W. Hertzberg, J.A. Manson, Fatigue of engineering plastics, Academic press1980.

[11] R.J. Crawford, Plastics engineering, Elsevier1998.

[12] D. Kujawski, F. Ellyin, A unified approach to mean stress effect on fatigue threshold conditions, International Journal of Fatigue 17(2) (1995) 101-106.

[13] G. Tao, Z. Xia, Mean stress/strain effect on fatigue behavior of an epoxy resin, International journal of fatigue 29(12) (2007) 2180-2190.

[14] M. Shariati, H. Hatami, H. Yarahmadi, H.R. Eipakchi, An experimental study on the ratcheting and fatigue behavior of polyacetal under uniaxial cyclic loading, Materials & Design 34 (2012) 302-312.

[15] S.R. Mellott, A. Fatemi, Fatigue behavior and modeling of thermoplastics including temperature and mean stress effects, Polymer Engineering & Science 54(3) (2014) 725-738.

[16] ASTM E606, Standard Test Method for Strain-Controlled Fatigue Testing, ASTM International, West Conshohocken, PA, (2019).

[17] J. Zaroulis, M. Boyce, Temperature, strain rate, and strain state dependence of the evolution in mechanical behaviour and structure of poly (ethylene terephthalate) with finite strain deformation, Polymer 38(6) (1997) 1303-1315.

[18] J. Simsiriwong, R. Shrestha, N. Shamsaei, M. Lugo, R.D. Moser, Effects of microstructural inclusions on fatigue life of polyether ether ketone (PEEK), journal of the mechanical behavior of biomedical materials 51 (2015) 388-397.

[19] J.E. Mark, Physical properties of polymers handbook, Springer2007.

[20] J. Sauer, G. Richardson, Fatigue of polymers, International journal of fracture 16(6) (1980) 499-532.

[21] ASTM D7791, Standard test method for uniaxial fatigue properties of plastics ASTM International, West Conshohocken, PA, (2017).
[22] P. Vincent, The necking and cold-drawing of rigid plastics, Polymer 1 (1960) 7-19.
[23] G.H. Michler, Electron microscopy of polymers, Springer Science & Business Media2008.
[24] N. Mills, Plastics; microstructure and engineering applications, Transport 148(149) (2005) 156-160.
[25] F. Rietsch, B. Bouette, The compression yield behaviour of polycarbonate over a wide range of strain rates and temperatures, European Polymer Journal 26(10) (1990) 1071-1075.
[26] J. Richeton, S. Ahzi, L. Daridon, Y. Rémond, A formulation of the cooperative model for the yield stress of amorphous polymers for a wide range of strain rates and temperatures, Polymer 46(16) (2005) 6035-6043.
[27] S. Rabinowitz, P. Beardmore, Cyclic deformation and fracture of polymers, Journal of Materials Science 9(1) (1974) 81-99.
[28] D.J. Krzypow, C.M. Rimnac, Cyclic steady state stress–strain behavior of UHMW polyethylene, Biomaterials 21(20) (2000) 2081-2087.
[29] G. Tao, Z. Xia, An experimental study of uniaxial fatigue behavior of an epoxy resin by a new noncontact real-time strain measurement and control system, Polymer Engineering & Science 47(6) (2007) 780-788.
[30] R.I. Stephens, A. Fatemi, R.R. Stephens, H.O. Fuchs, Metal fatigue in engineering, John Wiley & Sons2000.
[31] S. Mortazavian, A. Fatemi, Fatigue behavior and modeling of short fiber reinforced polymer composites: A literature review, International Journal of Fatigue 70 (2015) 297-321.
[32] A. Bernasconi, R.M. Kulin, Effect of frequency upon fatigue strength of a short glass fiber reinforced polyamide 6: a superposition method based on cyclic creep parameters, Polymer Composites 30(2) (2009) 154-161.
[33] S. Mortazavian, A. Fatemi, S.R. Mellott, A. Khosrovaneh, Effect of cycling frequency and self-heating on fatigue behavior of reinforced and unreinforced thermoplastic polymers, Polymer Engineering & Science 55(10) (2015) 2355-2367.
[34] ASTM E739, Standard Practice for Statistical Analysis of Linear or Linearized Stress-Life (S-N) and Strain-Life (ε-N) Fatigue Data, ASTM International, West Conshohocken, PA, (2015).
[35] D. Kujawski, A deviatoric version of the SWT parameter, International Journal of Fatigue 67 (2014) 95-102.
[36] J. Colin, A. Fatemi, Variable amplitude cyclic deformation and fatigue behavior of stainless steel 304L including step, periodic, and random loadings, Fatigue & Fracture of Engineering Materials & Structures 33(4) (2010) 205-220.
[37] K. Smith, T. Topper., P. Watson, A stress–strain function for the fatigue of metals (stress–strain function for metal fatigue including mean stress effect), Journal of Materials Science 5 (1970) 767-778.
[38] F. Ellyin, Fatigue damage, crack growth and life prediction, Springer Science & Business Media2012.

[39] G. Halford, The energy required for fatigue(Plastic strain hystersis energy required for fatigue in ferrous and nonferrous metals), Journal of materials 1 (1966) 3-18.
[40] S.M. Kurtz, T.H. Lanman, G. Higgs, D.W. MacDonald, S.H. Berven, J.E. Isaza, E. Phillips, M.J. Steinbeck, Retrieval analysis of PEEK rods for posterior fusion and motion preservation, European Spine Journal 22(12) (2013) 2752-2759.
[41] K.R. Chandran, Mechanical fatigue of polymers: A new approach to characterize the SN behavior on the basis of macroscopic crack growth mechanism, Polymer 91 (2016) 222-238.
[42] R. Shrestha, J. Simsiriwong, N. Shamsaei, R.D. Moser, Cyclic deformation and fatigue behavior of polyether ether ketone (PEEK), International Journal of Fatigue 82 (2016) 411-427.
[43] J.A. Sauer, A.D. McMaster, D.R. Morrow, Fatigue behavior of polystyrene and effect of mean stress, Journal of Macromolecular Science, Part B 12(4) (1976) 535-562.
[44] R.J. Crawford, P.P. Benham, Some fatigue characteristics of thermoplastics, Polymer 16(12) (1975) 908-914.
[45] G. Tao, Z. Xia, Ratcheting behavior of an epoxy polymer and its effect on fatigue life, Polymer Testing 26(4) (2007) 451-460.
[46] P. Chen, S.-C. Wong, Strain-controlled fatigue life and modeling of conduit polymers, Journal of materials science 46(6) (2011) 1902-1912.
[47] O. Krause, Frequency effects on lifetime, Optimat Blades Project (2002).
[48] Y. Murakami, Metal fatigue: effects of small defects and nonmetallic inclusions, Academic Press2019.
[49] L. Xueshu, C. Fei, A review of void formation and its effects on the mechanical performance of carbon fiber reinforced plastic, Engineering Transactions 64(1) (2016) 33–51.
[50] B. Tomkins, W. Biggs, Low endurance fatigue in metals and polymers, Journal of Materials Science 4(6) (1969) 544-553.
[51] A. Vinogradov, C. Jenkins, R. Winter, Cyclic loading effects on durability of polymer systems, Long Term Durability of Structural Materials, Elsevier2001, pp. 159-170.
[52] F.J. Arbeiter, A. Frank, G. Pinter, Influence of molecular structure and reinforcement on fatigue behavior of tough polypropylene materials, Journal of Applied Polymer Science 133(38) (2016).
[53] R. Shrestha, J. Simsiriwong, N. Shamsaei, Mean strain effects on cyclic deformation and fatigue behavior of polyether ether ketone (PEEK), Polymer Testing 55 (2016) 69-77.
[54] A. Chudnovsky, Z. Zhou, H. Zhang, K. Sehanobish, Lifetime assessment of engineering thermoplastics, International Journal of Engineering Science 59 (2012) 108-139.
[55] F.J. Medel, P. Pena, J. Cegoñino, E. Gomez-Barrena, J. Puertolas, Comparative fatigue behavior and toughness of remelted and annealed highly crosslinked polyethylenes, Journal of Biomedical Materials Research Part B: Applied Biomaterials: An Official Journal of The Society for Biomaterials, The Japanese Society for Biomaterials, and The Australian Society for Biomaterials and the Korean Society for Biomaterials 83(2) (2007) 380-390.

[56] J. Wainstein, M. Chapetti, P.E. Montemartini, P. Frontini, Fatigue crack propagation evaluation of several commercial grade propylene polymers, International Journal of Polymeric Materials 54(7) (2005) 575-587.
[57] N.A. Jones, A.J. Lesser, Morphological study of fatigue-induced damage in isotactic polypropylene, Journal of Polymer Science Part B: Polymer Physics 36(15) (1998) 2751-2760.
[58] M. Eftekhari, A. Fatemi, A. Khosrovaneh, Fatigue Behavior of Neat and Short Glass Fiber Reinforced Polymers under Two-Step Loadings and Periodic Overloads, SAE International Journal of Materials and Manufacturing 9(3) (2016) 585-593.
[59] O. Olabisi, K. Adewale, Handbook of thermoplastics, CRC press2016.
[60] S. Thomas, P. Visakh, Handbook of Engineering and Specialty Thermoplastics, Volume 3: Polyethers and Polyesters, John Wiley & Sons2011.
[61] M. Schmidt, D. Pohle, T. Rechtenwald, Selective laser sintering of PEEK, CIRP annals 56(1) (2007) 205-208.
[62] M. Berer, Z. Major, G. Pinter, D. Constantinescu, L. Marsavina, Investigation of the dynamic mechanical behavior of polyetheretherketone (PEEK) in the high stress tensile regime, Mechanics of Time-Dependent Materials 18(4) (2014) 663-684.
[63] M. Berer, D. Tscharnuter, G. Pinter, Dynamic mechanical response of polyetheretherketone (PEEK) exposed to cyclic loads in the high stress tensile regime, International Journal of Fatigue 80 (2015) 397-405.
[64] P. Beardmore, S. Rabinowitz, Treatise on materials science and technology, vol. 6, Academic Press, New York (1975) 267.
[65] D. Zhao, N. Moritz, P. Laurila, R. Mattila, L. Lassila, N. Strandberg, T. Mäntylä, P. Vallittu, H. Aro, Development of a multi-component fiber-reinforced composite implant for load-sharing conditions, Medical engineering & physics 31(4) (2009) 461-469.
[66] A. Schwitalla, W.-D. Müller, PEEK dental implants: a review of the literature, Journal of Oral Implantology 39(6) (2013) 743-749.
[67] D.-Y. Cho, W.-R. Liau, W.-Y. Lee, J.-T. Liu, C.-L. Chiu, P.-C. Sheu, Preliminary Experience Using a Polyetheretherketone (PEEK) Cage in the Treatment of Cervical Disc Disease, Neurosurgery 51(6) (2002) 1343-1350.
[68] K. Jockisch, S. Brown, T. Bauer, K. Merritt, Biological response to chopped-carbon-fiber-reinforced peek, Journal of biomedical materials research 26(2) (1992) 133-146.
[69] M. Eftekhari, A. Fatemi, On the strengthening effect of increasing cycling frequency on fatigue behavior of some polymers and their composites: Experiments and modeling, International Journal of Fatigue 87 (2016) 153-166.
[70] A. Fatemi, L. Yang, Cumulative fatigue damage and life prediction theories: a survey of the state of the art for homogeneous materials, International journal of fatigue 20(1) (1998) 9-34.
[71] S. Lin, C. Ma, N. Tai, Mechanical properties and morphology of different carbon fiber lengths in reinforced polyetheretherketone (PEEK) composites, Journal of advanced materials 28(2) (1997).

[72] C.P. Hoppel, R.N. Pangborn, R.W. Thomson, Damage accumulation during multiple stress level fatigue of short-glass-fiber reinforced styrene-maleic anhydride, Journal of Thermoplastic Composite Materials 14(1) (2001) 84-94.
[73] H. Noguchi, Y.-H. Kim, H. Nisitani, On the cumulative fatigue damage in short carbon fiber reinforced poly-ether-ether-ketone, Engineering fracture mechanics 51(3) (1995) 457-468.
[74] A. Zago, G.S. Springer, Constant amplitude fatigue of short glass and carbon fiber reinforced thermoplastics, Journal of reinforced plastics and composites 20(7) (2001) 564-595.
[75] A. Zago, G.S. Springer, M. Quaresimin, Cumulative damage of short glass fiber reinforced thermoplastics, Journal of reinforced plastics and composites 20(7) (2001) 596-605.
[76] W. Yao, N. Himmel, A new cumulative fatigue damage model for fibre-reinforced plastics, Composites science and technology 60(1) (2000) 59-64.
[77] R. Shrestha, J. Simsiriwong, N. Shamsaei, Load history and sequence effects on cyclic deformation and fatigue behavior of a thermoplastic polymer, Polymer Testing 56 (2016) 99-109.
[78] R. Shrestha, Fatigue behavior and modeling of polyether ether ketone (PEEK) under constant and variable amplitude loadings, Mississippi State University2016.
[79] K. Golos, F. Ellyin, Generalization of cumulative damage criterion to multilevel cyclic loading, Theoretical and Applied Fracture Mechanics 7(3) (1987) 169-176.
[80] M.J. Mahtabi, N. Shamsaei, A modified energy-based approach for fatigue life prediction of superelastic NiTi in presence of tensile mean strain and stress, International Journal of Mechanical Sciences 117 (2016) 321-333.
[81] J. Morrow, Cyclic plastic strain energy and fatigue of metals, Internal friction, damping, and cyclic plasticity, ASTM International1965.
[82] S. Manson, G.R. Halford, Practical implementation of the double linear damage rule and damage curve approach for treating cumulative fatigue damage, International journal of fracture 17(2) (1981) 169-192.
[83] Z. Hashin, A. Rotem, A cumulative damage theory of fatigue failure, Materials Science and Engineering 34(2) (1978) 147-160.
[84] A. Fatemi, N. Shamsaei, Multiaxial fatigue: An overview and some approximation models for life estimation, International Journal of Fatigue 33(8) (2011) 948-958.
[85] G. Tao, Z. Xia, Biaxial fatigue behavior of an epoxy polymer with mean stress effect, International Journal of Fatigue 31(4) (2009) 678-685.
[86] L. Wang, S. Shi, S. Fu, G. Chen, X. Chen, Evaluation of multiaxial fatigue life prediction criteria for PEEK, Theoretical and Applied Fracture Mechanics 73 (2014) 128-135.
[87] W. Mars, A. Fatemi, Multiaxial stress effects on fatigue behavior of filled natural rubber, International Journal of Fatigue 28(5) (2006) 521-529.
[88] W. Mars, A. Fatemi, Multiaxial fatigue of rubber: Part I: equivalence criteria and theoretical aspects, Fatigue & fracture of engineering materials & structures 28(6) (2005) 515-522.
[89] W. Mars, A. Fatemi, Multiaxial fatigue of rubber: Part II: experimental observations and life predictions, Fatigue & fracture of engineering materials & structures 28(6) (2005) 523-538.

[90] B. Klimkeit, Y. Nadot, S. Castagnet, C. Nadot-Martin, C. Dumas, S. Bergamo, C.M. Sonsino, A. Büter, Multiaxial fatigue life assessment for reinforced polymers, International Journal of Fatigue 33(6) (2011) 766-780.
[91] M. Amjadi, A. Fatemi, Multiaxial fatigue behavior of thermoplastics including mean stress and notch effects: Experiments and modeling, International Journal of Fatigue 136 (2020) 105571.
[92] A. Avanzini, C. Petrogalli, D. Battini, G. Donzella, Influence of micro-notches on the fatigue strength and crack propagation of unfilled and short carbon fiber reinforced PEEK, Materials & Design 139 (2018) 447-456.
[93] K. Friedrich, Z. Lu, A. Hager, Recent advances in polymer composites' tribology, Wear 190(2) (1995) 139-144.
[94] ASTM E2207-15, Standard practice for strain-controlled axial-torsional fatigue testing with thin-walled tubular specimens, ASTM International, West Conshohocken, PA, (2015)..
[95] N. Shamsaei, A. Fatemi, Effect of microstructure and hardness on non-proportional cyclic hardening coefficient and predictions, Materials Science and Engineering: A 527(12) (2010) 3015-3024.
[96] N. Shamsaei, Multiaxial fatigue and deformation including non-proportional hardening and variable amplitude loading effects, (2010).
[97] N. Shamsaei, A. Fatemi, D.F. Socie, Multiaxial cyclic deformation and non-proportional hardening employing discriminating load paths, International Journal of Plasticity 26(12) (2010) 1680-1701.
[98] E. Tanaka, S. Murakami, M. Ōoka, Effects of strain path shapes on non-proportional cyclic plasticity, Journal of the Mechanics and Physics of Solids 33(6) (1985) 559-575.
[99] F. Lu, G. Kang, Y. Zhu, C. Xi, H. Jiang, Experimental observation on multiaxial ratchetting of polycarbonate polymer at room temperature, Polymer Testing 50 (2016) 135-144.
[100] N. Shamsaei, A. Fatemi, D.F. Socie, Multiaxial fatigue evaluation using discriminating strain paths, International Journal of Fatigue 33(4) (2011) 597-609.
[101] D.F. Socie, G.B. Marquis, Multiaxial fatigue, Society of Automotive Engineers Warrendale, PA2000.
[102] R. Shrestha, J. Simsiriwong, N. Shamsaei, Fatigue modeling for a thermoplastic polymer under mean strain and variable amplitude loadings, International Journal of Fatigue 100 (2017) 429-443.
[103] R. Shrestha, J. Simsiriwong, N. Shamsaei, Fatigue data for polyether ether ketone (PEEK) under fully-reversed cyclic loading, Data in Brief 6 (2016) 881-884.
[104] N. Shamsaei, M. Gladskyi, K. Panasovskyi, S. Shukaev, A. Fatemi, Multiaxial fatigue of titanium including step loading and load path alteration and sequence effects, International Journal of Fatigue 32(11) (2010) 1862-1874.